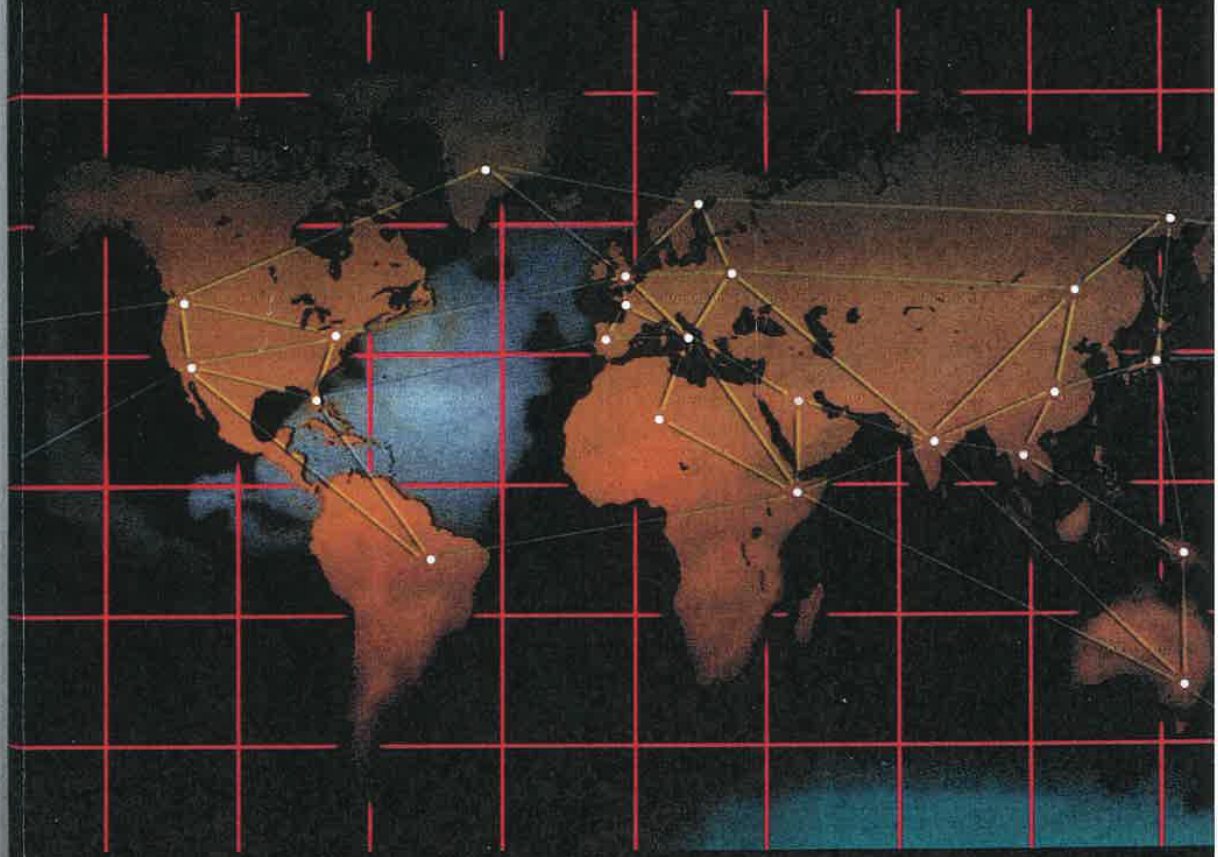
THE MOBILE COMMUNICATIONS HANDBOOK

Second Edition



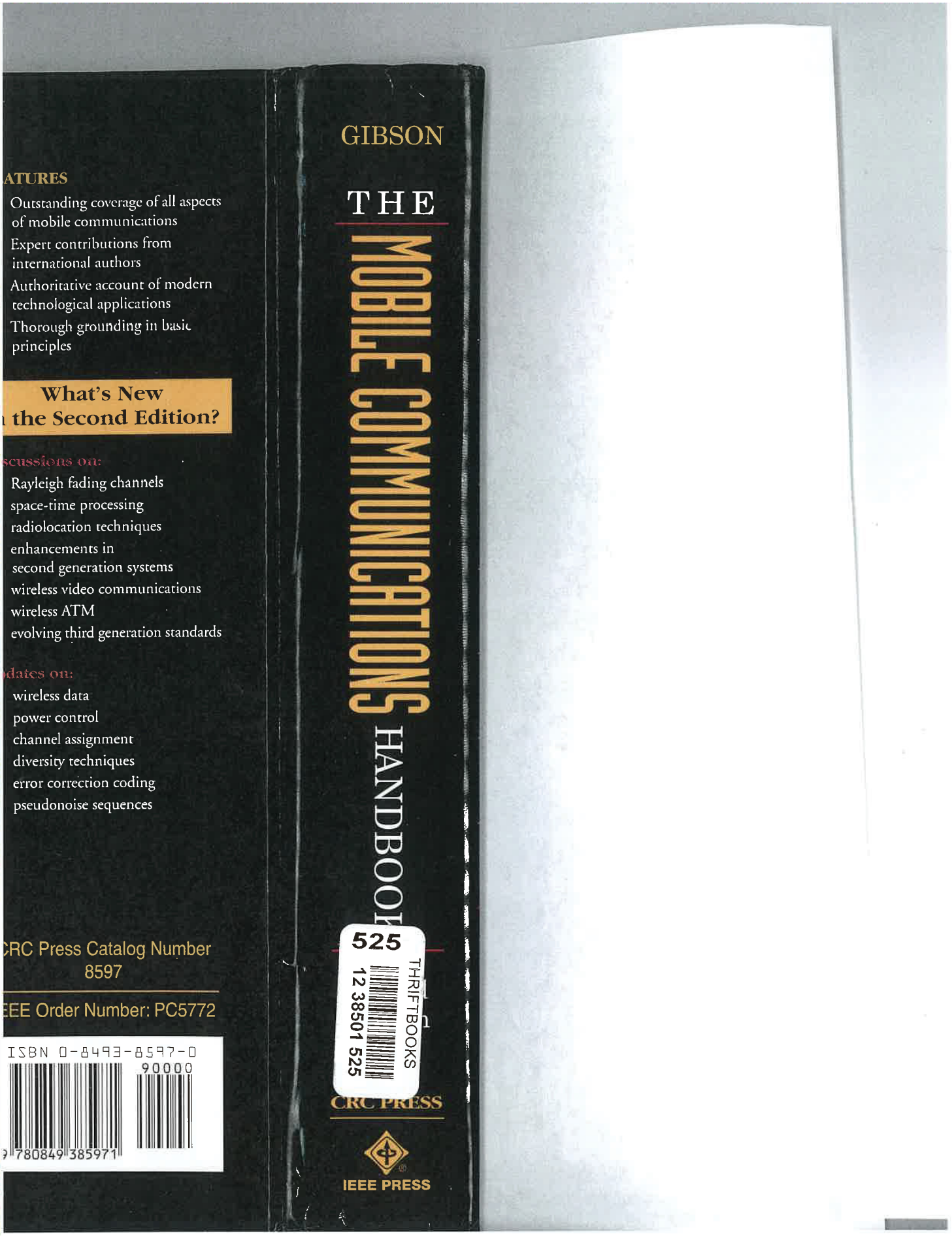
Editor-in-Chief

JERRY D. GIBSON

CRC PRESS

IEEE PRESS

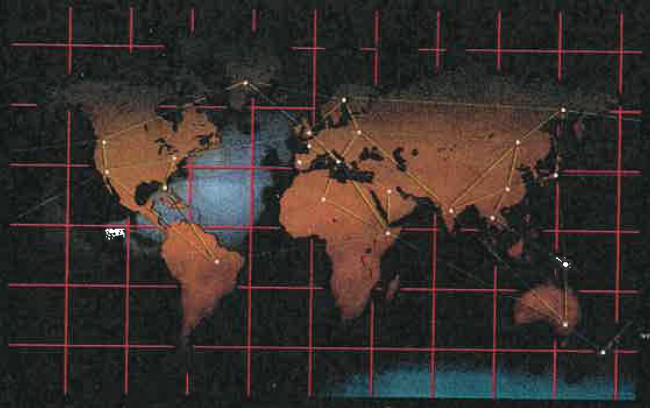
A CRC Handbook Published in Cooperation with IEEE Press


ATURES
Outstanding coverage of all aspects of mobile communications
Expert contributions from international authors
Authoritative account of modern technological applications
Thorough grounding in basic principles
What's New the Second Edition?
scussions on:
Rayleigh fading channels
space-time processing
radiolocation techniques
enhancements in second generation systems
wireless video communications
wireless ATM
evolving third generation standards
dates on:
wireless data
power control
channel assignment
diversity techniques
error correction coding
pseudonoise sequences
RC Press Catalog Number 8597
EEE Order Number: PC5772
ISBN 0-8493-8597-0
90000
9 780849 385971
GIBSON
THE MOBILE COMMUNICATIONS HANDBOOK
525
THRIFTBOOKS
12 38501 525
CRC PRESS
IEEE PRESS

DATA COMMUNICATIONS
NETWORKING

THE MOBILE COMMUNICATIONS HANDBOOK

Second Edition



Editor-in-Chief
JERRY D. GIBSON

The ***Mobile Communications Handbook*** covers the entire field — from principles of analog and digital communications to cordless telephones, wireless local area networks (LANs), and international technology standards. The amazing scope of the handbook ensures that it will be the primary reference for every aspect of mobile communications.

Organized into two sections, ***The Mobile Communications Handbook*** first introduces the basic principles of analog and digital communications. Consisting of tutorial articles, this section provides background information and technical details, offering a solid foundation for the spectrum of mobile communication technologies. The second part of the handbook consists of articles covering such topics as cellular mobile radio, personal communication systems, user location and addressing, wireless data, wireless LANs, and technology standards. Each article has been written as an independent contribution, but with intentional overlap between articles, providing essentially self-contained articles that can be read in whichever order desired by the reader. Nevertheless, the articles follow a logical order, thus creating continuity for the reader who wishes to proceed systematically through the handbook.

FEATURES

- Outstanding coverage of all aspects of mobile communications
- Expert contributions from international authors
- Authoritative account of modern technological applications
- Thorough grounding in basic principles

What's New in the Second Edition?

Discussions on:

- Rayleigh fading channels
- space-time processing
- radiolocation techniques
- enhancements in second generation systems
- wireless video communications
- wireless ATM
- evolving third generation standards

Updates on:

- wireless data
- power control
- channel assignment
- diversity techniques
- error correction coding
- pseudonoise sequences

CRC Press Catalog Number 8597

IEEE Order Number: PC5772

ISBN 0-8493-8597-0

9 780849 385971 90000

THE MOBILE COMMUNICATIONS HANDBOOK

Second Edition

The Electrical Engineering Handbook Series

Series Editor

Richard C. Dorf

University of California, Davis

Titles Included in the Series

The Avionics Handbook, Cary R. Spitzer

The Biomedical Engineering Handbook, Joseph D. Bronzino

The Circuits and Filters Handbook, Wai-Kai Chen

The Communications Handbook, Jerry D. Gibson

The Control Handbook, William S. Levine

The Digital Signal Processing Handbook, Vijay K. Madisetti & Douglas B. Williams

The Electrical Engineering Handbook, Richard C. Dorf

The Electric Power Engineering Handbook, L.L. Grigsby

The Electronics Handbook, Jerry C. Whitaker

The Engineering Handbook, Richard C. Dorf

The Handbook of Formulas and Tables for Signal Processing, Alexander D. Poularikas

The Industrial Electronics Handbook, J. David Irwin

The Measurement, Instrumentation, and Sensors Handbook, John G. Webster

The Mechanical Systems Design Handbook, Osita D.I. Nwokah

The Microwave Engineering Handbook, J. Michael Golio

The Mobile Communications Handbook, Jerry D. Gibson

The Ocean Engineering Handbook, Ferial El-Hawary

The Technology Management Handbook, Richard C. Dorf

The Transforms and Applications Handbook, Alexander D. Poularikas

The VLSI Handbook, Wai-Kai Chen

THE MOBILE COMMUNICATIONS HANDBOOK

Second Edition

Editor-in-Chief
JERRY D. GIBSON
Southern Methodist University
Dallas, Texas

Managing Editor
ELAINE M. GIBSON

CRC PRESS IEEE PRESS

A CRC Handbook Published in Cooperation with IEEE Press

Acquiring Editor:	Nora Konopka
Project Editor:	Carol Whitehead
Production Manager:	Suzanne Lassandro
Marketing Manager:	Barbara Glunn, Jane Lewis, Arline Massey, Jane Stark
Cover design:	Jonathan Pennell
PrePress:	Gary Bennett
Manufacturing:	Carol Slatter

Library of Congress Cataloging-in-Publication Data

The mobile communications handbook / editor-in-chief, Jerry D. Gibson.
-- 2nd ed.
p. cm.
Includes bibliographical references and index.
ISBN 0-8493-8597-0 (alk. paper)
1. Mobile communication systems. I. Gibson, Jerry D.
TK6570.M6M5934 1999
621.3845--dc21 98-46558
CIP

This book contains information obtained from authentic and highly regarded sources. Reprinted material is quoted with permission, and sources are indicated. A wide variety of references are listed. Reasonable efforts have been made to publish reliable data and information, but the author and the publisher cannot assume responsibility for the validity of all materials or for the consequences of their use.

Neither this book nor any part may be reproduced or transmitted in any form or by any means, electronic or mechanical, including photocopying, microfilming, and recording, or by any information storage or retrieval system, without prior permission in writing from the publisher.

All rights reserved. Authorization to photocopy items for internal or personal use, or the personal or internal use of specific clients, may be granted by CRC Press LLC, provided that $.50 per page photocopied is paid directly to Copyright Clearance Center, 222 Rosewood Drive, Danvers, MA 01923 USA. The fee code for users of the Transactional Reporting Service is ISBN 0-8493-8597-0/99/$0.00+$.50. The fee is subject to change without notice. For organizations that have been granted a photocopy license by the CCC, a separate system of payment has been arranged.

The consent of CRC Press LLC does not extend to copying for general distribution, for promotion, for creating new works, or for resale. Specific permission must be obtained in writing from CRC Press LLC for such copying.

Direct all inquiries to CRC Press LLC, 2000 Corporate Blvd., N.W., Boca Raton, Florida 33431.

Trademark Notice: Product or corporate names may be trademarks or registered trademarks, and are used only for identification and explanation, without intent to infringe.

© 1999 by CRC Press LLC

No claim to original U.S. Government works
International Standard Book Number 0-8493-8597-0
Library of Congress Card Number 98-46558
Printed in the United States of America 1 2 3 4 5 6 7 8 9 0
Printed on acid-free paper

Preface

To keep pace with the rapid evolution of the mobile and wireless communications field, this second edition of *The Mobile Communications Handbook* contains 12 revised chapters and 10 entirely new chapters to complement another 14 chapters carried forward from the first edition. We use the term mobile communications to include technologies ranging from cordless telephones, digital cellular mobile radio, and evolving personal communications systems to wireless data and wireless networks. To cover this range of topics, we present 36 concise chapters by experts from industry and academia. The chapters are written to provide a succinct overview of each topic, quickly bringing the reader up to date; additionally, the chapters contain sufficient detail and references to encourage further study. The chapters are more than a "just the facts" presentation, with many of the authors using their experience to provide insights into forthcoming developments in the various fields.

The Handbook is divided into two parts. The first part covers the basic principles of analog and digital communications that pertain to mobile communications, and consists of 14 tutorial/review chapters that lay a solid groundwork for the wide-ranging aspects of mobile communications technologies. The second part of the Handbook contains 22 chapters covering such topics as cellular mobile radio, Rayleigh fading channels, space-time processing, power control, personal communications systems, user location and addressing, wireless data, wireless local area networks (LANs), wireless ATM, and third generation wireless standards. The basic principles chapters readily allow the reader to jump right to the mobile communications topic of interest, with the option of efficiently filling in any gaps in his/her background by referring back to the Basic Principles section as needed, without searching through a textbook or shuffling off to the library.

Although there is an ordering to the articles, the sequence of articles does not have to be read from the beginning to end. Each article was written to be an independent contribution but with intentional overlap between some articles to prevent the reader from having to flip back and forth to extract the desired information. Interestingly, as the reader will discover, this overlap often admits alternative views of difficult issues.

As in the first edition, the lead-off article for the wireless section is written by an acknowledged leader and innovator in wireless communications, Dr. Don Cox of Stanford University. This chapter is unique in that Dr. Cox inserts comments and provides updates directly in the text of his chapter from the first edition. Besides being informative and easy to read, the article implicitly challenges those active in wireless communications to continually question the common knowledge in the field.

It has been a great pleasure to work with the authors to publish this second edition. The authors come from all parts of the world and constitute a literal who's who of workers in digital and mobile communications. Certainly, each article is an extraordinary contribution to the communications field, and the collection, I believe, is the most comprehensive treatment of the mobile communications field available in one volume today. I sincerely acknowledge the exceptional efforts and talents of my wife, Elaine M. Gibson, who served as Managing Editor for the project, and was the principal contact point for the authors and the publisher. Her energy and organizational skills in coordinating each contribution and in organizing the Handbook were essential to its timely delivery and to its quality. Elaine

and I both appreciate the patience, support, and guidance of the staff at CRC Press during all stages of developing and producing this Handbook.

Jerry D. Gibson
Dallas, Texas

About the Editor

Jerry D. Gibson currently serves as Chairman of the Department of Electrical Engineering at Southern Methodist University in Dallas, Texas. He has held positions at General Dynamics-Fort Worth (1969–1972), the University of Notre Dame (1973–1974), and the University of Nebraska-Lincoln (1974–1976), and during the Fall of 1991, Dr. Gibson was on sabbatical with the Information Systems Laboratory and the Telecommunications Program in the Department of Electrical Engineering at Stanford University. From 1987–1997, he held the J. W. Runyon, Jr. Professorship in the Department of Electrical Engineering at Texas A&M University.

Dr. Gibson is coauthor of the book *Introduction to Nonparametric Detection with Applications* (Academic Press, 1975 and IEEE Press, 1995), the author of the textbook, *Principles of Digital and Analog Communications* (Prentice-Hall, second edition, 1993), and coauthor of the book *Digital Compression for Multimedia* (Morgan Kaufmann, 1998). He was Associate Editor for Speech Processing for the *IEEE Transactions on Communications* from 1981 to 1985 and Associate Editor for Communications for the *IEEE Transactions on Information Theory* from 1988–1991. He has served as a member of the Speech Technical Committee of the IEEE Signal Processing Society (1992–1995), on the Editorial Board for the *Proceedings of the IEEE* (1991–1997), and as a member of the IEEE Information Theory Society Board of Governors (1990-1998). He was President of the IEEE Information Theory Society in 1996. Dr. Gibson is Editor-in-Chief of *The Mobile Communications Handbook* (CRC Press, 1996) and Editor-in-Chief of *The Communications Handbook* (CRC Press, 1997).

In 1990, Dr. Gibson received The Fredrick Emmons Terman Award from The American Society for Engineering Education, and in 1992, was elected Fellow of the IEEE "for contributions to the theory and practice of adaptive prediction and speech waveform coding." He was corecipient of the 1993 IEEE Signal Processing Society Senior Paper Award for the Speech Processing area. His research interests include data, speech, image, and video compression, multimedia over networks, wireless communications, information theory, and digital signal processing.

Contributors

Melbourne Barton
Bellcore
Red Bank, New Jersey

V. K. Bhargava
University of Victoria
Department of Electrical and Computer Engineering
Victoria, Canada

Madhukar Budagavi
Texas Instruments
DSP Solutions R and D Center
Dallas, Texas

James J. Caffery, Jr.
Georgia Institute of Technology
School of Electrical and Computer Engineering
Atlanta, Georgia

Wai-Yip Chan
Electrical and Computer Engineering Department
Illinois Institute of Technology
Chicago, Illinois

Li Fung Chang
Bellcore
Morristown, New Jersey

Matthew Cheng
Bellcore
Morristown, New Jersey

Giovanni Cherubini
IBM Zurich Research Laboratory
Ruschlikon, Switzerland

Leon W. Couch, II
University of Florida
Electrical and Computer Engineering
Gainesville, Florida

Donald C. Cox
Stanford University
Stanford, California

Marc Delprat
Alcatel Telcom/MCD
Colombes, France

Spiros Dimolitsas
Lawrence Livermore National Laboratory
Livermore, California

I. J. Fair
Department of Electrical and Computer Engineering
Technical University of Nova Scotia
Halifax, Nova Scotia
Canada

Ira Gerson
Motorola Semiconductor Products
Schaumburg, Illinois

Steven D. Gray
Nokia Research Center
Irving, Texas

Lajos Hanzo
Department of Electrical and Computer Science
University of Southampton
Highfield, Southampton
United Kingdom

Tor Helleseth
Department of Informatics
University of Bergen
Bergen, Norway

Michael L. Honig
Northwestern University
Department of EECS
Evanston, Illinois

Hwei P. Hsu
Fairleigh Dickinson University
Teaneck, New Jersey

Bijan Jabbari
George Mason University
Department of Electrical and Computer Engineering
Fairfax, Virginia

Ravi Jain
Bell Communications Research
Red Bank, New Jersey

P. Vijay Kumar
University of Southern California
Los Angeles, California

Vinod Kumar
Alcatel Telecom
Mobile Communication Division
Colombes, France

Allen H. Levesque
GTE Laboratories
Waltham, Massachusetts

Yi-Bing Lin
National Chaio Tung University
Hsinchu, Taiwan
Republic of China

Joseph L. LoCicero
Illinois Institute of Technology
Armour College of Engineering
Department of Electrical and Computer Engineering
Chicago, Illinois

Paul Mermelstein
INRS—Telecommunications
Ile des Soeurs
Verdun, Quebec
Canada

Toshio Miki
Mobile Communication Network, Inc.
Yokosuka, Kanagawa
Japan

Laurence B. Milstein
University of California–San Diego
Department of Electrical and Computer Engineering
La Jolla, California

Seshadri Mohan
Bell Communications Research
Morristown, New Jersey

Tero Ojanperä
Nokia Research Center
Irving, Texas

Michael Onufry
COMSAT Laboratories
Clarksburg, Maryland

Geoffrey C. Orsak
Southern Methodist University
Electrical Engineering Department
Dallas, Texas

Kaveh Pahlavan
Worcester Polytechnic Institute
Worcester, Massachusetts

Bernd-Peter Paris
George Mason University
Department of Electrical and Computer Engineering
Fairfax, Virginia

Bhasker P. Patel
Illinois Institute of Technology
Chicago, Illinois

Arogyaswami J. Paulraj
Stanford University
Department of Electrical Engineering
Stanford, California

Roman Pichna
University of Oulu
Center for Wireless Communication
Oulu, Finland

John G. Proakis
Northeastern University
Electrical Engineering
Boston, Massachusetts

Bala Rajagopalan
NEC C&C Research Laboratories
Princeton, New Jersey

Daniel Reininger
NEC USA, Inc.
Princeton, New Jersey

Marvin K. Simon
Jet Propulsion Laboratory
Pasadena, California

Suresh Singh
Oregon State University
Electrical and Computer Engineering Department
Corvallis, Oregon

Bernard Sklar
Communications Engineering Services
Tarzana, California

Raymond Steele
MAC, Ltd.
Southampton
United Kingdom

Gordon L. Stüber
Georgia Institute of Technology
School of Electrical and Computer Engineering
Atlanta, Georgia

Raj Talluri
Texas Instruments
DSP Solutions R and D Center
Dallas, Texas

Qiang Wang
University of Victoria
Victoria, British Columbia
Canada

Michel Daoud Yacoub
The University of Campinas
San Paulo, Brazil

Contents

SECTION I Basic Principles

1 Complex Envelope Representations for Modulated Signals *Leon W. Couch, II* 1-1

2 Sampling *Hwei P. Hsu* 2-1

3 Pulse Code Modulation *Leon W. Couch, II* 3-1

4 Baseband Signalling and Pulse Shaping *Michael L. Honig and Melbourne Barton* 4-1

5 Channel Equalization *John G. Proakis* 5-1

6 Line Coding *Joseph L. LoCicero and Bhasker P. Patel* 6-1

7 Echo Cancellation *Giovanni Cherubini* 7-1

8 Pseudonoise Sequences *Tor Helleseth and P. Vijay Kumar* 8-1

9 Optimum Receivers *Geoffrey C. Orsak* 9-1

10 Forward Error Correction Coding *V.K. Bhargava and I.J. Fair* 10-1

11 Spread Spectrum Communications *Laurence B. Milstein and Marvin K. Simon* 11-1

12 Diversity *Arogyaswami J. Paulraj* 12-1

13 Digital Communication System Performance *Bernard Sklar* 13-1

14 Telecommunications Standardization *Spiros Dimolitsas and Michael Onufry* 14-1

SECTION II Wireless

15 Wireless Personal Communications: A Perspective *Donald C. Cox* 15-1

16 Modulation Methods *Gordon L. Stüber* 16-1

17 Access Methods *Bernd-Peter Paris* 17-1

18 Rayleigh Fading Channels *Bernard Sklar* 18-1

19 Space-Time Processing *Arogyaswami J. Paulraj* 19-1

20 Location Strategies for Personal Communications Services *Ravi Jain, Yi-Bing Lin, and Seshadri Mohan* 20-1

21 Cell Design Principles *Michel Daoud Yacoub* 21-1

22 Microcellular Radio Communications *Raymond Steele* 22-1

23 Fixed and Dynamic Channel Assignment *Bijan Jabbari* 23-1

24 Radiolocation Techniques *Gordon L. Stüber and James J. Caffery, Jr.* 24-1

25 Power Control *Roman Pichna and Qiang Wang* 25-1

26 Enhancements in Second Generation Systems *Marc Delprat and Vinod Kumar* 26-1

27 The Pan-European Cellular System *Lajos Hanzo* 27-1

28 Speech and Channel Coding for North American TDMA Cellular Systems *Paul Mermelstein* 28-1

29 The British Cordless Telephone Standard: CT-2 *Lajos Hanzo* 29-1

30 Half-Rate Standards *Wai-Yip Chan, Ira Gerson, and Toshio Miki* 30-1

31 Wireless Video Communications *Madhukar Budagavi and Raj Talluri* . . . 31-1

32 Wireless LANs *Suresh Singh* 32-1

33 Wireless Data *Allen H. Levesque and Kaveh Pahlavan* 33-1

34 Wireless ATM: Interworking Aspects *Melbourne Barton, Matthew Cheng, and Li Fung Chang* 34-1

35 Wireless ATM: QoS and Mobility Management *Bala Rajagopalan and Daniel Reininger* 35-1

36 An Overview of cdma2000, WCDMA, and EDGE *Tero Ojanperä and Steven D. Gray* 36-1

Index I-1

I

Basic Principles

1 **Complex Envelope Representations for Modulated Signals** *Leon W. Couch, II* . 1-1
Introduction • Complex Envelope Representation • Representation of Modulated Signals • Generalized Transmitters and Receivers • Spectrum and Power of Bandpass Signals • Amplitude Modulation • Phase and Frequency Modulation • QPSK Signalling

2 **Sampling** *Hwei P. Hsu* 2-1
Introduction • Instantaneous Sampling • Sampling Theorem • Sampling of Sinusoidal Signals • Sampling of Bandpass Signals • Practical Sampling • Sampling Theorem in the Frequency Domain • Summary and Discussion

3 **Pulse Code Modulation** *Leon W. Couch, II* 3-1
Introduction • Generation of PCM • Percent Quantizing Noise • Practical PCM Circuits • Bandwidth of PCM • Effects of Noise • Nonuniform Quantizing: μ-Law and A-Law Companding • Example: Design of a PCM System

4 **Baseband Signalling and Pulse Shaping** *Michael L. Honig and Melbourne Barton* 4-1
Communications System Model • Intersymbol Interference and the Nyquist Criterion • Nyquist Criterion with Matched Filtering • Eye Diagrams • Partial-Response Signalling • Additional Considerations • Examples

5 **Channel Equalization** *John G. Proakis* 5-1
Characterization of Channel Distortion • Characterization of Intersymbol Interference • Linear Equalizers • Decision-Feedback Equalizer • Maximum-Likelihood Sequence Detection • Conclusions

6 **Line Coding** *Joseph L. LoCicero and Bhasker P. Patel* 6-1
Introduction • Common Line Coding Formats • Alternate Line Codes • Multilevel Signalling, Partial Response Signalling, and Duobinary Coding • Bandwidth Comparison • Concluding Remarks

7 **Echo Cancellation** *Giovanni Cherubini* 7-1
Introduction • Echo Cancellation for PAM Systems • Echo Cancellation for QAM Systems • Echo Cancellation for OFDM Systems • Summary and Conclusions

8 **Pseudonoise Sequences** *Tor Helleseth and P. Vijay Kumar* 8-1
Introduction • m Sequences • The q-ary Sequences with Low Autocorrelation • Families of Sequences with Low Crosscorrelation • Aperiodic Correlation • Other Correlation Measures

9 Optimum Receivers *Geoffrey C. Orsak* 9-1
Introduction • Preliminaries • Karhunen–Loève Expansion • Detection Theory • Performance • Signal Space • Standard Binary Signalling Schemes • M-ary Optimal Receivers • More Realistic Channels • Dispersive Channels

10 Forward Error Correction Coding *V.K. Bhargava and I.J. Fair* 10-1
Introduction • Fundamentals of Block Coding • Structure and Decoding of Block Codes • Important Classes of Block Codes • Principles of Convolutional Coding • Decoding of Convolutional Codes • Trellis-Coded Modulation • Additional Measures • Turbo Codes • Applications

11 Spread Spectrum Communications *Laurence B. Milstein and Marvin K. Simon* 11-1
A Brief History • Why Spread Spectrum? • Basic Concepts and Terminology • Spread Spectrum Techniques • Applications of Spread Spectrum

12 Diversity *Arogyaswami J. Paulraj* 12-1
Introduction • Diversity Schemes • Diversity Combining Techniques • Effect of Diversity Combining on Bit Error Rate • Concluding Remarks

13 Digital Communication System Performance *Bernard Sklar* 13-1
Introduction • Bandwidth and Power Considerations • Example 1: Bandwidth-Limited Uncoded System • Example 2: Power-Limited Uncoded System • Example 3: Bandwidth-Limited Power-Limited Coded System • Example 4: Direct-Sequence Spread-Spectrum Coded System • Conclusion

14 Telecommunications Standardization *Spiros Dimolitsas and Michael Onufry* .. 14-1
Introduction • Global Standardization • Regional Standardization • National Standardization • Intellectual Property • Standards Coordination • Scientific • Standards Development Cycle

1

Complex Envelope Representations for Modulated Signals[1]

1.1 Introduction 1-1
1.2 Complex Envelope Representation 1-2
1.3 Representation of Modulated Signals 1-4
1.4 Generalized Transmitters and Receivers 1-4
1.5 Spectrum and Power of Bandpass Signals 1-7
1.6 Amplitude Modulation 1-8
1.7 Phase and Frequency Modulation 1-10
1.8 QPSK Signalling 1-11
Defining Terms 1-14
References 1-15
Further Information 1-15

Leon W. Couch, II
University of Florida

1.1 Introduction

What is a general representation for bandpass digital and analog signals? How do we represent a **modulated signal**? How do we evaluate the spectrum and the power of these signals? These are some of the questions that are answered in this chapter.

A *baseband* waveform has a spectral magnitude that is nonzero for frequencies in the vicinity of the origin (i.e., $f = 0$) and negligible elsewhere. A *bandpass* waveform has a spectral magnitude that is nonzero for frequencies in some band concentrated about a frequency $f = \pm f_c$ (where $f_c \gg 0$), and the spectral magnitude is negligible elsewhere. f_c is called the *carrier frequency*. The value of f_c may be arbitrarily assigned for mathematical convenience in some problems. In others, namely, **modulation** problems, f_c is the frequency of an oscillatory signal in the transmitter circuit and is the assigned frequency of the transmitter, such as 850 kHz for an AM broadcasting station.

In communication problems, the information source signal is usually a baseband signal—for example, a transistor-transistor logic (TTL) waveform from a digital circuit or an audio (analog) signal from a microphone. The communication engineer has the job of building a system that will transfer the information from this source signal to the desired destination.

[1] *Source:* Couch, Leon W., II. 1997. *Digital and Analog Communication Systems,* 5th ed., Prentice Hall, Upper Saddle River, NJ.

0-8493-8597-0/99/$0.00+$.50

© 1999 by CRC Press LLC

As shown in Fig. 1.1, this usually requires the use of a bandpass signal, $s(t)$, which has a bandpass spectrum that is concentrated at $\pm f_c$ where f_c is selected so that $s(t)$ will propagate across the communication channel (either a wire or a wireless channel).

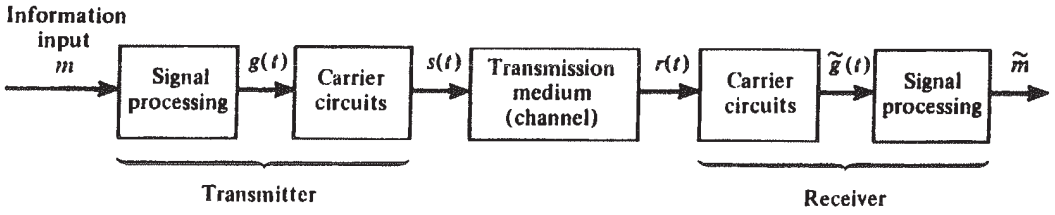


FIGURE 1.1 Bandpass communication system. *Source:* Couch, L.W., II. 1997. *Digital and Analog Communication Systems,* 5th ed., Prentice Hall, Upper Saddle River, NJ, p. 227. With permission.

Modulation is the process of imparting the source information onto a bandpass signal with a carrier frequency f_c by the introduction of amplitude and/or phase perturbations. This bandpass signal is called the *modulated* signal $s(t)$, and the baseband source signal is called the *modulating* signal $m(t)$. Examples of exactly how modulation is accomplished are given later in this chapter. This definition indicates that modulation may be visualized as a mapping operation that maps the source information onto the bandpass signal $s(t)$ that will be transmitted over the channel.

As the modulated signal passes through the channel, noise corrupts it. The result is a bandpass signal-plus-noise waveform that is available at the receiver input, $r(t)$, as illustrated in Fig. 1.1. The receiver has the job of trying to recover the information that was sent from the source; $\tilde{m}$ denotes the corrupted version of m.

1.2 Complex Envelope Representation

All bandpass waveforms, whether they arise from a modulated signal, interfering signals, or noise, may be represented in a convenient form given by the following theorem. $v(t)$ will be used to denote the **bandpass waveform** canonically. That is, $v(t)$ can represent the signal when $s(t) \equiv v(t)$, the noise when $n(t) \equiv v(t)$, the filtered signal plus noise at the channel output when $r(t) \equiv v(t)$, or any other type of bandpass waveform[2].

THEOREM 1.1 *Any physical bandpass waveform can be represented by*

$$v(t) = Re\left\{g(t)e^{j\omega_c t}\right\} \tag{1.1a}$$

$Re\{\cdot\}$ denotes the real part of $\{\cdot\}$. $g(t)$ is called the complex envelope of $v(t)$, and f_c is the associated carrier frequency (hertz) where $\omega_c = 2\pi f_c$. Furthermore, two other equivalent representations are

[2]The symbol $\equiv$ denotes an equivalence and the symbol $\stackrel{\triangle}{=}$ denotes a definition.

$$v(t) = R(t)\cos[\omega_c t + \theta(t)] \tag{1.1b}$$

and

$$v(t) = x(t)\cos\omega_c t - y(t)\sin\omega_c t \tag{1.1c}$$

where

$$g(t) = x(t) + jy(t) = |g(t)|e^{j\angle g(t)} \equiv R(t)e^{j\theta(t)} \tag{1.2}$$

$$x(t) = Re\{g(t)\} \equiv R(t)\cos\theta(t) \tag{1.3a}$$
$$y(x) = Im\{g(t)\} \equiv R(t)\sin\theta(t) \tag{1.3b}$$

$$R(t) \triangleq |g(t)| \equiv \sqrt{x^2(t) + y^2(t)} \tag{1.4a}$$
$$\theta(t) \triangleq \angle g(t) = \tan^{-1}\left(\frac{y(t)}{x(t)}\right) \tag{1.4b}$$

The waveforms $g(t), x(t), y(t), R(t)$, and $\theta(t)$ are all **baseband waveforms**, and, except for $g(t)$, they are all real waveforms. $R(t)$ is a nonnegative real waveform. Equation (1.1) is a low-pass-to-bandpass transformation. The $e^{j\omega_c t}$ factor in (1.1a) shifts (i.e., translates) the spectrum of the baseband signal $g(t)$ from baseband up to the carrier frequency f_c. In communications terminology the frequencies in the baseband signal $g(t)$ are said to be *heterodyned* up to f_c. The **complex envelope**, $g(t)$, is usually a complex function of time and it is the generalization of the phasor concept. That is, if $g(t)$ happens to be a complex constant, then $v(t)$ is a pure sine wave of frequency f_c and this complex constant is the phasor representing the sine wave. If $g(t)$ is not a constant, then $v(t)$ is not a pure sine wave because the amplitude and phase of $v(t)$ varies with time, caused by the variations of $g(t)$.

Representing the complex envelope in terms of two real functions in Cartesian coordinates, we have

$$g(x) \equiv x(t) + jy(t) \tag{1.5}$$

where $x(t) = \text{Re}\{g(t)\}$ and $y(t) = \text{Im}\{g(t)\}$. $x(t)$ is said to be the *in-phase modulation* associated with $v(t)$, and $y(t)$ is said to be the *quadrature modulation* associated with $v(t)$. Alternatively, the polar form of $g(t)$, represented by $R(t)$ and $\theta(t)$, is given by (1.2), where the identities between Cartesian and polar coordinates are given by (1.3) and (1.4). $R(t)$ and $\theta(t)$ are real waveforms and, in addition, $R(t)$ is always nonnegative. $R(t)$ is said to be the *amplitude modulation* (AM) on $v(t)$, and $\theta(t)$ is said to be the *phase modulation* (PM) on $v(t)$.

The usefulness of the complex envelope representation for bandpass waveforms cannot be overemphasized. In modern communication systems, the bandpass signal is often partitioned into two channels, one for $x(t)$ called the I (in-phase) channel and one for $y(t)$ called the Q (quadrature-phase) channel. In digital computer simulations of bandpass signals, the sampling rate used in the simulation can be minimized by working with the complex envelope, $g(t)$, instead of with the bandpass signal, $v(t)$, because $g(t)$ is the baseband equivalent of the bandpass signal [1].

1.3 Representation of Modulated Signals

Modulation is the process of encoding the source information $m(t)$ (modulating signal) into a bandpass signal $s(t)$ (modulated signal). Consequently, the modulated signal is just a special application of the bandpass representation. The *modulated signal* is given by

$$s(t) = \text{Re}\left\{g(t)e^{j\omega_c t}\right\} \tag{1.6}$$

where $\omega_c = 2\pi f_c$. f_c is the carrier frequency. The complex envelope $g(t)$ is a function of the modulating signal $m(t)$. That is,

$$g(t) = g[m(t)] \tag{1.7}$$

Thus $g[\cdot]$ performs a mapping operation on $m(t)$. This was shown in Fig. 1.1.

Table 1.1 gives an overview of the *big picture* for the modulation problem. Examples of the mapping function $g[m]$ are given for amplitude modulation (AM), double-sideband suppressed carrier (DSB-SC), phase modulation (PM), frequency modulation (FM), single-sideband AM suppressed carrier (SSB-AM-SC), single-sideband PM (SSB-PM), single-sideband FM (SSB-FM), single-sideband envelope detectable (SSB-EV), single-sideband square-law detectable (SSB-SQ), and quadrature modulation (QM). For each $g[m]$, Table 1.1 also shows the corresponding $x(t)$ and $y(t)$ quadrature modulation components, and the corresponding $R(t)$ and $\theta(t)$ amplitude and phase modulation components. Digitally modulated bandpass signals are obtained when $m(t)$ is a digital baseband signal—for example, the output of a transistor transistor logic (TTL) circuit.

Obviously, it is possible to use other $g[m]$ functions that are not listed in Table 1.1. The question is: Are they useful? $g[m]$ functions are desired that are easy to implement and that will give desirable spectral properties. Furthermore, in the receiver the inverse function $m[g]$ is required. The inverse should be single valued over the range used and should be easily implemented. The inverse mapping should suppress as much noise as possible so that $m(t)$ can be recovered with little corruption.

1.4 Generalized Transmitters and Receivers

A more detailed description of transmitters and receivers as first shown in Fig. 1.1 will now be illustrated.

There are two canonical forms for the generalized transmitter, as indicated by (1.1b) and (1.1c). Equation (1.1b) describes an AM-PM type circuit as shown in Fig. 1.2. The baseband signal processing circuit generates $R(t)$ and $\theta(t)$ from $m(t)$. The R and θ are functions of the modulating signal $m(t)$, as given in Table 1.1, for the particular modulation type desired. The signal processing may be implemented either by using nonlinear analog circuits or a digital computer that incorporates the R and θ algorithms under software program control. In the implementation using a digital computer, one analog-to-digital converter (ADC) will be needed at the input of the baseband signal processor and two digital-to-analog converters (DACs) will be needed at the output. The remainder of the AM-PM canonical form requires radio frequency (RF) circuits, as indicated in the figure.

Figure 1.3 illustrates the second canonical form for the generalized transmitter. This uses in-phase and quadrature-phase (IQ) processing. Similarly, the formulas relating $x(t)$ and $y(t)$ to $m(t)$ are shown in Table 1.1, and the baseband signal processing may be implemented by using either analog hardware or digital hardware with software. The remainder of the canonical form uses RF circuits as indicated.

TABLE 1.1 Complex Envelope Functions for Various Types of Modulation[a]

Type of Modulation	Mapping Functions $g(m)$	Corresponding Quadrature Modulation	
		$x(t)$	$y(t)$
AM	$A_c[1+m(t)]$	$A_c[1+m(t)]$	0
DSB-SC	$A_c m(t)$	$A_c m(t)$	0
PM	$A_c e^{jD_p m(t)}$	$A_c \cos[D_p m(t)]$	$A_c \sin[D_p m(t)]$
FM	$A_c e^{jD_f \int_{-\infty}^{t} m(\sigma)d\sigma}$	$A_c \cos\left[D_f \int_{-\infty}^{t} m(\sigma)d\sigma\right]$	$A_c \sin\left[D_f \int_{-\infty}^{t} m(\sigma)d\sigma\right]$
SSB-AM-SC[b]	$A_c[m(t) \pm j\hat{m}(t)]$	$A_c m(t)$	$\pm A_c \hat{m}(t)$
SSB-PM[b]	$A_c e^{jD_p[m(t)\pm j\hat{m}(t)]}$	$A_c e^{\mp D_p \hat{m}(t)} \cos[D_p m(t)]$	$A_c e^{\mp D_p \hat{m}(t)} \sin[D_p m(t)]$
SSB-FM[b]	$A_c e^{jD_f \int_{-\infty}^{t} [m(\sigma)\pm j\hat{m}(\sigma)]d\sigma}$	$A_c e^{\mp D_f \int_{-\infty}^{t} \hat{m}(\sigma)d\sigma} \cos\left[D_f \int_{-\infty}^{t} m(\sigma)d\sigma\right]$	$A_c e^{\mp D_f \int_{-\infty}^{t} \hat{m}(\sigma)d\sigma} \sin\left[D_f \int_{-\infty}^{t} m(\sigma)d\sigma\right]$
SSB-EV[b]	$A_c e^{\{\ln[1+m(t)]\pm j\hat{\ln}\lvert 1+m(t)\rvert\}}$	$A_c[1+m(t)] \cos\{\hat{\ln}[1+m(t)]\}$	$\pm A_c[1+m(t)] \sin\{\hat{\ln}[1+m(t)]\}$
SSB-SQ[b]	$A_c e^{(1/2)\{\ln[1+m(t)]\pm j\hat{\ln}\lvert 1+m(t)\rvert\}}$	$A_c \sqrt{1+m(t)} \cos\{\frac{1}{2}\hat{\ln}[1+m(t)]\}$	$\pm A_c \sqrt{1+m(t)} \sin\{\frac{1}{2}\hat{\ln}[1+m(t)]\}$
QM	$A_c[m_1(t)+jm_2(t)]$	$A_c m_1(t)$	$A_c m_2(t)$

TABLE 1.1 Complex Envelope Functions for Various Types of Modulation[a] *(Continued)*

Type of Modulation	Corresponding Amplitude and Phase Modulation		Linearity	Remarks
	$R(t)$	$\theta(t)$		
AM	$A_c\|1+m(t)\|$	$\begin{cases} 0, & m(t)>-1 \\ 180°, & m(t)<-1 \end{cases}$	L[c]	$m(t)>-1$ required for envelope detection
DSB-SC	$A_c\|m(t)\|$	$\begin{cases} 0, & m(t)>0 \\ 180°, & m(t)<0 \end{cases}$	L	Coherent detection required
PM	A_c	$D_p m(t)$	NL	D_p is the phase deviation constant (rad/volt)
FM	A_c	$D_f\int_{-\infty}^{t} m(\sigma)d\sigma$	NL	D_f is the frequency deviation constant (rad/volt-sec)
SSB-AM-SC[b]	$A_c\sqrt{[m(t)]^2+[\hat{m}(t)]^2}$	$\tan^{-1}[\pm\hat{m}(t)/m(t)]$	L	Coherent detection required
SSB-PM[b]	$A_c e^{\pm D_p\hat{m}(t)}$	$D_p m(t)$	NL	
SSB-FM[b]	$A_c e^{\pm D_f\int_{-\infty}^{t}\hat{m}(\sigma)d\sigma}$	$D_f\int_{-\infty}^{t} m(\sigma)d\sigma$	NL	
SSB-EV[b]	$A_c\|1+m(t)\|$	$\pm\hat{\ln}[1+m(t)]$	NL	$m(t)>-1$ is required so that the $\ln(\cdot)$ will have a real value
SSB-SQ[b]	$A_c\sqrt{1+m(t)}$	$\pm\frac{1}{2}\hat{\ln}[1+m(t)]$	NL	$m(t)>-1$ is required so that the $\ln(\cdot)$ will have a real value
QM	$A_c\sqrt{m_1^2(t)+m_2^2(t)}$	$\tan^{-1}[m_2(t)/m_1(t)]$	L	Used in NTSC color television; requires coherent detection

Source: Couch, L.W., II, 1997, *Digital and Analog Communication Systems,* 5th ed., Prentice Hall, Upper Saddle River, NJ, pp. 231-232. With permission.

[a] $A_c>0$ is a constant that sets the power level of the signal as evaluated by use of (1.11); L, linear; NL, nonlinear; and $\hat{[\cdot]}$ is the Hilbert transform (a $-90°$ phase-shifted version of $[\cdot]$). For example, $\hat{m}(t)=m(t)*\frac{1}{\pi t}=\frac{1}{\pi}\int_{-\infty}^{\infty}\frac{m(\lambda)}{t-\lambda}d\lambda$.

[b] Use upper signs for upper sideband signals and lower signals for lower sideband signals.

[c] In the strict sense, AM signals are not linear because the carrier term does not satisfy the linearity (superposition) condition.

Analogous to the transmitter realizations, there are two canonical forms of receiver. Each one consists of RF carrier circuits followed by baseband signal processing as illustrated in Fig. 1.1. Typically the carrier circuits are of the superheterodyne-receiver type which consist of an RF amplifier, a down converter (mixer plus local oscillator) to some intermediate frequency (IF), an IF amplifier and then detector circuits [1]. In the first canonical form of the receiver, the carrier circuits have amplitude and phase detectors that output $\tilde{R}(t)$ and $\tilde{\theta}(t)$, respectively. This pair, $\tilde{R}(t)$ and $\tilde{\theta}(t)$, describe the polar form of the received complex envelope, $\tilde{g}(t)$. $\tilde{R}(t)$ and $\tilde{\theta}(t)$ are then fed into the signal processor which uses the inverse functions of Table 1.1 to generate the recovered modulation, $\tilde{m}(t)$. The second canonical form of the receiver uses quadrature product detectors in the carrier circuits to produce the Cartesian form of the received complex envelope, $\tilde{x}(t)$ and $\tilde{y}(t)$. $\tilde{x}(t)$ and $\tilde{y}(t)$ are then inputted to the signal processor which generates $\tilde{m}(t)$ at its output.

Once again, it is stressed that any type of signal modulation (see Table 1.1) may be generated (transmitted) or detected (received) by using either of these two canonical forms. Both of these forms conveniently separate baseband processing from RF processing. Digital

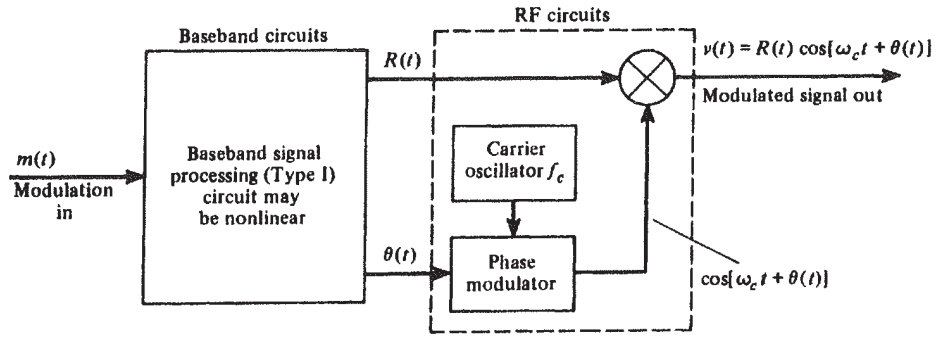


FIGURE 1.2 Generalized transmitter using the AM-PM generation technique. *Source:* Couch, L.W., II. 1997. *Digital and Analog Communication Systems,* 5th ed., Prentice Hall, Upper Saddle River, NJ, p. 278. With permission.

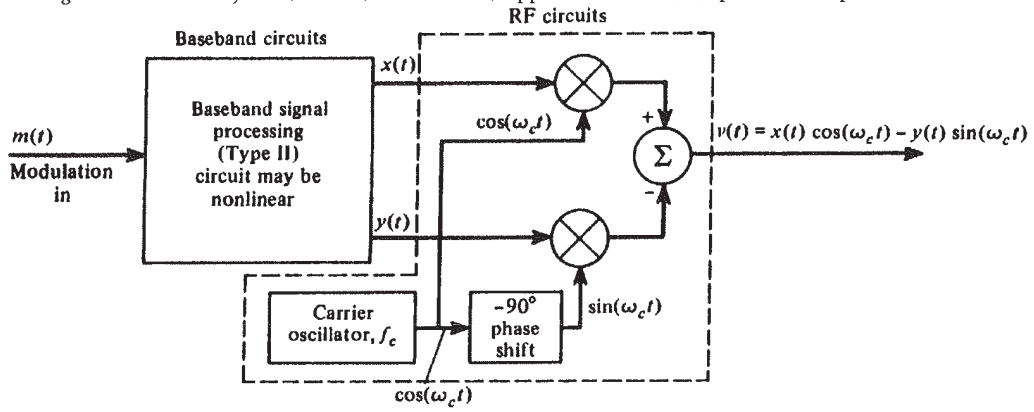


FIGURE 1.3 Generalized transmitter using the quadrature generation technique. *Source:* Couch, L.W., II. 1997. *Digital and Analog Communication Systems,* 5th ed., Prentice Hall, Upper Saddle River, NJ, p. 278. With permission.

techniques are especially useful to realize the baseband processing portion. Furthermore, if digital computing circuits are used, any desired modulation type can be realized by selecting the appropriate software algorithm.

1.5 Spectrum and Power of Bandpass Signals

The spectrum of the bandpass signal is the translation of the spectrum of its complex envelope. Taking the **Fourier transform** of (1.1a), the spectrum of the bandpass waveform is [1]

$$V(f) = \frac{1}{2}\left[G\left(f - f_c\right) + G^*\left(-f - f_c\right)\right] \tag{1.8}$$

where $G(f)$ is the Fourier transform of $g(t)$,

$$G(f) = \int_{-\infty}^{\infty} g(t)e^{-j2\pi ft}dt \ ,$$

and the asterisk superscript denotes the complex conjugate operation. The *power spectra density* (PSD) of the bandpass waveform is [1]

$$\mathcal{P}_v(f) = \frac{1}{4}\left[\mathcal{P}_g\left(f - f_c\right) + \mathcal{P}_g\left(-f - f_c\right)\right] \tag{1.9}$$

where $\mathcal{P}_g(f)$ is the PSD of $g(t)$.

The average power dissipated in a resistive load is V_{rms}^2/R_L or $I_{\text{rms}}^2 R_L$ where V_{rms} is the rms value of the voltage waveform across the load and I_{rms} is the rms value of the current through the load. For bandpass waveforms, Eq. (1.1) may represent either the voltage or the current. Furthermore, the rms values of $v(t)$ and $g(t)$ are related by [1]

$$v_{\text{rms}}^2 = \langle v^2(t) \rangle = \frac{1}{2} \langle |g(t)|^2 \rangle = \frac{1}{2} g_{\text{rms}}^2 \tag{1.10}$$

where $\langle \cdot \rangle$ denotes the time average and is given by

$$\left\langle \left[\quad \right] \right\rangle = \lim_{t \to \infty} \frac{1}{T} \int_{-T/2}^{T/2} \left[\quad \right] dt$$

Thus, if $v(t)$ of (1.1) represents the bandpass voltage waveform across a resistive load, the average power dissipated in the load is

$$P_L = \frac{v_{\text{rms}}^2}{R_L} = \frac{\langle v^2(t) \rangle}{R_L} = \frac{\langle |g(t)|^2 \rangle}{2R_L} = \frac{g_{\text{rms}}^2}{2R_L} \tag{1.11}$$

where g_{rms} is the rms value of the complex envelope and R_L is the resistance of the load.

1.6 Amplitude Modulation

Amplitude modulation (AM) will now be examined in more detail. From Table 1.1 the complex envelope of an AM signal is

$$g(t) = A_c[1 + m(t)] \tag{1.12}$$

so that the spectrum of the complex envelope is

$$G(f) = A_c \delta(f) + A_c M(f) \tag{1.13}$$

Using (1.6), we obtain the AM signal waveform

$$s(t) = A_c[1 + m(t)] \cos \omega_c t \tag{1.14}$$

and, using (1.8), the AM spectrum

$$S(f) = \frac{1}{2} A_c \left[\delta(f - f_c) + M(f - f_c) + \delta(f + f_c) + M(f + f_c) \right] \tag{1.15}$$

where $\delta(f) = \delta(-f)$ and, because $m(t)$ is real, $M^*(f) = M(-f)$. Suppose that the magnitude spectrum of the modulation happens to be a triangular function, as shown in Fig. 1.4(a). This spectrum might arise from an analog audio source where the bass frequencies are emphasized. The resulting AM spectrum, using (1.15), is shown in Fig. 1.4(b). Note that because $G(f - f_c)$ and $G^*(-f - f_c)$ do not overlap, the magnitude spectrum is

$$|S(f)| = \begin{cases} \frac{1}{2} A_c \delta(f - f_c) + \frac{1}{2} A_c |M(f - f_c)|, & f > 0 \\ \frac{1}{2} A_c \delta(f + f)_c + \frac{1}{2} A_c |M(-f - f)_c|, & f < 0 \end{cases} \tag{1.16}$$

The 1 in

$$g(t) = A_c[1 + m(t)]$$

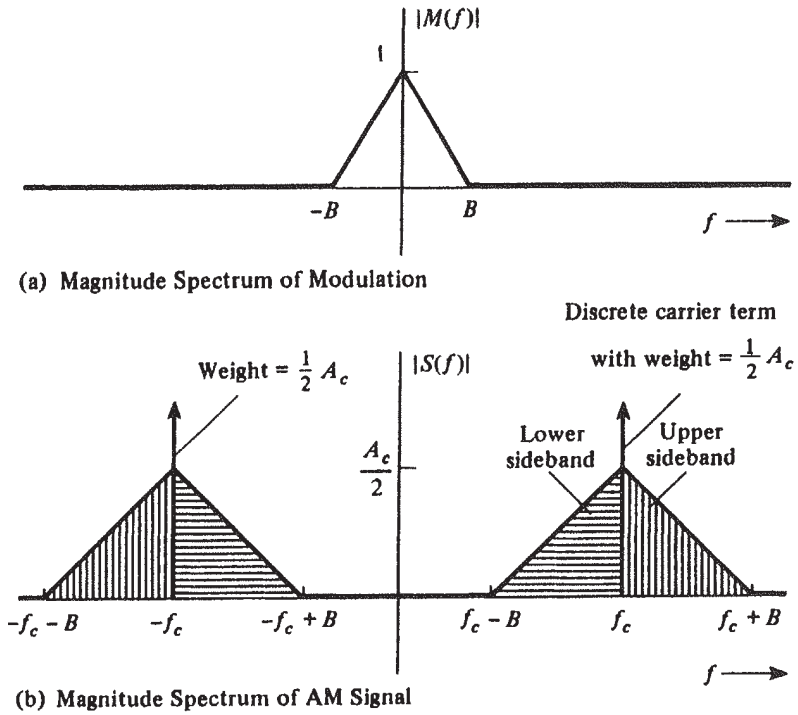


FIGURE 1.4 Spectrum of an AM signal. *Source:* Couch, L.W., II. 1997. *Digital and Analog Communication Systems,* 5th ed., Prentice Hall, Upper Saddle River, NJ, p. 235. With permission.

causes delta functions to occur in the spectrum at $f = \pm f_c$, where f_c is the assigned carrier frequency. Also, from Fig. 1.4 and (1.16), it is realized that the bandwidth of the AM signal is 2B. That is, the bandwidth of the AM signal is twice the bandwidth of the baseband modulating signal.

The average power dissipated into a resistive load is found by using (1.11).

$$P_L = \frac{A_c^2}{2R_L}\left\langle |1 + m(t)|^2 \right\rangle = \frac{A_c^2}{2R_L}\left[1 + 2\langle m(t)\rangle + \langle m^2(t)\rangle\right]$$

If we assume that the *dc* value of the modulation is zero, $\langle m(t)\rangle = 0$, then the average power dissipated into the load is

$$P_L = \frac{A_c^2}{2R_L}\left\langle 1 + m_{\text{rms}}^2 \right\rangle \quad . \tag{1.17}$$

where m_{rms} is the rms value of the modulation, $m(t)$. Thus, the average power of an AM signal changes if the rms value of the modulating signal changes. For example, if $m(t)$ is a sine wave test tone with a peak value of 1.0 for 100% modulation,

$$m_{\text{rms}} = 1/\sqrt{2} \; .$$

Assume that $A_c = 1000$ volts and $R_L = 50$ ohms, which are typical values used in AM broadcasting. Then the averagepower dissipated into the 50 Ω load for this AM signal is

$$P_L = \frac{(1000)^2}{2(50)}\left[1 + \frac{1}{2}\right] = 15{,}000 \text{ watts} \tag{1.18}$$

The Federal Communications Commission (FCC) rated carrier power is obtained when $m(t) = 0$. In this case, (1.17) becomes $P_L = (1000)^2/100 = 10{,}000$ watts and the FCC would rate this as a 10,000 watt AM station. The sideband power for 100% sine wave modulation is 5,000 watts.

Now let the modulation on the AM signal be a binary digital signal such that $m(t) = \pm 1$ where $+1$ is used for a binary one and -1 is used for a binary 0. Referring to (1.14), this AM signal becomes an *on-off keyed* (OOK) digital signal where the signal is on when a binary one is transmitted and off when a binary zero is transmitted. For $A_c = 1000$ and $R_L = 50\ \Omega$, the average power dissipated would be 20,000 watts since $m_{\text{rms}} = 1$ for $m(t) = \pm 1$.

1.7 Phase and Frequency Modulation

Phase modulation (PM) and *frequency modulation* (FM) are special cases of angle-modulated signalling. In angle-modulated signalling the complex envelope is

$$g(t) = A_c e^{j\theta(t)} \tag{1.19}$$

Using (1.6), the resulting *angle-modulated* signal is

$$s(t) = A_c \cos[\omega_c + \theta(t)] \tag{1.20}$$

For PM the phase is directly proportional to the modulating signal:

$$\theta(t) = D_p m(t) \tag{1.21}$$

where the proportionality constant D_p is the phase sensitivity of the phase modulator, having units of radians per volt [assuming that $m(t)$ is a voltage waveform]. For FM the phase is proportional to the integral of $m(t)$:

$$\theta(t) = D_f \int_{-\infty}^{t} m(\sigma) d\sigma \tag{1.22}$$

where the frequency deviation constant D_f has units of radians/volt-second. These concepts are summarized by the PM and FM entries in Table 1.1.

By comparing the last two equations, it is seen that if we have a PM signal modulated by $m_p(t)$, there is *also* FM on the signal corresponding to a *different* modulating waveshape that is given by

$$m_f(t) = \frac{D_p}{D_f}\left[\frac{dm_p(t)}{dt}\right] \tag{1.23}$$

where the subscripts f and p denote frequency and phase, respectively. Similarly, if we have an FM signal modulated by $m_f(t)$, the corresponding phase modulation on this signal is

$$m_p(t) = \frac{D_f}{D_p} \int_{-\infty}^{t} m_f(\sigma) d\sigma \tag{1.24}$$

By using (1.24), a PM circuit may be used to synthesize an FM circuit by inserting an integrator in cascade with the phase modulator input.

Other properties of PM and FM are that the **real envelope**, $R(t) = |g(t)| = A_c$, is a constant, as seen from (1.19). Also, $g(t)$ is a *nonlinear* function of the modulation. However,

from (1.21) and (1.22), $\theta(t)$ is a linear function of the modulation, $m(t)$. Using (1.11), the average power dissipated by a PM or FM signal is the constant

$$P_L = \frac{A_c^2}{2R_L} \tag{1.25}$$

That is, the average power of a PM or FM signal does not depend on the modulating waveform, $m(t)$.

The *instantaneous frequency deviation* for an FM signal from its carrier frequency is given by the derivative of its phase $\theta(t)$. Taking the derivative of (1.22), the *peak frequency deviation* is

$$\Delta F = \frac{1}{2\pi} D_f M_p \text{ Hz} \tag{1.26}$$

where $M_p = \max[m(t)]$ is the peak value of the modulation waveform and the derivative has been divided by 2π to convert from radians/sec to Hz units.

For FM and PM signals, Carson's rule estimates the transmission bandwidth containing approximately 98% of the total power. This FM or PM signal bandwidth is

$$B_T = 2(\beta + 1)B \tag{1.27}$$

where B is bandwidth (highest frequency) of the modulation. The modulation index β, is $\beta = \Delta F/B$ for FM and $\beta = \max[D_p m(t)] = D_p M_p$ for PM.

The AMPS (Advanced Mobile Phone System) analog cellular phones use FM signalling. A peak deviation of 12 kHz is specified with a modulation bandwidth of 3 kHz. From (1.27), this gives a bandwidth of 30 kHz for the AMPS signal and allows a channel spacing of 30 kHz to be used. To accommodate more users, narrow-band AMPS (NAMPS) with a 5 kHz peak deviation is used in some areas. This allows 10 kHz channel spacing if the carrier frequencies are carefully selected to minimize interference to used adjacent channels. A maximum FM signal power of 3 watts is allowed for the AMPS phones. However, hand-held AMPS phones usually produce no more than 600 mW which is equivalent to 5.5 volts rms across the 50 Ω antenna terminals.

The GSM (Group Special Mobile) digital cellular phones use FM with *minimum frequency-shift-keying* (MSK) where the peak frequency deviation is selected to produce orthogonal waveforms for binary one and binary zero data. (Digital phones use a speech codec to convert the analog voice source to a digital data source for transmission over the system.) Orthogonality occurs when $\Delta F = 1/4R$ where R is the bit rate (bits/sec) [1]. Actually, GSM uses Gaussian shaped MSK (GMSK). That is, the digital data waveform (with rectangular binary one and binary zero pulses) is first filtered by a low-pass filter having a Gaussian shaped frequency response (to attenuate the higher frequencies). This Gaussian filtered data waveform is then fed into the frequency modulator to generate the GMSK signal. This produces a digitally modulated FM signal with a relatively small bandwidth.

Other digital cellular standards use QPSK signalling as discussed in the next section.

1.8 QPSK Signalling

Quadrature phase-shift-keying (QPSK) is a special case of quadrature modulation as shown in Table 1.1 where $m_1(t) = \pm 1$ and $m_2(t) = \pm 1$ are two binary bit streams. The complex envelope for QPSK is

$$g(t) = x(t) + jy(t) = A_c\left[m_1(t) + jm_2(t)\right]$$

where $x(t) = \pm A_c$ and $y(t) = \pm A_c$. The permitted values for the complex envelope are illustrated by the QPSK **signal constellation** shown in Fig. 1.5a. The *signal constellation* is a plot of the permitted values for the complex envelope, $g(t)$. QPSK may be generated by using the quadrature generation technique of Fig. 1.3 where the baseband signal processor is a serial-to-parallel converter that reads in two bits of data at a time from the serial binary input stream, $m(t)$ and outputs the first of the two bits to $x(t)$ and the second bit to $y(t)$. If the two input bits are both binary ones, (11), then $m_1(t) = +A_c$ and $m_2(t) = +A_c$. This is represented by the top right-hand dot for $g(t)$ in the signal constellation for QPSK signalling in Fig. 1.5a. Likewise, the three other possible two-bit words, (10), (01), and (00), are also shown. The QPSK signal is also equivalent to a four-phase phase-shift-keyed signal (4PSK) since all the points in the signal constellation fall on a circle where the permitted phases are $\theta(t) = 45°$, 135°, 225°, and 315°. There is no amplitude modulation on the QPSK signal since the distances from the origin to all the signal points on the signal constellation are equal.

For QPSK, the spectrum of $g(t)$ is of the $\sin x/x$ type since $x(t)$ and $y(t)$ consists of rectangular data pulses of value $\pm A_c$. Moreover, it can be shown that for equally likely independent binary one and binary zero data, the power spectral density of $g(t)$ for digitally modulated signals with M point signal constellations is [1]

$$\mathcal{P}_g(f) = K\left(\frac{\sin \pi f \ell T_b}{\pi f \ell T_b}\right)^2 \tag{1.28}$$

where K is a constant, $R = 1/T_b$ is the data rate (bits/sec) of $m(t)$ and $M = 2^\ell$. M is the number of points in the signal constellation. For QPSK, $M = 4$ and $\ell = 2$. This PSD for the complex envelope, $\mathcal{P}_g(f)$, is plotted in Fig. 1.6. The PSD for the QPSK signal ($\ell = 2$) is given by translating $\mathcal{P}_g(f)$ up to the carrier frequency as indicated by (1.9).

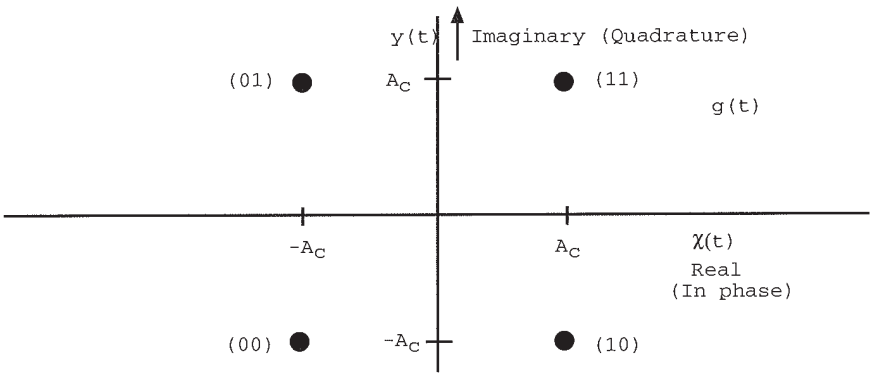
Referring to Fig. 1.6 or using (1.28), the first-null bandwidth of $g(t)$ is R/ℓ Hz. Consequently, the null-to-null bandwidth of the modulated RF signal is

$$B_{\text{null}} = \frac{2R}{\ell} \text{ Hz} \tag{1.29}$$

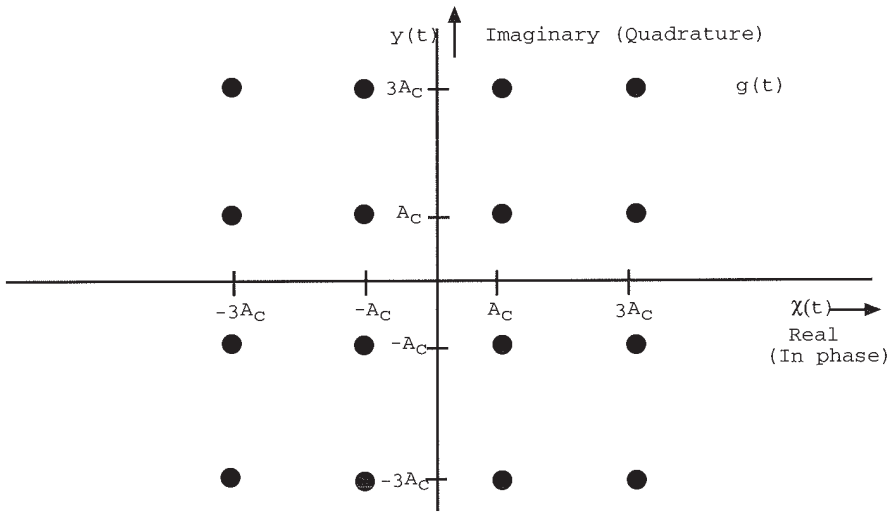
For example, if the data rate of the baseband information source is 9600 bits/sec, then the null-to-null bandwidth of the QPSK signal would be 9.6 Hz since $\ell = 2$.

Referring to Fig. 1.6, it is seen that the sidelobes of the spectrum are relatively large so, in practice, the sidelobes of the spectrum are filtered off to prevent interference to the adjacent channels. This filtering rounds off the edges of the rectangular data pulses and this causes some amplitude modulation on the QPSK signal. That is, the points in the signal constellation for the filtered QPSK signal would be fuzzy since the transition from one constellation point to another point is not instantaneous because the filtered data pulses are not rectangular. QPSK is the modulation used for digital cellular phones with the IS-95 Code Division Multiple Access (CDMA) standard.

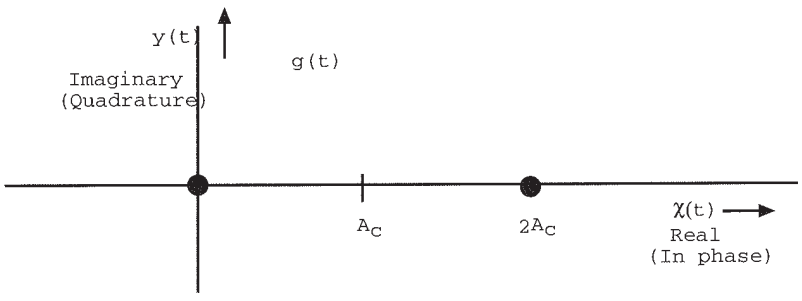
Equation (1.28) and Fig. 1.6 also represent the spectrum for *quadrature modulation amplitude modulation* (QAM) signalling. QAM signalling allows more than two values for $x(t)$ and $y(t)$. For example QAM where $M = 16$ has 16 points in the signal constellation with 4 values for $x(t)$ and 4 values for $y(t)$ such as, for example, $x(t) = +A_c$, $-A_c$, $+3A_c$, $-3A_c$ and $y(t) = +A_c$, $-A_c$, $+3A_c$, $-3A_c$. This is shown in Fig. 1.5b. Each point in the $M = 16$ QAM signal constellation would represent a unique four-bit data word, as compared with the $M = 4$ QPSK signal constellation shown in Fig. 1.5a where each point represents a unique two-bit data word. For a $R = 9600$ bits/sec information source data rate, a $M = 16$ QAM signal would have a null-to-null bandwidth of 4.8 kHz since $\ell = 4$.



(a) QPSK Signal Constellation



(b) 16 QAM Signal Constellation



(c) OOK Signal Constellation

FIGURE 1.5 Signal constellations (permitted values of the complex envelope).

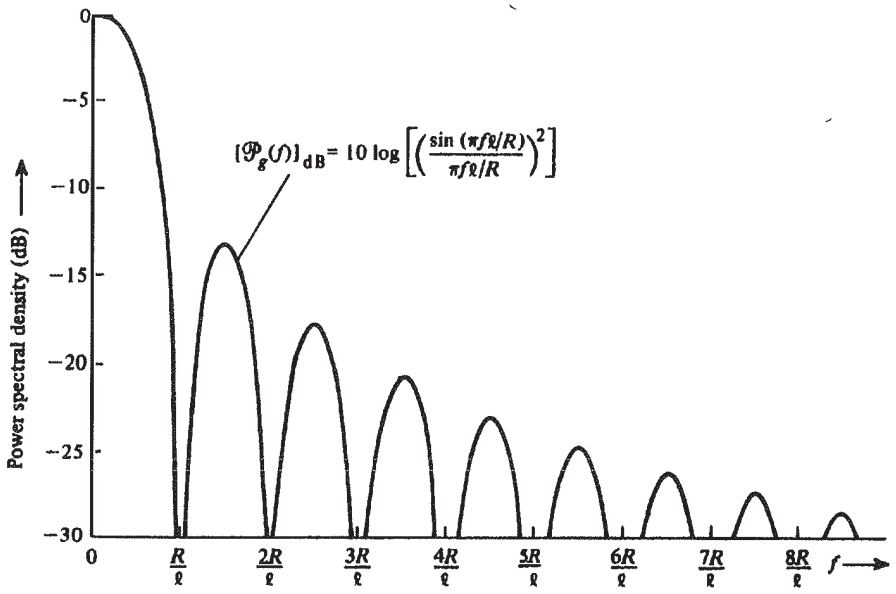


FIGURE 1.6 PSD for the complex envelope of MPSK and QAM where $M = 2^\ell$ and R is bit rate (positive frequencies shown). *Source:* Couch, L.W., II. 1997. *Digital and Analog Communication Systems,* 5th ed., Prentice Hall, Upper Saddle River, NJ, p. 350. With permission.

For OOK signalling as described at the end of Section 1.6, the signal constellation would consist of $M = 2$ points along the x axis where $x = 0, 2A_c$ and $y = 0$. This is illustrated in Fig. 1.5c. For a $R = 9600$ bit/sec information source data rate, an OOK signal would have a null-to-null bandwidth of 19.2 kHz since $\ell = 1$.

Defining Terms

Bandpass waveform: The spectrum of the waveform is nonzero for frequencies in some band concentrated about a frequency $f_c \gg 0$; f_c is called the carrier frequency.

Baseband waveform: The spectrum of the waveform is nonzero for frequencies near $f = 0$.

Complex envelope: The function $g(t)$ of a bandpass waveform $v(t)$ where the bandpass waveform is described by

$$v(t) = Re\left\{g(t)e^{j\omega_c t}\right\}$$

Fourier transform: If $w(t)$ is a waveform, then the Fourier transform of $w(t)$ is

$$W(f) = \Im[w(t)] = \int_{-\infty}^{\infty} w(t)e^{-j2\pi ft}dt$$

where f has units of hertz.

Modulated signal: The bandpass signal

$$s(t) = Re\left\{g(t)e^{j\omega_c t}\right\}$$

where fluctuations of $g(t)$ are caused by the information source such as audio, video, or data.

Modulation: The information source, $m(t)$, that causes fluctuations in a bandpass signal.

Real envelope: The function $R(t) = |g(t)|$ of a bandpass waveform $v(t)$ where the bandpass waveform is described by

$$v(t) = Re\left\{g(t)e^{j\omega_c t}\right\}$$

Signal constellation: The permitted values of the complex envelope for a digital modulating source.

References

[1] Couch, L.W., II, *Digital and Analog Communication Systems,* 5th ed., Prentice Hall, Upper Saddle River, NJ, 1997.

Further Information

[1] Bedrosian, E., The analytic signal representation of modulated waveforms. *Proc. IRE,* vol. 50, October, 2071–2076, 1962.

[2] Couch, L.W., II, *Modern Communication Systems: Principles and Applications,* Macmillan Publishing, New York, (now Prentice Hall, Upper Saddle River, NJ), 1995.

[3] Dugundji, J., Envelopes and pre-envelopes of real waveforms. *IRE Trans. Information Theory,* vol. IT-4, March, 53–57, 1958.

[4] Voelcker, H.B., Toward the unified theory of modulation—Part I: Phase-envelope relationships. *Proc. IRE,* vol.54, March, 340–353, 1966.

[5] Voelcker, H.B., Toward the unified theory of modulation—Part II: Zero manipulation. *Proc. IRE,* vol. 54, May, 735–755, 1966.

[6] Ziemer, R.E. and Tranter, W.H., *Principles of Communications,* 4th ed., John Wiley and Sons, New York, 1995.

2

Sampling

2.1 Introduction 2-1
2.2 Instantaneous Sampling 2-1
Ideal Sampled Signal • Band-Limited Signals
2.3 Sampling Theorem 2-3
2.4 Sampling of Sinusoidal Signals 2-4
2.5 Sampling of Bandpass Signals 2-4
2.6 Practical Sampling 2-6
Natural Sampling • Flat-Top Sampling
2.7 Sampling Theorem in the Frequency Domain 2-9
2.8 Summary and Discussion 2-9
Defining Terms 2-10
References 2-10
Further Information 2-10

Hwei P. Hsu
Fairleigh Dickinson University

2.1 Introduction

To transmit analog message signals, such as speech signals or video signals, by digital means, the signal has to be converted into digital form. This process is known as analog-to-digital conversion. The sampling process is the first process performed in this conversion, and it converts a continuous-time signal into a discrete-time signal or a sequence of numbers. Digital transmission of analog signals is possible by virtue of the sampling theorem, and the sampling operation is performed in accordance with the sampling theorem.

In this chapter, using the Fourier transform technique, we present this remarkable sampling theorem and discuss the operation of sampling and practical aspects of sampling.

2.2 Instantaneous Sampling

Suppose we sample an arbitrary analog signal $m(t)$ shown in Fig. 2.1(a) instantaneously at a uniform rate, once every T_s seconds. As a result of this sampling process, we obtain an infinite sequence of samples $\{m(nT_s)\}$, where n takes on all possible integers. This form of sampling is called *instantaneous sampling.* We refer to T_s as the **sampling interval,** and its reciprocal $1/T_s = f_s$ as the **sampling rate.** Sampling rate (samples per second) is often cited in terms of sampling frequency expressed in hertz.

0-8493-8597-0/99/$0.00+$.50

© 1999 by CRC Press LLC

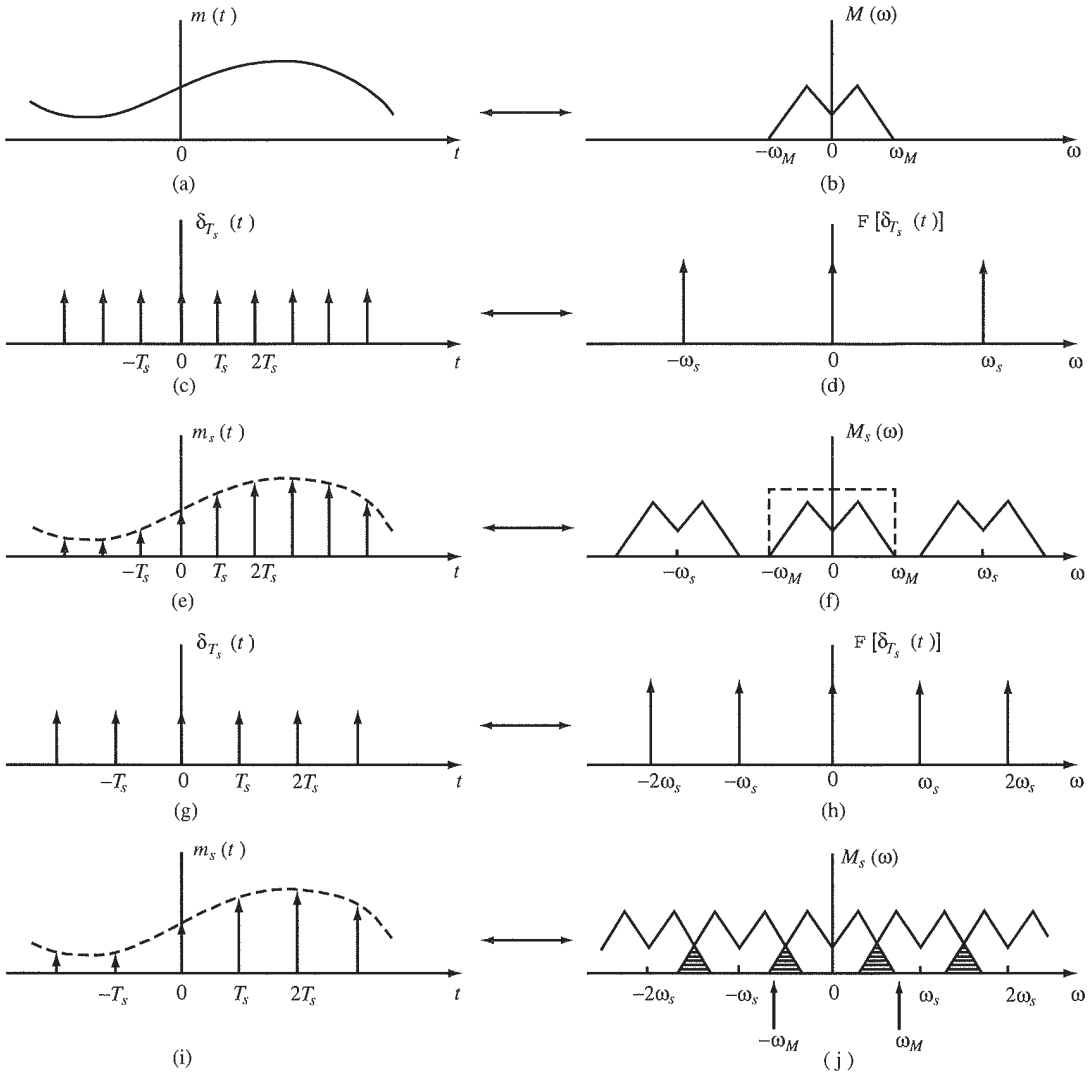


FIGURE 2.1 Illustration of instantaneous sampling and sampling theorem.

2.2.1 Ideal Sampled Signal

Let $m_s(t)$ be obtained by multiplication of $m(t)$ by the unit impulse train $\delta_T(t)$ with period T_s [Fig. 2.1(c)], that is,

$$\begin{aligned} m_s(t) &= m(t)\delta_{T_s}(t) = m(t)\sum_{n=-\infty}^{\infty}\delta(t-nT_s) \\ &= \sum_{n=-\infty}^{\infty} m(t)\delta(t-nT_s) = \sum_{n=-\infty}^{\infty} m(nT_s)\,\delta(t-nT_s) \end{aligned} \tag{2.1}$$

where we used the property of the δ function, $m(t)\delta(t-t_0) = m(t_0)\delta(t-t_0)$. The signal $m_s(t)$ [Fig. 2.1(e)] is referred to as the **ideal sampled signal.**

2.2.2 Band-Limited Signals

A real-valued signal $m(t)$ is called a **band-limited signal** if its Fourier transform $M(\omega)$ satisfies the condition

$$M(\omega) = 0 \qquad \text{for } |\omega| > \omega_M \tag{2.2}$$

where $\omega_M = 2\pi f_M$ [Fig. 2.1(b)]. A band-limited signal specified by Eq. (2.2) is often referred to as a *low-pass signal.*

2.3 Sampling Theorem

The sampling theorem states that a band-limited signal $m(t)$ specified by Eq. (2.2) can be uniquely determined from its values $m(nT_s)$ sampled at uniform interval T_s if $T_s \leq \pi/\omega_M = 1/(2f_M)$. In fact, when $T_s = \pi/\omega_M, m(t)$ is given by

$$m(t) = \sum_{n=-\infty}^{\infty} m(nT_s) \frac{\sin \omega_M (t - nT_s)}{\omega_M (t - nT_s)} \tag{2.3}$$

which is known as the **Nyquist–Shannon interpolation formula** and it is also sometimes called the *cardinal series.* The sampling interval $T_s = 1/(2f_M)$is called the *Nyquist interval* and the minimum rate $f_s = 1/T_s = 2f_M$ is known as the **Nyquist rate.**

Illustration of the instantaneous sampling process and the sampling theorem is shown in Fig. 2.1. The Fourier transform of the unit impulse train is given by [Fig. 2.1(d)]

$$\mathcal{F}\{\delta_{T_s}(t)\} = \omega_s \sum_{n=-\infty}^{\infty} \delta(\omega - n\omega_s) \qquad \omega_s = 2\pi/T_s \tag{2.4}$$

Then, by the convolution property of the Fourier transform, the Fourier transform $M_s(\omega)$ of the ideal sampled signal $m_s(t)$ is given by

$$\begin{aligned} M_s(\omega) &= \frac{1}{2\pi}\left[M(\omega) * \omega_s \sum_{n=-\infty}^{\infty} \delta(\omega - n\omega_s)\right] \\ &= \frac{1}{T_s} \sum_{n=-\infty}^{\infty} M(\omega - n\omega_s) \end{aligned} \tag{2.5}$$

where $*$ denotes convolution and we used the convolution property of the δ-function $M(\omega) * \delta(\omega - \omega_0) = M(\omega - \omega_0)$. Thus, the sampling has produced images of $M(\omega)$ along the frequency axis. Note that $M_s(\omega)$ will repeat periodically without overlap as long as $\omega_s \geq 2\omega_M$ or $f_s \geq 2f_M$ [Fig. 2.1(f)]. It is clear from Fig. 2.1(f) that we can recover $M(\omega)$ and, hence, $m(t)$ by passing the sampled signal $m_s(t)$ through an ideal low-pass filter having frequency response

$$H(\omega) = \begin{cases} T_s, & |\omega| \leq \omega_M \\ 0, & \text{otherwise} \end{cases} \tag{2.6}$$

where $\omega_M = \pi/T_s$. Then

$$M(\omega) = M_s(\omega)H(\omega) \tag{2.7}$$

Taking the inverse Fourier transform of Eq. (2.6), we obtain the impulse response $h(t)$ of the ideal low-pass filter as

$$h(t) = \frac{\sin \omega_M t}{\omega_M t} \tag{2.8}$$

Taking the inverse Fourier transform of Eq. (2.7), we obtain

$$\begin{aligned} m(t) &= m_s(t) * h(t) \\ &= \sum_{n=-\infty}^{\infty} m(nT_s)\,\delta(t-nT_s) * \frac{\sin \omega_M t}{\omega_M t} \\ &= \sum_{n=-\infty}^{\infty} m(nT_s)\,\frac{\sin \omega_M (t-nT_s)}{\omega_M (t-nT_s)} \end{aligned} \tag{2.9}$$

which is Eq. (2.3).

The situation shown in Fig. 2.1(j) corresponds to the case where $f_s < 2f_M$. In this case there is an overlap between $M(\omega)$ and $M(\omega - \omega_M)$. This overlap of the spectra is known as *aliasing* or *foldover*. When this aliasing occurs, the signal is distorted and it is impossible to recover the original signal $m(t)$ from the sampled signal. To avoid aliasing, in practice, the signal is sampled at a rate slightly higher than the Nyquist rate. If $f_s > 2f_M$, then as shown in Fig. 2.1(f), there is a gap between the upper limit ω_M of $M(\omega)$ and the lower limit $\omega_s - \omega_M$ of $M(\omega - \omega_s)$. This range from ω_M to $\omega_s - \omega_M$ is called a *guard band.* As an example, speech transmitted via telephone is generally limited to $f_M = 3.3$ kHz (by passing the sampled signal through a low-pass filter). The Nyquist rate is, thus, 6.6 kHz. For digital transmission, the speech is normally sampled at the rate $f_s = 8$ kHz. The guard band is then $f_s - 2f_M = 1.4$ kHz. The use of a sampling rate higher than the Nyquist rate also has the desirable effect of making it somewhat easier to design the low-pass reconstruction filter so as to recover the original signal from the sampled signal.

2.4 Sampling of Sinusoidal Signals

A special case is the sampling of a sinusoidal signal having the frequency f_M. In this case we require that $f_s > 2f_M$ rather that $f_s \geq 2f_M$. To see that this condition is necessary, let $f_s = 2f_M$. Now, if an initial sample is taken at the instant the sinusoidal signal is zero, then all successive samples will also be zero. This situation is avoided by requiring $f_s > 2f_M$.

2.5 Sampling of Bandpass Signals

A real-valued signal $m(t)$ is called a **bandpass signal** if its Fourier transform $M(\omega)$ satisfies the condition

$$M(\omega) = 0 \quad \text{except for} \quad \begin{cases} \omega_1 < \omega < \omega_2 \\ -\omega_2 < \omega < -\omega_1 \end{cases} \tag{2.10}$$

where $\omega_1 = 2\pi f_1$ and $\omega_2 = 2\pi f_2$ [Fig. 2.2(a)].

The sampling theorem for a band-limited signal has shown that a sampling rate of $2f_2$ or greater is adequate for a low-pass signal having the highest frequency f_2. Therefore, treating $m(t)$ specified by Eq. (2.10) as a special case of such a low-pass signal, we conclude that a sampling rate of $2f_2$ is adequate for the sampling of the bandpass signal $m(t)$. But it is not necessary to sample this fast. The minimum allowable sampling rate depends on f_1, f_2, and the bandwidth $f_B = f_2 - f_1$.

Let us consider the direct sampling of the bandpass signal specified by Eq. (2.10). The spectrum of the sampled signal is periodic with the period $\omega_s = 2\pi f_s$, where f_s is the sampling frequency, as in Eq. (2.4). Shown in Fig. 2.2(b) are the two right shifted spectra of the negative side spectrum $M_-(\omega)$. If the recovering of the bandpass signal is achieved by

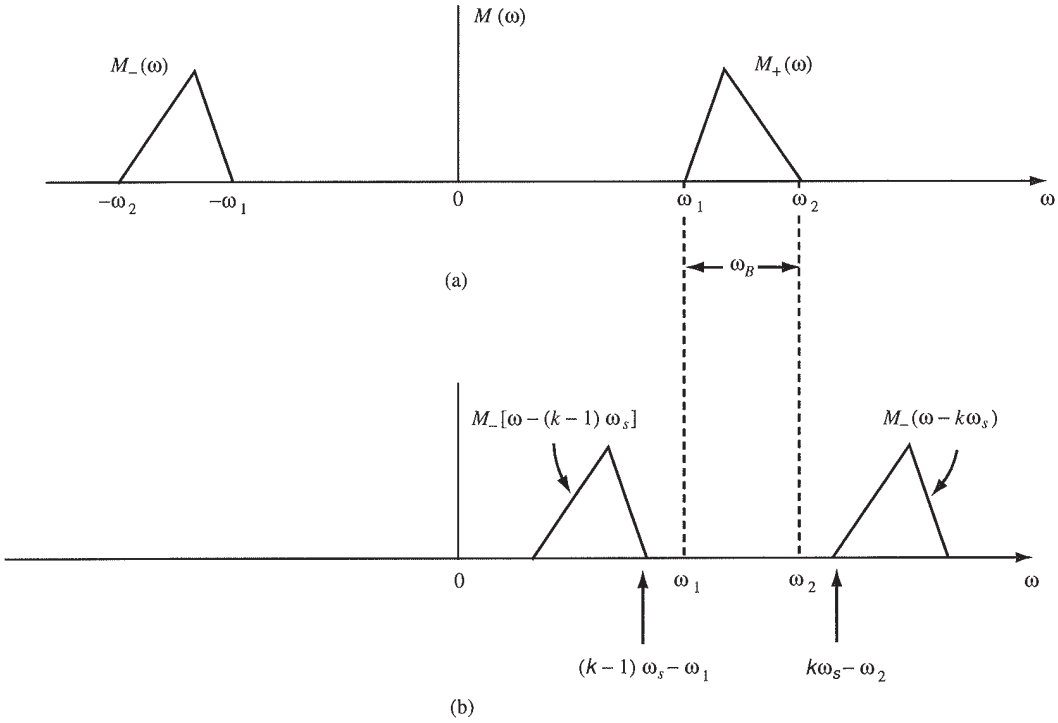


FIGURE 2.2 (a) Spectrum of a bandpass signal; (b) Shifted spectra of $M_{-}(\omega)$.

passing the sampled signal through an ideal bandpass filter covering the frequency bands $(-\omega_2, -\omega_1)$ and (ω_1, ω_2), it is necessary that there be no aliasing problem. From Fig. 2.2(b), it is clear that to avoid overlap it is necessary that

$$\omega_s \geq 2(\omega_2 - \omega_1) \tag{2.11}$$

$$(k-1)\omega_s - \omega_1 \leq \omega_1 \tag{2.12}$$

and

$$k\omega_s - \omega_2 \geq \omega_2 \tag{2.13}$$

where $\omega_1 = 2\pi f_1$, $\omega_2 = 2\pi f_2$, and k is an integer $(k = 1, 2, \ldots)$. Since $f_1 = f_2 - f_B$, these constraints can be expressed as

$$1 \leq k \leq \frac{f_2}{f_B} \leq \frac{k}{2}\frac{f_s}{f_B} \tag{2.14}$$

and

$$\frac{k-1}{2}\frac{f_s}{f_B} \leq \frac{f_2}{f_B} - 1 \tag{2.15}$$

A graphical description of Eqs. (2.14) and (2.15) is illustrated in Fig. 2.3. The unshaded regions represent where the constraints are satisfied, whereas the shaded regions represent the regions where the constraints are not satisfied and overlap will occur. The solid line in Fig. 2.3 shows the locus of the minimum sampling rate. The minimum sampling rate is given by

$$\min\{f_s\} = \frac{2f_2}{m} \tag{2.16}$$

where m is the largest integer not exceeding f_2/f_B. Note that if the ratio f_2/f_B is an integer, then the minimum sampling rate is $2f_B$. As an example, consider a bandpass signal with $f_1 = 1.5$ kHz and $f_2 = 2.5$ kHz. Here $f_B = f_2 - f_1 = 1$ kHz, and $f_2/f_B = 2.5$. Then from Eq. (2.16) and Fig. 2.3 we see that the minimum sampling rate is $2f_2/2 = f_2 = 2.5$ kHz, and allowable ranges of sampling rate are 2.5 kHz $\leq f_s \leq 3$ kHz and $f_s \geq 5$ kHz $(= 2f_2)$.

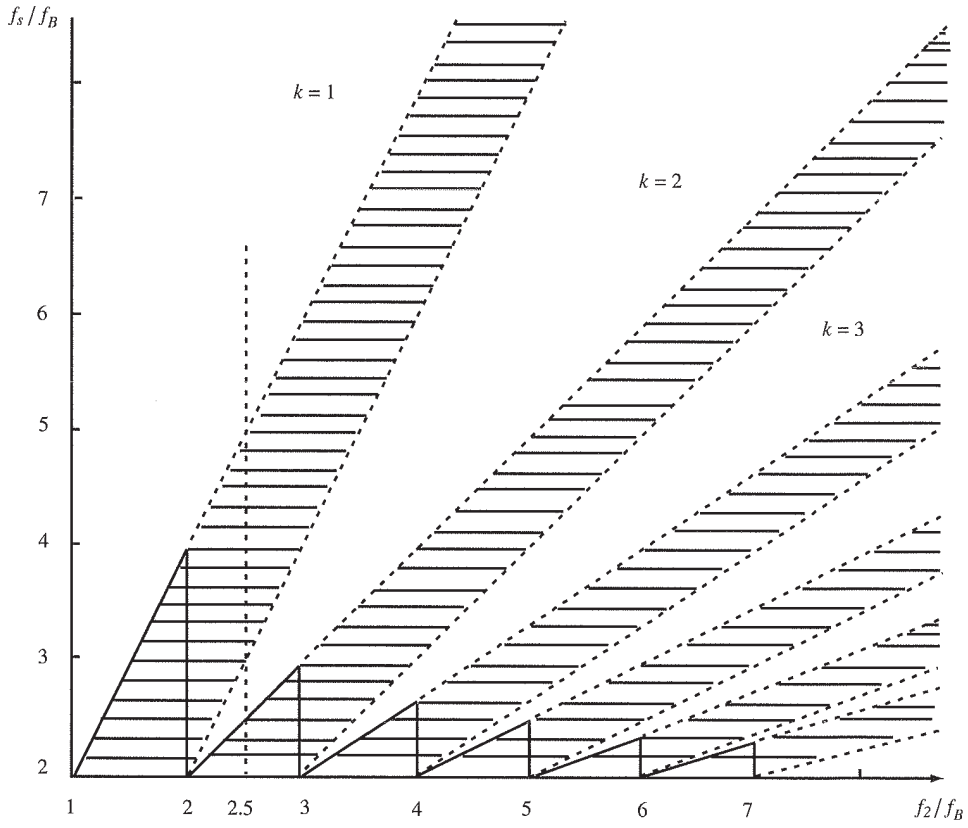


FIGURE 2.3 Minimum and permissible sampling rates for a bandpass signal.

2.6 Practical Sampling

In practice, the sampling of an analog signal is performed by means of high-speed switching circuits, and the sampling process takes the form of *natural sampling* or **flat-top sampling.**

2.6.1 Natural Sampling

Natural sampling of a band-limited signal $m(t)$ is shown in Fig. 2.4. The sampled signal $m_{\text{ns}}(t)$ can be expressed as

$$m_{\text{ns}}(t) = m(t)x_p(t) \tag{2.17}$$

where $x_p(t)$ is the periodic train of rectangular pulses with fundamental period T_s, and each rectangular pulse in $x_p(t)$ has duration d and unit amplitude [Fig. 2.4(b)]. Observe that the sampled signal $m_{\rm ns}(t)$ consists of a sequence of pulses of varying amplitude whose tops follow the waveform of the signal $m(t)$ [Fig. 2.4(c)].

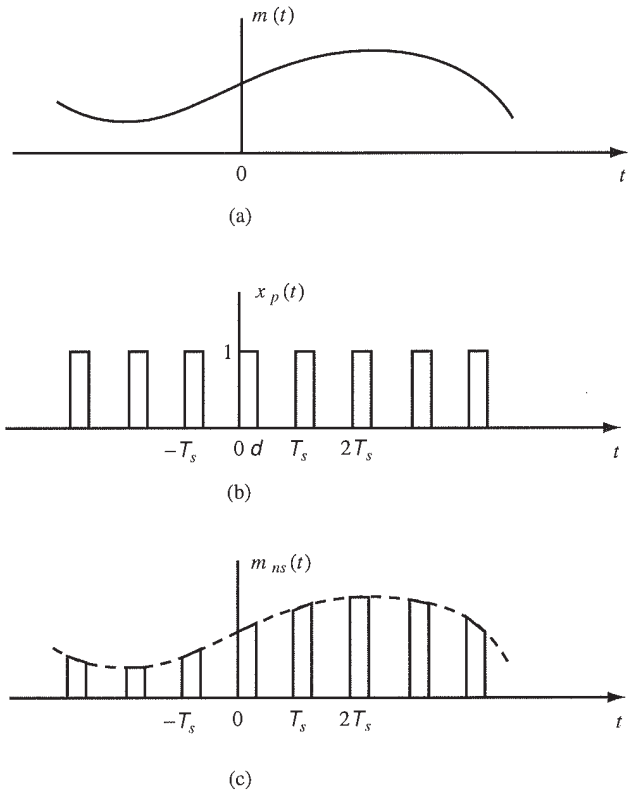


FIGURE 2.4 Natural sampling.

The Fourier transform of $x_p(t)$ is

$$X_p(\omega) = \sum_{n=-\infty}^{\infty} c_n \delta(\omega - n\omega_s) \qquad \omega_s = 2\pi/T_s \tag{2.18}$$

where

$$c_n = \frac{d}{T_s} \frac{\sin(n\omega_s d/2)}{n\omega_s d/2} e^{-jn\omega_s d/2} \tag{2.19}$$

Then the Fourier transform of $m_{\rm ns}(t)$ is given by

$$M_{\rm ns}(\omega) = M(\omega) * X_p(\omega) = \sum_{n=-\infty}^{\infty} c_n M(\omega - n\omega_s) \tag{2.20}$$

from which we see that the effect of the natural sampling is to multiply the nth shifted spectrum $M(\omega - n\omega_s)$ by a constant c_n. Thus, the original signal $m(t)$ can be reconstructed from $m_{\rm ns}(t)$ with no distortion by passing $m_{\rm ns}(t)$ through an ideal low-pass filter if the sampling rate f_s is equal to or greater than the Nyquist rate $2f_M$.

2.6.2 Flat-Top Sampling

The sampled waveform, produced by practical sampling devices that are the sample and hold types, has the form [Fig. 2.5(c)]

$$m_{\text{fs}}(t) = \sum_{n=-\infty}^{\infty} m(nT_s)\, p(t - nT_s) \tag{2.21}$$

where $p(t)$ is a rectangular pulse of duration d with unit amplitude [Fig. 2.5(a)]. This type of sampling is known as **flat-top sampling.** Using the ideal sampled signal $m_s(t)$ of Eq. (2.1), $m_{\text{fs}}(t)$ can be expressed as

$$m_{\text{fs}}(t) = p(t) * \left[\sum_{n=-\infty}^{\infty} m(nT_s)\, \delta(t - nT_s) \right] = p(t) * m_s(t) \tag{2.22}$$

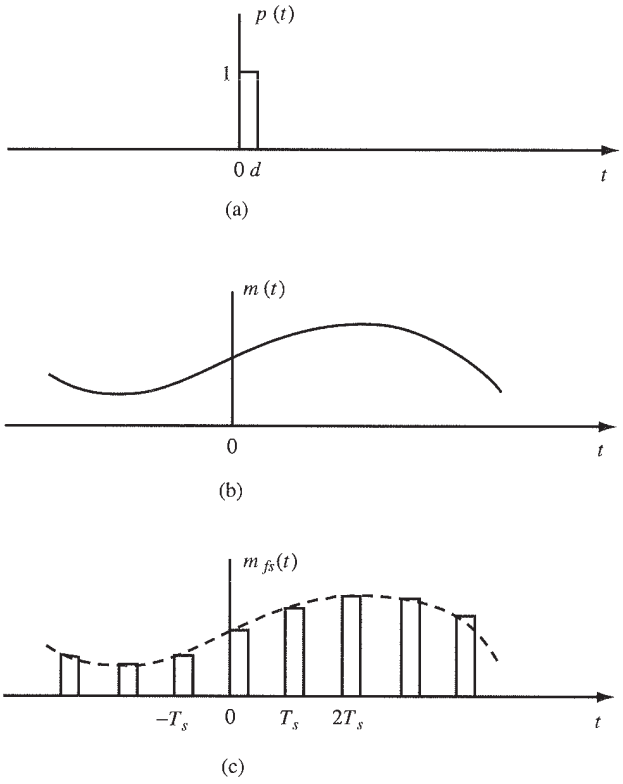


FIGURE 2.5 Flat-top sampling.

Using the convolution property of the Fourier transform and Eq. (2.4), the Fourier transform of $m_{\text{fs}}(t)$ is given by

$$M_{\text{fs}}(\omega) = P(\omega)M_s(\omega) = \frac{1}{T_s} \sum_{n=-\infty}^{\infty} P(\omega)M(\omega - n\omega_s) \tag{2.23}$$

where

$$P(\omega) = d\frac{\sin(\omega d/2)}{\omega d/2}e^{-j\omega d/2} \tag{2.24}$$

From Eq.(2.23) we see that by using flat-top sampling we have introduced amplitude distortion and time delay, and the primary effect is an attenuation of high-frequency components. This effect is known as the *aperture effect.* The aperture effect can be compensated by an equalizing filter with a frequency response $H_{\text{eq}}(\omega) = 1/P(\omega)$. If the pulse duration d is chosen such that $d \ll T_s$, however, then $P(\omega)$ is essentially constant over the baseband and no equalization may be needed.

2.7 Sampling Theorem in the Frequency Domain

The sampling theorem expressed in Eq. (2.4) is the time-domain sampling theorem. There is a dual to this time-domain sampling theorem, i.e., the sampling theorem in the frequency domain.

Time-limited signals: A continuous-time signal $m(t)$ is called **time limited** if

$$m(t) = 0 \qquad \text{for} \quad |t| > |T_0| \tag{2.25}$$

Frequency-domain sampling theorem: The frequency-domain sampling theorem states that the Fourier transform $M(\omega)$ of a time-limited signal $m(t)$ specified by Eq. (2.25) can be uniquely determined from its values $M(n\omega_s)$ sampled at a uniform rate ω_s if $\omega_s \leq \pi/T_0$. In fact, when $\omega_s = \pi/T_0$, then $M(\omega)$ is given by

$$M(\omega) = \sum_{n=-\infty}^{\infty} M(n\omega_s)\frac{\sin T_0(\omega - n\omega_s)}{T_0(\omega - n\omega_s)} \tag{2.26}$$

2.8 Summary and Discussion

The sampling theorem is the fundamental principle of digital communications. We state the sampling theorem in two parts.

THEOREM 2.1 *If the signal contains no frequency higher than f_M* Hz, *it is completely described by specifying its samples taken at instants of time spaced $1/2f_M$* s.

THEOREM 2.2 *The signal can be completely recovered from its samples taken at the rate of $2f_M$ samples per second or higher.*

The preceding sampling theorem assumes that the signal is strictly band limited. It is known that if a signal is band limited it cannot be time limited and vice versa. In many practical applications, the signal to be sampled is time limited and, consequently, it cannot be strictly band limited. Nevertheless, we know that the frequency components of physically occurring signals attenuate rapidly beyond some defined bandwidth, and for practical purposes we consider these signals are band limited. This approximation of real signals by band limited ones introduces no significant error in the application of the sampling theorem. When such a signal is sampled, we band limit the signal by filtering before sampling and sample at a rate slightly higher than the nominal Nyquist rate.

Defining Terms

Band-limited signal: A signal whose frequency content (Fourier transform) is equal to zero above some specified frequency.

Bandpass signal: A signal whose frequency content (Fourier transform) is nonzero only in a band of frequencies not including the origin.

Flat-top sampling: Sampling with finite width pulses that maintain a constant value for a time period less than or equal to the sampling interval. The constant value is the amplitude of the signal at the desired sampling instant.

Ideal sampled signal: A signal sampled using an ideal impulse train.

Nyquist rate: The minimum allowable sampling rate of $2f_M$ samples per second, to reconstruct a signal band limited to f_M hertz.

Nyquist-Shannon interpolation formula: The infinite series representing a time domain waveform in terms of its ideal samples taken at uniform intervals.

Sampling interval: The time between samples in uniform sampling.

Sampling rate: The number of samples taken per second (expressed in Hertz and equal to the reciprocal of the sampling interval).

Time-limited: A signal that is zero outside of some specified time interval.

References

[1] Brown, J.L. Jr., First order sampling of bandpass signals—A new approach. *IEEE Trans. Information Theory,* IT-26(5), 613–615, 1980.

[2] Byrne, C.L. and Fitzgerald, R.M., Time-limited sampling theorem for band-limited signals, *IEEE Trans. Information Theory,* IT-28(5), 807–809, 1982.

[3] Hsu, H.P., *Applied Fourier Analysis,* Harcourt Brace Jovanovich, San Diego, CA, 1984.

[4] Hsu, H.P., *Analog and Digital Communications,* McGraw-Hill, New York, 1993.

[5] Hulthén, R., Restoring causal signals by analytical continuation: A generalized sampling theorem for causal signals. *IEEE Trans. Acoustics, Speech, and Signal Processing,* ASSP-31(5), 1294–1298, 1983.

[6] Jerri, A.J., The Shannon sampling theorem—Its various extensions and applications: A tutorial review, *Proc. IEEE.* 65(11), 1565–1596, 1977.

Further Information

For a tutorial review of the sampling theorem, historical notes, and earlier references see Jerri [6].

3

Pulse Code Modulation[1]

3.1 Introduction 3-1
3.2 Generation of PCM 3-2
3.3 Percent Quantizing Noise 3-3
3.4 Practical PCM Circuits 3-4
3.5 Bandwidth of PCM 3-6
3.6 Effects of Noise 3-6
3.7 Nonuniform Quantizing: μ-Law and A-Law Companding 3-9
3.8 Example: Design of a PCM System 3-11
Defining Terms 3-12
References 3-12
Further Information 3-13

Leon W. Couch, II
University of Florida

3.1 Introduction

Pulse code modulation (PCM) is analog-to-digital conversion of a special type where the information contained in the instantaneous samples of an analog signal is represented by digital words in a serial bit stream.

If we assume that each of the digital words has n binary digits, there are $M = 2^n$ unique code words that are possible, each code word corresponding to a certain amplitude level. Each sample value from the analog signal, however, can be any one of an infinite number of levels, so that the digital word that represents the amplitude closest to the actual sampled value is used. This is called **quantizing**. That is, instead of using the exact sample value of the analog waveform, the sample is replaced by the closest allowed value, where there are M allowed values, and each allowed value corresponds to one of the code words.

PCM is very popular because of the many advantages it offers. Some of these advantages are as follows.

- Relatively inexpensive digital circuitry may be used extensively in the system.
- PCM signals derived from all types of analog sources (audio, video, etc.) may be time-division multiplexed with data signals (e.g., from digital computers) and transmitted over a common high-speed digital communication system.

[1] *Source:* Leon W. Couch, II. 1997. *Digital and Analog Communication Systems,* 5th ed., Prentice Hall, Upper Saddle River, NJ. With permission.

0-8493-8597-0/99/$0.00+$.50

© 1999 by CRC Press LLC

- In long-distance digital telephone systems requiring repeaters, a *clean* PCM waveform can be regenerated at the output of each repeater, where the input consists of a noisy PCM waveform. The noise at the input, however, may cause bit errors in the regenerated PCM output signal.
- The noise performance of a digital system can be superior to that of an analog system. In addition, the probability of error for the system output can be reduced even further by the use of appropriate coding techniques.

These advantages usually outweigh the main disadvantage of PCM: a much wider bandwidth than that of the corresponding analog signal.

3.2 Generation of PCM

The PCM signal is generated by carrying out three basic operations: sampling, quantizing, and encoding (see Fig. 3.1). The sampling operation generates an instantaneously-sampled flat-top **pulse-amplitude modulated** (PAM) signal.

The quantizing operation is illustrated in Fig. 3.2 for the $M = 8$ level case. This quantizer is said to be *uniform* since all of the steps are of equal size. Since we are approximating the analog sample values by using a finite number of levels ($M = 8$ in this illustration), *error* is introduced into the recovered output analog signal because of the quantizing effect. The error waveform is illustrated in Fig. 3.2c. The quantizing error consists of the difference between the analog signal at the sampler input and the output of the quantizer. Note that the peak value of the error (± 1) is one-half of the quantizer step size (2). If we sample at the Nyquist rate ($2B$, where B is the absolute bandwidth, in hertz, of the input analog signal) or faster and there is negligible channel noise, there will still be noise, called *quantizing noise,* on the recovered analog waveform due to this error. The quantizing noise can also be thought of as a round-off error. The quantizer output is a *quantized* (i.e., only M possible amplitude values) PAM signal.

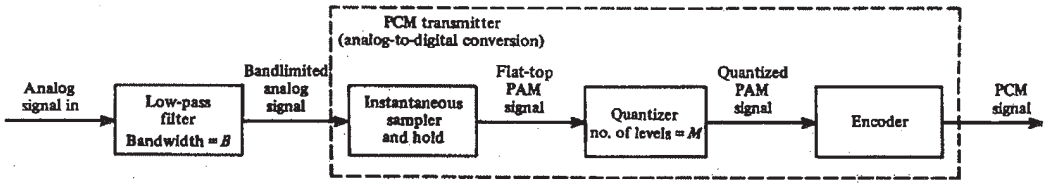


FIGURE 3.1 A PCM transmitter. *Source:* Couch, L.W. II 1997. *Digital and Analog Communication Systems,* 5th ed., Prentice Hall, Upper Saddle River, NJ, p. 138. With permission.

The PCM signal is obtained from the quantized PAM signal by encoding each quantized sample value into a digital word. It is up to the system designer to specify the exact code word that will represent a particular quantized level. If a Gray code of Table 3.1 is used, the resulting PCM signal is shown in Fig. 3.2d where the PCM word for each quantized sample is strobed out of the encoder by the next clock pulse. The Gray code was chosen because it has only 1-b change for each step change in the quantized level. Consequently, single errors in the received PCM code word will cause minimum errors in the recovered analog level, provided that the sign bit is not in error.

Here we have described PCM systems that represent the quantized analog sample values by *binary* code words. Of course, it is possible to represent the quantized analog samples by

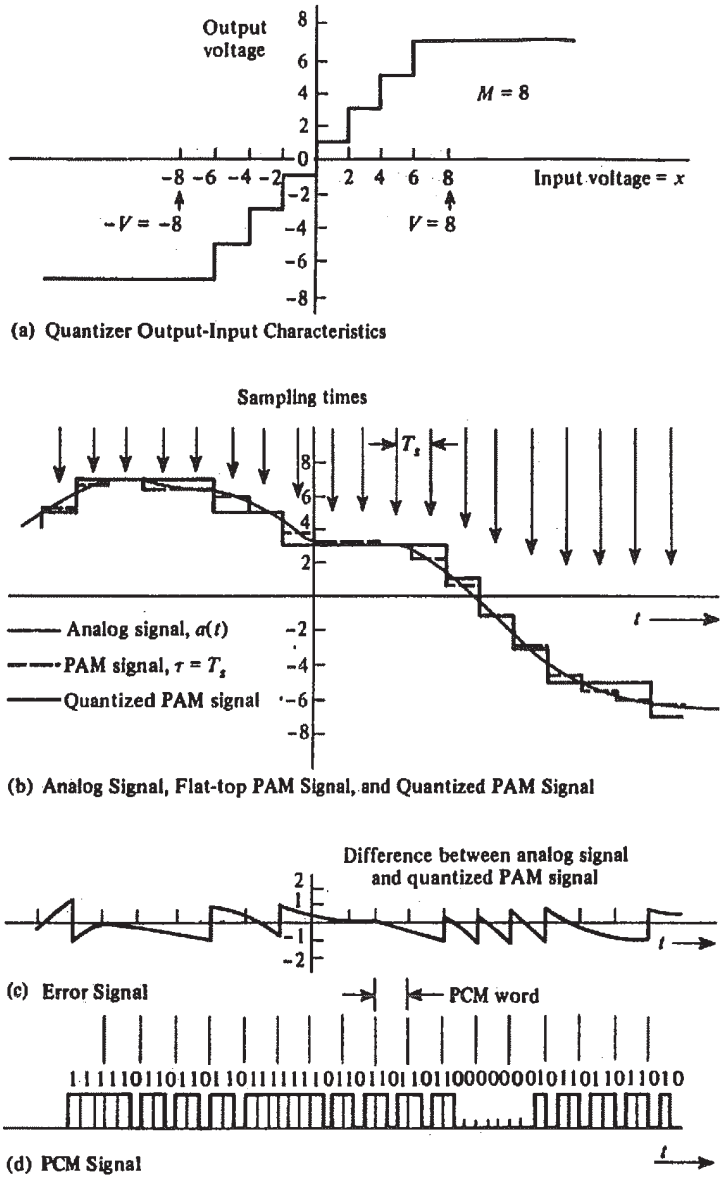


FIGURE 3.2 Illustration of waveforms in a PCM system. *Source:* Couch, L.W. II 1997. *Digital and Analog Communication Systems,* 5th ed., Prentice Hall, Upper Saddle River, NJ, p. 139. With permission.

digital words using other than base 2. That is, for base q, the number of quantized levels allowed is $M = q^n$, where n is the number of q base digits in the code word. We will not pursue this topic since binary ($q = 2$) digital circuits are most commonly used.

3.3 Percent Quantizing Noise

The quantizer at the PCM encoder produces an error signal at the PCM decoder output as illustrated in Fig. 3.2c. The peak value of this error signal may be expressed as a percentage

TABLE 3.1 3-b Gray Code for $M = 8$ Levels

Quantized Sample Voltage	Gray Code Word (PCM Output)	
+7	110	
+5	111	
+3	101	
+1	100	
		Mirror image except for sign bit
−1	000	
−3	001	
−5	011	
−7	010	

Source: Couch, L.W., II. 1997. *Digital and Analog Communication Systems*, 5th ed., Prentice Hall, Upper Saddle River, NJ, p. 140. With permission.

of the maximum possible analog signal amplitude. Referring to Fig. 3.2c, a peak error of 1 V occurs for a maximum analog signal amplitude of $M = 8$ V as shown Fig. 3.1c. Thus, in general,

$$\frac{2P}{100} = \frac{1}{M} = \frac{1}{2^n}$$

or

$$2^n = \frac{50}{P} \tag{3.1}$$

where P is the peak percentage error for a PCM system that uses n bit code words. The design value of n needed in order to have less than P percent error is obtained by taking the base 2 logarithm of both sides of Eq. (3.1), where it is realized that $\log_2(x) = [\log_{10}(x)]/\log_{10}(2) = 3.32\log_{10}(x)$. That is,

$$n \geq 3.32\log_{10}\left(\frac{50}{P}\right) \tag{3.2}$$

where n is the number of bits needed in the PCM word in order to obtain less than P percent error in the recovered analog signal (i.e., decoded PCM signal).

3.4 Practical PCM Circuits

Three techniques are used to implement the analog-to-digital converter (ADC) encoding operation. These are the *counting* or *ramp, serial* or *successive approximation*, and *parallel* or *flash* encoders.

In the counting encoder, at the same time that the sample is taken, a ramp generator is energized and a binary counter is started. The output of the ramp generator is continuously compared to the sample value; when the value of the ramp becomes equal to the sample value, the binary value of the counter is read. This count is taken to be the PCM word. The binary counter and the ramp generator are then reset to zero and are ready to be reenergized at the next sampling time. This technique requires only a few components, but the speed of this type of ADC is usually limited by the speed of the counter. The Maxim ICL7126 CMOS ADC integrated circuit uses this technique.

The serial encoder compares the value of the sample with trial quantized values. Successive trials depend on whether the past comparator outputs are positive or negative. The

trial values are chosen first in large steps and then in small steps so that the process will converge rapidly. The trial voltages are generated by a series of voltage dividers that are configured by (on-off) switches. These switches are controlled by digital logic. After the process converges, the value of the switch settings is read out as the PCM word. This technique requires more precision components (for the voltage dividers) than the ramp technique. The speed of the feedback ADC technique is determined by the speed of the switches. The National Semiconductor ADC0804 8-b ADC uses this technique.

The parallel encoder uses a set of parallel comparators with reference levels that are the permitted quantized values. The sample value is fed into all of the parallel comparators simultaneously. The high or low level of the comparator outputs determines the binary PCM word with the aid of some digital logic. This is a fast ADC technique but requires more hardware than the other two methods. The Harris CA3318 8-b ADC integrated circuit is an example of the technique.

All of the integrated circuits listed as examples have parallel digital outputs that correspond to the digital word that represents the analog sample value. For generation of PCM, the parallel output (digital word) needs to be converted to serial form for transmission over a two-wire channel. This is accomplished by using a parallel-to-serial converter integrated circuit, which is also known as a **serial-input-output** (SIO) chip. The SIO chip includes a shift register that is set to contain the parallel data (usually, from 8 or 16 input lines). Then the data are shifted out of the last stage of the shift register bit by bit onto a single output line to produce the serial format. Furthermore, the SIO chips are usually full duplex; that is, they have two sets of shift registers, one that functions for data flowing in each direction. One shift register converts parallel input data to serial output data for transmission over the channel, and, simultaneously, the other shift register converts received serial data from another input to parallel data that are available at another output. Three types of SIO chips are available: the *universal asynchronous receiver/transmitter* (UART), the *universal synchronous receiver/transmitter* (USRT), and the *universal synchronous/asynchronous receiver transmitter* (USART). The UART transmits and receives asynchronous serial data, the USRT transmits and receives synchronous serial data, and the USART combines both a UART and a USRT on one chip.

At the receiving end the PCM signal is decoded back into an analog signal by using a digital-to-analog converter (DAC) chip. If the DAC chip has a parallel data input, the received serial PCM data are first converted to a parallel form using a SIO chip as described in the preceding paragraph. The parallel data are then converted to an approximation of the analog sample value by the DAC chip. This conversion is usually accomplished by using the parallel digital word to set the configuration of electronic switches on a resistive current (or voltage) divider network so that the analog output is produced. This is called a *multiplying* DAC since the analog output voltage is directly proportional to the divider reference voltage multiplied by the value of the digital word. The Motorola MC1408 and the National Semiconductor DAC0808 8-b DAC chips are examples of this technique. The DAC chip outputs samples of the quantized analog signal that approximates the analog sample values. This may be smoothed by a low-pass reconstruction filter to produce the analog output.

The Communications Handbook [6, pp 107–117] and The Electrical Engineering Handbook [5, pp. 771–782] give more details on ADC, DAC, and PCM circuits.

3.5 Bandwidth of PCM

A good question to ask is: What is the spectrum of a PCM signal? For the case of PAM signalling, the spectrum of the PAM signal could be obtained as a function of the spectrum of the input analog signal because the PAM signal is a linear function of the analog signal. This is not the case for PCM. As shown in Figs. 3.1 and 3.2, the PCM signal is a nonlinear function of the input signal. Consequently, the spectrum of the PCM signal is not directly related to the spectrum of the input analog signal. It can be shown that the spectrum of the PCM signal depends on the bit rate, the correlation of the PCM data, and on the PCM waveform pulse shape (usually rectangular) used to describe the bits [2, 3]. From Fig. 3.2, the bit rate is

$$R = nf_s \tag{3.3}$$

where n is the number of bits in the PCM word ($M = 2^n$) and f_s is the sampling rate. For no aliasing we require $f_s \geq 2B$ where B is the bandwidth of the analog signal (that is to be converted to the PCM signal). The dimensionality theorem [2, 3] shows that the bandwidth of the PCM waveform is bounded by

$$B_{\text{PCM}} \geq \frac{1}{2}R = \frac{1}{2}nf_s \tag{3.4}$$

where equality is obtained if a $(\sin x)/x$ type of pulse shape is used to generate the PCM waveform. The exact spectrum for the PCM waveform will depend on the pulse shape that is used as well as on the type of line encoding. For example, if one uses a rectangular pulse shape with polar nonreturn to zero (NRZ) line coding, the first null bandwidth is simply

$$B_{\text{PCM}} = R = nf_s \text{ Hz} \tag{3.5}$$

Table 3.2 presents a tabulation of this result for the case of the minimum sampling rate, $f_s = 2B$. Note that Eq. (3.4) demonstrates that the bandwidth of the PCM signal has a lower bound given by

$$B_{\text{PCM}} \geq nB \tag{3.6}$$

where $f_s > 2B$ and B is the bandwidth of the corresponding analog signal. Thus, for reasonable values of n, the bandwidth of the PCM signal will be significantly larger than the bandwidth of the corresponding analog signal that it represents. For the example shown in Fig. 3.2 where $n = 3$, the PCM signal bandwidth will be at least three times wider than that of the corresponding analog signal. Furthermore, if the bandwidth of the PCM signal is reduced by improper filtering or by passing the PCM signal through a system that has a poor frequency response, the filtered pulses will be elongated (stretched in width) so that pulses corresponding to any one bit will smear into adjacent bit slots. If this condition becomes too serious, it will cause errors in the detected bits. This pulse smearing effect is called **intersymbol interference** (ISI).

3.6 Effects of Noise

The analog signal that is recovered at the PCM system output is corrupted by noise. Two main effects produce this noise or distortion: 1) quantizing noise that is caused by the M-step quantizer at the PCM transmitter and 2) bit errors in the recovered PCM signal. The bit errors are caused by *channel noise* as well as improper channel filtering, which causes ISI. In addition, if the input analog signal is not strictly band limited, there will be some

TABLE 3.2 Performance of a PCM System with Uniform Quantizing and No Channel Noise

Number of Quantizer Levels Used, M	Length of the PCM Word, n (bits)	Bandwidth of PCM Signal (First Null Bandwidth)[a]	Recovered Analog Signal Power-to-Quantizing Noise Power Ratios (dB) $(S/N)_{out}$
2	1	2B	6.0
4	2	4B	12.0
8	3	6B	18.1
16	4	8B	24.1
32	5	10B	30.1
64	6	12B	36.1
128	7	14B	42.1
256	8	16B	48.2
512	9	18B	54.2
1,024	10	20B	60.2
2,048	11	22B	66.2
4,096	12	24B	72.2
8,192	13	26B	78.3
16,384	14	28B	84.3
32,768	15	30B	90.3
65,536	16	32B	96.3

[a] B is the absolute bandwidth of the input analog signal. *Source:* Couch, L.W. II 1997. *Digital and Analog Communication Systems,* 5th ed., Prentice Hall, Upper Saddle River, NJ, p. 142. With permission.

aliasing noise on the recovered analog signal [12]. Under certain assumptions, it can be shown that the recovered analog *average* signal power to the average noise power [2] is

$$\left(\frac{S}{N}\right)_{\text{out}} = \frac{M^2}{1 + 4\left(M^2 - 1\right) P_e} \tag{3.7}$$

where M is the number of uniformly spaced quantizer levels used in the PCM transmitter and P_e is the probability of bit error in the recovered binary PCM signal at the receiver DAC before it is converted back into an analog signal. Most practical systems are designed so that P_e is negligible. Consequently, if we assume that there are no bit errors due to channel noise (i.e., $P_e = 0$), the S/N due only to quantizing errors is

$$\left(\frac{S}{N}\right)_{\text{out}} = M^2 \tag{3.8}$$

Numerical values for these S/N ratios are given in Table 3.2.

To realize these S/N ratios, one critical assumption is that the peak-to-peak level of the analog waveform at the input to the PCM encoder is set to the design level of the quantizer. For example, referring to Fig. 3.2, this corresponds to the input traversing the range $-V$ to $+V$ volts where $V = 8$ V is the design level of the quantizer. Equation (3.7) was derived for waveforms with equally likely values, such as a triangle waveshape, that have a peak-to-peak value of $2V$ and an rms value of $V/\sqrt{3}$, where V is the design peak level of the quantizer.

From a practical viewpoint, the quantizing noise at the output of the PCM decoder can be categorized into four types depending on the operating conditions. The four types are overload noise, random noise, granular noise, and hunting noise. As discussed earlier, the level of the analog waveform at the input of the PCM encoder needs to be set so that its peak level does not exceed the design peak of V volts. If the peak input does exceed V, the recovered analog waveform at the output of the PCM system will have flat tops near the peak values. This produces *overload noise.* The flat tops are easily seen on an oscilloscope, and the recovered analog waveform sounds distorted since the flat topping

produces unwanted harmonic components. For example, this type of distortion can be heard on PCM telephone systems when there are high levels such as dial tones, busy signals, or off-hook warning signals.

The second type of noise, *random noise,* is produced by the random quantization errors in the PCM system under normal operating conditions when the input level is properly set. This type of condition is assumed in Eq. (3.8). Random noise has a white hissing sound. If the input level is not sufficiently large, the S/N will deteriorate from that given by Eq. (3.8); the quantizing noise will still remain more or less random.

If the input level is reduced further to a relatively small value with respect to the design level, the error values are not equally likely from sample to sample, and the noise has a harsh sound resembling gravel being poured into a barrel. This is called *granular noise.* This type of noise can be randomized (noise power decreased) by increasing the number of quantization levels and, consequently, increasing the PCM bit rate. Alternatively, granular noise can be reduced by using a nonuniform quantizer, such as the μ-law or A-law quantizers that are described in Section 3.7.

The fourth type of quantizing noise that may occur at the output of a PCM system is *hunting noise.* It can occur when the input analog waveform is nearly constant, including when there is no signal (i.e., zero level). For these conditions the sample values at the quantizer output (see Fig. 3.2) can oscillate between two adjacent quantization levels, causing an undesired sinusoidal type tone of frequency $1/2f_s$ at the output of the PCM system. Hunting noise can be reduced by filtering out the tone or by designing the quantizer so that there is no vertical step at the constant value of the inputs, such as at 0-V input for the no signal case. For the no signal case, the hunting noise is also called *idle channel noise.* Idle channel noise can be reduced by using a horizontal step at the origin of the quantizer output–input characteristic instead of a vertical step as shown in Fig. 3.2.

Recalling that $M = 2^n$, we may express Eq. (3.8) in decibels by taking $10 \log_{10}(\cdot)$ of both sides of the equation,

$$\left(\frac{S}{N}\right)_{\text{dB}} = 6.02n + \alpha \tag{3.9}$$

where n is the number of bits in the PCM word and $\alpha = 0$. This equation—called the 6-dB rule—points out the significant performance characteristic for PCM: an additional 6-dB improvement in S/N is obtained for each bit added to the PCM word. This is illustrated in Table 3.2. Equation (3.9) is valid for a wide variety of assumptions (such as various types of input waveshapes and quantification characteristics), although the value of α will depend on these assumptions [7]. Of course, it is assumed that there are no bit errors and that the input signal level is large enough to range over a significant number of quantizing levels.

One may use Table 3.2 to examine the design requirements in a proposed PCM system. For example, high fidelity enthusiasts are turning to digital audio recording techniques. Here PCM signals are recorded instead of the analog audio signal to produce superb sound reproduction. For a dynamic range of 90 dB, it is seen that at least 15-b PCM words would be required. Furthermore, if the analog signal had a bandwidth of 20 kHz, the first null bandwidth for rectangular bit-shape PCM would be 2×20 kHz $\times 15 = 600$ kHz. Consequently, video-type tape recorders are needed to record and reproduce high-quality digital audio signals. Although this type of recording technique might seem ridiculous at first, it is realized that expensive high-quality analog recording devices are hard pressed to reproduce a dynamic range of 70 dB. Thus, digital audio is one way to achieve improved performance. This is being proven in the marketplace with the popularity of the digital compact disk (CD). The CD uses a 16-b PCM word and a sampling rate of 44.1 kHz on

each stereo channel [9, 10]. Reed–Solomon coding with interleaving is used to correct burst errors that occur as a result of scratches and fingerprints on the compact disk.

3.7 Nonuniform Quantizing: μ-Law and A-Law Companding

Voice analog signals are more likely to have amplitude values near zero than at the extreme peak values allowed. For example, when digitizing voice signals, if the peak value allowed is 1 V, weak passages may have voltage levels on the order of 0.1 V (20 dB down). For signals such as these with nonuniform amplitude distribution, the granular quantizing noise will be a serious problem if the step size is not reduced for amplitude values near zero and increased for extremely large values. This is called nonuniform quantizing since a variable step size is used. An example of a nonuniform quantizing characteristic is shown in Fig. 3.3.

The effect of nonuniform quantizing can be obtained by first passing the analog signal through a compression (nonlinear) amplifier and then into the PCM circuit that uses a uniform quantizer. In the U.S., a μ-law type of compression characteristic is used. It is defined [11] by

$$|w_2(t)| = \frac{\ln(1 + \mu |w_1(t)|)}{\ln(1 + \mu)} \tag{3.10}$$

where the allowed peak values of $w_1(t)$ are ± 1 (i.e., $|w_1(t)| \leq 1$), μ is a positive constant that is a parameter. This compression characteristic is shown in Fig. 3.3(b) for several values of μ, and it is noted that $\mu \to 0$ corresponds to linear amplification (uniform quantization overall). In the United States, Canada, and Japan, the telephone companies use a $\mu = 255$ compression characteristic in their PCM systems [4].

Another compression law, used mainly in Europe, is the A-law characteristic. It is defined [1] by

$$|w_2(t)| = \begin{cases} \dfrac{A|w_1(t)|}{1 + \ln A}, & 0 \leq |w_1(t)| \leq \dfrac{1}{A} \\ \dfrac{1 + \ln(A|w_1(t)|)}{1 + \ln A}, & \dfrac{1}{A} \leq |w_1(t)| \leq 1 \end{cases} \tag{3.11}$$

where $|w_1(t)| < 1$ and A is a positive constant. The A-law compression characteristic is shown in Fig. 3.3(c). The typical value for A is 87.6.

When compression is used at the transmitter, *expansion* (i.e., decompression) must be used at the receiver output to restore signal levels to their correct relative values. The *expandor* characteristic is the inverse of the compression characteristic, and the combination of a compressor and an expandor is called a *compandor*.

Once again, it can be shown that the output S/N follows the 6-dB law [2]

$$\left(\frac{S}{N}\right)_{\text{dB}} = 6.02 + \alpha \tag{3.12}$$

where for uniform quantizing

$$\alpha = 4.77 - 20\log(V/x_{\text{rms}}) \tag{3.13}$$

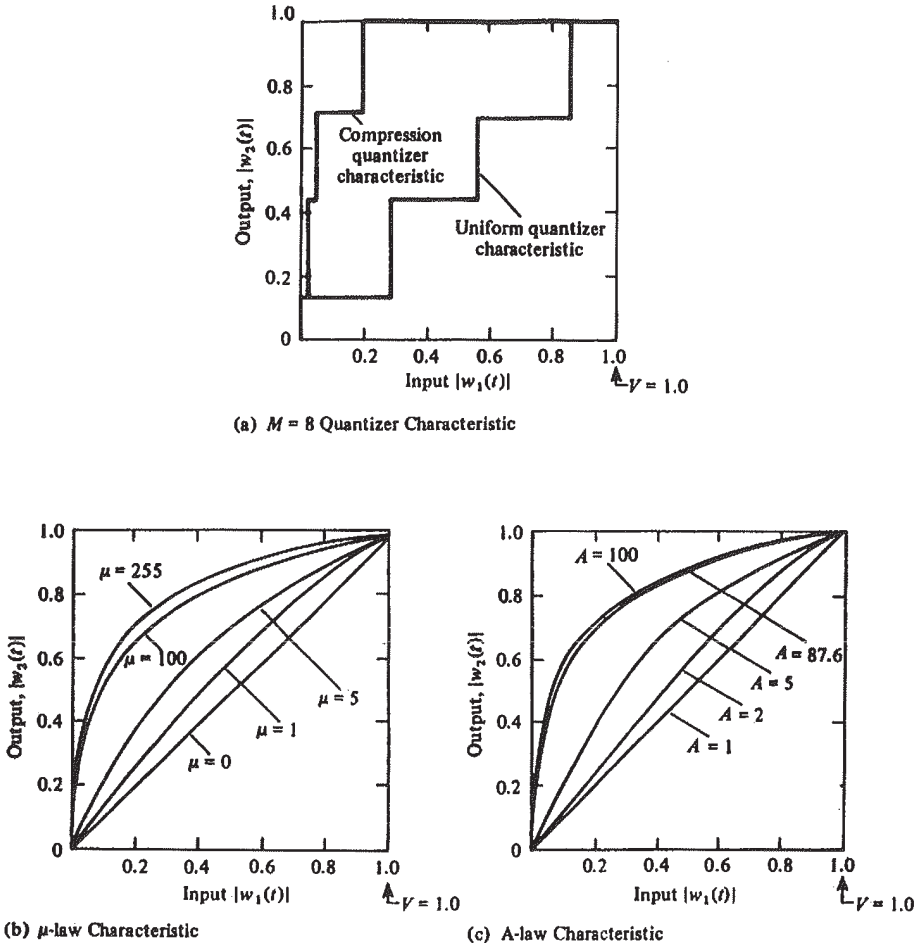


FIGURE 3.3 Compression characteristics (first quadrant shown). *Source:* Couch, L.W. II 1997. *Digital and Analog Communication Systems,* 5th ed., Prentice Hall, Upper Saddle River, NJ, p. 147. With permission.

and for sufficiently large input levels[2] for μ-law companding

$$\alpha \approx 4.77 - 20\log[\ln(1+\mu)] \tag{3.14}$$

and for A-law companding [7]

$$\alpha \approx 4.77 - 20\log[1+\ln A] \tag{3.15}$$

n is the number of bits used in the PCM word, V is the peak design level of the quantizer, and x_{rms} is the rms value of the input analog signal. Notice that the output S/N is a function of the input level for the uniform quantizing (no companding) case but is relatively insensitive to input level for μ-law and A-law companding, as shown in Fig. 3.4. The ratio V/x_{rms} is called the *loading factor.* The input level is often set for a loading factor of 4 (12 dB) to

[2]See Lathi, 1998 for a more complicated expression that is valid for any input level.

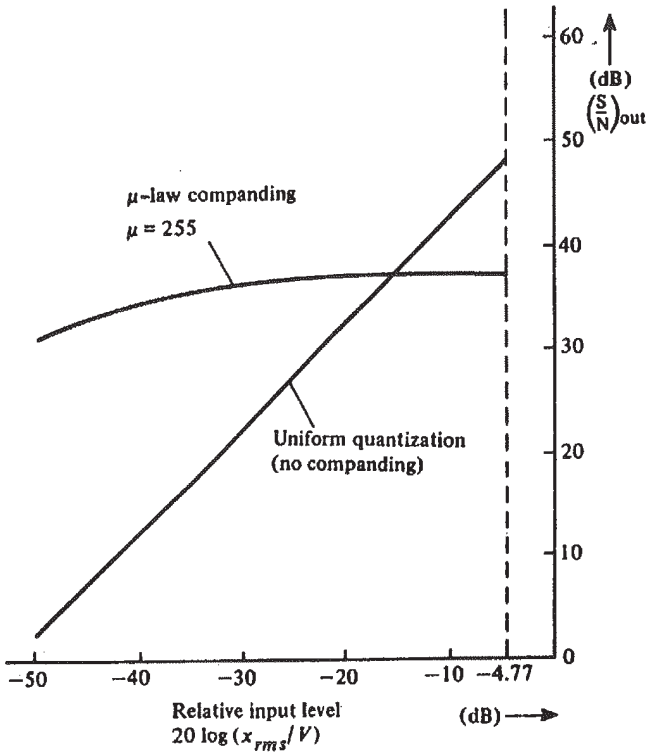


FIGURE 3.4 Output S/N of 8-b PCM systems with and without companding. *Source:* Couch, L.W. II 1997. *Digital and Analog Communication Systems,* 5th ed., Prentice Hall, Upper Saddle River, NJ, p. 149. With permission.

ensure that the overload quantizing noise will be negligible. In practice this gives $\alpha = -7.3$ for the case of uniform encoding as compared to $\alpha = 0$, which was obtained for the ideal conditions associated with Eq. (3.8).

3.8 Example: Design of a PCM System

Assume that an analog voice-frequency signal, which occupies a band from 300 to 3400 Hz, is to be transmitted over a binary PCM system. The minimum sampling frequency would be $2 \times 3.4 = 6.8$ kHz. In practice the signal is oversampled, and in the U.S. a sampling frequency of 8 kHz is the standard used for voice-frequency signals in telephone communication systems. Assume that each sample value is represented by 8 b; then the bit rate of the PCM signal is

$$\begin{aligned} R &= (f_s \text{ samples}/s)\,(n \text{ b}/s) \\ &= (8\ k \text{ samples}/s)(8 \text{ b}/s) = 64 \text{ kb}/s \end{aligned} \tag{3.16}$$

Referring to the dimensionality theorem [Eq. (3.4)], we realize that the theoretically minimum absolute bandwidth of the PCM signal is

$$B_{\min} = \frac{1}{2}D = 32 \text{ kHz} \tag{3.17}$$

and this is realized if the PCM waveform consists of $(\sin x)/x$ pulse shapes. If rectangular pulse shaping is used, the absolute bandwidth is infinity, and the first null bandwidth

[Eq. (3.5)] is

$$B_{\text{null}} = R = \frac{1}{T_b} = 64 \text{ kHz} \tag{3.18}$$

That is, we require a bandwidth of 64 kHz to transmit this digital voice PCM signal where the bandwidth of the original analog voice signal was, at most, 4 kHz. Using $n = 8$ in Eq. (3.1), the error on the recovered analog signal is $\pm 0.2\%$. Using Eqs. (3.12) and (3.13) for the case of uniform quantizing with a loading factor, V/x_{rms}, of 10 (20 dB), we get for uniform quantizing

$$\left(\frac{S}{N}\right)_{\text{dB}} = 32.9 \text{ dB} \tag{3.19}$$

Using Eqs. (3.12) and (3.14) for the case of $\mu = 255$ companding, we get

$$\left(\frac{S}{N}\right) = 38.05 \text{ dB} \tag{3.20}$$

These results are illustrated in Fig. 3.4.

Defining Terms

Intersymbol interference: Filtering of a digital waveform so that a pulse corresponding to 1 b will smear (stretch in width) into adjacent bit slots.

Pulse amplitude modulation: An analog signal is represented by a train of pulses where the pulse amplitudes are proportional to the analog signal amplitude.

Pulse code modulation: A serial bit stream that consists of binary words which represent quantized sample values of an analog signal.

Quantizing: Replacing a sample value with the closest allowed value.

References

[1] Cattermole, K.W., *Principles of Pulse-code Modulation,* American Elsevier, New York, NY, 1969.

[2] Couch, L.W., *Digital and Analog Communication Systems,* 5th ed., Prentice Hall, Upper Saddle River, NJ, 1997.

[3] Couch, L.W., *Modern Communication Systems: Principles and Applications,* Macmillan Publishing, New York, NY, 1995.

[4] Dammann, C.L., McDaniel, L.D., and Maddox, C.L., D2 Channel Bank—Multiplexing and Coding. *B. S. T. J.,* 12(10), 1675–1700, 1972.

[5] Dorf, R.C., *The Electrical Engineering Handbook,* CRC Press, Inc., Boca Raton, FL, 1993.

[6] Gibson, J.D., *The Communications Handbook,* CRC Press, Inc., Boca Raton, FL, 1997.

[7] Jayant, N.S. and Noll, P., *Digital Coding of Waveforms,* Prentice Hall, Englewood Cliffs, NJ, 1984.

[8] Lathi, B.P., *Modern Digital and Analog Communication Systems,* 3rd ed., Oxford University Press, New York, NY, 1998.

[9] Miyaoka, S., Digital Audio is Compact and Rugged. *IEEE Spectrum,* 21(3), 35–39, 1984.

[10] Peek, J.B.H., Communication Aspects of the Compact Disk Digital Audio System. *IEEE Comm. Mag.,* 23(2), 7–15, 1985.

[11] Smith, B., Instantaneous Companding of Quantized Signals. *B. S. T. J.*, 36(5), 653–709, 1957.

[12] Spilker, J.J., *Digital Communications by Satellite,* Prentice Hall, Englewood Cliffs, NJ, 1977.

Further Information

Many practical design situations and applications of PCM transmission via twisted-pair T-1 telephone lines, fiber optic cable, microwave relay, and satellite systems are given in [2] and [3].

4

Baseband Signalling and Pulse Shaping

4.1 Communications System Model 4-1
4.2 Intersymbol Interference and the Nyquist Criterion ... 4-4
Raised Cosine Pulse
4.3 Nyquist Criterion with Matched Filtering 4-8
4.4 Eye Diagrams 4-10
Vertical Eye Opening • Horizontal Eye Opening • Slope of the Inner Eye
4.5 Partial-Response Signalling 4-12
Precoding
4.6 Additional Considerations 4-18
Average Transmitted Power and Spectral Constraints • Peak-to-Average Power • Channel and Receiver Characteristics • Complexity • Tolerance to Interference • Probability of Intercept and Detection
4.7 Examples 4-20
Global System for Mobile Communications (GSM) • U.S. Digital Cellular (IS-136) • Interim Standard-95 • Personal Access Communications System (PACS)
Defining Terms 4-21
References 4-22
Further Information 4-23

Michael L. Honig
Northwestern University

Melbourne Barton
Bellcore

Many physical communications channels, such as radio channels, accept a continuous-time waveform as input. Consequently, a sequence of source bits, representing data or a digitized analog signal, must be converted to a continuous-time waveform at the transmitter. In general, each successive group of bits taken from this sequence is mapped to a particular continuous-time pulse. In this chapter we discuss the basic principles involved in selecting such a pulse for channels that can be characterized as linear and time invariant with finite bandwidth.

4.1 Communications System Model

Figure 4.1a shows a simple block diagram of a communications system. The sequence of source bits $\{b_i\}$ are grouped into sequential blocks (vectors) of m bits $\{\boldsymbol{b}_i\}$, and each binary vector $\boldsymbol{b}_i$ is mapped to one of 2^m pulses, $p(\boldsymbol{b}_i; t)$, which is transmitted over the channel.

0-8493-8597-0/99/$0.00+$.50

© 1999 by CRC Press LLC

The transmitted signal as a function of time can be written as

$$s(t) = \sum_i p(\boldsymbol{b}_i; t - iT) \tag{4.1}$$

where $1/T$ is the rate at which each group of m bits, or pulses, is introduced to the channel. The information (bit) rate is therefore m/T.

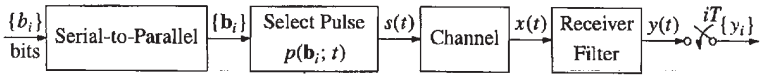


Figure 4.1a Communication system model. The source bits are grouped into binary vectors, which are mapped to a sequence of pulse shapes.

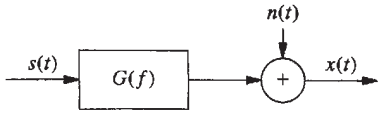


Figure 4.1b Channel model consisting of a linear, time-invariant system (transfer function) followed by additive noise.

The channel in Fig. 4.1a can be a radio link, which may distort the input signal $s(t)$ in a variety of ways. For example, it may introduce pulse dispersion (due to finite bandwidth) and multipath, as well as additive background noise. The output of the channel is denoted as $x(t)$, which is processed by the receiver to determine estimates of the source bits. The receiver can be quite complicated; however, for the purpose of this discussion, it is sufficient to assume only that it contains a front-end filter and a sampler, as shown in Fig. 4.1a. This assumption is valid for a wide variety of detection strategies. The purpose of the receiver filter is to remove noise outside of the transmitted frequency band and to compensate for the channel frequency response.

A commonly used channel model is shown in Fig. 4.1b and consists of a linear, time-invariant filter, denoted as $G(f)$, followed by additive noise $n(t)$. The channel output is, therefore,

$$x(t) = [g(t) * s(t)] + n(t) \tag{4.2}$$

where $g(t)$ is the channel impulse response associated with $G(f)$, and the asterisk denotes convolution,

$$g(t) * s(t) = \int_{-\infty}^{\infty} g(t - \tau)s(\tau)\, \mathrm{d}\tau$$

This channel model accounts for all linear, time-invariant channel impairments, such as finite bandwidth and time-invariant multipath. It does not account for time-varying impairments, such as rapid fading due to time-varying multipath. Nevertheless, this model can be considered valid over short time periods during which the multipath parameters remain constant.

In Figs. 4.1a, and 4.1b, it is assumed that all signals are **baseband signals**, which means that the frequency content is centered around $f = 0$ (DC). The channel passband, therefore, partially coincides with the transmitted spectrum. In general, this condition requires that the transmitted signal be modulated by an appropriate carrier frequency and demodulated at the receiver. In that case, the model in Figs. 4.1a, and 4.1b still applies; however, *baseband-equivalent* signals must be derived from their modulated (passband) counterparts.

Baseband signalling and *pulse shaping* refers to the way in which a group of source bits is mapped to a baseband transmitted pulse.

As a simple example of baseband signalling, we can take $m = 1$ (map each source bit to a pulse), assign a 0 bit to a pulse $p(t)$, and a 1 bit to the pulse $-p(t)$. Perhaps the simplest example of a baseband pulse is the *rectangular* pulse given by $p(t) = 1$, $0 < t \leq T$, and $p(t) = 0$ elsewhere. In this case, we can write the transmitted signal as

$$s(t) = \sum_i A_i p(t - iT) \tag{4.3}$$

where each symbol A_i takes on a value of $+1$ or -1, depending on the value of the ith bit, and $1/T$ is the *symbol rate*, namely, the rate at which the symbols A_i are introduced to the channel.

The preceding example is called *binary* **pulse amplitude modulation (PAM)**, since the data symbols A_i are binary valued, and they amplitude modulate the transmitted pulse $p(t)$. The information rate (bits per second) in this case is the same as the symbol rate $1/T$. As a simple extension of this signalling technique, we can increase m and choose A_i from one of $M = 2^m$ values to transmit at bit rate m/T. This is known as M-ary PAM. For example, letting $m = 2$, each pair of bits can be mapped to a pulse in the set $\{p(t), -p(t), 3p(t), -3p(t)\}$.

In general, the transmitted symbols $\{A_i\}$, the baseband pulse $p(t)$, and channel impulse response $g(t)$ can be *complex valued.* For example, each successive pair of bits might select a symbol from the set $\{1, -1, j, -j\}$, where $j = \sqrt{-1}$. This is a consequence of considering the baseband equivalent of passband modulation. (That is, generating a transmitted spectrum which is centered around a carrier frequency f_c.) Here we are not concerned with the relation between the passband and baseband equivalent models and simply point out that the discussion and results in this chapter apply to complex-valued symbols and pulse shapes.

As an example of a signalling technique which is not PAM, let $m = 1$ and

$$\begin{aligned} p(0;t) &= \begin{cases} \sqrt{2}\sin(2\pi f_1 t) & 0 < t < T \\ 0 & \text{elsewhere} \end{cases} \\ p(1;t) &= \begin{cases} \sqrt{2}\sin(2\pi f_2 t) & 0 < t < T \\ 0 & \text{elsewhere} \end{cases} \end{aligned} \tag{4.4}$$

where f_1 and $f_2 \neq f_1$ are fixed frequencies selected so that $f_1 T$ and $f_2 T$ (number of cycles for each bit) are multiples of $1/2$. These pulses are *orthogonal*, namely,

$$\int_0^T p(1;t)p(0;t)\,\mathrm{d}t = 0$$

This choice of pulse shapes is called binary **frequency-shift keying (FSK)**.

Another example of a set of orthogonal pulse shapes for $m = 2$ bits$/T$ is shown in Fig. 4.2. Because these pulses may have as many as three transitions within a symbol period, the transmitted spectrum occupies roughly four times the transmitted spectrum of binary PAM with a rectangular pulse shape. The spectrum is, therefore, spread across a much larger band than the smallest required for reliable transmission, assuming a data rate of $2/T$. This type of signalling is referred to as **spread-spectrum**. Spread-spectrum signals are more

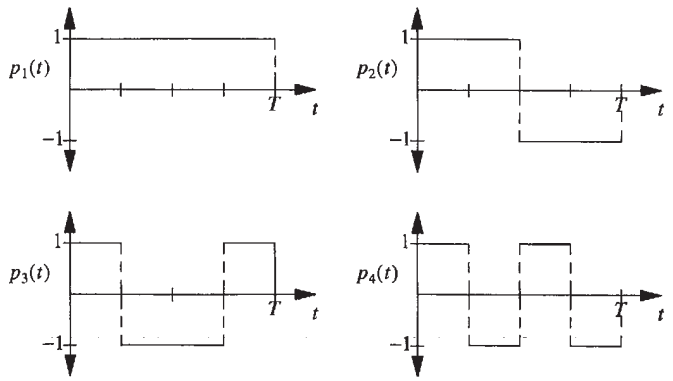


FIGURE 4.2 Four orthogonal spread-spectrum pulse shapes.

robust with respect to interference from other transmitted signals than are narrowband signals.[1]

4.2 Intersymbol Interference and the Nyquist Criterion

Consider the transmission of a PAM signal illustrated in Fig. 4.3. The source bits $\{b_i\}$ are mapped to a sequence of levels $\{A_i\}$, which modulate the transmitter pulse $p(t)$. The channel input is, therefore, given by Eq. (4.3) where $p(t)$ is the impulse response of the transmitter *pulse-shaping filter* $P(f)$ shown in Fig. 4.3. The input to the transmitter filter $P(f)$ is the modulated sequence of delta functions $\sum_i A_i\delta(t-iT)$. The channel is represented by the transfer function $G(f)$ (plus noise), which has impulse response $g(t)$, and the receiver filter has transfer function $R(f)$ with associated impulse response $r(t)$.

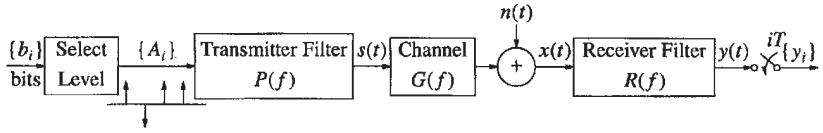


FIGURE 4.3 Baseband model of a pulse amplitude modulation system.

Let $h(t)$ be the overall impulse response of the combined transmitter, channel, and receiver, which has transfer function $H(f) = P(f)G(f)R(f)$. We can write $h(t) = p(t) * g(t) * r(t)$. The output of the receiver filter is then

$$y(t) = \sum_i A_i h(t - iT) + \tilde{n}(t) \tag{4.5}$$

where $\tilde{n}(t) = r(t) * n(t)$ is the output of the filter $R(f)$ with input $n(t)$. Assuming that samples are collected at the output of the filter $R(f)$ at the symbol rate $1/T$, we can write

[1] This example can also be viewed as coded binary PAM. Namely, each pair of two source bits are mapped to 4 coded bits, which are transmitted via binary PAM with a rectangular pulse. The current IS-95 air interface uses an extension of this signalling method in which groups of 6 b are mapped to 64 orthogonal pulse shapes with as many as 63 transitions during a symbol.

the kth sample of $y(t)$ as

$$\begin{aligned} y(kT) &= \sum_i A_i h(kT - iT) + \tilde{n}(kT) \\ &= A_k h(0) + \sum_{i \neq k} A_i h(kT - iT) + \tilde{n}(kT) \end{aligned} \tag{4.6}$$

The first term on the right-hand side of Eq. (4.6) is the kth transmitted symbol scaled by the system impulse response at $t = 0$. If this were the only term on the right side of Eq. (4.6), we could obtain the source bits without error by scaling the received samples by $1/h(0)$. The second term on the right-hand side of Eq. (4.6) is called **intersymbol interference**, which reflects the view that neighboring symbols interfere with the detection of each desired symbol.

One possible criterion for choosing the transmitter and receiver filters is to minimize intersymbol interference. Specifically, if we choose $p(t)$ and $r(t)$ so that

$$h(kT) = \begin{cases} 1 & k = 0 \\ 0 & k \neq 0 \end{cases} \tag{4.7}$$

then the kth received sample is

$$y(kT) = A_k + \tilde{n}(kT) \tag{4.8}$$

In this case, the intersymbol interference has been eliminated. This choice of $p(t)$ and $r(t)$ is called a **zero-forcing** solution, since it forces the intersymbol interference to zero. Depending on the type of detection scheme used, a zero-forcing solution may not be desirable. This is because the probability of error also depends on the noise intensity, which generally increases when intersymbol interference is suppressed. It is instructive, however, to examine the properties of the zero-forcing solution.

We now view Eq. (4.7) in the frequency domain. Since $h(t)$ has Fourier transform

$$H(f) = P(f)G(f)R(f) \tag{4.9}$$

where $P(f)$ is the Fourier transform of $p(t)$, the bandwidth of $H(f)$ is limited by the bandwidth of the channel $G(f)$. We will assume that $G(f) = 0$, $|f| > W$. The sampled impulse response $h(kT)$ can, therefore, be written as the inverse Fourier transform

$$h(kT) = \int_{-W}^{W} H(f) e^{j2\pi f kT} \, \mathrm{d}f$$

Through a series of manipulations, this integral can be rewritten as an inverse discrete Fourier transform,

$$h(kT) = T \int_{-1/(2T)}^{1/(2T)} H_{\mathrm{eq}}\left(e^{j2\pi fT}\right) e^{j2\pi fkT} \, \mathrm{d}f \tag{4.10a}$$

where

$$\begin{aligned} H_{\mathrm{eq}}(e^{j2\pi fT}) &= \frac{1}{T} \sum_k H\left(f + \frac{k}{T}\right) \\ &= \frac{1}{T} \sum_k P\left(f + \frac{k}{T}\right) G\left(f + \frac{k}{T}\right) R\left(f + \frac{k}{T}\right) \end{aligned} \tag{4.10b}$$

This relation states that $H_{\text{eq}}(z), z = e^{j2\pi fT}$, is the discrete Fourier transform of the sequence $\{h_k\}$, where $h_k = h(kT)$. Sampling the impulse response $h(t)$ therefore changes the transfer function $H(f)$ to the *aliased* frequency response $H_{\text{eq}}(e^{j2\pi fT})$. From Eqs. (4.10), and (4.6) we conclude that $H_{\text{eq}}(z)$ is the transfer function that relates the sequence of input data symbols $\{A_i\}$ to the sequence of received samples $\{y_i\}$, where $y_i = y(iT)$, in the absence of noise. This is illustrated in Fig. 4.4. For this reason, $H_{\text{eq}}(z)$ is called the **equivalent discrete-time transfer function** for the overall system transfer function $H(f)$.

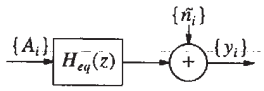


FIGURE 4.4 Equivalent discrete-time channel for the PAM system shown in Fig. 4.3 $[y_i = y(iT), \tilde{n}_i = \tilde{n}(iT)]$

Since $H_{\text{eq}}(e^{j2\pi fT})$ is the discrete Fourier transform of the sequence $\{h_k\}$, the time-domain, or sequence condition (4.7) is equivalent to the frequency-domain condition

$$H_{\text{eq}}\left(e^{j2\pi fT}\right) = 1 \tag{4.11}$$

This relation is called the **Nyquist criterion**. From Eqs. (4.10b) and (4.11) we make the following observations.

1. To satisfy the Nyquist criterion, the channel bandwidth W must be at least $1/(2T)$. Otherwise, $G(f + n/T) = 0$ for f in some interval of positive length for all n, which implies that $H_{\text{eq}}(e^{j2\pi fT}) = 0$ for f in the same interval.
2. For the minimum bandwidth $W = 1/(2T)$, Eqs. (4.10b) and (4.11) imply that $H(f) = T$ for $|f| < 1/(2T)$ and $H(f) = 0$ elsewhere. This implies that the system impulse response is given by

$$h(t) = \frac{\sin(\pi t/T)}{\pi t/T} \tag{4.12}$$

(Since $\int_{-\infty}^{\infty} h^2(t)\,\mathrm{d}t = T$, the transmitted signal $s(t) = \sum_i A_i h(t - iT)$ has power equal to the symbol variance $E[|A_i|^2]$.) The impulse response in Eq. (4.12) is called a *minimum bandwidth* or Nyquist pulse. The frequency band $[-1/(2T), 1/(2T)]$ [i.e., the passband of $H(f)$] is called the **Nyquist band**.

3. Suppose that the channel is bandlimited to twice the Nyquist bandwidth. That is, $G(f) = 0$ for $|f| > 1/T$. The condition (4.11) then becomes

$$H(f) + H\left(f - \frac{1}{T}\right) + H\left(f + \frac{1}{T}\right) = T \tag{4.13}$$

Assume for the moment that $H(f)$ and $h(t)$ are both real valued, so that $H(f)$ is an even function of $f[H(f) = H(-f)]$. This is the case when the receiver filter is the matched filter (see Section 4.3). We can then rewrite Eq. (4.13) as

$$H(f) + H\left(\frac{1}{T} - f\right) = T, \quad 0 < f < \frac{1}{2T} \tag{4.14}$$

which states that $H(f)$ must have odd symmetry about $f = 1/(2T)$. This is illustrated in Fig. 4.5, which shows two different transfer functions $H(f)$ that

satisfy the Nyquist criterion.

4. The pulse shape $p(t)$ enters into Eq. (4.11) only through the product $P(f)R(f)$. Consequently, either $P(f)$ or $R(f)$ can be fixed, and the other filter can be adjusted or adapted to the particular channel. Typically, the pulse shape $p(t)$ is fixed, and the receiver filter is adapted to the (possibly time-varying) channel.

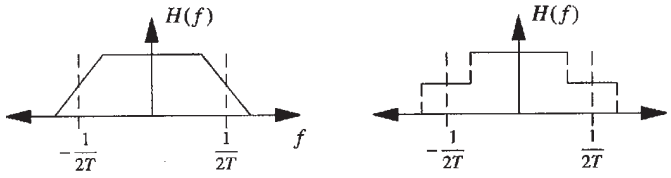


FIGURE 4.5 Two examples of frequency responses that satisfy the Nyquist criterion.

4.2.1 Raised Cosine Pulse

Suppose that the channel is ideal with transfer function

$$G(f) = \begin{cases} 1, & |f| < W \\ 0, & |f| > W \end{cases} \tag{4.15}$$

To maximize bandwidth efficiency, Nyquist pulses given by Eq. (4.12) should be used where $W = 1/(2T)$. This type of signalling, however, has two major drawbacks. First, Nyquist pulses are noncausal and of infinite duration. They can be approximated in practice by introducing an appropriate delay, and truncating the pulse. The pulse, however, decays very slowly, namely, as $1/t$, so that the truncation window must be wide. This is equivalent to observing that the ideal bandlimited frequency response given by Eq. (4.15) is difficult to approximate closely. The second drawback, which is more important, is the fact that this type of signalling is not robust with respect to sampling jitter. Namely, a small sampling offset ε produces the output sample

$$y(kT + \varepsilon) = \sum_i A_i \frac{\sin[\pi(k - i + \varepsilon/T)]}{\pi(k - i + \varepsilon/T)} \tag{4.16}$$

Since the Nyquist pulse decays as $1/t$, this sum is not guaranteed to converge. A particular choice of symbols $\{A_i\}$ can, therefore, lead to very large intersymbol interference, no matter how small the offset. Minimum bandwidth signalling is therefore impractical.

The preceding problem is generally solved in one of two ways in practice:

1. The pulse bandwidth is increased to provide a faster pulse decay than $1/t$.
2. A *controlled* amount of intersymbol interference is introduced at the transmitter, which can be subtracted out at the receiver.

The former approach sacrifices bandwidth efficiency, whereas the latter approach sacrifices power efficiency. We will examine the latter approach in Section 4.5. The most common example of a pulse, which illustrates the first technique, is the **raised cosine pulse**, given by

$$h(t) = \left[\frac{\sin(\pi t/T)}{\pi t/T}\right]\left[\frac{\cos(\alpha\pi t/T)}{1 - (2\alpha t/T)^2}\right] \tag{4.17}$$

which has Fourier transform

$$H(f) = \begin{cases} T & 0 \le |f| \le \dfrac{1-\alpha}{2T} \\ \dfrac{T}{2}\left\{1 + \cos\left[\dfrac{\pi T}{\alpha}\left(|f| - \dfrac{1-\alpha}{2T}\right)\right]\right\} & \dfrac{1-\alpha}{2T} \le |f| \le \dfrac{1+\alpha}{2T} \\ 0 & |f| > \dfrac{1+\alpha}{2T} \end{cases} \tag{4.18}$$

where $0 \le \alpha \le 1$.

Plots of $p(t)$ and $P(f)$ are shown in Figs. 4.6a, and 4.6b for different values of α. It is easily verified that $h(t)$ satisfies the Nyquist criterion (4.7) and, consequently, $H(f)$ satisfies Eq. (4.11). When $\alpha = 0$, $H(f)$ is the Nyquist pulse with minimum bandwidth $1/(2T)$, and when $\alpha > 0, H(f)$ has bandwidth $(1+\alpha)/(2T)$ with a raised cosine rolloff. The parameter α, therefore, represents the additional, or **excess bandwidth** as a fraction of the minimum bandwidth $1/(2T)$. For example, when $\alpha = 1$, we say that the pulse is a raised cosine pulse with 100% excess bandwidth. This is because the pulse bandwidth $1/T$ is twice the minimum bandwidth. Because the raised cosine pulse decays as $1/t^3$, performance is robust with respect to sampling offsets.

The raised cosine frequency response (4.18) applies to the combination of transmitter, channel, and receiver. If the transmitted pulse shape $p(t)$ is a raised cosine pulse, then $h(t)$ is a raised cosine pulse only if the combined receiver and channel frequency response is constant. Even with an ideal (transparent) channel, however, the optimum (matched) receiver filter response is generally not constant in the presence of additive Gaussian noise. An alternative is to transmit the *square-root raised cosine* pulse shape, which has frequency response $P(f)$ given by the square-root of the raised cosine frequency response in Eq. (4.18). Assuming an ideal channel, setting the receiver frequency response $R(f) = P(f)$ then results in an overall raised cosine system response $H(f)$.

4.3 Nyquist Criterion with Matched Filtering

Consider the transmission of an isolated pulse $A_0\delta(t)$. In this case the input to the receiver in Fig. 4.3 is

$$x(t) = A_0\tilde{g}(t) + n(t) \tag{4.19}$$

where $\tilde{g}(t)$ is the inverse Fourier transform of the combined transmitter-channel transfer function $\tilde{G}(f) = P(f)G(f)$. We will assume that the noise $n(t)$ is white with spectrum $N_0/2$. The output of the receiver filter is then

$$y(t) = r(t) * x(t) = A_0[r(t) * \tilde{g}(t)] + [r(t) * n(t)] \tag{4.20}$$

The first term on the right-hand side is the desired signal, and the second term is noise. Assuming that $y(t)$ is sampled at $t = 0$, the ratio of signal energy to noise energy, or signal-to-noise ratio (SNR) at the sampling instant, is

$$SNR = \frac{E\left[|A_0|^2\right]\left|\displaystyle\int_{-\infty}^{\infty} r(-t)\tilde{g}(t)\,\mathrm{d}t\right|^2}{\dfrac{N_0}{2}\displaystyle\int_{-\infty}^{\infty}|r(t)|^2\,\mathrm{d}t} \tag{4.21}$$

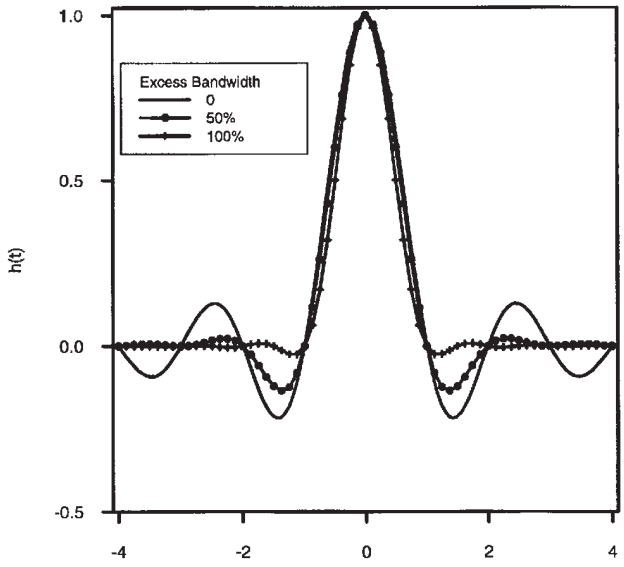


Figure 4.6a Raised cosine pulse.

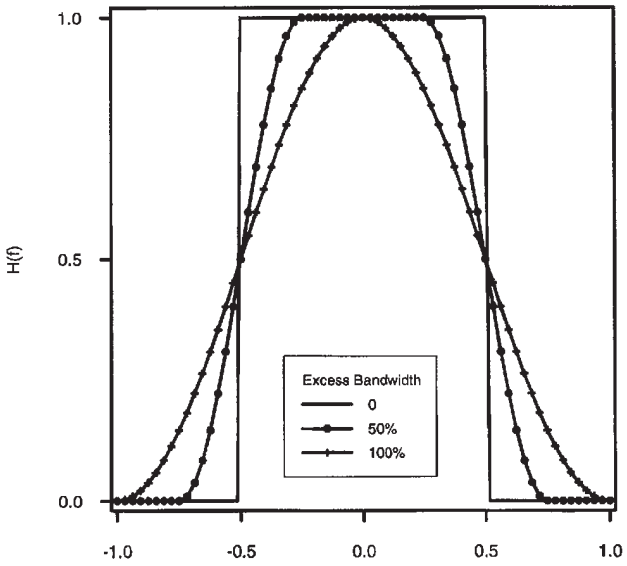


Figure 4.6b Raised cosine spectrum.

The receiver impulse response that maximizes this expression is $r(t) = \tilde{g}^*(-t)$ [complex conjugate of $\tilde{g}(-t)$], which is known as the **matched filter** impulse response. The associated transfer function is $R(f) = \tilde{G}^*(f)$.

Choosing the receiver filter to be the matched filter is optimal in more general situations, such as when detecting a sequence of channel symbols with intersymbol interference (assuming the additive noise is Gaussian). We, therefore, reconsider the Nyquist criterion when the receiver filter is the matched filter. In this case, the baseband model is shown in Fig. 4.7, and the output of the receiver filter is given by

$$y(t) = \sum_i A_i h(t - iT) + \tilde{n}(t) \tag{4.22}$$

where the baseband pulse $h(t)$ is now the impulse response of the filter with transfer function $|\tilde{G}(f)|^2 = |P(f)G(f)|^2$. This impulse response is the *autocorrelation* of the impulse response of the combined transmitter-channel filter $\tilde{G}(f)$,

$$h(t) = \int_{-\infty}^{\infty} \tilde{g}^*(s)\tilde{g}(s+t)\,\mathrm{d}s \tag{4.23}$$

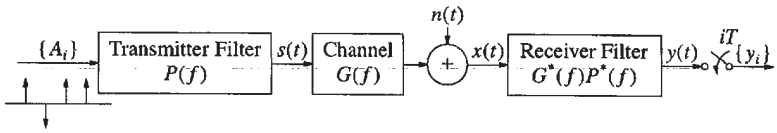


FIGURE 4.7 Baseband PAM model with a matched filter at the receiver.

With a matched filter at the receiver, the equivalent discrete-time transfer function is

$$\begin{aligned} H_{\mathrm{eq}}(e^{j2\pi fT}) &= \frac{1}{T}\sum_k \left|\tilde{G}\left(f-\frac{k}{T}\right)\right|^2 \\ &= \frac{1}{T}\sum_k \left|P\left(f-\frac{k}{T}\right)G\left(f-\frac{k}{T}\right)\right|^2 \end{aligned} \tag{4.24}$$

which relates the sequence of transmitted symbols $\{A_k\}$ to the sequence of received samples $\{y_k\}$ in the absence of noise. Note that $H_{\mathrm{eq}}(e^{j2\pi fT})$ is positive, real valued, and an even function of f. If the channel is bandlimited to twice the Nyquist bandwidth, then $H(f) = 0$ for $|f| > 1/T$, and the Nyquist condition is given by Eq. (4.14) where $H(f) = |G(f)P(f)|^2$. The aliasing sum in Eq. (4.10b) can therefore be described as a folding operation in which the channel response $|H(f)|^2$ is folded around the Nyquist frequency $1/(2T)$. For this reason, $H_{\mathrm{eq}}(e^{j2\pi fT})$ with a matched receiver filter is often referred to as the folded channel spectrum.

4.4 Eye Diagrams

One way to assess the severity of distortion due to intersymbol interference in a digital communications system is to examine the **eye diagram**. The eye diagram is illustrated in Figs. 4.8a and 4.8b, for a raised cosine pulse shape with 25% excess bandwidth and an ideal bandlimited channel. Figure 4.8a shows the data signal at the receiver

$$y(t) = \sum_i A_i h(t-iT) + \tilde{n}(t) \tag{4.25}$$

where $h(t)$ is given by Eq. (4.17), $\alpha = 1/4$, each symbol A_i is independently chosen from the set $\{\pm 1, \pm 3\}$, where each symbol is equally likely, and $\tilde{n}(t)$ is bandlimited white Gaussian noise. (The received SNR is 30 dB.) The eye diagram is constructed from the time-domain data signal $y(t)$ as follows (assuming nominal sampling times at $kT, k = 0, 1, 2, \ldots$):

1. Partition the waveform $y(t)$ into successive segments of length T starting from $t = T/2$.
2. Translate each of these waveform segments $[y(t),\ (k+1/2)T \le t \le (k+3/2)T,$ $k = 0, 1, 2, \ldots]$ to the interval $[-T/2, T/2]$, and superimpose.

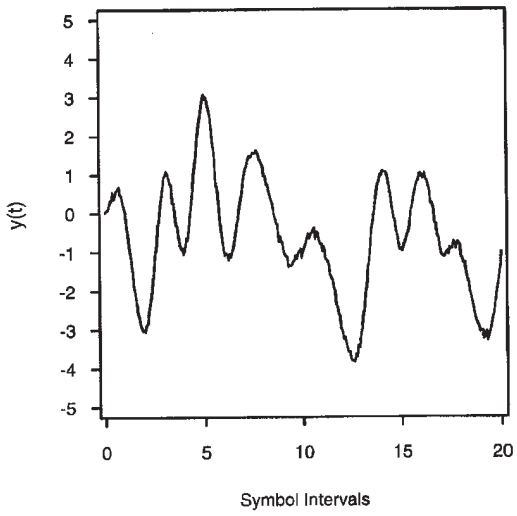


Figure 4.8a Received signal $y(t)$.

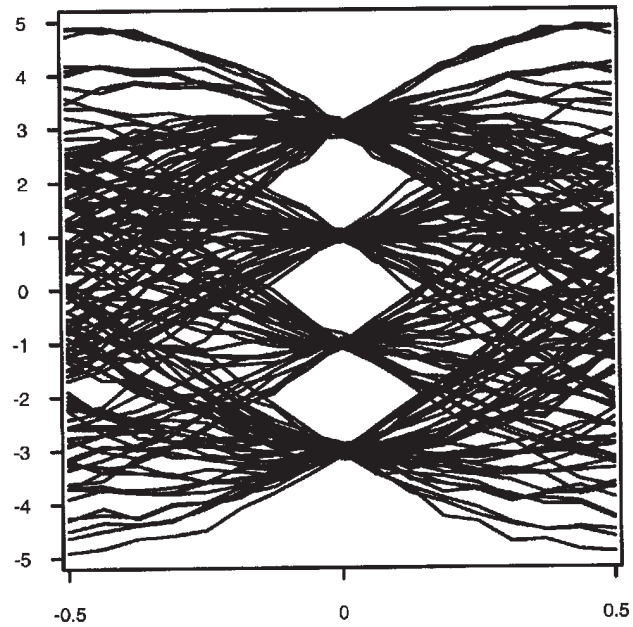


Figure 4.8b Eye diagram for received signal shown in Fig. 4.8a.

The resulting picture is shown in Fig. 4.8b for the $y(t)$ shown in Fig. 4.8a. (Partitioning $y(t)$ into successive segments of length iT, $i > 1$, is also possible. This would result in i successive eye diagrams.) The number of eye openings is one less than the number of transmitted signal levels. In practice, the eye diagram is easily viewed on an oscilloscope by applying the received waveform $y(t)$ to the vertical deflection plates of the oscilloscope and applying a sawtooth waveform at the symbol rate $1/T$ to the horizontal deflection plates. This causes successive symbol intervals to be translated into one interval on the oscilloscope display.

Each waveform segment $y(t)$, $(k + 1/2)T \leq t \leq (k + 3/2)T$, depends on the particular sequence of channel symbols surrounding A_k. The number of channel symbols that affects a

particular waveform segment depends on the extent of the intersymbol interference, shown in Eq. (4.6). This, in turn, depends on the duration of the impulse response $h(t)$. For example, if $h(t)$ has most of its energy in the interval $0 < t < mT$, then each waveform segment depends on approximately m symbols. Assuming binary transmission, this implies that there are a total of 2^m waveform segments that can be superimposed in the eye diagram. (It is possible that only one sequence of channel symbols causes significant intersymbol interference, and this sequence occurs with very low probability.) In current digital wireless applications the impulse response typically spans only a few symbols.

The eye diagram has the following important features which measure the performance of a digital communications system.

4.4.1 Vertical Eye Opening

The vertical openings at any time t_0, $-T/2 \leq t_0 \leq T/2$, represent the separation between signal levels with worst-case intersymbol interference, assuming that $y(t)$ is sampled at times $t = kT + t_0$, $k = 0, 1, 2, \ldots$. It is possible for the intersymbol interference to be large enough so that this vertical opening between some, or all, signal levels disappears altogether. In that case, the eye is said to be closed. Otherwise, the eye is said to be open. A closed eye implies that if the estimated bits are obtained by thresholding the samples $y(kT)$, then the decisions will depend primarily on the intersymbol interference rather than on the desired symbol. The probability of error will, therefore, be close to $1/2$. Conversely, wide vertical spacings between signal levels imply a large degree of immunity to additive noise. In general, $y(t)$ should be sampled at the times $kT + t_0$, $k = 0, 1, 2, \ldots$, where t_0 is chosen to maximize the vertical eye opening.

4.4.2 Horizontal Eye Opening

The width of each opening indicates the sensitivity to timing offset. Specifically, a very narrow eye opening indicates that a small timing offset will result in sampling where the eye is closed. Conversely, a wide horizontal opening indicates that a large timing offset can be tolerated, although the error probability will depend on the vertical opening.

4.4.3 Slope of the Inner Eye

The slope of the inner eye indicates sensitivity to timing jitter or variance in the timing offset. Specifically, a very steep slope means that the eye closes rapidly as the timing offset increases. In this case, a significant amount of jitter in the sampling times significantly increases the probability of error.

The shape of the eye diagram is determined by the pulse shape. In general, the faster the baseband pulse decays, the wider the eye opening. For example, a rectangular pulse produces a box-shaped eye diagram (assuming binary signalling). The minimum bandwidth pulse shape Eq. (4.12) produces an eye diagram which is closed for all t except for $t = 0$. This is because, as shown earlier, an arbitrarily small timing offset can lead to an intersymbol interference term that is arbitrarily large, depending on the data sequence.

4.5 Partial-Response Signalling

To avoid the problems associated with Nyquist signalling over an ideal bandlimited channel, bandwidth and/or power efficiency must be compromised. Raised cosine pulses compromise

bandwidth efficiency to gain robustness with respect to timing errors. Another possibility is to introduce a controlled amount of intersymbol interference at the transmitter, which can be removed at the receiver. This approach is called **partial-response (PR) signalling**. The terminology reflects the fact that the sampled system impulse response does not have the full response given by the Nyquist condition Eq. (4.7).

To illustrate PR signalling, suppose that the Nyquist condition Eq. (4.7) is replaced by the condition

$$h_k = \begin{cases} 1 & k = 0, 1 \\ 0 & \text{all other } k \end{cases} \tag{4.26}$$

The kth received sample is then

$$y_k = A_k + A_{k-1} + \tilde{n}_k \tag{4.27}$$

so that there is intersymbol interference from one neighboring transmitted symbol. For now we focus on the spectral characteristics of PR signalling and defer discussion of how to detect the transmitted sequence $\{A_k\}$ in the presence of intersymbol interference. The equivalent discrete-time transfer function in this case is the discrete Fourier transform of the sequence in Eq. (4.26),

$$\begin{aligned} H_{\text{eq}}(e^{j2\pi fT}) &= \frac{1}{T}\sum_k H\left(f + \frac{k}{T}\right) \\ &= 1 + e^{-j2\pi fT} = 2e^{-j\pi fT}\cos(\pi fT) \end{aligned} \tag{4.28}$$

As in the full-response case, for Eq. (4.28) to be satisfied, the *minimum* bandwidth of the channel $G(f)$ and transmitter filter $P(f)$ is $W = 1/(2T)$. Assuming $P(f)$ has this minimum bandwidth implies

$$H(f) = \begin{cases} 2Te^{-j\pi fT}\cos(\pi fT) & |f| < 1/(2T) \\ 0 & |f| > 1/(2T) \end{cases} \tag{4.29a}$$

and

$$h(t) = T\{\ \text{sinc}\ (t/T) + \ \text{sinc}\ [(t-T)/T]\} \tag{4.29b}$$

where sinc $x = (\sin \pi x)/(\pi x)$. This pulse is called a *duobinary* pulse and is shown along with the associated $H(f)$ in Fig. 4.9. [Notice that $h(t)$ satisfies Eq. (4.26).] Unlike the ideal bandlimited frequency response, the transfer function $H(f)$ in Eq. (4.29a) is continuous and is, therefore, easily approximated by a physically realizable filter. Duobinary PR was first proposed by Lender, [7], and later generalized by Kretzmer, [6].

The main advantage of the duobinary pulse Eq. (4.29b), relative to the minimum bandwidth pulse Eq. (4.12), is that signalling at the Nyquist symbol rate is feasible with zero excess bandwidth. Because the pulse decays much more rapidly than a Nyquist pulse, it is robust with respect to timing errors. Selecting the transmitter and receiver filters so that the overall system response is duobinary is appropriate in situations where the channel frequency response $G(f)$ is near zero or has a rapid rolloff at the Nyquist band edge $f = 1/(2T)$.

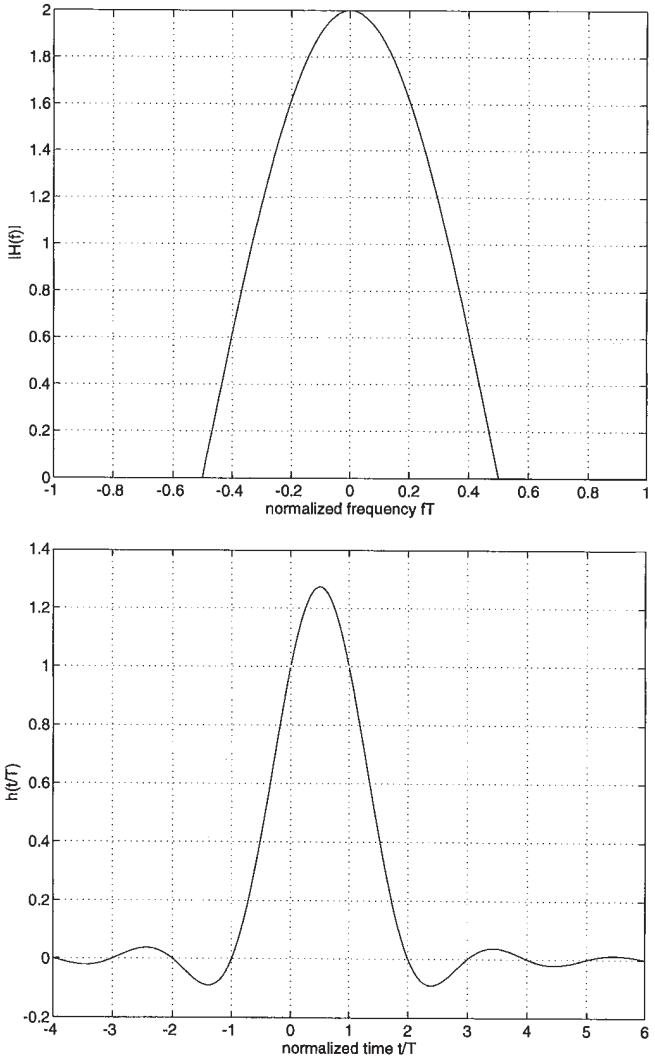


FIGURE 4.9 Duobinary frequency response and minimum bandwidth pulse.

As another example of PR signalling, consider the *modified* duobinary partial response

$$h_k = \begin{cases} 1 & k = -1 \\ -1 & k = 1 \\ 0 & \text{all other } k \end{cases} \tag{4.30}$$

which has equivalent discrete-time transfer function

$$\begin{aligned} H_{\text{eq}}\left(e^{j2\pi fT}\right) &= e^{j2\pi fT} - e^{-j2\pi fT} \\ &= j2\sin(2\pi fT) \end{aligned} \tag{4.31}$$

With zero excess bandwidth, the overall system response is

$$H(f) = \begin{cases} j2T\sin(2\pi fT) & |f| < 1/(2T) \\ 0 & |f| > 1/(2T) \end{cases} \tag{4.32a}$$

and

$$h(t) = T\{\text{sinc } [(t+T)/T] - \text{sinc } [(t-T)/T]\} \tag{4.32b}$$

These functions are plotted in Fig. 4.10. This pulse shape is appropriate when the channel response $G(f)$ is near zero at both DC ($f = 0$) and at the Nyquist band edge. This is often the case for wire (twisted-pair) channels where the transmitted signal is coupled to the channel through a transformer. Like duobinary PR, modified duobinary allows minimum bandwidth signalling at the Nyquist rate.

A particular partial response is often identified by the polynomial

$$\sum_{k=0}^{K} h_k D^k$$

where D (for delay) takes the place of the usual z^{-1} in the z transform of the sequence $\{h_k\}$. For example, duobinary is also referred to as $1 + D$ partial response.

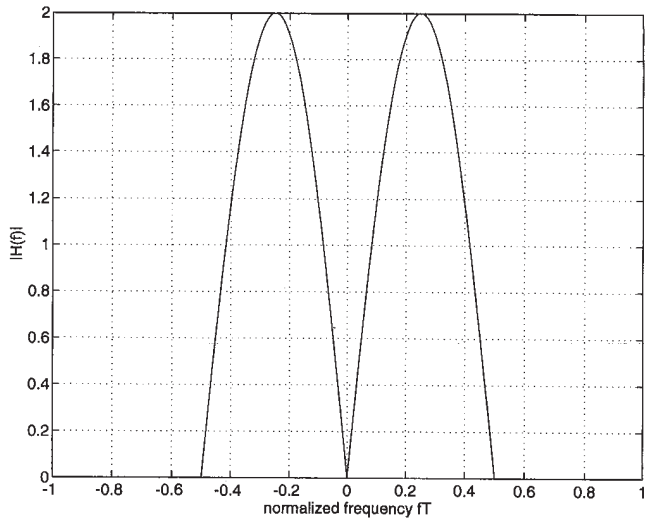
In general, more complicated system responses than those shown in Figs. 4.9 and 4.10 can be generated by choosing more nonzero coefficients in the sequence $\{h_k\}$. This complicates detection, however, because of the additional intersymbol interference that is generated.

Rather than modulating a PR pulse $h(t)$, a PR signal can also be generated by filtering the sequence of transmitted levels $\{A_i\}$. This is shown in Fig. 4.11. Namely, the transmitted levels are first passed through a discrete-time (digital) filter with transfer function $P_d(e^{j2\pi fT})$ (where the subscript d indicates discrete). [Note that $P_d(e^{j2\pi fT})$ can be selected to be $H_{\text{eq}}(e^{j2\pi fT})$.] The outputs of this filter form the PAM signal, where the pulse shaping filter $P(f) = 1$, $|f| < 1/(2T)$ and is zero elsewhere. If the transmitted levels $\{A_k\}$ are selected independently and are identically distributed, then the transmitted spectrum is $\sigma_A^2|P_d(e^{j2\pi fT})|^2$ for $|f| < 1/(2T)$ and is zero for $|f| > 1/(2T)$, where $\sigma_A^2 = E[|A_k|^2]$.

Shaping the transmitted spectrum to have nulls coincident with nulls in the channel response potentially offers significant performance advantages. By introducing intersymbol interference, however, PR signalling increases the number of received signal levels, which increases the complexity of the detector and may reduce immunity to noise. For example, the set of received signal levels for duobinary signalling is $\{0, \pm 2\}$ from which the transmitted levels $\{\pm 1\}$ must be estimated. The performance of a particular PR scheme depends on the channel characteristics, as well as the type of detector used at the receiver. We now describe a simple suboptimal detection strategy.

4.5.1 Precoding

Consider the received signal sample Eq. (4.27) with duobinary signalling. If the receiver has correctly decoded the symbol A_{k-1}, then in the absence of noise A_k can be decoded by subtracting A_{k-1} from the received sample y_k. If an error occurs, however, then subtracting the preceding symbol estimate from the received sample will cause the error to propagate to successive detected symbols. To avoid this problem, the transmitted levels can be **precoded** in such a way as to compensate for the intersymbol interference introduced by the overall partial response.



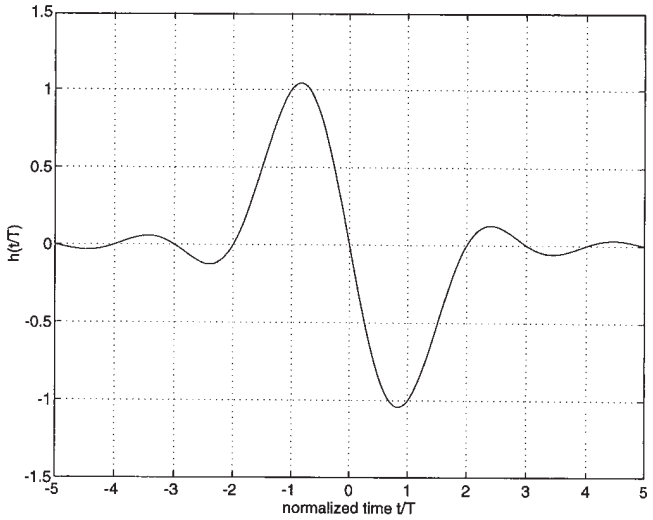


FIGURE 4.10 Modified duobinary frequency response and minimum bandwidth pulse.

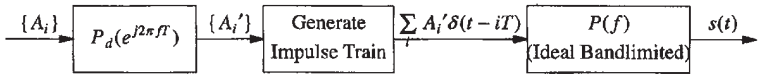


FIGURE 4.11 Generation of PR signal.

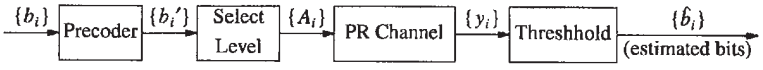


FIGURE 4.12 Precoding for a PR channel.

We first illustrate precoding for duobinary PR. The sequence of operations is illustrated in Fig. 4.12. Let $\{b_k\}$ denote the sequence of source bits where $b_k \in \{0, 1\}$. This sequence is transformed to the sequence $\{b'_k\}$ by the operation

$$b'_k = b_k \oplus b'_{k-1} \tag{4.33}$$

TABLE 4.1 Example of Precoding for Duobinary PR.

$\{b_i\}$:		1	0	0	1	1	1	0	0	1	0
$\{b'_i\}$:	0	1	1	1	0	1	0	0	0	1	1
$\{A_i\}$:	−1	1	1	1	−1	1	−1	−1	−1	1	1
$\{y_i\}$:		0	2	2	0	0	0	−2	−2	0	2

where $\oplus$ denotes modulo 2 addition (exclusive OR). The sequence $\{b'_k\}$ is mapped to the sequence of binary transmitted signal levels $\{A_k\}$ according to

$$A_k = 2b'_k - 1 \tag{4.34}$$

That is, $b'_k = 0$ ($b'_k = 1$) is mapped to the transmitted level $A_k = -1$ ($A_k = 1$). In the absence of noise, the received symbol is then

$$y_k = A_k + A_{k-1} = 2\left(b'_k + b'_{k-1} - 1\right) \tag{4.35}$$

and combining Eqs. (4.33) and (4.35) gives

$$b_k = \left(\frac{1}{2}y_k + 1\right) \bmod 2 \tag{4.36}$$

That is, if $y_k = \pm 2$, then $b_k = 0$, and if $y_k = 0$, then $b_k = 1$. Precoding, therefore, enables the detector to make *symbol-by-symbol* decisions that do not depend on previous decisions. Table 4.1 shows a sequence of transmitted bits $\{b_i\}$, precoded bits $\{b'_i\}$, transmitted signal levels $\{A_i\}$, and received samples $\{y_i\}$.

The preceding precoding technique can be extended to multilevel PAM and to other PR channels. Suppose that the PR is specified by

$$H_{\text{eq}}(D) = \sum_{k=0}^{K} h_k D^k$$

where the coefficients are integers and that the source symbols $\{b_k\}$ are selected from the set $\{0, 1, \ldots, M-1\}$. These symbols are transformed to the sequence $\{b'_k\}$ via the precoding operation

$$b'_k = \left(b_k - \sum_{i=1}^{K} h_i b'_{k-i}\right) \bmod M \tag{4.37}$$

Because of the modulo operation, each symbol b'_k is also in the set $\{0, 1, \ldots, M-1\}$. The kth transmitted signal level is given by

$$A_k = 2b'_k - (M-1) \tag{4.38}$$

so that the set of transmitted levels is $\{-(M-1), \ldots, (M-1)\}$ (i.e., a shifted version of the set of values assumed by b_k). In the absence of noise the received sample is

$$y_k = \sum_{i=0}^{K} h_i A_{k-i} \tag{4.39}$$

and it can be shown that the kth source symbol is given by

$$b_k = \frac{1}{2}\left(y_k + (M-1) \cdot H_{\text{eq}}(1)\right) \bmod M \tag{4.40}$$

Precoding the symbols $\{b_k\}$ in this manner, therefore, enables symbol-by-symbol decisions at the receiver. In the presence of noise, more sophisticated detection schemes (e.g., maximum likelihood) can be used with PR signalling to obtain improvements in performance.

4.6 Additional Considerations

In many applications, bandwidth and intersymbol interference are not the only important considerations for selecting baseband pulses. Here we give a brief discussion of additional practical constraints that may influence this selection.

4.6.1 Average Transmitted Power and Spectral Constraints

The constraint on average transmitted power varies according to the application. For example, low-average power is highly desirable for mobile wireless applications that use battery-powered transmitters. In many applications (e.g., digital subscriber loops, as well as digital radio), constraints are imposed to limit the amount of interference, or crosstalk, radiated into neighboring receivers and communications systems. Because this type of interference is frequency dependent, the constraint may take the form of a spectral mask that specifies the maximum allowable transmitted power as a function of frequency. For example, crosstalk in wireline channels is generally caused by capacitive coupling and increases as a function of frequency. Consequently, to reduce the amount of crosstalk generated at a particular transmitter, the pulse shaping filter generally attenuates high frequencies more than low frequencies.

In radio applications where signals are assigned different frequency bands, constraints on the transmitted spectrum are imposed to limit *adjacent-channel interference*. This interference is generated by transmitters assigned to adjacent frequency bands. Therefore, a constraint is needed to limit the amount of *out-of-band power* generated by each transmitter, in addition to an overall average power constraint. To meet this constraint, the transmitter filter in Fig. 4.3 must have a sufficiently steep rolloff at the edges of the assigned frequency band. (Conversely, if the transmitted signals are time multiplexed, then the duration of the system impulse response must be contained within the assigned time slot.)

4.6.2 Peak-to-Average Power

In addition to a constraint on average transmitted power, a *peak-power* constraint is often imposed as well. This constraint is important in practice for the following reasons:

1. The dynamic range of the transmitter is limited. In particular, saturation of the output amplifier will "clip" the transmitted waveform.
2. Rapid fades can severely distort signals with high peak-to-average power.
3. The transmitted signal may be subjected to nonlinearities. Saturation of the output amplifier is one example. Another example that pertains to wireline applications is the companding process in the voice telephone network [5]. Namely, the compander used to reduce quantization noise for pulse-code modulated voice signals introduces amplitude-dependent distortion in data signals.

The preceding impairments or constraints indicate that the transmitted waveform should have a low **peak-to-average power ratio (PAR)**. For a transmitted waveform $x(t)$, the PAR is defined as

$$\text{PAR} = \frac{\max |x(t)|^2}{E\{|x(t)|^2\}}$$

where $E(\cdot)$ denotes expectation. Using binary signalling with rectangular pulse shapes minimizes the PAR. However, this compromises bandwidth efficiency. In applications where PAR

should be low, binary signalling with rounded pulses are often used. Operating RF power amplifiers with power back-off can also reduce PAR, but leads to inefficient amplification.

For an **orthogonal frequency division multiplexing (OFDM)** system, it is well known that the transmitted signal can exhibit a very high PAR compared to an equivalent single-carrier system. Hence more sophisticated approaches to PAR reduction are required for OFDM. Some proposed approaches are described in [8] and references therein. These include altering the set of transmitted symbols and setting aside certain OFDM tones specifically to minimize PAR.

4.6.3 Channel and Receiver Characteristics

The type of channel impairments encountered and the type of detection scheme used at the receiver can also influence the choice of a transmitted pulse shape. For example, a constant amplitude pulse is appropriate for a fast fading environment with noncoherent detection. The ability to track channel characteristics, such as phase, may allow more bandwidth efficient pulse shapes in addition to multilevel signalling.

High-speed data communications over time-varying channels requires that the transmitter and/or receiver adapt to the changing channel characteristics. Adapting the transmitter to compensate for a time-varying channel requires a feedback channel through which the receiver can notify the transmitter of changes in channel characteristics. Because of this extra complication, adapting the receiver is often preferred to adapting the transmitter pulse shape. However, the following examples are notable exceptions.

1. The current IS-95 air interface for direct-sequence code-division multiple access adapts the transmitter power to control the amount of interference generated and to compensate for channel fades. This can be viewed as a simple form of adaptive transmitter pulse shaping in which a single parameter associated with the pulse shape is varied.
2. Multitone modulation divides the channel bandwidth into small subbands, and the transmitted power and source bits are distributed among these subbands to maximize the information rate. The received signal-to-noise ratio for each subband must be transmitted back to the transmitter to guide the allocation of transmitted bits and power [1].

In addition to multitone modulation, *adaptive precoding* (also known as Tomlinson–Harashima precoding [4, 11]) is another way in which the transmitter can adapt to the channel frequency response. Adaptive precoding is an extension of the technique described earlier for partial-response channels. Namely, the equivalent discrete-time channel impulse response is measured at the receiver and sent back to the transmitter, where it is used in a precoder. The precoder compensates for the intersymbol interference introduced by the channel, allowing the receiver to detect the data by a simple threshhold operation. Both multitone modulation and precoding have been used with wireline channels (voiceband modems and digital subscriber loops).

4.6.4 Complexity

Generation of a bandwidth-efficient signal requires a filter with a sharp cutoff. In addition, bandwidth-efficient pulse shapes can complicate other system functions, such as timing and carrier recovery. If sufficient bandwidth is available, the cost can be reduced by using a rectangular pulse shape with a simple detection strategy (low-pass filter and threshold).

4.6.5 Tolerance to Interference

Interference is one of the primary channel impairments associated with digital radio. In addition to adjacent-channel interference described earlier, *cochannel interference* may be generated by other transmitters assigned to the same frequency band as the desired signal. Cochannel interference can be controlled through frequency (and perhaps time slot) assignments and by pulse shaping. For example, assuming fixed average power, increasing the bandwidth occupied by the signal lowers the power spectral density and decreases the amount of interference into a narrowband system that occupies part of the available bandwidth. Sufficient bandwidth spreading, therefore, enables wideband signals to be overlaid on top of narrowband signals without disrupting either service.

4.6.6 Probability of Intercept and Detection

The broadcast nature of wireless channels generally makes eavesdropping easier than for wired channels. A requirement for most commercial, as well as military applications, is to guarantee the privacy of user conversations (low probability of intercept). An additional requirement, in some applications, is that determining whether or not communications is taking place must be difficult (low probability of detection). Spread-spectrum waveforms are attractive in these applications since spreading the pulse energy over a wide frequency band decreases the power spectral density and, hence, makes the signal less visible. Power-efficient modulation combined with coding enables a further reduction in transmitted power for a target error rate.

4.7 Examples

We conclude this chapter with a brief description of baseband pulse shapes used in existing and emerging standards for digital mobile cellular and Personal Communications Services (PCS).

4.7.1 Global System for Mobile Communications (GSM)

The European GSM standard for digital mobile cellular communications operates in the 900-MHz frequency band, and is based on time-division multiple access (TDMA) [9]. The U.S. version operates at 1900 MHz, and is called PCS-1900. A special variant of binary FSK is used called *Gaussian minimum-shift keying (GMSK)*. The GMSK modulator is illustrated in Fig. 4.13. The input to the modulator is a binary PAM signal $s(t)$, given by Eq. (4.3), where the pulse $p(t)$ is a Gaussian function and $|s(t)| < 1$. This waveform frequency modulates the carrier f_c, so that the (passband) transmitted signal is

$$w(t) = K\cos\left[2\pi f_c t + 2\pi f_d \int_{-\infty}^{t} s(\tau)\,\mathrm{d}\tau\right]$$

The maximum frequency deviation from the carrier is $f_d = 1/(2T)$, which characterizes minimum-shift keying. This technique can be used with a noncoherent receiver that is easy to implement. Because the transmitted signal has a constant envelope, the data can be reliably detected in the presence of rapid fades that are characteristic of mobile radio channels.



FIGURE 4.13 Generation of GMSK signal; LPF is low-pass filter.

4.7.2 U.S. Digital Cellular (IS-136)

The IS-136 air interface (formerly IS-54) operates in the 800 MHz band and is based on TDMA [3]. There is also a 1900 MHz version of IS-136. The baseband signal is given by Eq. (4.3) where the symbols are complex-valued, corresponding to quadrature phase modulation. The pulse has a square-root raised cosine spectrum with 35% excess bandwidth.

4.7.3 Interim Standard-95

The IS-95 air interface for digital mobile cellular uses spread-spectrum signalling (CDMA) in the 800-MHz band [10]. There is also a 1900 MHz version of IS-95. The baseband transmitted pulse shapes are analogous to those shown in Fig. 4.2, where the number of square pulses (chips) per bit is 128. To improve spectral efficiency the (wideband) transmitted signal is filtered by an approximation to an ideal low-pass response with a small amount of excess bandwidth. This shapes the chips so that they resemble minimum bandwidth pulses.

4.7.4 Personal Access Communications System (PACS)

Both PACS and the Japanese personal handy phone (PHP) system are TDMA systems which have been proposed for personal communications systems (PCS), and operate near 2 GHz [2]. The baseband signal is given by Eq. (4.3) with four complex symbols representing four-phase quadrature modulation. The baseband pulse has a square-root raised cosine spectrum with 50% excess bandwidth.

Defining Terms

Baseband signal: A signal with frequency content centered around DC.

Equivalent discrete-time transfer function: A discrete-time transfer function (z transform) that relates the transmitted amplitudes to received samples in the absence of noise.

Excess bandwidth: That part of the baseband transmitted spectrum which is not contained within the Nyquist band.

Eye diagram: Superposition of segments of a received PAM signal that indicates the amount of intersymbol interference present.

Frequency-shift keying: A digital modulation technique in which the transmitted pulse is sinusoidal, where the frequency is determined by the source bits.

Intersymbol interference: The additive contribution (interference) to a received sample from transmitted symbols other than the symbol to be detected.

Matched filter: The receiver filter with impulse response equal to the time-reversed, complex conjugate impulse response of the combined transmitter filter-channel impulse response.

Nyquist band: The narrowest frequency band that can support a PAM signal without intersymbol interference (the interval $[-1/(2T), 1/(2T)]$ where $1/T$ is the symbol rate).

Nyquist criterion: A condition on the overall frequency response of a PAM system that ensures the absence of intersymbol interference.

Orthogonal frequency division multiplexing (OFDM): Modulation technique in which the transmitted signal is the sum of low-bit-rate narrowband digital signals modulated on orthogonal carriers.

Partial-response signalling: A signalling technique in which a controlled amount of intersymbol interference is introduced at the transmitter in order to shape the transmitted spectrum.

Precoding: A transformation of source symbols at the transmitter that compensates for intersymbol interference introduced by the channel.

Pulse amplitude modulation (PAM): A digital modulation technique in which the source bits are mapped to a sequence of amplitudes that modulate a transmitted pulse.

Raised cosine pulse: A pulse shape with Fourier transform that decays to zero according to a raised cosine; see Eq. (4.18). The amount of excess bandwidth is conveniently determined by a single parameter (α).

Spread spectrum: A signalling technique in which the pulse bandwidth is many times wider than the Nyquist bandwidth.

Zero-forcing criterion: A design constraint which specifies that intersymbol interference be eliminated.

References

[1] Bingham, J.A.C., Multicarrier modulation for data transmission: an idea whose time has come. *IEEE Commun. Mag.*, 28(May), 5–14, 1990.

[2] Cox, D.C., Wireless personal communications: what is it? *IEEE Personal Comm.*, 2(2), 20–35, 1995.

[3] Electronic Industries Association/Telecommunications Industry Association. Recommended minimum performance standards for 800 MHz dual-mode mobile stations. Incorp. EIA/TIA 19B, EIA/TIA Project No. 2216, Mar.,1991

[4] Harashima, H. and Miyakawa, H., Matched-transmission technique for channels with intersymbol interference. *IEEE Trans. on Commun.*, COM-20(Aug.), 774–780, 1972.

[5] Kalet, I. and Saltzberg, B.R., QAM transmission through a companding channel—signal constellations and detection. *IEEE Trans. on Comm.*, 42(2–4), 417–429, 1994.

[6] Kretzmer, E.R., Generalization of a technique for binary data communication. *IEEE Trans. Comm. Tech.*, COM-14 (Feb.), 67, 68, 1966.

[7] Lender, A., The duobinary technique for high-speed data Transmission. *AIEE Trans. on Comm. Electronics*, 82 (March), 214–218, 1963.

[8] Muller, S.H. and Huber, J.B., A comparison of peak power reduction schemes for OFDM. *Proc. GLOBECOM '97*, (Mon.), 1–5, 1997.

[9] Rahnema, M., Overview of the GSM system and protocol architecture. *IEEE Commun. Mag.*, (April), 92–100, 1993.

[10] Telecommunication Industry Association. Mobile station-base station compatibility standard for dual-mode wideband spread spectrum cellular system. TIA/EIA/IS-95-A. May, 1995.

[11] Tomlinson, M., New automatic equalizer employing modulo arithmetic. *Electron. Lett.*, 7 (March), 138, 139, 1971.

Further Information

Baseband signalling and pulse shaping is fundamental to the design of any digital communications system and is, therefore, covered in numerous texts on digital communications. For more advanced treatments see E.A. Lee and D.G. Messerschmitt, *Digital Communication*, Kluwer 1994, and J.G. Proakis, *Digital Communications*, McGraw-Hill 1995.

5

Channel Equalization

5.1 Characterization of Channel Distortion 5-1
5.2 Characterization of Intersymbol Interference 5-2
5.3 Linear Equalizers 5-9
Adaptive Linear Equalizers
5.4 Decision-Feedback Equalizer 5-18
5.5 Maximum-Likelihood Sequence Detection 5-21
5.6 Conclusions 5-22
Defining Terms 5-24
References 5-24
Further Information 5-24

John G. Proakis
Northeastern University

5.1 Characterization of Channel Distortion

Many communication channels, including telephone channels, and some radio channels, may be generally characterized as band-limited linear filters. Consequently, such channels are described by their frequency response $C(f)$, which may be expressed as

$$C(f) = A(f)e^{j\theta(f)} \tag{5.1}$$

where $A(f)$ is called the *amplitude response* and $\theta(f)$ is called the *phase response.* Another characteristic that is sometimes used in place of the phase response is the *envelope delay* or *group delay,* which is defined as

$$\tau(f) = -\frac{1}{2\pi}\frac{\mathrm{d}\theta(f)}{\mathrm{d}f} \tag{5.2}$$

A channel is said to be nondistorting or ideal if, within the bandwidth W occupied by the transmitted signal, $A(f) = \text{const}$ and $\theta(f)$ is a linear function of frequency [or the envelope delay $\tau(f) = \text{const}$]. On the other hand, if $A(f)$ and $\tau(f)$ are not constant within the bandwidth occupied by the transmitted signal, the channel distorts the signal. If $A(f)$ is not constant, the distortion is called *amplitude distortion* and if $\tau(f)$ is not constant, the distortion on the transmitted signal is called *delay distortion.*

As a result of the amplitude and delay distortion caused by the nonideal channel frequency response characteristic $C(f)$, a succession of pulses transmitted through the channel at rates comparable to the bandwidth W are smeared to the point that they are no longer distinguishable as well-defined pulses at the receiving terminal. Instead, they overlap and, thus, we have **intersymbol interference (ISI)**. As an example of the effect of delay distortion on a transmitted pulse, Fig. 5.1(a) illustrates a band-limited pulse having zeros

0-8493-8597-0/99/$0.00+$.50

© 1999 by CRC Press LLC

periodically spaced in time at points labeled $\pm T$, $\pm 2T$, etc. If information is conveyed by the pulse amplitude, as in pulse amplitude modulation (PAM), for example, then one can transmit a sequence of pulses, each of which has a peak at the periodic zeros of the other pulses. Transmission of the pulse through a channel modeled as having a linear envelope delay characteristic $\tau(f)$ [quadratic phase $\theta(f)$], however, results in the received pulse shown in Fig. 5.1(b) having zero crossings that are no longer periodically spaced. Consequently a sequence of successive pulses would be smeared into one another, and the peaks of the pulses would no longer be distinguishable. Thus, the channel delay distortion results in intersymbol interference. As will be discussed in this chapter, it is possible to compensate for the nonideal frequency response characteristic of the channel by use of a filter or equalizer at the demodulator. Figure 5.1(c) illustrates the output of a linear equalizer that compensates for the linear distortion in the channel.

The extent of the intersymbol interference on a telephone channel can be appreciated by observing a frequency response characteristic of the channel. Figure 5.2 illustrates the measured average amplitude and delay as a function of frequency for a medium-range (180–725 mi) telephone channel of the switched telecommunications network as given by Duffy and Tratcher, 1971. We observe that the usable band of the channel extends from about 300 Hz to about 3000 Hz. The corresponding impulse response of the average channel is shown in Fig. 5.3. Its duration is about 10 ms. In comparison, the transmitted symbol rates on such a channel may be of the order of 2500 pulses or symbols per second. Hence, intersymbol interference might extend over 20–30 symbols.

Besides telephone channels, there are other physical channels that exhibit some form of time dispersion and, thus, introduce intersymbol interference. Radio channels, such as short-wave ionospheric propagation (HF), tropospheric scatter, and mobile cellular radio are three examples of time-dispersive wireless channels. In these channels, time dispersion and, hence, intersymbol interference is the result of multiple propagation paths with different path delays. The number of paths and the relative time delays among the paths vary with time and, for this reason, these radio channels are usually called time-variant multipath channels. The time-variant multipath conditions give rise to a wide variety of frequency response characteristics. Consequently, the frequency response characterization that is used for telephone channels is inappropriate for time-variant multipath channels. Instead, these radio channels are characterized statistically in terms of the scattering function, which, in brief, is a two-dimensional representation of the average received signal power as a function of relative time delay and Doppler frequency (see Proakis [4]).

For illustrative purposes, a scattering function measured on a medium-range (150 mi) tropospheric scatter channel is shown in Fig. 5.4. The total time duration (multipath spread) of the channel response is approximately 0.7 μs on the average, and the spread between half-power points in Doppler frequency is a little less than 1 Hz on the strongest path and somewhat larger on the other paths. Typically, if one is transmitting at a rate of 10^7 symbols/s over such a channel, the multipath spread of 0.7 μs will result in intersymbol interference that spans about seven symbols.

5.2 Characterization of Intersymbol Interference

In a digital communication system, channel distortion causes intersymbol interference, as illustrated in the preceding section. In this section, we shall present a model that characterizes the ISI. The digital modulation methods to which this treatment applies are PAM, phase-shift keying (PSK) and quadrature amplitude modulation (QAM). The transmitted

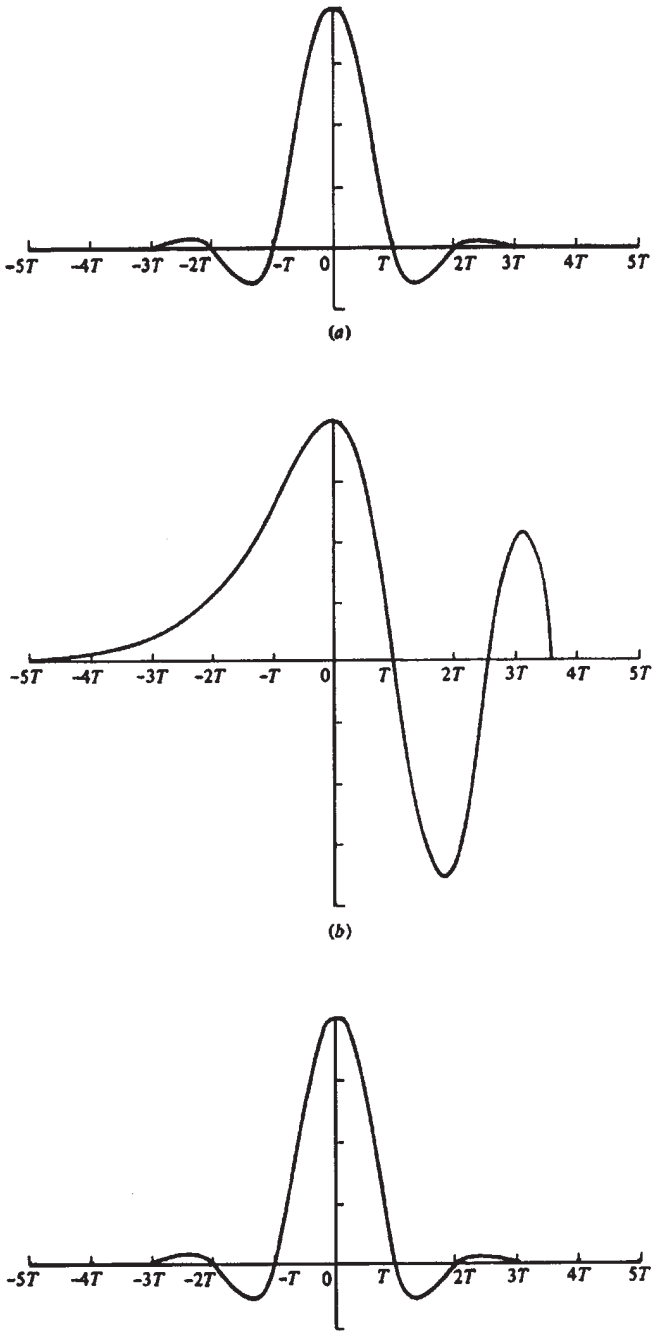


FIGURE 5.1 Effect of channel distortion: (a) channel input, (b) channel output, (c) equalizer output.

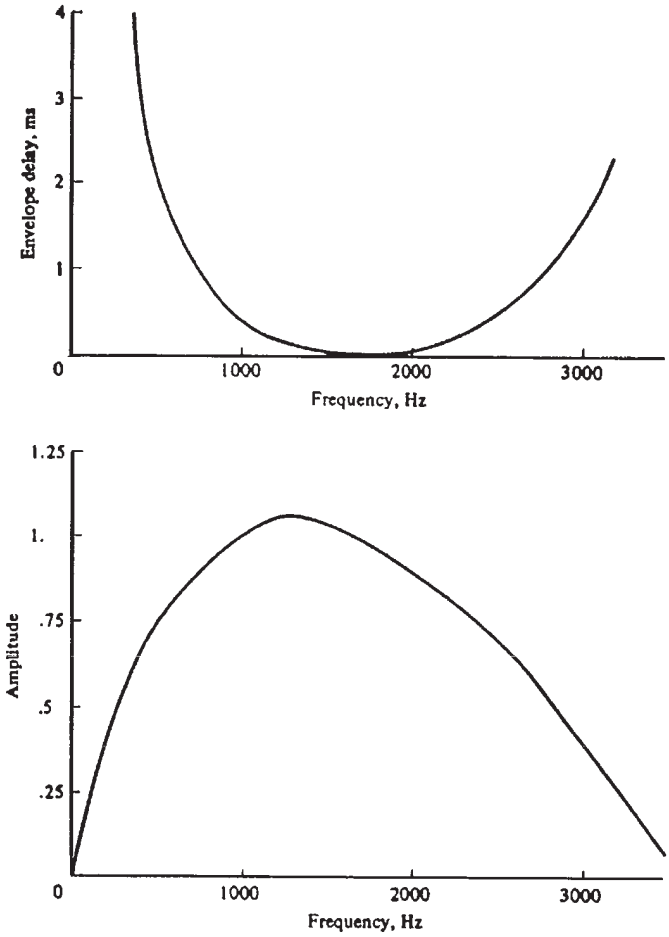


FIGURE 5.2 Average amplitude and delay characteristics of medium-range telephone channel.

signal for these three types of modulation may be expressed as

$$\begin{aligned} s(t) &= v_c(t)\cos 2\pi f_c t - v_s(t)\sin 2\pi f_c t \\ &= \text{Re}\left[v(t)\, e^{j2\pi f_c t}\right] \end{aligned} \tag{5.3}$$

where $v(t) = v_c(t) + jv_s(t)$ is called the *equivalent low-pass signal*, f_c is the carrier frequency, and Re[ ] denotes the real part of the quantity in brackets.

In general, the equivalent low-pass signal is expressed as

$$v(t) = \sum_{n=0}^{\infty} I_n\, g_T(t - nT) \tag{5.4}$$

where $g_T(t)$ is the basic pulse shape that is selected to control the spectral characteristics of the transmitted signal, $\{I_n\}$ the sequence of transmitted information symbols selected from a signal constellation consisting of M points, and T the signal interval ($1/T$ is the symbol rate). For PAM, PSK, and QAM, the values of I_n are points from M-ary signal constellations. Figure 5.5 illustrates the signal constellations for the case of $M = 8$ signal points. Note that for PAM, the signal constellation is one dimensional. Hence, the equivalent low-pass signal $v(t)$ is real valued, i.e., $v_s(t) = 0$ and $v_c(t) = v(t)$. For M-ary ($M > 2$)

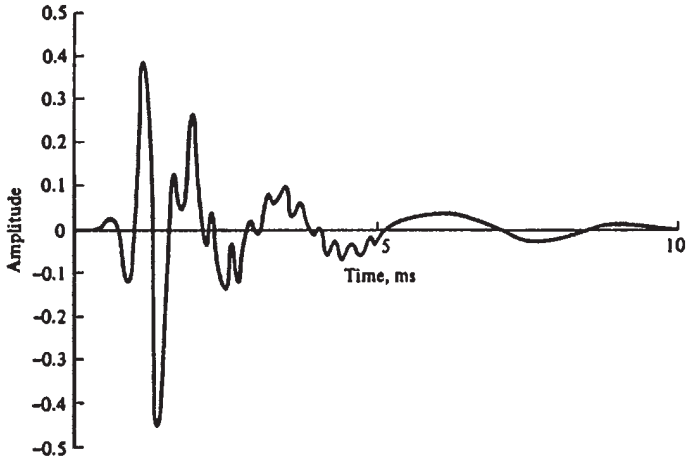


FIGURE 5.3 Impulse response of average channel with amplitude and delay shown in Fig.5.2.

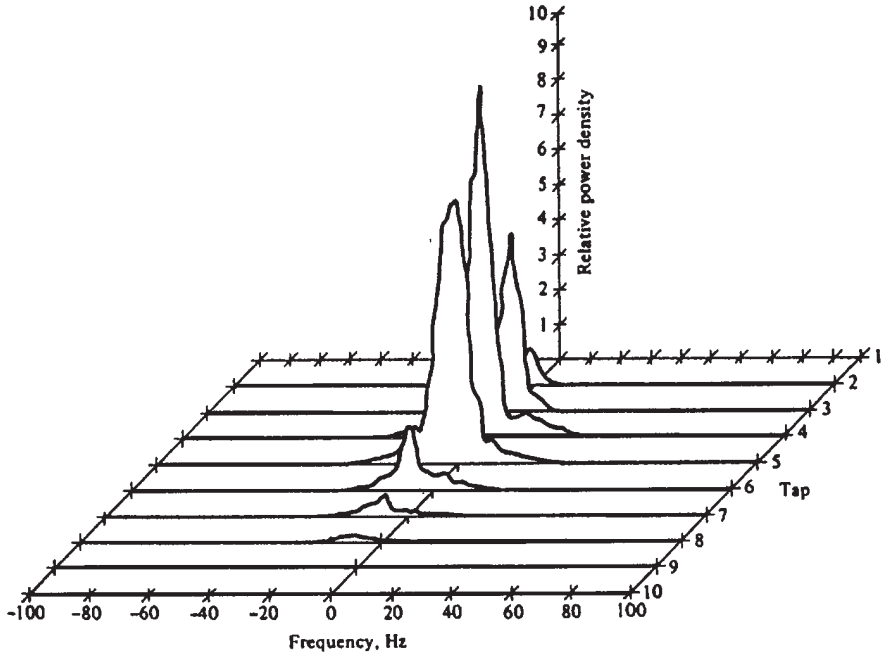


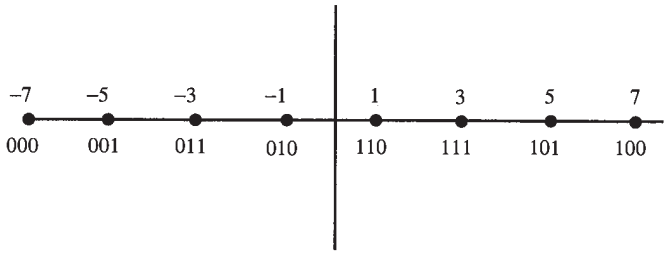
FIGURE 5.4 Scattering function of a medium-range tropospheric scatter channel.

PSK and QAM, the signal constellations are two dimensional and, hence, $v(t)$ is complex valued.

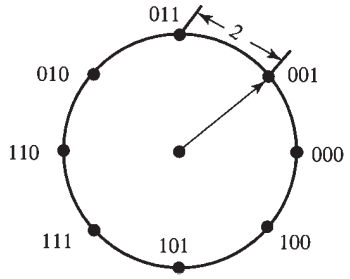
The signal $s(t)$ is transmitted over a bandpass channel that may be characterized by an equivalent low-pass frequency response $C(f)$. Consequently, the equivalent low-pass received signal can be represented as

$$r(t) = \sum_{n=0}^{\infty} I_n \, h(t - nT) + w(t) \tag{5.5}$$

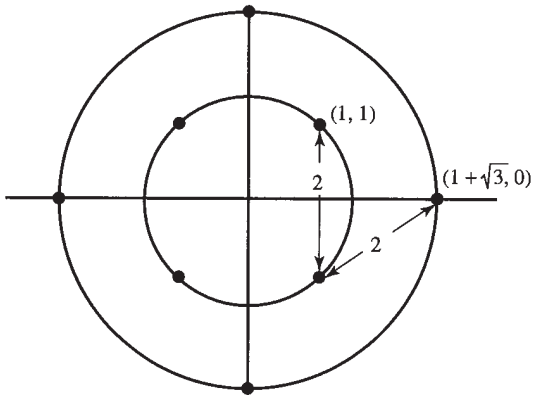
where $h(t) = g_T(t) * c(t)$, and $c(t)$ is the impulse response of the equivalent low-pass channel, the asterisk denotes convolution, and $w(t)$ represents the additive noise in the channel.



(a) PAM



(b) PSK



(c) QAM

FIGURE 5.5 $M = 8$ signal constellations for PAM, PSK, and QAM.

To characterize the ISI, suppose that the received signal is passed through a receiving filter and then sampled at the rate $1/T$ samples/s. In general, the optimum filter at the receiver is matched to the received signal pulse $h(t)$. Hence, the frequency response of this filter is $H^*(f)$. We denote its output as

$$y(t) = \sum_{n=0}^{\infty} I_n x(t - nT) + \nu(t) \tag{5.6}$$

where $x(t)$ is the signal pulse response of the receiving filter, i.e., $X(f) = H(f)H^*(f) = |H(f)|^2$, and $\nu(t)$ is the response of the receiving filter to the noise $w(t)$. Now, if $y(t)$ is sampled at times $t = kT$, $k = 0, 1, 2, \ldots$, we have

$$\begin{aligned} y(kT) \equiv y_k &= \sum_{n=0}^{\infty} I_n x(kT - nT) + \nu(kT) \\ &= \sum_{n=0}^{\infty} I_n x_{k-n} + \nu_k, \qquad k = 0, 1, \ldots \end{aligned} \tag{5.7}$$

The sample values $\{y_k\}$ can be expressed as

$$y_k = x_0 \left(I_k + \frac{1}{x_0} \sum_{\substack{n=0 \\ n \neq k}}^{\infty} I_n x_{k-n} \right) + \nu_k, \qquad k = 0, 1, \ldots \tag{5.8}$$

The term x_0 is an arbitrary scale factor, which we arbitrarily set equal to unity for convenience. Then

$$y_k = I_k + \sum_{\substack{n=0 \\ n \neq k}}^{\infty} I_n x_{k-n} + \nu_k \tag{5.9}$$

The term I_k represents the desired information symbol at the kth sampling instant, the term

$$\sum_{\substack{n=0 \\ n \neq k}}^{\infty} I_n x_{k-n} \tag{5.10}$$

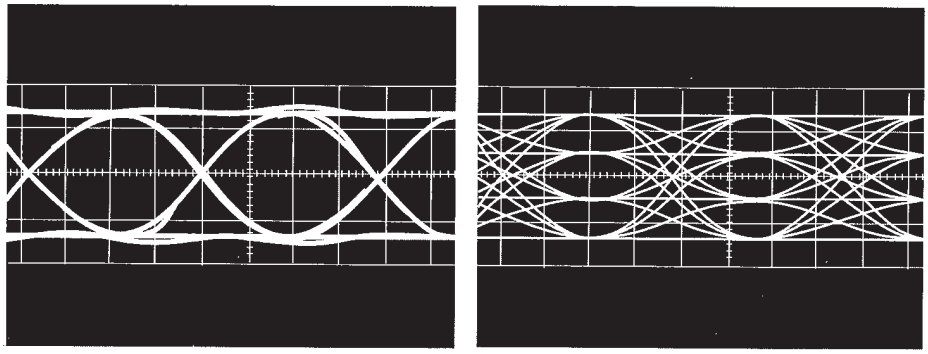
represents the ISI, and ν_k is the additive noise variable at the kth sampling instant.

The amount of ISI, and noise in a digital communications system can be viewed on an oscilloscope. For PAM signals, we can display the received signal $y(t)$ on the vertical input with the horizontal sweep rate set at $1/T$. The resulting oscilloscope display is called an *eye pattern* because of its resemblance to the human eye. For example, Fig. 5.6 illustrates the eye patterns for binary and four-level PAM modulation. The effect of ISI is to cause the eye to close, thereby reducing the margin for additive noise to cause errors. Figure 5.7 graphically illustrates the effect of ISI in reducing the opening of a binary eye. Note that intersymbol interference distorts the position of the zero crossings and causes a reduction in the eye opening. Thus, it causes the system to be more sensitive to a synchronization error.

For PSK and QAM it is customary to display the eye pattern as a two-dimensional scatter diagram illustrating the sampled values $\{y_k\}$ that represent the decision variables at the sampling instants. Figure 5.8 illustrates such an eye pattern for an 8-PSK signal. In the absence of intersymbol interference and noise, the superimposed signals at the sampling instants would result in eight distinct points corresponding to the eight transmitted signal phases. Intersymbol interference and noise result in a deviation of the received samples $\{y_k\}$ from the desired 8-PSK signal. The larger the intersymbol interference and noise, the larger the scattering of the received signal samples relative to the transmitted signal points.

In practice, the transmitter and receiver filters are designed for zero ISI at the desired sampling times $t = kT$. Thus, if $G_T(f)$ is the frequency response of the transmitter filter and $G_R(f)$ is the frequency response of the receiver filter, then the product $G_T(f)\,G_R(f)$ is designed to yield zero ISI. For example, the product $G_T(f)\,G_R(f)$ may be selected as

$$G_T(f)G_R(f) = X_{rc}(f) \tag{5.11}$$



BINARY QUATERNARY

FIGURE 5.6 Examples of eye patterns for binary and quaternary amplitude shift keying (or PAM).

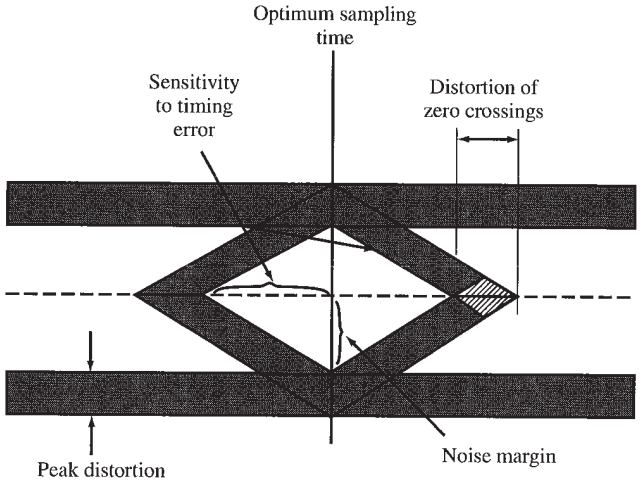


FIGURE 5.7 Effect of intersymbol interference on eye opening.

where $X_{rc}(f)$ is the raised-cosine frequency response characteristic, defined as

$$X_{rc}(f) = \begin{cases} T, & 0 \le |f| \le (1-\alpha)/2T \\ \dfrac{T}{2}\left[1 + \cos\dfrac{\pi T}{\alpha}\left(|f| - \dfrac{1-\alpha}{2T}\right)\right], & \dfrac{1-\alpha}{2T} \le |f| \le \dfrac{1+\alpha}{2T} \\ 0, & |f| > \dfrac{1+\alpha}{2T} \end{cases} \tag{5.12}$$

where α is called the *rolloff* factor, which takes values in the range $0 \le \alpha \le 1$, and $1/T$ is the symbol rate. The frequency response $X_{rc}(f)$ is illustrated in Fig. 5.9(a) for $\alpha = 0, 1/2$, and 1. Note that when $\alpha = 0$, $X_{rc}(f)$ reduces to an ideal brick wall physically nonrealizable frequency response with bandwidth occupancy $1/2T$. The frequency $1/2T$ is called the *Nyquist frequency.* For $\alpha > 0$, the bandwidth occupied by the desired signal $X_{rc}(f)$ beyond the Nyquist frequency $1/2T$ is called the *excess bandwidth,* and is usually expressed as a percentage of the Nyquist frequency. For example, when $\alpha = 1/2$, the excess bandwidth is 50% and when $\alpha = 1$, the excess bandwidth is 100%. The signal pulse $x_{rc}(t)$ having the

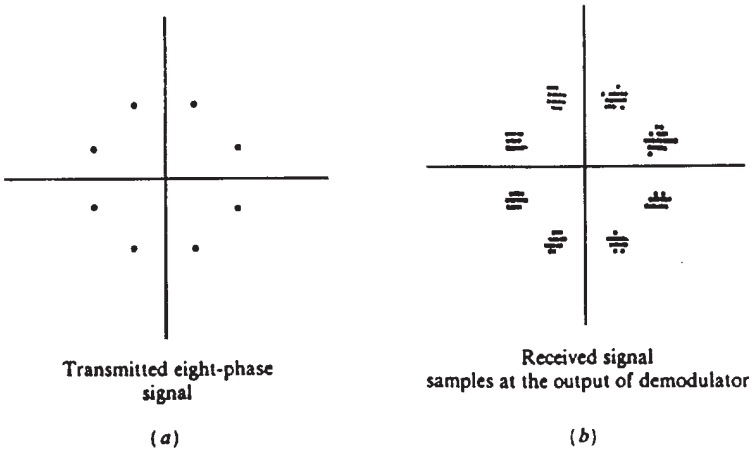


FIGURE 5.8 Two-dimensional digital eye patterns.

raised-cosine spectrum is

$$x_{rc}(t) = \frac{\sin \pi t/T}{\pi t/T} \quad \frac{\cos(\pi \alpha t/T)}{1 - 4\alpha^2 t^2/T^2} \tag{5.13}$$

Figure 5.9(b) illustrates $x_{rc}(t)$ for $\alpha = 0$, $1/2$, and 1. Note that $x_{rc}(t) = 1$ at $t = 0$ and $x_{rc}(t) = 0$ at $t = kT$, $k = \pm 1, \pm 2, \ldots$. Consequently, at the sampling instants $t = kT$, $k \neq 0$, there is no ISI from adjacent symbols when there is no channel distortion. In the presence of channel distortion, however, the ISI given by Eq. (5.10) is no longer zero, and a **channel equalizer** is needed to minimize its effect on system performance.

5.3 Linear Equalizers

The most common type of channel equalizer used in practice to reduce SI is a linear transversal filter with adjustable coefficients $\{c_i\}$, as shown in Fig. 5.10.

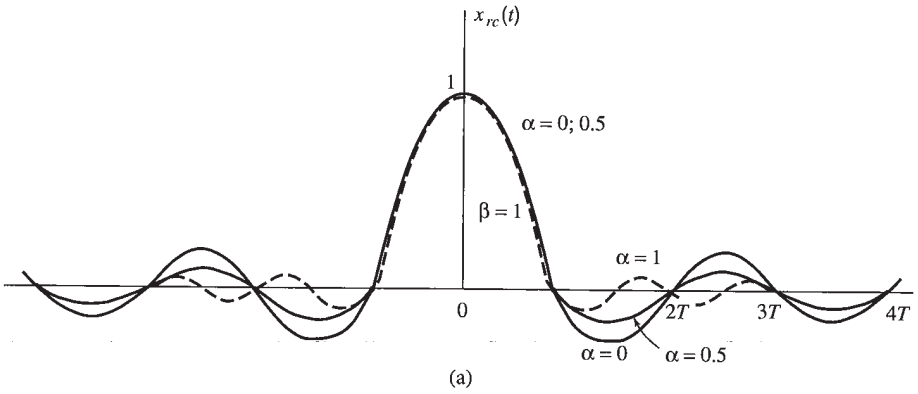
On channels whose frequency response characteristics are unknown, but time invariant, we may measure the channel characteristics and adjust the parameters of the equalizer; once adjusted, the parameters remain fixed during the transmission of data. Such equalizers are called **preset equalizers.** On the other hand, **adaptive equalizers** update their parameters on a periodic basis during the transmission of data and, thus, they are capable of tracking a slowly time-varying channel response.

First, let us consider the design characteristics for a linear equalizer from a frequency domain viewpoint. Figure 5.11 shows a block diagram of a system that employs a linear filter as a **channel equalizer.**

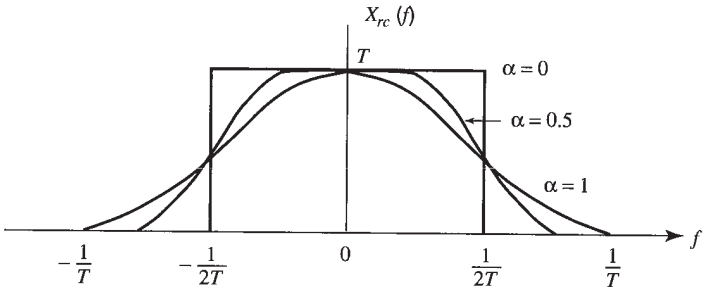
The demodulator consists of a receiver filter with frequency response $G_R(f)$ in cascade with a channel equalizing filter that has a frequency response $G_E(f)$. As indicated in the preceding section, the receiver filter response $G_R(f)$ is matched to the transmitter response, i.e., $G_R(f) = G_T^*(f)$, and the product $G_R(f)G_T(f)$ is usually designed so that there is zero ISI at the sampling instants as, for example, when $G_R(t)G_T(f) = X_{rc}(f)$.

For the system shown in Fig. 5.11, in which the channel frequency response is not ideal, the desired condition for zero ISI is

$$G_T(f)C(f)G_R(f)G_E(f) = X_{rc}(f) \tag{5.14}$$



(a)



(b)

FIGURE 5.9 Pulses having a raised cosine spectrum.

where $X_{rc}(f)$ is the desired raised-cosine spectral characteristic. Since $G_T(f)G_R(f) = X_{rc}(f)$ by design, the frequency response of the equalizer that compensates for the channel distortion is

$$G_E(f) = \frac{1}{C(f)} = \frac{1}{|C(f)|} e^{-j\theta_c(f)} \tag{5.15}$$

Thus, the amplitude response of the equalizer is $|G_E(f)| = 1/|C(f)|$ and its phase response is $\theta_E(f) = -\theta_c(f)$. In this case, the equalizer is said to be the *inverse channel filter* to the channel response.

We note that the inverse channel filter completely eliminates ISI caused by the channel. Since it forces the ISI to be zero at the sampling instants $t = kT$, $k = 0, 1, \ldots$, the equalizer is called a **zero-forcing equalizer.** Hence, the input to the detector is simply

$$z_k = I_k + \eta_k, \qquad k = 0, 1, \ldots \tag{5.16}$$

where η_k represents the additive noise and I_k is the desired symbol.

In practice, the ISI caused by channel distortion is usually limited to a finite number of symbols on either side of the desired symbol. Hence, the number of terms that constitute the ISI in the summation given by Eq. (5.10) is finite. As a consequence, in practice the channel equalizer is implemented as a finite duration impulse response (FIR) filter, or transversal filter, with adjustable tap coefficients $\{c_n\}$, as illustrated in Fig. 5.10. The time delay τ between adjacent taps may be selected as large as T, the symbol interval, in which case the FIR equalizer is called a **symbol-spaced equalizer.** In this case, the input to the

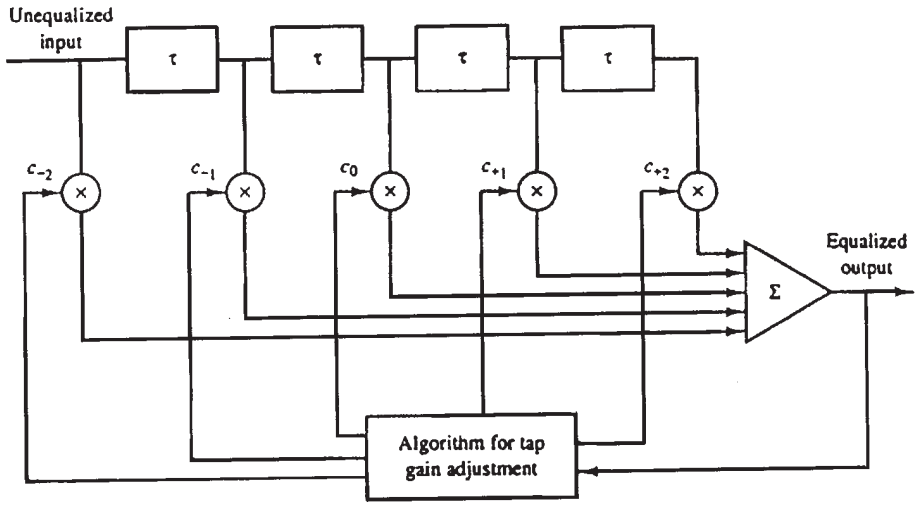


FIGURE 5.10 Linear transversal filter.

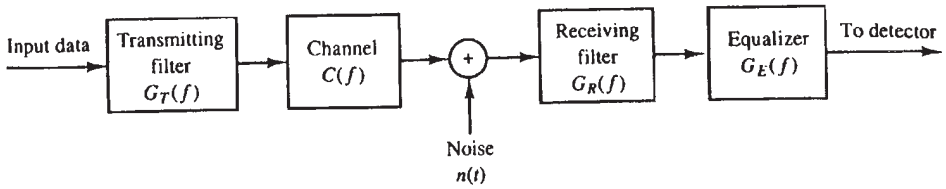


FIGURE 5.11 Block diagram of a system with an equalizer.

equalizer is the sampled sequence given by Eq. (5.7). We note that when the symbol rate $1/T < 2W$, however, frequencies in the received signal above the folding frequency $1/T$ are aliased into frequencies below $1/T$. In this case, the equalizer compensates for the aliased channel-distorted signal.

On the other hand, when the time delay τ between adjacent taps is selected such that $1/\tau \geq 2W > 1/T$, no aliasing occurs and, hence, the inverse channel equalizer compensates for the true channel distortion. Since $\tau < T$, the channel equalizer is said to have *fractionally spaced taps* and it is called a **fractionally spaced equalizer.** In practice, τ is often selected as $\tau = T/2$. Notice that, in this case, the sampling rate at the output of the filter $G_R(f)$ is $2/T$.

The impulse response of the FIR equalizer is

$$g_E(t) = \sum_{n=-N}^{N} c_n \delta(t - n\tau) \tag{5.17}$$

and the corresponding frequency response is

$$G_E(f) = \sum_{n=-N}^{N} c_n e^{-j2\pi f n\tau} \tag{5.18}$$

where $\{c_n\}$ are the $(2N+1)$ equalizer coefficients and N is chosen sufficiently large so that the equalizer spans the length of the ISI, i.e., $2N+1 \geq L$, where L is the number of signal samples spanned by the ISI. Since $X(f) = G_T(f)C(f)G_R(f)$ and $x(t)$ is the signal pulse

corresponding to $X(f)$, then the equalized output signal pulse is

$$q(t) = \sum_{n=-N}^{N} c_n x(t - n\tau) \tag{5.19}$$

The zero-forcing condition can now be applied to the samples of $q(t)$ taken at times $t = mT$. These samples are

$$q(mT) = \sum_{n=-N}^{N} c_n x(mT - n\tau), \qquad m = 0, \pm 1, \ldots, \pm N \tag{5.20}$$

Since there are $2N + 1$ equalizer coefficients, we can control only $2N + 1$ sampled values of $q(t)$. Specifically, we may force the conditions

$$q(mT) = \sum_{n=-N}^{N} c_n x(mT - n\tau) = \begin{cases} 1, & m = 0 \\ 0, & m = \pm 1, \pm 2, \ldots, \pm N \end{cases} \tag{5.21}$$

which may be expressed in matrix form as $\boldsymbol{X}\boldsymbol{c} = \boldsymbol{q}$, where $\boldsymbol{X}$ is a $(2N+1) \times (2N+1)$ matrix with elements $\{x(mT - n\tau)\}$, $\boldsymbol{c}$ is the $(2N + 1)$ coefficient vector and $\boldsymbol{q}$ is the $(2N + 1)$ column vector with one nonzero element. Thus, we obtain a set of $2N + 1$ linear equations for the coefficients of the zero-forcing equalizer.

We should emphasize that the FIR zero-forcing equalizer does not completely eliminate ISI because it has a finite length. As N is increased, however, the residual ISI can be reduced, and in the limit as $N \to \infty$, the ISI is completely eliminated.

EXAMPLE 5.1:

Consider a channel distorted pulse $x(t)$, at the input to the equalizer, given by the expression

$$x(t) = \frac{1}{1 + \left(\frac{2t}{T}\right)^2}$$

where $1/T$ is the symbol rate. The pulse is sampled at the rate $2/T$ and equalized by a zero-forcing equalizer. Determine the coefficients of a five-tap zero-forcing equalizer.

Solution 5.1 According to Eq. (5.21), the zero-forcing equalizer must satisfy the equations

$$q(mT) = \sum_{n=-2}^{2} c_n x\left(mT - nT/2\right) = \begin{cases} 1, & m = 0 \\ 0, & m = \pm 1, \pm 2 \end{cases}$$

The matrix $\boldsymbol{X}$ with elements $x(mT - nT/2)$ is given as

$$\boldsymbol{X} = \begin{bmatrix} 1 & \frac{1}{5} & \frac{1}{10} & \frac{1}{17} & \frac{1}{26} & \frac{1}{37} \\ \frac{1}{5} & 1 & \frac{1}{2} & \frac{1}{5} & \frac{1}{10} & \frac{1}{17} \\ \frac{1}{10} & \frac{1}{2} & 1 & \frac{1}{2} & \frac{1}{5} & \frac{1}{10} \\ \frac{1}{17} & \frac{1}{5} & \frac{1}{2} & 1 & \frac{1}{2} & \frac{1}{5} \\ \frac{1}{26} & \frac{1}{10} & \frac{1}{5} & \frac{1}{2} & 1 & \frac{1}{2} \\ \frac{1}{37} & \frac{1}{17} & \frac{1}{10} & \frac{1}{5} & \frac{1}{2} & 1 \end{bmatrix} \tag{5.22}$$

The coefficient vector $\boldsymbol{c}$ and the vector $\boldsymbol{q}$ are given as

$$\boldsymbol{c} = \begin{bmatrix} c_{-2} \\ c_{-1} \\ c_0 \\ c_1 \\ c_2 \end{bmatrix} \qquad \boldsymbol{q} = \begin{bmatrix} 0 \\ 0 \\ 1 \\ 0 \\ 0 \end{bmatrix} \tag{5.23}$$

Then, the linear equations $\boldsymbol{X}\boldsymbol{c} = \boldsymbol{q}$ can be solved by inverting the matrix $\boldsymbol{X}$. Thus, we obtain

$$\boldsymbol{c}_{\text{opt}} = \boldsymbol{X}^{-1}\boldsymbol{q} = \begin{bmatrix} -2.2 \\ 4.9 \\ -3 \\ 4.9 \\ -2.2 \end{bmatrix} \tag{5.24}$$

One drawback to the zero-forcing equalizer is that it ignores the presence of additive noise. As a consequence, its use may result in significant noise enhancement. This is easily seen by noting that in a frequency range where $C(f)$ is small, the channel equalizer $G_E(f) = 1/C(f)$ compensates by placing a large gain in that frequency range. Consequently, the noise in that frequency range is greatly enhanced. An alternative is to relax the zero ISI condition and select the channel equalizer characteristic such that the combined power in the residual ISI and the additive noise at the output of the equalizer is minimized. A channel equalizer that is optimized based on the minimum mean square error (MMSE) criterion accomplishes the desired goal.

To elaborate, let us consider the noise corrupted output of the FIR equalizer, which is

$$z(t) = \sum_{n=-N}^{N} c_n y(t - n\tau) \tag{5.25}$$

where $y(t)$ is the input to the equalizer, given by Eq. (5.6). The equalizer output is sampled at times $t = mT$. Thus, we obtain

$$z(mT) = \sum_{n=-N}^{N} c_n y(mT - n\tau) \tag{5.26}$$

The desired response at the output of the equalizer at $t = mT$ is the transmitted symbol I_m. The error is defined as the difference between I_m and $z(mT)$. Then, the mean square error (MSE) between the actual output sample $z(mT)$ and the desired values I_m is

$$\begin{aligned} MSE &= E\left|z(mT) - I_m\right|^2 \\ &= E\left[\left|\sum_{n=-N}^{N} c_n y(mT - n\tau) - I_m\right|^2\right] \\ &= \sum_{n=-N}^{N}\sum_{k=-N}^{N} c_n c_k R_Y(n-k) \\ &\quad - 2\sum_{k=-N}^{N} c_k R_{IY}(k) + E\left(|I_m|^2\right) \end{aligned} \tag{5.27}$$

where the correlations are defined as

$$\begin{aligned} R_Y(n-k) &= E\left[y^*(mT-n\tau)y(mT-k\tau)\right] \\ R_{IY}(k) &= E\left[y(mT-k\tau)I_m^*\right] \end{aligned} \tag{5.28}$$

and the expectation is taken with respect to the random information sequence $\{I_m\}$ and the additive noise.

The minimum *MSE* solution is obtained by differentiating Eq. (5.27) with respect to the equalizer coefficients $\{c_n\}$. Thus, we obtain the necessary conditions for the minimum *MSE* as

$$\sum_{n=-N}^{N} c_n R_Y(n-k) = R_{IY}(k), \qquad k = 0, \pm 1, 2, \ldots, \pm N \tag{5.29}$$

These are the $(2N+1)$ linear equations for the equalizer coefficients. In contrast to the zero-forcing solution already described, these equations depend on the statistical properties (the autocorrelation) of the noise as well as the ISI through the autocorrelation $R_Y(n)$.

In practice, the autocorrelation matrix $R_Y(n)$ and the crosscorrelation vector $R_{IY}(n)$ are unknown a priori. These correlation sequences can be estimated, however, by transmitting a test signal over the channel and using the time-average estimates

$$\begin{aligned} \hat{R}_Y(n) &= \frac{1}{K}\sum_{k=1}^{K} y^*(kT-n\tau)y(kT) \\ \hat{R}_{IY}(n) &= \frac{1}{K}\sum_{k=1}^{K} y(kT-n\tau)I_k^* \end{aligned} \tag{5.30}$$

in place of the ensemble averages to solve for the equalizer coefficients given by Eq. (5.29).

5.3.1 Adaptive Linear Equalizers

We have shown that the tap coefficients of a linear equalizer can be determined by solving a set of linear equations. In the zero-forcing optimization criterion, the linear equations are given by Eq. (5.21). On the other hand, if the optimization criterion is based on minimizing the *MSE,* the optimum equalizer coefficients are determined by solving the set of linear equations given by Eq. (5.29).

In both cases, we may express the set of linear equations in the general matrix form

$$\boldsymbol{B}\boldsymbol{c} = \boldsymbol{d} \tag{5.31}$$

where $\boldsymbol{B}$ is a $(2N+1)\times(2N+1)$ matrix, $\boldsymbol{c}$ is a column vector representing the $2N+1$ equalizer coefficients, and $\boldsymbol{d}$ a $(2N+1)$-dimensional column vector. The solution of Eq. (5.31) yields

$$\boldsymbol{c}_{\text{opt}} = \boldsymbol{B}^{-1}\boldsymbol{d} \tag{5.32}$$

In practical implementations of equalizers, the solution of Eq. (5.31) for the optimum coefficient vector is usually obtained by an iterative procedure that avoids the explicit computation of the inverse of the matrix $\boldsymbol{B}$. The simplest iterative procedure is the method of steepest descent, in which one begins by choosing arbitrarily the coefficient vector $\boldsymbol{c}$, say $\boldsymbol{c}_0$. This initial choice of coefficients corresponds to a point on the criterion function that is being optimized. For example, in the case of the *MSE* criterion, the initial guess $\boldsymbol{c}_0$

corresponds to a point on the quadratic *MSE* surface in the $(2N+1)$-dimensional space of coefficients. The gradient vector, defined as $\boldsymbol{g}_0$, which is the derivative of the *MSE* with respect to the $2N+1$ filter coefficients, is then computed at this point on the criterion surface, and each tap coefficient is changed in the direction opposite to its corresponding gradient component. The change in the jth tap coefficient is proportional to the size of the jth gradient component.

For example, the gradient vector denoted as $\boldsymbol{g}_k$, for the MSE criterion, found by taking the derivatives of the MSE with respect to each of the $2N+1$ coefficients, is

$$\boldsymbol{g}_k = \boldsymbol{B}\boldsymbol{c}_k - \boldsymbol{d}, \qquad k = 0, 1, 2, \ldots \tag{5.33}$$

Then the coefficient vector $\boldsymbol{c}_k$ is updated according to the relation

$$\boldsymbol{c}_{k+1} = \boldsymbol{c}_k - \Delta \boldsymbol{g}_k \tag{5.34}$$

where Δ is the *step-size parameter* for the iterative procedure. To ensure convergence of the iterative procedure, Δ is chosen to be a small positive number. In such a case, the gradient vector $\boldsymbol{g}_k$ converges toward zero, i.e., $\boldsymbol{g}_k \to \boldsymbol{0}$ as $k \to \infty$, and the coefficient vector $\boldsymbol{c}_k \to \boldsymbol{c}_{\text{opt}}$ as illustrated in Fig. 5.12 based on two-dimensional optimization. In general, convergence of the equalizer tap coefficients to $\boldsymbol{c}_{\text{opt}}$ cannot be attained in a finite number of iterations with the steepest-descent method. The optimum solution $\boldsymbol{c}_{\text{opt}}$, however, can be approached as closely as desired in a few hundred iterations. In digital communication systems that employ channel equalizers, each iteration corresponds to a time interval for sending one symbol and, hence, a few hundred iterations to achieve convergence to $\boldsymbol{c}_{\text{opt}}$ corresponds to a fraction of a second.

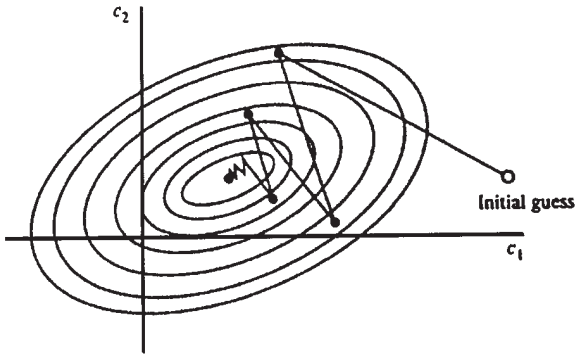


FIGURE 5.12 Examples of convergence characteristics of a gradient algorithm.

Adaptive channel equalization is required for channels whose characteristics change with time. In such a case, the ISI varies with time. The channel equalizer must track such time variations in the channel response and adapt its coefficients to reduce the ISI. In the context of the preceding discussion, the optimum coefficient vector $\boldsymbol{c}_{\text{opt}}$ varies with time due to time variations in the matrix $\boldsymbol{B}$ and, for the case of the *MSE* criterion, time variations in the vector $\boldsymbol{d}$. Under these conditions, the iterative method described can be modified to use estimates of the gradient components. Thus, the algorithm for adjusting the equalizer tap coefficients may be expressed as

$$\hat{\boldsymbol{c}}_{k+1} = \hat{\boldsymbol{c}}_k - \Delta \hat{\boldsymbol{g}}_k \tag{5.35}$$

where $\hat{\boldsymbol{g}}_k$ denotes an estimate of the gradient vector $\boldsymbol{g}_k$ and $\hat{\boldsymbol{c}}_k$ denotes the estimate of the tap coefficient vector.

In the case of the *MSE* criterion, the gradient vector $\boldsymbol{g}_k$ given by Eq. (5.33) may also be expressed as

$$\boldsymbol{g}_k = -E\left(e_k \boldsymbol{y}_k^*\right)$$

An estimate $\hat{\boldsymbol{g}}_k$ of the gradient vector at the kth iteration is computed as

$$\hat{\boldsymbol{g}}_k = -e_k \boldsymbol{y}_k^* \tag{5.36}$$

where e_k denotes the difference between the desired output from the equalizer at the kth time instant and the actual output $z(kT)$, and $\boldsymbol{y}_k$ denotes the column vector of $2N+1$ received signal values contained in the equalizer at time instant k. The *error signal* e_k is expressed as

$$e_k = I_k - z_k \tag{5.37}$$

where $z_k = z(kT)$ is the equalizer output given by Eq. (5.26) and I_k is the desired symbol. Hence, by substituting Eq. (5.36) into Eq. (5.35), we obtain the adaptive algorithm for optimizing the tap coefficients (based on the *MSE* criterion) as

$$\hat{\boldsymbol{c}}_{k+1} = \hat{\boldsymbol{c}}_k + \Delta e_k \boldsymbol{y}_k^* \tag{5.38}$$

Since an estimate of the gradient vector is used in Eq. (5.38) the algorithm is called a **stochastic gradient algorithm;** it is also known as the **LMS algorithm.**

A block diagram of an adaptive equalizer that adapts its tap coefficients according to Eq. (5.38) is illustrated in Fig. 5.13. Note that the difference between the desired output I_k and the actual output z_k from the equalizer is used to form the error signal e_k. This error is scaled by the step-size parameter Δ, and the scaled error signal Δe_k multiplies the received signal values $\{y(kT - n\tau)\}$ at the $2N+1$ taps. The products $\Delta e_k y^*(kT - n\tau)$ at the $(2N+1)$ taps are then added to the previous values of the tap coefficients to obtain the updated tap coefficients, according to Eq. (5.38). This computation is repeated as each new symbol is received. Thus, the equalizer coefficients are updated at the symbol rate.

Initially, the adaptive equalizer is trained by the transmission of a known pseudo-random sequence $\{I_m\}$ over the channel. At the demodulator, the equalizer employs the known sequence to adjust its coefficients. Upon initial adjustment, the adaptive equalizer switches from a **training mode** to a **decision-directed mode,** in which case the decisions at the output of the detector are sufficiently reliable so that the error signal is formed by computing the difference between the detector output and the equalizer output, i.e.,

$$e_k = \tilde{I}_k - z_k \tag{5.39}$$

where $\tilde{I}_k$ is the output of the detector. In general, decision errors at the output of the detector occur infrequently and, consequently, such errors have little effect on the performance of the tracking algorithm given by Eq. (5.38).

A rule of thumb for selecting the step-size parameter so as to ensure convergence and good tracking capabilities in slowly varying channels is

$$\Delta = \frac{1}{5(2N+1)P_R} \tag{5.40}$$

where P_R denotes the received signal-plus-noise power, which can be estimated from the received signal (see Proakis [4]).

The convergence characteristic of the stochastic gradient algorithm in Eq. (5.38) is illustrated in Fig. 5.14. These graphs were obtained from a computer simulation of an 11-tap adaptive equalizer operating on a channel with a rather modest amount of ISI. The input

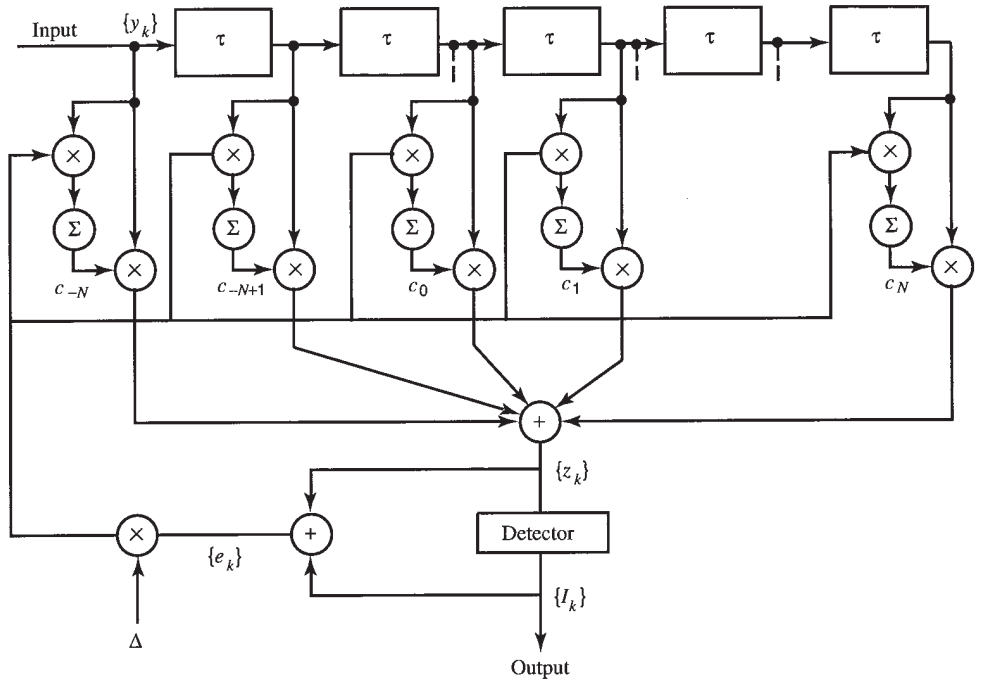


FIGURE 5.13 Linear adaptive equalizer based on the *MSE* criterion.

signal-plus-noise power P_R was normalized to unity. The rule of thumb given in Eq. (5.40) for selecting the step size gives $\Delta = 0.018$. The effect of making Δ too large is illustrated by the large jumps in *MSE* as shown for $\Delta = 0.115$. As Δ is decreased, the convergence is slowed somewhat, but a lower MSE is achieved, indicating that the estimated coefficients are closer to $\mathbf{c}_{\text{opt}}$.

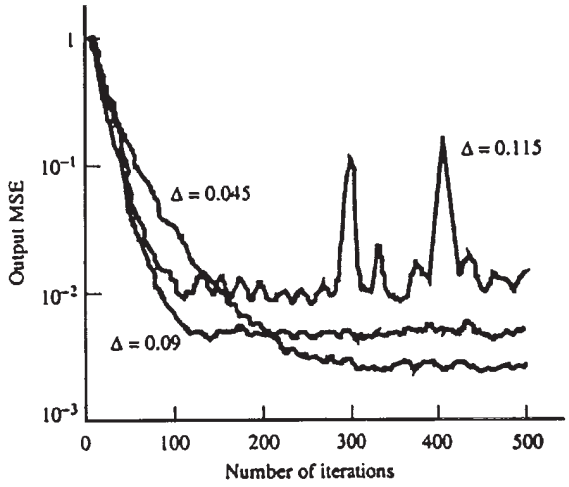


FIGURE 5.14 Initial convergence characteristics of the *LMS* algorithm with different step sizes.

Although we have described in some detail the operation of an adaptive equalizer that is optimized on the basis of the MSE criterion, the operation of an adaptive equalizer based on the zero-forcing method is very similar. The major difference lies in the method for estimating the gradient vectors $\boldsymbol{g}_k$ at each iteration. A block diagram of an adaptive zero-forcing equalizer is shown in Fig. 5.15.

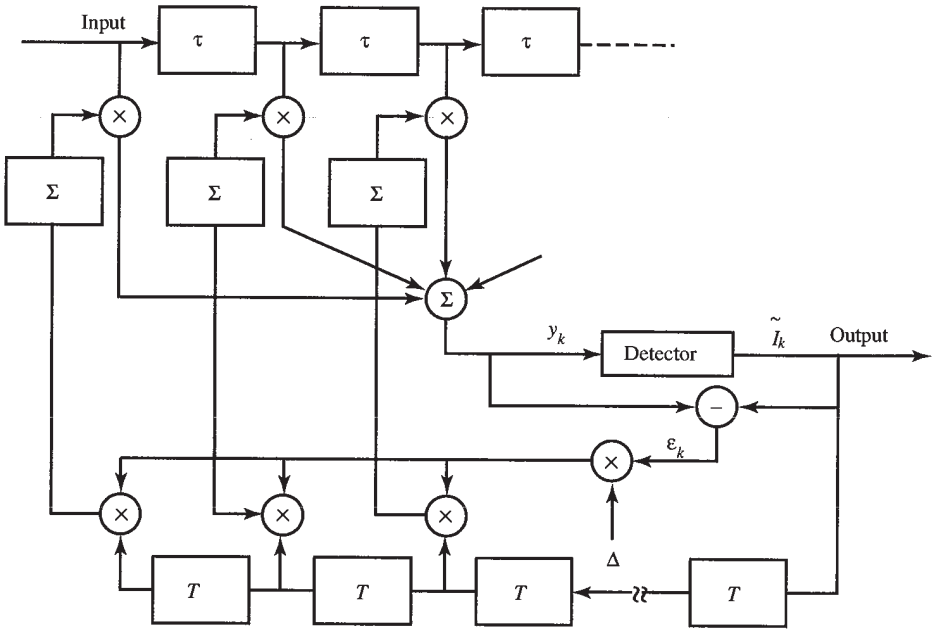


FIGURE 5.15 An adaptive zero-forcing equalizer.

For more details on the tap coefficient update method for a zero-forcing equalizer, the reader is referred to the papers by Lucky [2, 3], and the text by Proakis [4].

5.4 Decision-Feedback Equalizer

The linear filter equalizers described in the preceding section are very effective on channels, such as wire line telephone channels, where the ISI is not severe. The severity of the ISI is directly related to the spectral characteristics and not necessarily to the time span of the ISI. For example, consider the ISI resulting from the two channels that are illustrated in Fig. 5.16. The time span for the ISI in channel A is 5 symbol intervals on each side of the desired signal component, which has a value of 0.72. On the other hand, the time span for the ISI in channel B is one symbol interval on each side of the desired signal component, which has a value of 0.815. The energy of the total response is normalized to unity for both channels.

In spite of the shorter ISI span, channel B results in more severe ISI. This is evidenced in the frequency response characteristics of these channels, which are shown in Fig. 5.17. We observe that channel B has a spectral null [the frequency response $C(f) = 0$ for some frequencies in the band $|f| \leq W$] at $f = 1/2T$, whereas this does not occur in the case of channel A. Consequently, a linear equalizer will introduce a large gain in its frequency response to compensate for the channel null. Thus, the noise in channel B will be enhanced

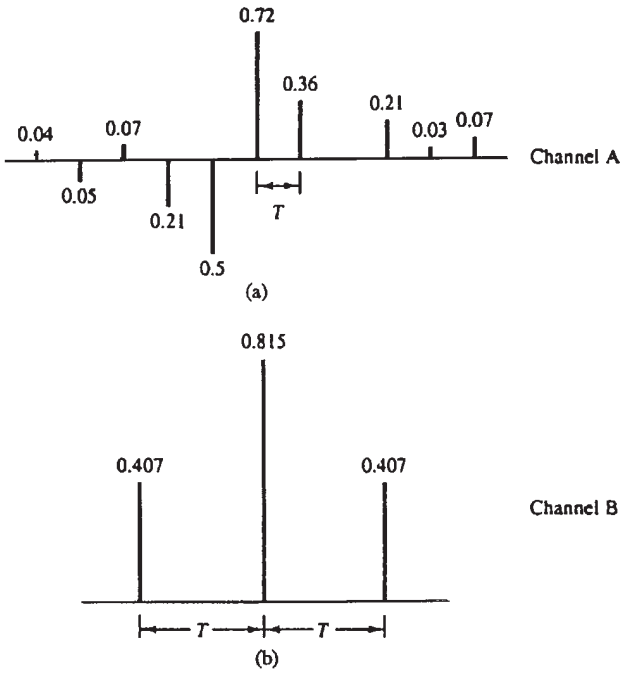


FIGURE 5.16 Two channels with ISI.

much more than in channel A. This implies that the performance of the linear equalizer for channel B will be sufficiently poorer than that for channel A. This fact is borne out by the computer simulation results for the performance of the two linear equalizers shown in Fig. 5.18. Hence, the basic limitation of a linear equalizer is that it performs poorly on channels having spectral nulls. Such channels are often encountered in radio communications, such as ionospheric transmission at frequencies below 30 MHz and mobile radio channels, such as those used for cellular radio communications.

A **decision-feedback equalizer (DFE)** is a nonlinear equalizer that employs previous decisions to eliminate the ISI caused by previously detected symbols on the current symbol to be detected. A simple block diagram for a DFE is shown in Fig. 5.19. The DFE consists of two filters. The first filter is called a *feedforward filter* and it is generally a fractionally spaced FIR filter with adjustable tap coefficients. This filter is identical in form to the linear equalizer already described. Its input is the received filtered signal $y(t)$ sampled at some rate that is a multiple of the symbol rate, e.g., at rate $2/T$. The second filter is a *feedback filter*. It is implemented as an FIR filter with symbol-spaced taps having adjustable coefficients. Its input is the set of previously detected symbols. The output of the feedback filter is subtracted from the output of the feedforward filter to form the input to the detector. Thus, we have

$$z_m = \sum_{n=-N_1}^{0} c_n y(mT - n\tau) - \sum_{n=1}^{N_2} b_n \tilde{I}_{m-n} \tag{5.41}$$

where $\{c_n\}$ and $\{b_n\}$ are the adjustable coefficients of the feedforward and feedback filters, respectively, $\tilde{I}_{m-n}, n = 1, 2, \ldots, N_2$ are the previously detected symbols, $N_1 + 1$ is the length of the feedforward filter, and N_2 is the length of the feedback filter. Based on the input z_m, the detector determines which of the possible transmitted symbols is closest in distance to the input signal I_m. Thus, it makes its decision and outputs $\tilde{I}_m$. What makes the

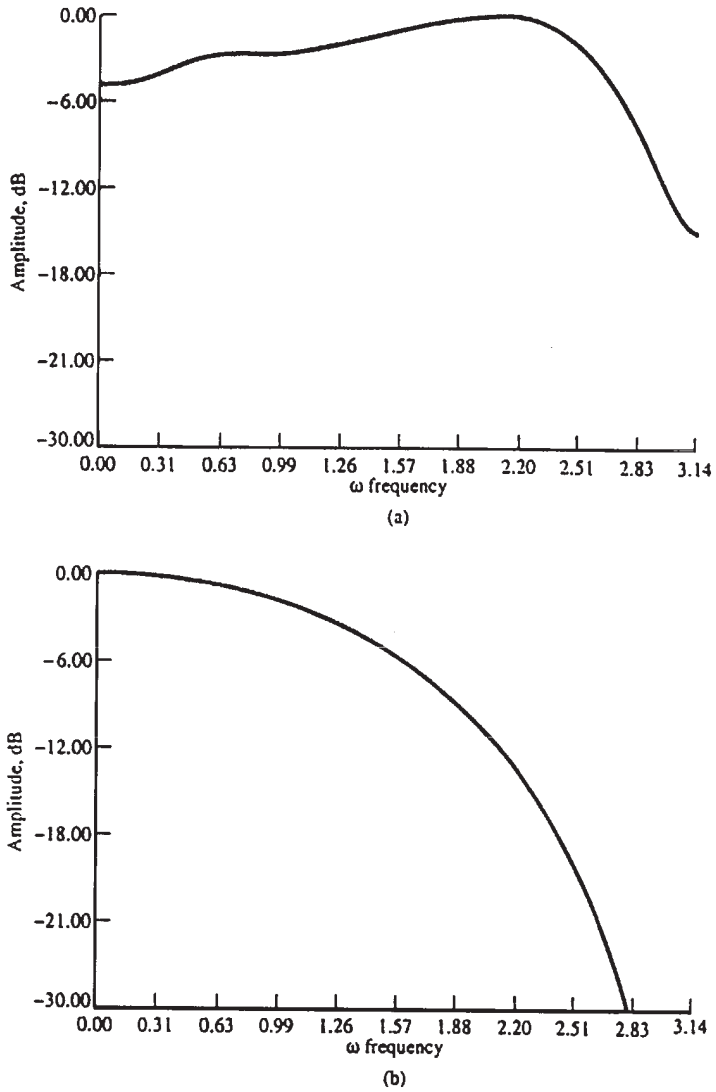


FIGURE 5.17 Amplitude spectra for (a) channel A shown in Fig.5.16(a) and (b) channel B shown in Fig.5.16(b).

DFE nonlinear is the nonlinear characteristic of the detector that provides the input to the feedback filter.

The tap coefficients of the feedforward and feedback filters are selected to optimize some desired performance measure. For mathematical simplicity, the *MSE* criterion is usually applied, and a stochastic gradient algorithm is commonly used to implement an adaptive DFE. Figure 5.20 illustrates the block diagram of an adaptive DFE whose tap coefficients are adjusted by means of the LMS stochastic gradient algorithm. Figure 5.21 illustrates the probability of error performance of the DFE, obtained by computer simulation, for binary PAM transmission over channel B. The gain in performance relative to that of a linear equalizer is clearly evident.

We should mention that decision errors from the detector that are fed to the feedback filter have a small effect on the performance of the DFE. In general, a small loss in performance

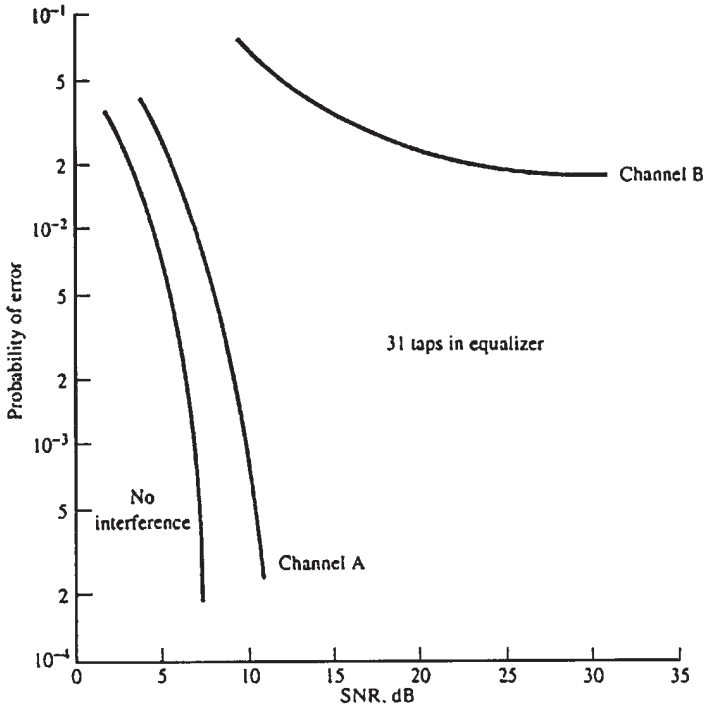


FIGURE 5.18 Error-rate performance of linear *MSE* equalizer.

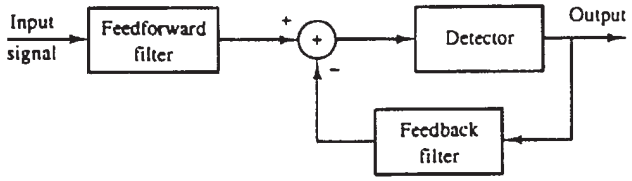


FIGURE 5.19 Block diagram of DFE.

of one to two decibels is possible at error rates below 10^{-2}, as illustrated in Fig. 5.21, but the decision errors in the feedback filters are not catastrophic.

5.5 Maximum-Likelihood Sequence Detection

Although the DFE outperforms a linear equalizer, it is not the optimum equalizer from the viewpoint of minimizing the probability of error in the detection of the information sequence $\{I_k\}$ from the received signal samples $\{y_k\}$ given in Eq. (5.5). In a digital communication system that transmits information over a channel that causes ISI, the optimum detector is a maximum-likelihood symbol sequence detector which produces at its output the most probable symbol sequence $\{\tilde{I}_k\}$ for the given received sampled sequence $\{y_k\}$. That is, the detector finds the sequence $\{\tilde{I}_k\}$ that maximizes the *likelihood function*

$$\Lambda(\{I_k\}) = \ln p(\{y_k\} \mid \{I_k\}) \tag{5.42}$$

where $p(\{y_k\} \mid \{I_k\})$ is the joint probability of the received sequence $\{y_k\}$ conditioned on $\{I_k\}$. The sequence of symbols $\{\tilde{I}_k\}$ that maximizes this joint conditional probability is called the **maximum-likelihood sequence detector.**

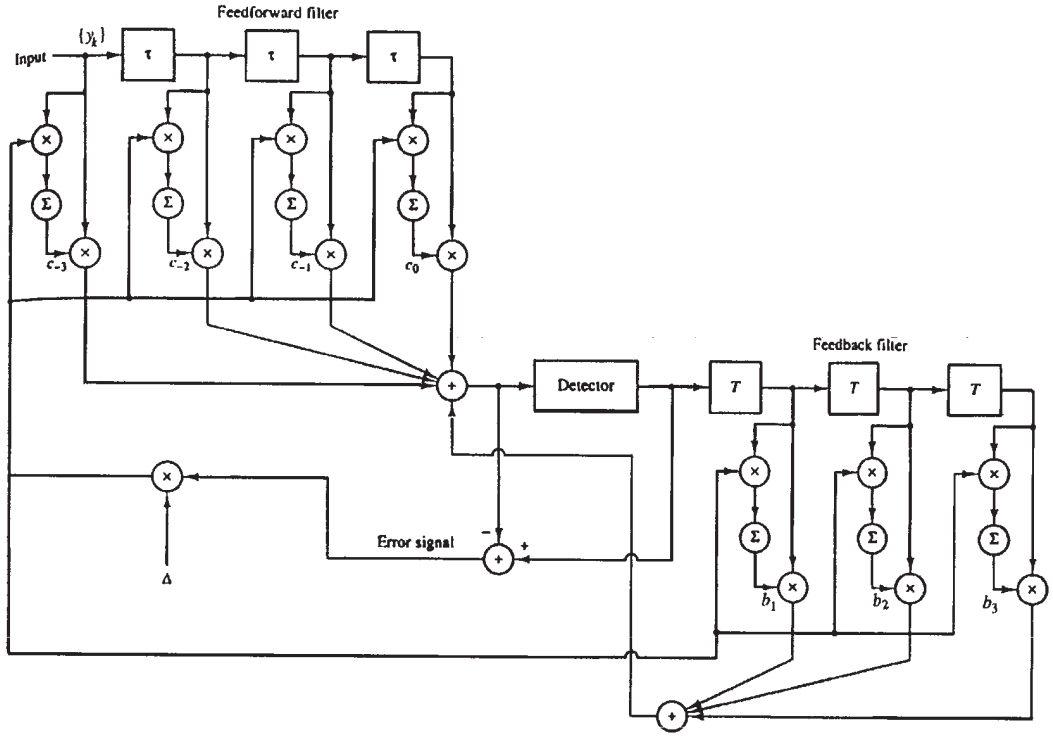


FIGURE 5.20 Adaptive DFE.

An algorithm that implements maximum-likelihood sequence detection (MLSD) is the Viterbi algorithm, which was originally devised for decoding convolutional codes. For a description of this algorithm in the context of sequence detection in the presence of ISI, the reader is referred to the paper by Forney [1] and the text by Proakis [4].

The major drawback of MLSD for channels with ISI is the exponential behavior in computational complexity as a function of the span of the ISI. Consequently, MLSD is practical only for channels where the ISI spans only a few symbols and the ISI is severe, in the sense that it causes a severe degradation in the performance of a linear equalizer or a decision-feedback equalizer. For example, Fig. 5.22 illustrates the error probability performance of the Viterbi algorithm for a binary PAM signal transmitted through channel B (see Fig. 5.16). For purposes of comparison, we also illustrate the probability of error for a DFE. Both results were obtained by computer simulation. We observe that the performance of the maximum likelihood sequence detector is about 4.5 dB better than that of the DFE at an error probability of 10^{-4}. Hence, this is one example where the ML sequence detector provides a significant performance gain on a channel with a relatively short ISI span.

5.6 Conclusions

Channel equalizers are widely used in digital communication systems to mitigate the effects of ISI caused by channel distortion. Linear equalizers are widely used for high-speed modems that transmit data over telephone channels. For wireless (radio) transmission, such as in mobile cellular communications and interoffice communications, the multipath propagation of the transmitted signal results in severe ISI. Such channels require more powerful equalizers to combat the severe ISI. The decision-feedback equalizer and the MLSD are two nonlinear channel equalizers that are suitable for radio channels with severe ISI.

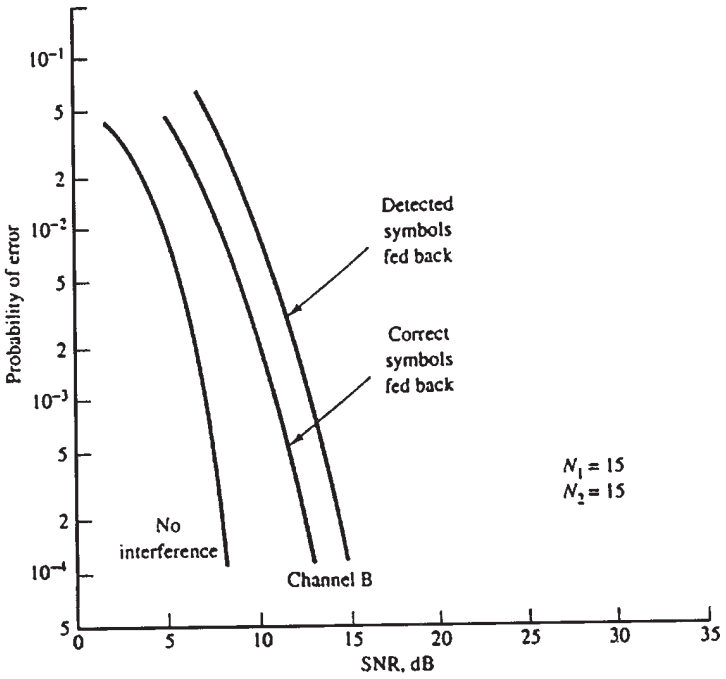


FIGURE 5.21 Performance of DFE with and without error propagation.

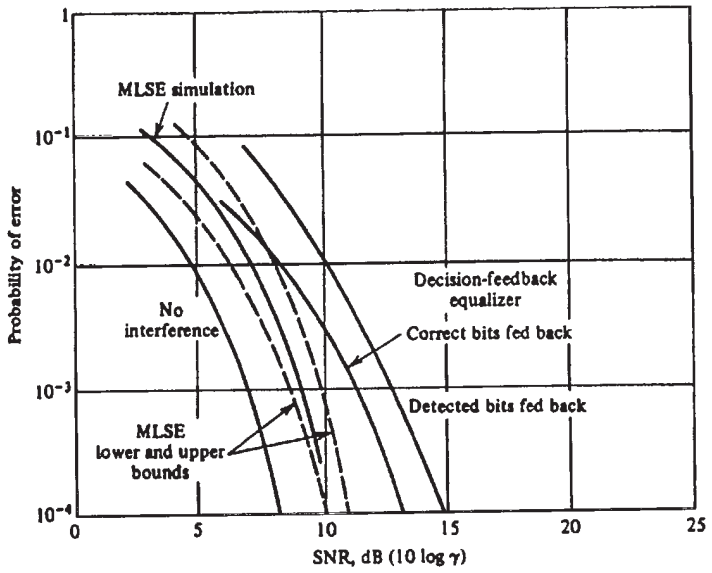


FIGURE 5.22 Comparison of performance between MLSE and decision-feedback equalization for channel B of Fig.5.16.

Defining Terms

Adaptive equalizer: A channel equalizer whose parameters are updated automatically and adaptively during transmission of data.

Channel equalizer: A device that is used to reduce the effects of channel distortion in a received signal.

Decision-directed mode: Mode for adjustment of the equalizer coefficient adaptively based on the use of the detected symbols at the output of the detector.

Decision-feedback equalizer (DFE): An adaptive equalizer that consists of a feedforward filter and a feedback filter, where the latter is fed with previously detected symbols that are used to eliminate the intersymbol interference due to the tail in the channel impulse response.

Fractionally spaced equalizer: A tapped-delay line channel equalizer in which the delay between adjacent taps is less than the duration of a transmitted symbol.

Intersymbol interference: Interference in a received symbol from adjacent (nearby) transmitted symbols caused by channel distortion in data transmission.

LMS algorithm: See stochastic gradient algorithm.

Maximum-likelihood sequence detector: A detector for estimating the most probable sequence of data symbols by maximizing the likelihood function of the received signal.

Preset equalizer: A channel equalizer whose parameters are fixed (time-invariant) during transmission of data.

Stochastic gradient algorithm: An algorithm for adaptively adjusting the coefficients of an equalizer based on the use of (noise-corrupted) estimates of the gradients.

Symbol-spaced equalizer: A tapped-delay line channel equalizer in which the delay between adjacent taps is equal to the duration of a transmitted symbol.

Training mode: Mode for adjustment of the equalizer coefficients based on the transmission of a known sequence of transmitted symbols.

Zero-forcing equalizer: A channel equalizer whose parameters are adjusted to completely eliminate intersymbol interference in a sequence of transmitted data symbols.

References

[1] Forney, G.D., Jr., Maximum-likelihood sequence estimation of digital sequences in the presence of intersymbol interference. *IEEE Trans. Inform. Theory,* IT-18, 363–378, May 1972.

[2] Lucky, R.W., Automatic equalization for digital communications. *Bell Syst. Tech. J.,* 44, 547–588, Apr. 1965.

[3] Lucky, R.W., Techniques for adaptive equalization of digital communication. *Bell Syst. Tech. J.,* 45, 255–286, Feb. 1966.

[4] Proakis, J.G., *Digital Communications,* 3rd ed., McGraw-Hill, New York, 1995.

Further Information

For a comprehensive treatment of adaptive equalization techniques and their performance characteristics, the reader may refer to the book by Proakis [4]. The two papers by

Lucky [2, 3], provide a treatment on linear equalizers based on the zero-forcing criterion. Additional information on decision-feedback equalizers may be found in the journal papers "An Adaptive Decision-Feedback Equalizer" by D.A. George, R.R. Bowen, and J.R. Storey, *IEEE Transactions on Communications Technology,* Vol. COM-19, pp. 281–293, June 1971, and "Feedback Equalization for Fading Dispersive Channels" by P. Monsen, *IEEE Transactions on Information Theory,* Vol. IT-17, pp. 56–64, January 1971. A through treatment of channel equalization based on maximum-likelihood sequence detection is given in the paper by Forney [1].

6

Line Coding

6.1 Introduction 6-1
6.2 Common Line Coding Formats 6-2
Unipolar NRZ (Binary On-Off Keying) • Unipolar RZ • Polar NRZ • Polar RZ [Bipolar, Alternate Mark Inversion (AMI), or Pseudoternary] • Manchester Coding (Split Phase or Digital Biphase)
6.3 Alternate Line Codes 6-10
Delay Modulation (Miller Code) • Split Phase (Mark) • Biphase (Mark) • Code Mark Inversion (CMI) • NRZ (I) • Binary N Zero Substitution (BNZS) • High-Density Bipolar N (HDBN) • Ternary Coding
6.4 Multilevel Signalling, Partial Response Signalling, and Duobinary Coding 6-16
Multilevel Signalling • Partial Response Signalling and Duobinary Coding
6.5 Bandwidth Comparison 6-18
6.6 Concluding Remarks 6-18
Defining Terms 6-18
References 6-19

Joseph L. LoCicero
Illinois Institute of Technology

Bhasker P. Patel
Illinois Institute of Technology

6.1 Introduction

The terminology **line coding** originated in telephony with the need to transmit digital information across a copper telephone *line;* more specifically, binary data over a digital repeatered line. The concept of line coding, however, readily applies to any transmission line or channel. In a digital communication system, there exists a known set of symbols to be transmitted. These can be designated as $\{m_i\}$, $i = 1, 2, \ldots, N$, with a probability of occurrence $\{p_i\}$, $i = 1, 2, \ldots, N$, where the sequentially transmitted symbols are generally assumed to be statistically independent. The conversion or *coding* of these abstract symbols into real, temporal waveforms to be transmitted in baseband is the process of line coding. Since the most common type of line coding is for binary data, such a waveform can be succinctly termed a direct format for serial bits. The concentration in this section will be line coding for binary data.

Different channel characteristics, as well as different applications and performance requirements, have provided the impetus for the development and study of various types of line coding [1, 2]. For example, the channel might be ac coupled and, thus, could not support a line code with a dc component or large dc content. Synchronization or timing

0-8493-8597-0/99/$0.00+$.50

© 1999 by CRC Press LLC

recovery requirements might necessitate a discrete component at the data rate. The channel bandwidth and **crosstalk** limitations might dictate the type of line coding employed. Even such factors as the complexity of the encoder and the economy of the decoder could determine the line code chosen. Each line code has its own distinct properties. Depending on the application, one property may be more important than the other. In what follows, we describe, in general, the most desirable features that are considered when choosing a line code.

It is commonly accepted [1, 2, 5, 8] that the dominant considerations effecting the choice of a line code are: 1) timing, 2) dc content, 3) power spectrum, 4) performance monitoring, 5) probability of error, and 6) transparency. Each of these are detailed in the following paragraphs.

1) *Timing:* The waveform produced by a line code should contain enough timing information such that the receiver can synchronize with the transmitter and decode the received signal properly. The timing content should be relatively independent of source statistics, i.e., a long string of **1**s or **0**s should not result in loss of timing or jitter at the receiver.

2) *DC content:* Since the repeaters used in telephony are ac coupled, it is desirable to have zero dc in the waveform produced by a given line code. If a signal with significant dc content is used in ac coupled lines, it will cause **dc wander** in the received waveform. That is, the received signal baseline will vary with time. Telephone lines do not pass dc due to ac coupling with transformers and capacitors to eliminate dc ground loops. Because of this, the telephone channel causes a droop in constant signals. This causes dc wander. It can be eliminated by dc restoration circuits, feedback systems, or with specially designed line codes.

3) *Power spectrum:* The power spectrum and bandwidth of the transmitted signal should be matched to the frequency response of the channel to avoid significant distortion. Also, the power spectrum should be such that most of the energy is contained in as small bandwidth as possible. The smaller is the bandwidth, the higher is the transmission efficiency.

4) *Performance monitoring:* It is very desirable to detect errors caused by a noisy transmission channel. The error detection capability in turn allows performance monitoring while the channel is in use (i.e., without elaborate testing procedures that require suspending use of the channel).

5) *Probability of error:* The average error probability should be as small as possible for a given transmitter power. This reflects the reliability of the line code.

6) *Transparency:* A line code should allow all the possible patterns of **1**s and **0**s. If a certain pattern is undesirable due to other considerations, it should be mapped to a unique alternative pattern.

6.2 Common Line Coding Formats

A line coding format consists of a formal definition of the line code that specifies how a string of binary digits are converted to a line code waveform. There are two major classes of binary line codes: **level codes** and **transition codes.** Level codes carry information in their voltage level, which may be high or low for a full bit period or part of the bit period. Level codes are usually instantaneous since they typically encode a binary digit into a distinct waveform, independent of any past binary data. However, some level codes do exhibit memory. Transition codes carry information in the change in level appearing in the line code waveform. Transition codes may be instantaneous, but they generally have memory, using past binary data to dictate the present waveform. There are two common forms of level line codes: one is called **return to zero (RZ)** and the other is called

nonreturn to zero (NRZ). In RZ coding, the level of the pulse returns to zero for a portion of the bit interval. In NRZ coding, the level of the pulse is maintained during the entire bit interval.

Line coding formats are further classified according to the polarity of the voltage levels used to represent the data. If only one polarity of voltage level is used, i.e., positive or negative (in addition to the zero level) then it is called **unipolar** signalling. If both positive and negative voltage levels are being used, with or without a zero voltage level, then it is called **polar** signalling. The term **bipolar** signalling is used by some authors to designate a specific line coding scheme with positive, negative, and zero voltage levels. This will be described in detail later in this section. The formal definition of five common line codes is given in the following along with a representative waveform, the *power spectral density* (PSD), the probability of error, and a discussion of advantages and disadvantages. In some cases specific applications are noted.

6.2.1 Unipolar NRZ (Binary On-Off Keying)

In this line code, a binary **1** is represented by a non-zero voltage level and a binary **0** is represented by a zero voltage level as shown in Fig. 6.1(a). This is an instantaneous level code. The PSD of this code with equally likely **1**s and **0**s is given by [5, 8]

$$S_1(f) = \frac{V^2T}{4}\left(\frac{\sin \pi fT}{\pi fT}\right)^2 + \frac{V^2}{4}\delta(f) \tag{6.1}$$

where V is the binary **1** voltage level, $T = 1/R$ is the bit duration, and R is the bit rate in bits per second. The spectrum of unipolar NRZ is plotted in Fig. 6.2a. This PSD is a two-sided even spectrum, although only half of the plot is shown for efficiency of presentation. If the probability of a binary **1** is p, and the probability of a binary **0** is $(1-p)$, then the PSD of this code, in the most general case, is $4p(1-p)\,S_1(f)$. Considering the frequency of the first spectral null as the bandwidth of the waveform, the bandwidth of unipolar NRZ is R in hertz. The error rate performance of this code, for equally likely data, with additive white Gaussian noise (AWGN) and optimum, i.e., matched filter, detection is given by [1, 5]

$$P_e = \frac{1}{2}\text{erfc}\left(\sqrt{\frac{E_b}{2N_0}}\right) \tag{6.2}$$

where E_b/N_0 is a measure of the signal-to-noise ratio (SNR) of the received signal. In general, E_b is the energy per bit and $N_0/2$ is the two-sided PSD of the AWGN. More specifically, for unipolar NRZ, E_b is the energy in a binary **1**, which is V^2T. The performance of the unipolar NRZ code is plotted in Fig. 6.3

The principle advantages of unipolar NRZ are ease of generation, since it requires only a single power supply, and a relatively low bandwidth of R Hz. There are quite a few disadvantages of this line code. A loss of synchronization and timing jitter can result with a long sequence of **1**s or **0**s because no pulse transition is present. The code has no error detection capability and, hence, performance cannot be monitored. There is a significant dc component as well as a dc content. The error rate performance is not as good as that of polar line codes.

6.2.2 Unipolar RZ

In this line code, a binary **1** is represented by a nonzero voltage level during a portion of the bit duration, usually for half of the bit period, and a zero voltage level for rest of the bit

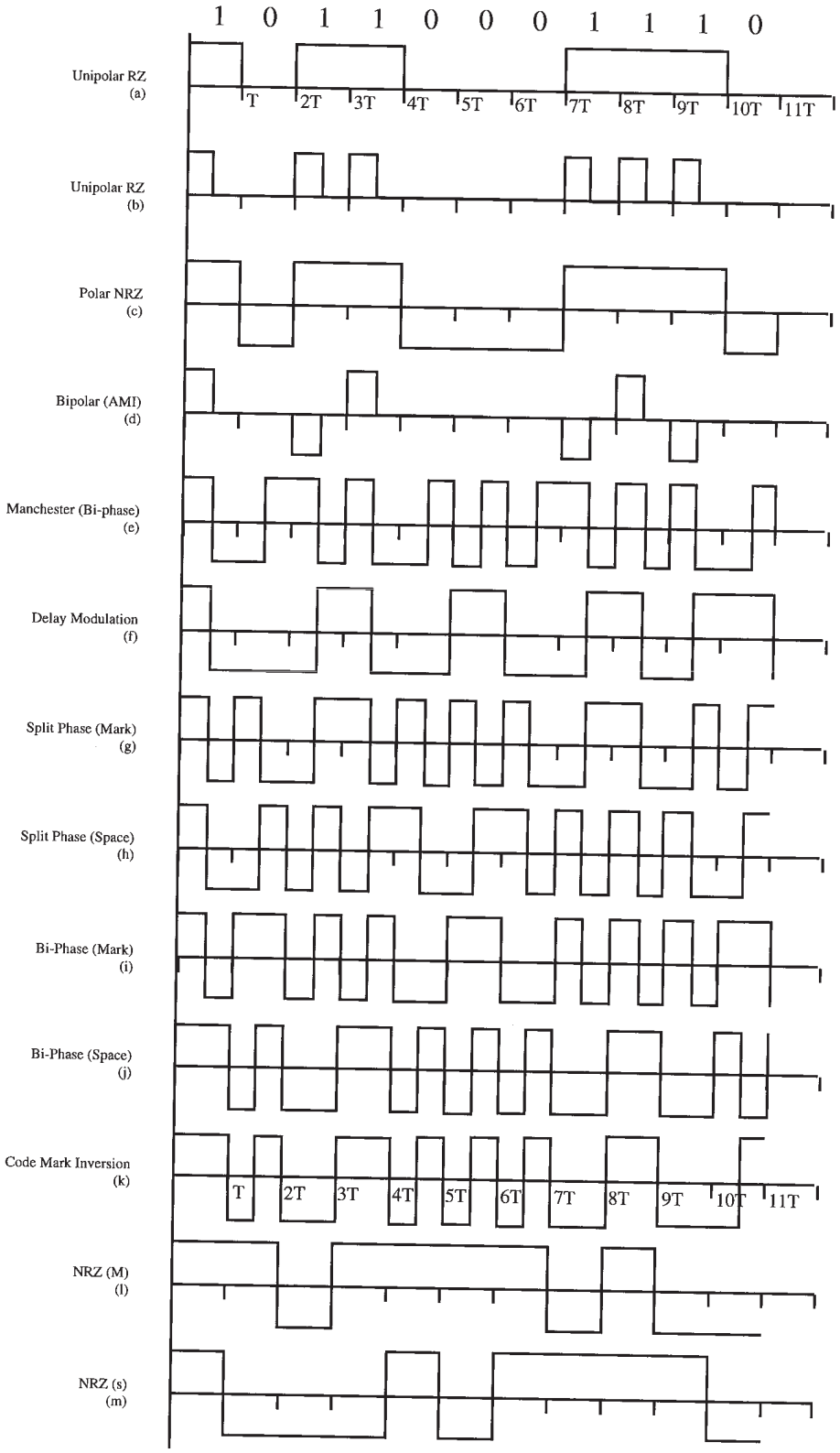


FIGURE 6.1 Waveforms for different line codes.

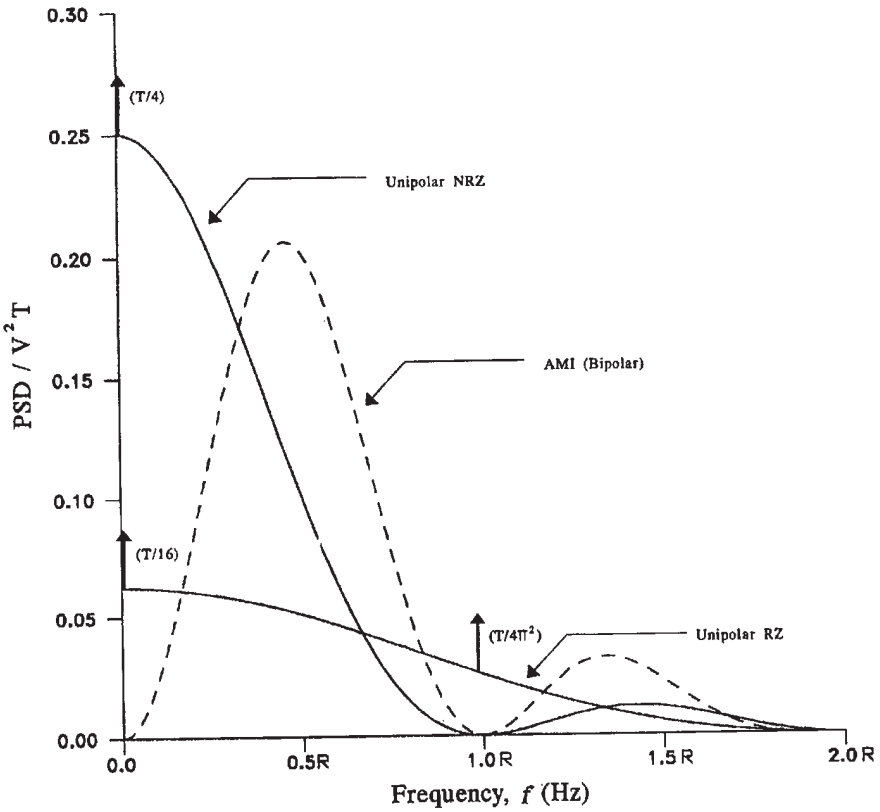


Figure 6.2a Power spectral density of different line codes, where $R = 1/\mathrm{T}$ is the bit rate.

duration. A binary **0** is represented by a zero voltage level during the entire bit duration. Thus, this is an instantaneous level code. Figure 6.1(b) illustrates a unipolar RZ waveform in which the **1** is represented by a nonzero voltage level for half the bit period. The PSD of this line code, with equally likely binary digits, is given by [5, 6, 8]

$$S_2(f) = \frac{V^2T}{16}\left(\frac{\sin \pi fT/2}{\pi fT/2}\right)^2 + \frac{V^2}{4\pi^2}\left[\frac{\pi^2}{4}\delta(f) + \sum_{n=-\infty}^{\infty}\frac{1}{(2n+1)^2}\delta(f-(2n+1)R)\right] \tag{6.3}$$

where again V is the binary **1** voltage level, and $T = 1/R$ is the bit period. The spectrum of this code is drawn in Fig. 6.2a. In the most general case, when the probability of a **1** is p, the continuous portion of the PSD in Eq. (6.3) is scaled by the factor $4p(1-p)$ and the discrete portion is scaled by the factor $4p^2$. The first null bandwidth of unipolar RZ is $2R$ Hz. The error rate performance of this line code is the same as that of the unipolar NRZ provided we increase the voltage level of this code such that the energy in binary **1**, E_b, is the same for both codes. The probability of error is given by Eq. (6.2) and identified in Fig. 6.3. If the voltage level and bit period are the same for unipolar NRZ and unipolar RZ, then the energy in a binary **1** for unipolar RZ will be $V^2T/2$ and the probability of error is worse by 3 dB.

The main advantages of unipolar RZ are, again, ease of generation since it requires a single power supply and the presence of a discrete spectral component at the symbol rate, which

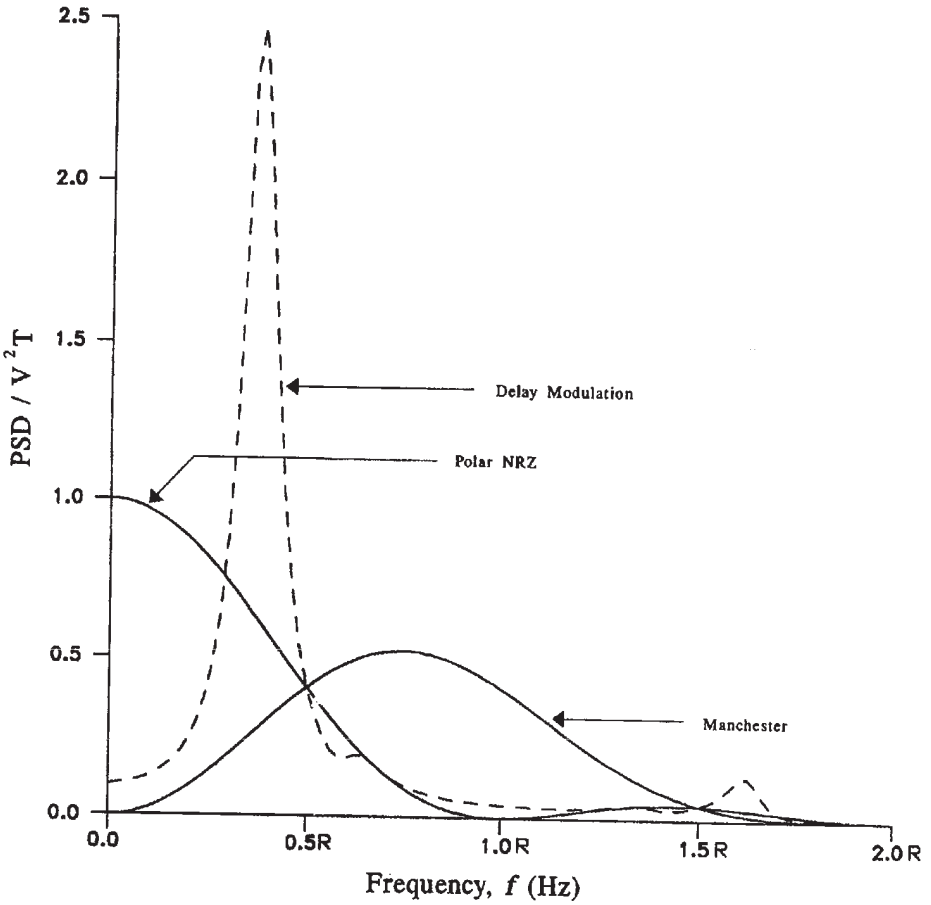


Figure 6.2b Power spectral density of different line codes, where $R = 1/\mathrm{T}$ is the bit rate.

allows simple timing recovery. A number of disadvantages exist for this line code. It has a nonzero dc component and nonzero dc content, which can lead to dc wander. A long string of **0**s will lack pulse transitions and could lead to loss of synchronization. There is no error detection capability and, hence, performance monitoring is not possible. The bandwidth requirement ($2R$ Hz) is higher than that of NRZ signals. The error rate performance is worse than that of polar line codes.

Unipolar NRZ as well as unipolar RZ are examples of pulse/no-pulse type of signalling. In this type of signalling, the pulse for a binary **0**, $g_2(t)$, is zero and the pulse for a binary **1** is specified generically as $g_1(t) = g(t)$. Using $G(f)$ as the Fourier transform of $g(t)$, the PSD of pulse/no-pulse signalling is given as [6, 7, 10]

$$S_{\mathrm{PNP}}(f) = p(1-p)R|G(f)|^2 + p^2R^2 \sum_{n=-\infty}^{\infty} |G(nR)|^2 \delta(f - nR) \tag{6.4}$$

where p is the probability of a binary **1**, and R is the bit rate.

6.2.3 Polar NRZ

In this line code, a binary **1** is represented by a positive voltage $+V$ and a binary **0** is represented by a negative voltage $-V$ over the full bit period. This code is also referred to

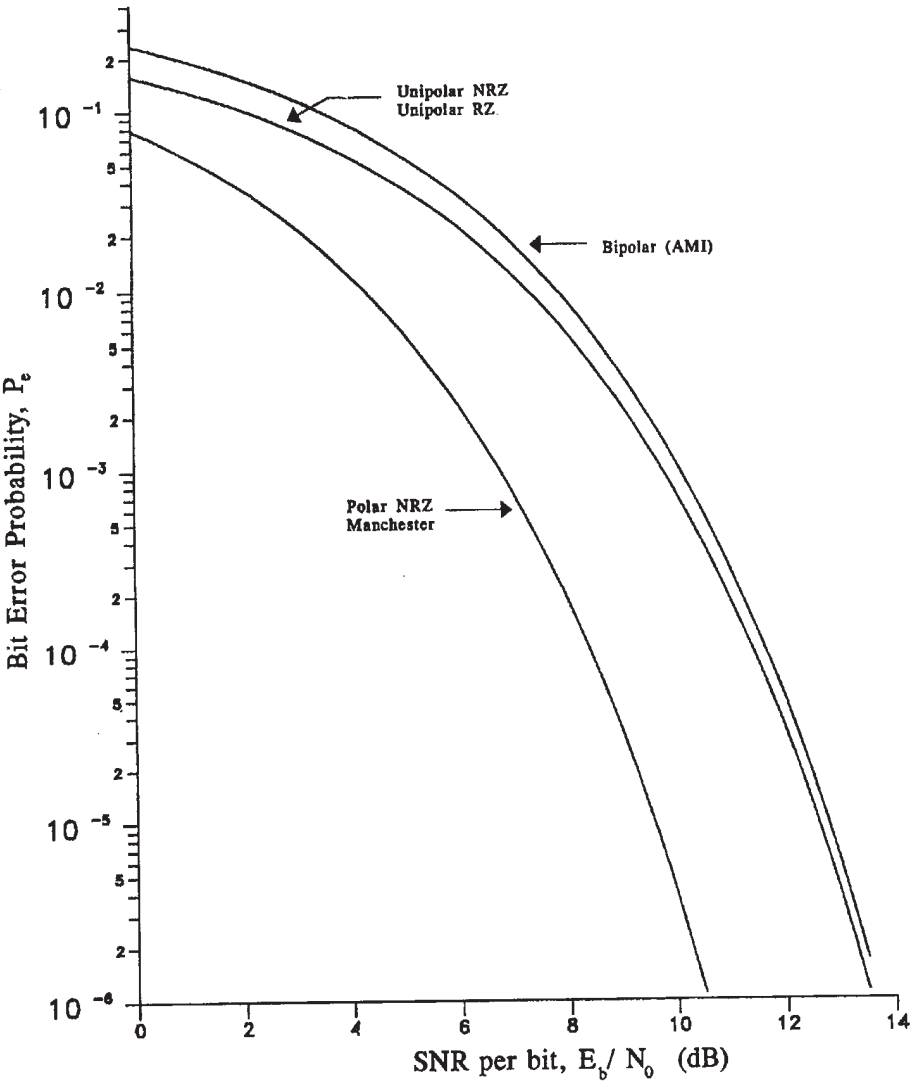


FIGURE 6.3 Bit error probability for different line codes.

as NRZ (L), since a bit is represented by maintaining a level (L) during its entire period. A polar NRZ waveform is shown in Fig. 6.1(c). This is again an instantaneous level code. Alternatively, a **1** may be represented by a $-V$ voltage level and a **0** by a $+V$ voltage level, without changing the spectral characteristics and performance of the line code. The PSD of this line code with equally likely bits is given by [5, 8]

$$S_3(f) = V^2 T \left(\frac{\sin \pi f T}{\pi f T} \right)^2 \tag{6.5}$$

This is plotted in Fig. 6.2b. When the probability of a **1** is p, and p is not 0.5, a dc component exists, and the PSD becomes [10]

$$S_{3p}(f) = 4V^2 T p(1-p) \left(\frac{\sin \pi f T}{\pi f T} \right)^2 + V^2 (1-2p)^2 \delta(f) \tag{6.6}$$

The first null bandwidth for this line code is again R Hz, independent of p. The probability of error of this line code when $p = 0.5$ is given by [1, 5]

$$P_e = \frac{1}{2}\text{erfc}\left(\sqrt{\frac{E_b}{N_0}}\right) \tag{6.7}$$

The performance of polar NRZ is plotted in Fig. 6.3. This is better than the error performance of the unipolar codes by 3 dB.

The advantages of polar NRZ include a low-bandwidth requirement, R Hz, comparable to unipolar NRZ, very good error probability, and greatly reduced dc because the waveform has a zero dc component when $p = 0.5$ even though the dc content is never zero. A few notable disadvantages are that there is no error detection capability, and that a long string of **1**s or **0**s could result in loss of synchronization, since there are no transitions during the string duration. Two power supplies are required to generate this code.

6.2.4 Polar RZ [Bipolar, Alternate Mark Inversion (AMI), or Pseudoternary]

In this scheme, a binary **1** is represented by alternating the positive and negative voltage levels, which return to zero for a portion of the bit duration, generally half the bit period. A binary **0** is represented by a zero voltage level during the entire bit duration. This line coding scheme is often called **alternate mark inversion (AMI)** since **1**s (marks) are represented by alternating positive and negative pulses. It is also called *pseudoternary* since three different voltage levels are used to represent binary data. Some authors designate this line code as bipolar RZ (BRZ). An AMI waveform is shown in Fig. 6.1(d). Note that this is a level code with memory. The AMI code is well known for its use in telephony. The PSD of this line code with memory is given by [1, 2, 7]

$$S_{4p}(f) = 2p(1-p)R|G(f)|^2\left(\frac{1-\cos 2\pi fT}{1+(2p-1)^2+2(2p-1)\cos 2\pi fT}\right) \tag{6.8}$$

where $G(f)$ is the Fourier transform of the pulse used to represent a binary **1**, and p is the probability of a binary **1**. When $p = 0.5$ and square pulses with amplitude $\pm V$ and duration $T/2$ are used to represent binary **1**s, the PSD becomes

$$S_4(f) = \frac{V^2T}{4}\left(\frac{\sin \pi fT/2}{\pi fT/2}\right)^2 \sin^2(\pi fT) \tag{6.9}$$

This PSD is plotted in Fig. 6.2a. The first null bandwidth of this waveform is R Hz. This is true for RZ rectangular pulses, independent of the value of p in Eq. (6.8). The error rate performance of this line code for equally likely binary data is given by [5]

$$P_e \approx \frac{3}{4}\text{erfc}\left(\sqrt{\frac{E_b}{2N_0}}\right), \qquad E_b/N_0 > 2 \tag{6.10}$$

This curve is plotted in Fig. 6.3 and is seen to be no more than 0.5 dB worse than the unipolar codes.

The advantages of polar RZ (or AMI, as it is most commonly called) outweigh the disadvantages. This code has no dc component and zero dc content, completely avoiding the dc wander problem. Timing recovery is rather easy since squaring, or full-wave rectifying, this type of signal yields a unipolar RZ waveform with a discrete component at the bit rate, R Hz. Because of the alternating polarity pulses for binary **1**s, this code has error detection

and, hence, performance monitoring capability. It has a low-bandwidth requirement, R Hz, comparable to unipolar NRZ. The obvious disadvantage is that the error rate performance is worse than that of the unipolar and polar waveforms. A long string of **0**s could result in loss of synchronization, and two power supplies are required for this code.

6.2.5 Manchester Coding (Split Phase or Digital Biphase)

In this coding, a binary **1** is represented by a pulse that has positive voltage during the first-half of the bit duration and negative voltage during second-half of the bit duration. A binary **0** is represented by a pulse that is negative during the first-half of the bit duration and positive during the second-half of the bit duration. The negative or positive midbit transition indicates a binary **1** or binary **0,** respectively. Thus, a Manchester code is classified as an instantaneous transition code; it has no memory. The code is also called diphase because a square wave with a 0° phase is used to represent a binary **1** and a square wave with a phase of 180° used to represent a binary **0;** or vice versa. This line code is used in Ethernet local area networks (LANs). The waveform for Manchester coding is shown in Fig. 6.1(e). The PSD of a Manchester waveform with equally likely bits is given by [5, 8]

$$S_5(f) = V^2 T \left(\frac{\sin \pi f T/2}{\pi f T/2} \right)^2 \sin^2 (\pi f T/2) \tag{6.11}$$

where $\pm V$ are used as the positive/negative voltage levels for this code. Its spectrum is plotted in Fig. 6.2b. When the probability p of a binary **1,** is not equal to one-half, the continuous portion of the PSD is reduced in amplitude and discrete components appear at integer multiples of the bit rate, $R = 1/T$. The resulting PSD is [6, 10]

$$\begin{aligned} S_{5p}(f) &= V^2 T 4p(1-p) \left(\frac{\sin \pi f T/2}{\pi f T/2} \right)^2 \sin^2 \frac{\pi f T}{2} \\ &\quad + V^2 (1-2p)^2 \sum_{n=-\infty, n \neq 0}^{\infty} \left(\frac{2}{n\pi} \right)^2 \delta(f - nR) \end{aligned} \tag{6.12}$$

The first null bandwidth of the waveform generated by a Manchester code is $2R$ Hz. The error rate performance of this waveform when $p = 0.5$ is the same as that of polar NRZ, given by Eq. (6.9), and plotted in Fig. 6.3.

The advantages of this code include a zero dc content on an individual pulse basis, so no pattern of bits can cause dc buildup; midbit transitions are always present making it is easy to extract timing information; and it has good error rate performance, identical to polar NRZ. The main disadvantage of this code is a larger bandwidth than any of the other common codes. Also, it has no error detection capability and, hence, performance monitoring is not possible.

Polar NRZ and Manchester coding are examples of the use of pure polar signalling where the pulse for a binary **0,** $g_2(t)$ is the negative of the pulse for a binary **1,** i.e., $g_2(t) = -g_1(t)$. This is also referred to as an antipodal signal set. For this broad type of polar binary line code, the PSD is given by [10]

$$S_{\mathrm{BP}}(f) = 4p(1-p)R|G(f)|^2 + (2p-1)^2 R^2 \sum_{n=-\infty}^{\infty} |G(nR)|^2 \delta(f - nR) \tag{6.13}$$

where $|G(f)|$ is the magnitude of the Fourier transform of either $g_1(t)$ or $g_2(t)$.

A further generalization of the PSD of binary line codes can be given, wherein a continuous spectrum and a discrete spectrum is evident. Let a binary **1,** with probability p, be represented by $g_1(t)$ over the $T = 1/R$ second bit interval; and let a binary **0,** with probability $1-p$, be represented by $g_2(t)$ over the same T second bit interval. The two-sided PSD for this general binary line code is [10]

$$\begin{aligned} S_{\mathrm{GB}}(f) &= p(1-p)R\,|G_1(f) - G_2(f)|^2 \\ &\quad + R^2 \sum_{n=-\infty}^{\infty} |pG_1(nR) + (1-p)G_2(nR)|^2\, \delta(f - nR) \end{aligned} \tag{6.14}$$

where the Fourier transform of $g_1(t)$ and $g_2(t)$ are given by $G_1(f)$ and $G_2(f)$, respectively.

6.3 Alternate Line Codes

Most of the line codes discussed thus far were instantaneous level codes. Only AMI had memory, and Manchester was an instantaneous transition code. The alternate line codes presented in this section all have memory. The first four are transition codes, where binary data is represented as the presence or absence of a transition, or by the direction of transition, i.e., positive to negative or vice versa. The last four codes described in this section are level line codes with memory.

6.3.1 Delay Modulation (Miller Code)

In this line code, a binary **1** is represented by a transition at the midbit position, and a binary **0** is represented by no transition at the midbit position. If a **0** is followed by another **0,** however, the signal transition also occurs at the end of the bit interval, that is, between the two **0**s. An example of delay modulation is shown in Fig. 6.1(f). It is clear that delay modulation is a transition code with memory. This code achieves the goal of providing good timing content without sacrificing bandwidth. The PSD of the Miller code for equally likely data is given by [10]

$$\begin{aligned} S_6(f) &= \frac{V^2 T}{2(\pi fT)^2(17 + 8\cos 2\pi fT)} \\ &\quad \times (23 - 2\cos \pi fT - 22\cos 2\pi fT \\ &\quad - 12\cos 3\pi fT + 5\cos 4\pi fT + 12\cos 5\pi fT \\ &\quad + 2\cos 6\pi fT - 8\cos 7\pi fT + 2\cos 8\pi fT) \end{aligned} \tag{6.15}$$

This spectrum is plotted in Fig. 6.2b. The advantages of this code are that it requires relatively low bandwidth, most of the energy is contained in less than $0.5R$. However, there is no distinct spectral null within the $2R$-Hz band. It has low dc content and no dc component. It has very good timing content, and carrier tracking is easier than Manchester coding. Error rate performance is comparable to that of the common line codes. One important disadvantage is that it has no error detection capability and, hence, performance cannot be monitored.

6.3.2 Split Phase (Mark)

This code is similar to Manchester in the sense that there are always midbit transitions. Hence, this code is relatively easy to synchronize and has no dc. Unlike Manchester, however, split phase (mark) encodes a binary digit into a midbit transition dependent on the

midbit transition in the previous bit period [12]. Specifically, a binary **1** produces a reversal of midbit transition relative to the previous midbit transition. A binary **0** produces no reversal of the midbit transition. Certainly this is a transition code with memory. An example of a split phase (mark) coded waveform is shown in Fig. 6.1(g), where the waveform in the first bit period is chosen arbitrarily. Since this method encodes bits differentially, there is no 180°-phase ambiguity associated with some line codes. This phase ambiguity may not be an issue in most baseband links but is important if the line code is modulated. Split phase (space) is very similar to split phase (mark), where the role of the binary **1** and binary **0** are interchanged. An example of a split phase (space) coded waveform is given in Fig. 6.1(h); again, the first bit waveform is arbitrary.

6.3.3 Biphase (Mark)

This code, designated as Bi ϕ-M, is similar to a Miller code in that a binary **1** is represented by a midbit transition, and a binary **0** has no midbit transition. However, this code always has a transition at the beginning of a bit period [10]. Thus, the code is easy to synchronize and has no dc. An example of Bi ϕ-M is given in Fig. 6.1(i), where the direction of the transition at $t = 0$ is arbitrarily chosen. Biphase (space) or Bi ϕ-S is similar to Bi ϕ-M, except the role of the binary data is reversed. Here a binary **0** (space) produces a midbit transition, and a binary **1** does not have a midbit transition. A waveform example of Bi ϕ-S is shown in Fig. 6.1(j). Both Bi ϕ-S and Bi ϕ-M are transition codes with memory.

6.3.4 Code Mark Inversion (CMI)

This line code is used as the interface to a Consultative Committee on International Telegraphy and Telephony (CCITT) multiplexer and is very similar to Bi ϕ-S. A binary **1** is encoded as an NRZ pulse with alternate polarity, $+V$ or $-V$. A binary **0** is encoded with a definitive midbit transition (or square wave phase) [1]. An example of this waveform is shown in Fig. 6.1(k) where a negative to positive transition (or 180° phase) is used for a binary **0.** The voltage level of the first binary **1** in this example is chosen arbitrarily. This example waveform is identical to Bi ϕ-S shown in Fig. 6.1(j), except for the last bit. CMI has good synchronization properties and has no dc.

6.3.5 NRZ (I)

This type of line code uses an inversion (I) to designate binary digits, specifically, a change in level or no change in level. There are two variants of this code, NRZ mark (M) and NRZ space (S) [5, 12]. In NRZ (M), a change of level is used to indicate a binary **1,** and no change of level is used to indicate a binary **0.** In NRZ (S) a change of level is used to indicate a binary **0,** and no change of level is used to indicate a binary **1.** Waveforms for NRZ (M) and NRZ (S) are depicted in Fig. 6.1(l) and Fig. 6.1(m), respectively, where the voltage level of the first binary **1** in the example is chosen arbitrarily. These codes are level codes with memory. In general, line codes that use differential encoding, like NRZ (I), are insensitive to 180° phase ambiguity. Clock recovery with NRZ (I) is not particularly good, and dc wander is a problem as well. Its bandwidth is comparable to polar NRZ.

6.3.6 Binary N Zero Substitution (BNZS)

The common bipolar code AMI has many desirable properties of a line code. Its major limitation, however, is that a long string of zeros can lead to loss of synchronization and

timing jitter because there are no pulses in the waveform for relatively long periods of time. **Binary N zero substitution (BNZS)** attempts to improve AMI by substituting a special code of length N for all strings of N zeros. This special code contains pulses that look like binary **1**s but purposely produce violations of the AMI pulse convention. Two consecutive pulses of the same polarity violate the AMI pulse convention, independent of the number of zeros between the two consecutive pulses. These violations can be detected at the receiver, and the special code replaced by N zeros. The special code contains pulses facilitating synchronization even when the original data has long string of zeros. The special code is chosen such that the desirable properties of AMI coding are retained despite the AMI pulse convention violations, i.e., dc balance and error detection capability. The only disadvantage of BNZS compared to AMI is a slight increase in crosstalk due to the increased number of pulses and, hence, an increase in the average energy in the code.

Choosing different values of N yields different BNZS codes. The value of N is chosen to meet the timing requirements of the application. In telephony, there are three commonly used BNZS codes: B6ZS, B3ZS, and B8ZS. All BNZS codes are level codes with memory.

In a B6ZS code, a string of six consecutive zeros is replaced by one of two the special codes according to the rule:

If the last pulse was positive (+), the special code is: $0\ +\ -\ 0\ -\ +$.
If the last pulse was negative (−), the special code is: $0\ -\ +\ 0\ +\ -$.

Here a zero indicates a zero voltage level for the bit period; a plus designates a positive pulse; and a minus indicates a negative pulse.

This special code causes two AMI pulse violations: in its second bit position and in its fifth bit position. These violations are easily detected at the receiver and zeros resubstituted. If the number of consecutive zeros is $12, 18, 24, \ldots$, the substitution is repeated $2, 3, 4, \ldots$ times. Since the number of violations is even, the B6ZS waveform is the same as the AMI waveform outside the special code, i.e., between special code sequences.

There are four pulses introduced by the special code that facilitates timing recovery. Also, note that the special code is dc balanced. An example of the B6ZS code is given as follows, where the special code is indicated by the bold characters.

Original data:	0	1	0	0	0	0	0	0	1	1	0	1	0	0	0	0	0	0	1	1
B6ZS format:	0	+	**0**	+	−	**0**	−	+	−	+	0	−	**0**	−	+	**0**	+	−	+	−

The computation of the PSD of a B6ZS code is tedious. Its shape is given in Fig. 6.4, for comparison purposes with AMI, for the case of equally likely data.

In a B3ZS code, a string of three consecutive zeros is replaced by either $B\mathbf{0}V$ or $\mathbf{00V}$, where B denotes a pulse obeying the AMI (bipolar) convention and V denotes a pulse violating the AMI convention. $B\mathbf{0}V$ or $\mathbf{00}V$ is chosen such that the number of bipolar (B) pulses between the violations is odd. The B3ZS rules are summarized in Table 6.1.

TABLE 6.1 B3ZS Substitution Rules

Number of B Pulses Since Last Violation	Polarity of Last B Pulse	Substitution Code	Substitution Code Form
Odd	Negative (−)	**00−**	**00**V
Odd	Positive (+)	**00+**	**00**V
Even	Negative (−)	**+0+**	$B\mathbf{0}V$
Even	Positive (+)	**−0−**	$B\mathbf{0}V$

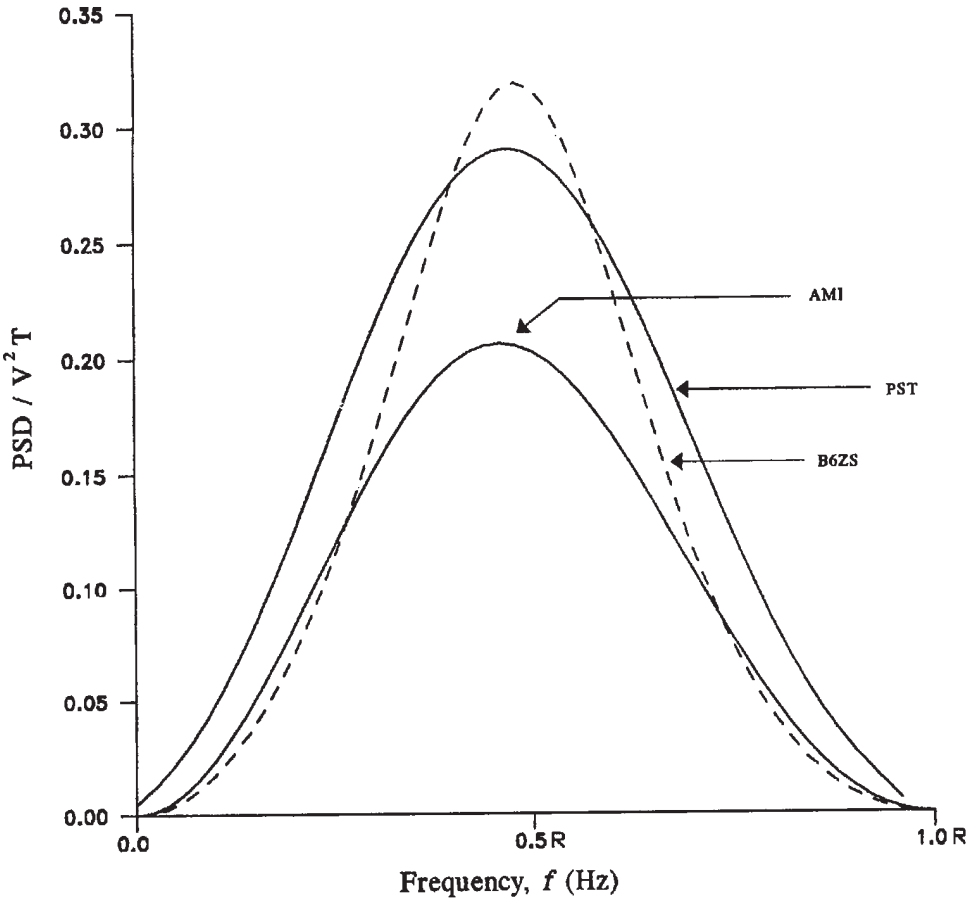


FIGURE 6.4 Power spectral density of different line codes, where $R = 1/\mathrm{T}$ is the bit rate.

Observe that the violation always occurs in the third bit position of the substitution code, and so it can be easily detected and zero replacement made at the receiver. Also, the substitution code selection maintains dc balance. There is either one or two pulses in the substitution code, facilitating synchronization. The error detection capability of AMI is retained in B3ZS because a single channel error would make the number of bipolar pulses between violations even instead of being odd. Unlike B6ZS, the B3ZS waveform between violations may not be the same as the AMI waveform. B3ZS is used in the digital signal-3 (DS-3) signal interface in North America and also in the long distance-4 (LD-4) coaxial transmission system in Canada. Next is an example of a B3ZS code, using the same symbol meaning as in the B6ZS code.

Original data:	1	0	0	1	0	0	0	1	1	0	0	0	0	1	0	0	0	1
B3ZS format:																		
Even No. of B pulses:	+	0	0	−	+	**0**	+	−	+	−	**0**	−	0	+	**0**	**0**	+	−
Odd No. of B pulses:	+	0	0	−	**0**	**0**	−	+	−	+	**0**	+	0	−	**0**	**0**	−	+

The last BNZS code considered here uses $N = 8$. A B8ZS code is used to provide transparent channels for the Integrated Services Digital Network (ISDN) on T1 lines and is similar to the B6ZS code. Here a string of eight consecutive zeros is replaced by one of two

special codes according to the following rule:

If the last pulse was positive (+), the special code is: 0 0 0 + − 0 − +.
If the last pulse was negative (−), the special code is: 0 0 0 − + 0 + −.

There are two bipolar violations in the special codes, at the fourth and seventh bit positions. The code is dc balanced, and the error detection capability of AMI is retained. The waveform between substitutions is the same as that of AMI. If the number of consecutive zeros is $16, 24, \ldots$, then the substitution is repeated $2, 3, \ldots$, times.

6.3.7 High-Density Bipolar N (HDBN)

This coding algorithm is a CCITT standard recommended by the Conference of European Posts and Telecommunications Administrations (CEPT), a European standards body. It is quite similar to BNZS coding. It is thus a level code with memory. Whenever there is a string of $N + 1$ consecutive zeros, they are replaced by a special code of length $N + 1$ containing AMI violations. Specific codes can be constructed for different values of N. A specific **high-density bipolar N (HDBN)** code, HDB3, is implemented as a CEPT primary digital signal. It is very similar to the B3ZS code. In this code, a string of four consecutive zeros is replaced by either $B00V$ or $000V$. $B00V$ or $000V$ is chosen such that the number of bipolar (B) pulses between violations is odd. The HDB3 rules are summarized in Table 6.2.

TABLE 6.2 HDB3 Substitution Rules

Number of B Pulses Since Last Violation	Polarity of Last B Pulse	Substitution Code	Substitution Code Form
Odd	Negative (−)	000−	$000V$
Odd	Positive (+)	000+	$000V$
Even	Negative (−)	+00+	$B00V$
Even	Positive (+)	−00−	$B00V$

Here the violation always occurs in the fourth bit position of the substitution code, so that it can be easily detected and zero replacement made at the receiver. Also, the substitution code selection maintains dc balance. There is either one or two pulses in the substitution code facilitating synchronization. The error detection capability of AMI is retained in HDB3 because a single channel error would make the number of bipolar pulses between violations even instead of being odd.

6.3.8 Ternary Coding

Many line coding schemes employ three symbols or levels to represent only one bit of information, like AMI. Theoretically, it should be possible to transmit information more efficiently with three symbols, specifically the maximum efficiency is $\log_2 3 = 1.58$ bits per symbol. Alternatively, the redundancy in the code signal space can be used to provide better error control. Two examples of ternary coding are described next [1, 2]: **pair selected ternary (PST)** and **4 binary 3 ternary (4B3T).** The PST code has many of the desirable properties of line codes, but its transmission efficiency is still 1 bit per symbol. The 4B3T code also has many of the desirable properties of line codes, and it has increased transmission efficiency.

In the PST code, two consecutive bits, termed a binary pair, are grouped together to form a word. These binary pairs are assigned codewords consisting of two ternary symbols, where each ternary symbol can be +, −, or 0, just as in AMI. There are nine possible ternary codewords. Ternary codewords with identical elements, however, are avoided, i.e., ++, −−, and 00. The remaining six codewords are transmitted using two modes called + mode and − mode. The modes are switched whenever a codeword with a single pulse is transmitted. The PST code and mode switching rules are summarized in Table 6.3.

TABLE 6.3 PST Codeword Assignment and Mode Switching Rules

	Ternary Codewords		Mode
Binary Pair	+ Mode	− Mode	Switching
11	+ −	+ −	No
10	+ 0	− 0	Yes
01	0 +	0 −	Yes
00	− +	− +	No

PST is designed to maintain dc balance and include a strong timing component. One drawback of this code is that the bits must be framed into pairs. At the receiver, an *out-of-frame* condition is signalled when unused ternary codewords (++, −−, and 00) are detected. The mode switching property of PST provides error detection capability. PST can be classified as a level code with memory.

If the original data for PST coding contains only **1**s or **0**s, an alternating sequence of +− +− ⋯ is transmitted. As a result, an out-of-frame condition can not be detected. This problem can be minimized by using the modified PST code as shown in Table 6.4.

TABLE 6.4 Modified PST Codeword Assignment and Mode Switching Rules

	Ternary Codewords		Mode
Binary Pair	+ Mode	− Mode	Switching
11	+ 0	0 −	Yes
10	+ −	+ −	No
01	− +	− +	No
00	0 +	− 0	Yes

It is tedious to derive the PSD of a PST coded waveform. Again, Fig. 6.4 shows the PSD of the PST code along with the PSD of AMI and B6ZS for comparison purposes, all for equally likely binary data. Observe that PST has more power than AMI and, thus, a larger amount of energy per bit, which translates into slightly increased crosstalk.

In 4B3T coding, words consisting of four binary digits are mapped into three ternary symbols. Four bits imply $2^4 = 16$ possible binary words, whereas three ternary symbols allow $3^3 = 27$ possible ternary codewords. The binary-to-ternary conversion in 4B3T insures dc balance and a strong timing component. The specific codeword assignment is as shown in Table 6.5.

TABLE 6.5 4B3T Codeword Assignment

	Ternary Codewords		
Binary Words	Column 1	Column 2	Column 3
0000	− − −		+ + +
0001	− − 0		+ + 0
0010	− 0 −		+ 0 +
0011	0 − −		0 + +
0100	− − +		+ + −
0101	− + −		+ − +
0110	+ − −		− + +
0111	− 0 0		+ 0 0
1000	0 − 0		0 + 0
1001	0 0 −		0 0 +
1010		0 + −	
1011		0 − +	
1100		+ 0 −	
1101		− 0 +	
1110		+ − 0	
1111		− + 0	

There are three types of codewords in Table 6.5, organized into three columns. The codewords in the first column have negative dc, codewords in the second column have zero dc, and those in the third column have positive dc. The encoder monitors the integer variable

$$I = N_p - N_n \ , \tag{6.16}$$

where N_p is the number of positive pulses transmitted and N_n are the number of negative pulses transmitted. Codewords are chosen according to following rule:

If $I < 0$, choose the ternary codeword from columns 1 and 2.

If $I > 0$, choose the ternary codeword from columns 2 and 3.

If $I = 0$, choose the ternary word from column 2, and from column 1 if the previous $I > 0$ or from column 3 if the previous $I < 0$.

Note that the ternary codeword 000 is not used, but the remaining 26 codewords are used in a complementary manner. For example, the column 1 codeword for 0001 is $--0$, whereas the column 3 codeword is $++0$. The maximum transmission efficiency for the 4B3T code is 1.33 bits per symbol compared to 1 bit per symbol for the other line codes. The disadvantages of 4B3T are that framing is required and that performance monitoring is complicated. The 4B3T code is used in the T148 span line developed by ITT Telecommunications. This code allows transmission of 48 channels using only 50% more bandwidth than required by T1 lines, instead of 100% more bandwidth.

6.4 Multilevel Signalling, Partial Response Signalling, and Duobinary Coding

Ternary coding, such as 4B3T, is an example of the use of more than two levels to improve the transmission efficiency. To increase the transmission efficiency further, more

levels and/or more signal processing is needed. Multilevel signalling allows an improvement in the transmission efficiency at the expense of an increase in the error rate, i.e., more transmitter power will be required to maintain a given probability of error. In partial response signalling, intersymbol interference is deliberately introduced by using pulses that are wider and, hence, require less bandwidth. The controlled amount of interference from each pulse can be removed at the receiver. This improves the transmission efficiency, at the expense of increased complexity. **Duobinary coding,** a special case of partial response signalling, requires only the minimum theoretical bandwidth of $0.5R$ Hz. In what follows these techniques are discussed in slightly more detail.

6.4.1 Multilevel Signalling

The number of levels that can be used for a line code is not restricted to two or three. Since more levels or symbols allow higher transmission efficiency, multilevel signalling can be considered in bandwidth-limited applications. Specifically, if the signalling rate or baud rate is R_s and the number of levels used is L, the equivalent transmission bit rate R_b is given by

$$R_b = R_s \log_2[L] \ . \tag{6.17}$$

Alternatively, multilevel signalling can be used to reduce the baud rate, which in turn can reduce crosstalk for the same equivalent bit rate. The penalty, however, is that the SNR must increase to achieve the same error rate. The T1G carrier system of AT&T uses multilevel signalling with $L = 4$ and a baud rate of 3.152 mega-symbols/s to double the capacity of the T1C system from 48 channels to 96 channels. Also, a four level signalling scheme at 80-kB is used to achieve 160 kb/s as a basic rate in a digital subscriber loop (DSL) for ISDN.

6.4.2 Partial Response Signalling and Duobinary Coding

This class of signalling is also called *correlative* coding because it purposely introduces a controlled or correlated amount of intersymbol interference in each symbol. At the receiver, the known amount of interference is effectively removed from each symbol. The advantage of this signalling is that wider pulses can be used requiring less bandwidth, but the SNR must be increased to realize a given error rate. Also, errors can propagate unless *precoding* is used.

There are many commonly used partial response signalling schemes, often described in terms of the delay operator D, which represents one signalling interval delay. For example, in $(1 + D)$ signalling the current pulse and the previous pulse are added. The T1D system of AT&T uses $(1 + D)$ signalling with precoding, referred to as duobinary signalling, to convert binary (two level) data into ternary (three level) data at the same rate. This requires the minimum theoretical channel bandwidth without the deleterious effects of intersymbol interference and avoids error propagation. Complete details regarding duobinary coding are found in Lender, 1963 and Schwartz, 1980. Some partial response signalling schemes, such as $(1 - D)$, are used to shape the bandwidth rather than control it. Another interesting example of duobinary coding is a $(1 - D^2)$, which can be analyzed as the product $(1 - D)$ $(1 + D)$. It is used by GTE in its modified T carrier system. AT&T also uses $(1 - D^2)$ with four input levels to achieve an equivalent data rate of 1.544 Mb/s in only a 0.5-MHz bandwidth.

6.5 Bandwidth Comparison

We have provided the PSD expressions for most of the commonly used line codes. The actual bandwidth requirement, however, depends on the pulse shape used and the definition of bandwidth itself. There are many ways to define bandwidth, for example, as a percentage of the total power or the sidelobe suppression relative to the main lobe. Using the first null of the PSD of the code as the definition of bandwidth, Table 6.6 provides a useful bandwidth comparison.

TABLE 6.6 First Null Bandwidth Comparison

Bandwidth	Codes	
	Unipolar NRZ	BNZS
R	Polar NRZ	HDBN
	Polar RZ (AMI)	PST
$2R$	Unipolar RZ	Split Phase
	Manchester	CMI

The notable omission in Table 6.6 is delay modulation (Miller code). It does not have a first null in the $2R$-Hz band, but most of its power is contained in less than $0.5R$ Hz.

6.6 Concluding Remarks

An in-depth presentation of line coding, particularly applicable to telephony, has been included in this chapter. The most desirable characteristics of line codes were discussed. We introduced five common line codes and eight alternate line codes. Each line code was illustrated by an example waveform. In most cases expressions for the PSD and the probability of error were given and plotted. Advantages and disadvantages of all codes were included in the discussion, and some specific applications were noted. Line codes for optical fiber channels and networks built around them, such as fiber distributed data interface (FDDI) were not included in this section. A discussion of line codes for optical fiber channels, and other new developments in this topic area can be found in [1, 3, 4].

Defining Terms

Alternate mark inversion (AMI): A popular name for bipolar line coding using three levels: zero, positive, and negative.

Binary N zero substitution (BNZS): A class of coding schemes that attempts to improve AMI line coding.

Bipolar: A particular line coding scheme using three levels: zero, positive, and negative.

Crosstalk: An unwanted signal from an adjacent channel.

DC wander: The dc level variation in the received signal due to a channel that cannot support dc.

Duobinary coding: A coding scheme with binary input and ternary output requiring the minimum theoretical channel bandwidth.

4 Binary 3 Ternary (4B3T): A line coding scheme that maps four binary digits into three ternary symbols.

High-density bipolar N (HDBN): A class of coding schemes that attempts to improve AMI.

Level codes: Line codes carrying information in their voltage levels.

Line coding: The process of converting abstract symbols into real, temporal waveforms to be transmitted through a baseband channel.

Nonreturn to zero (NRZ): A signal that stays at a nonzero level for the entire bit duration.

Pair selected ternary (PST): A coding scheme based on selecting a pair of three level symbols.

Polar: A line coding scheme using both polarity of voltages, with or without a zero level.

Return to zero (RZ): A signal that returns to zero for a portion of the bit duration.

Transition codes: Line codes carrying information in voltage level transitions.

Unipolar: A line coding scheme using only one polarity of voltage, in addition to a zero level.

References

[1] Bellamy, J., *Digital Telephony,* John Wiley & Sons, New York, NY, 1991.

[2] Bell Telephone Laboratories Technical Staff Members. *Transmission Systems for Communications,* 4th ed., Western Electric Company, Technical Publications, Winston-Salem, NC, 1970.

[3] Bic, J.C., Duponteil, D., and Imbeaux, J.C., *Elements of Digital Communication,* John Wiley & Sons, New York, NY, 1991.

[4] Bylanski, P., *Digital Transmission Systems,* Peter Peregrinus, Herts, England, 1976.

[5] Couch, L.W., *Modern Communication Systems: Principles and Applications,* Prentice-Hall, Englewood Cliffs, NJ, 1994.

[6] Feher, K., *Digital Modulation Techniques in an Interference Environment,* EMC Encyclopedia Series, Vol. IX. Don White Consultants, Germantown, MD, 1977.

[7] Gibson, J.D., *Principles of Analog and Digital Communications,* MacMillan Publishing, New York, NY, 1993.

[8] Lathi, B.P., *Modern Digital and Analog Communication Systems,* Holt, Rinehart and Winston, Philadelphia, PA, 1989.

[9] Lender, A., Duobinary Techniques for High Speed Data Transmission, *IEEE Trans. Commun. Electron.,* CE-82, 214–218, May 1963.

[10] Lindsey, W.C. and Simon, M.K., *Telecommunication Systems Engineering,* Prentice-Hall, Englewood Cliffs, NJ, 1973.

[11] Schwartz, M., *Information Transmission, Modulation, and Noise,* McGraw-Hill, New York, NY, 1980.

[12] Stremler, F.G., *Introduction to Communication Systems,* Addison-Wesley Publishing, Reading, MA, 1990.

7

Echo Cancellation

7.1 Introduction 7-1
7.2 Echo Cancellation for PAM Systems 7-2
7.3 Echo Cancellation for QAM Systems 7-9
7.4 Echo Cancellation for OFDM Systems 7-11
7.5 Summary and Conclusions 7-14
References 7-14
Further Information 7-15

Giovanni Cherubini
IBM Zurich Research Laboratory

7.1 Introduction

Full-duplex data transmission over a single twisted-pair cable permits the simultaneous flow of information in two directions when the same frequency band is used. Examples of applications of this technique are found in digital communications systems that operate over the telephone network. In a digital subscriber loop, at each end of the full-duplex link, a circuit known as a hybrid separates the two directions of transmission. To avoid signal reflections at the near- and far-end hybrid, a precise knowledge of the line impedance would be required. Since the line impedance depends on line parameters that, in general, are not exactly known, an attenuated and distorted replica of the transmit signal leaks to the receiver input as an echo signal. Data-driven adaptive echo cancellation mitigates the effects of impedance mismatch.

A similar problem is caused by crosstalk in transmission systems over voice-grade unshielded twisted-pair cables for local-area network applications, where multipair cables are used to physically separate the two directions of transmission. Crosstalk is a statistical phenomenon due to randomly varying differential capacitive and inductive coupling between adjacent two-wire transmission lines. At the rates of several megabits per second that are usually considered for local-area network applications, near-end crosstalk (NEXT) represents the dominant disturbance; hence adaptive NEXT cancellation must be performed to ensure reliable communications.

In voiceband data modems, the model for the echo channel is considerably different from the echo model adopted in baseband transmission. The transmitted signal is a passband signal obtained by quadrature amplitude modulation (QAM), and the far-end echo may exhibit significant carrier-phase jitter and carrier-frequency shift, which are caused by signal processing at intermediate points in the telephone network. Therefore, a digital adaptive echo canceller for voiceband modems needs to embody algorithms that account for the presence of such additional impairments.

0-8493-8597-0/99/$0.00+$.50

© 1999 by CRC Press LLC

In this chapter, we describe the echo channel models and adaptive echo canceller structures that are obtained for various digital communications systems, which are classified according to the employed modulation techniques. We also address the tradeoffs between complexity, speed of adaptation, and accuracy of cancellation in adaptive echo cancellers.

7.2 Echo Cancellation for Pulse–Amplitude Modulation (PAM) Systems

The model of a full-duplex baseband data transmission system employing pulse–amplitude modulation (PAM) and adaptive echo cancellation is shown in Fig. 7.1. To describe system operations, we consider one end of the full-duplex link. The configuration of an echo canceller for a PAM transmission system is shown in Fig. 7.2. The transmitted data consist of a sequence $\{a_n\}$ of independent and identically distributed (i.i.d.) real-valued symbols from the M-ary alphabet $\mathcal{A} = \{\pm 1, \pm 3, \ldots, \pm(M-1)\}$. The sequence $\{a_n\}$ is converted into an analog signal by a digital-to-analog (D/A) converter. The conversion to a staircase signal by a zero-order hold D/A converter is described by the frequency response $H_{\mathrm{D/A}}(f) = T \sin(\pi f T)/(\pi f T)$, where T is the modulation interval. The D/A converter output is filtered by the analog transmit filter and is input to the channel through the hybrid.

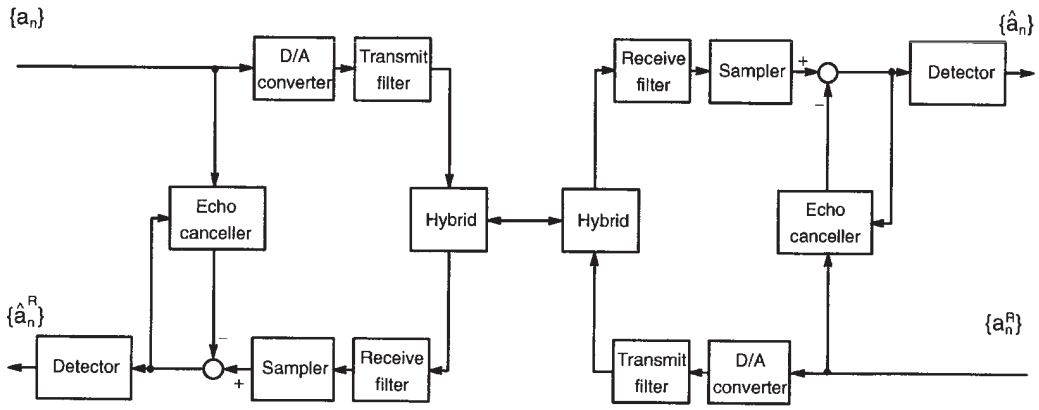


FIGURE 7.1 Model of a full-duplex PAM transmission system.

The signal $x(t)$ at the output of the low-pass analog receive filter has three components, namely, the signal from the far-end transmitter $r(t)$, the echo $u(t)$, and additive Gaussian noise $w(t)$. The signal $x(t)$ is given by

$$\begin{aligned} x(t) &= r(t) + u(t) + w(t) \\ &= \sum_{n=-\infty}^{\infty} a_n^R h(t - nT) + \sum_{n=-\infty}^{\infty} a_n h_E(t - nT) + w(t) \ , \end{aligned} \tag{7.1}$$

where $\{a_n^R\}$ is the sequence of symbols from the remote transmitter, and $h(t)$ and $h_E(t) = \{h_{\mathrm{D/A}} \otimes g_E\}(t)$ are the impulse responses of the overall channel and the echo channel, respectively. In the expression of $h_E(t)$, the function $h_{\mathrm{D/A}}(t)$ is the inverse Fourier transform of $H_{\mathrm{D/A}}(f)$, and the operator $\otimes$ denotes convolution. The signal obtained after echo cancellation is processed by a detector that outputs the sequence of estimated symbols $\{\hat{a}_n^R\}$. In

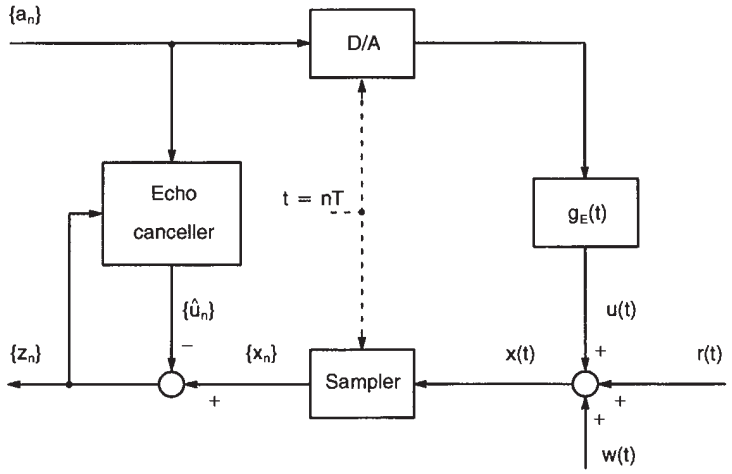


FIGURE 7.2 Configuration of an echo canceller for a PAM transmission system.

the case of full-duplex PAM data transmission over multi-pair cables for local-area network applications, where NEXT represents the main disturbance, the configuration of a digital NEXT canceller is obtained from Fig. 7.2, with the echo channel replaced by the crosstalk channel. For these applications, however, instead of *mono-duplex* transmission, where one pair is used to transmit only in one direction and the other pair to transmit only in the reverse direction, *dual-duplex* transmission may be adopted. Bi-directional transmission at rate ϱ over two pairs is then accomplished by full-duplex transmission of data streams at rate $\varrho/2$ over each of the two pairs. The lower modulation rate and/or spectral efficiency required per pair for achieving an aggregate rate equal to ϱ represents an advantage of dual-duplex over mono-duplex transmission. Dual-duplex transmission requires two transmitters and two receivers at each end of a link, as well as separation of the simultaneously transmitted and received signals on each pair, as illustrated in Fig. 7.3. In dual-duplex transceivers it is therefore necessary to suppress echoes returning from the hybrids and impedance discontinuities in the cable, as well as self NEXT, by adaptive digital echo and NEXT cancellation [3]. Although a dual-duplex scheme might appear to require higher implementation complexity than a mono-duplex scheme, it turns out that the two schemes are equivalent in terms of the number of multiply-and-add operations per second that are needed to perform the various filtering operations.

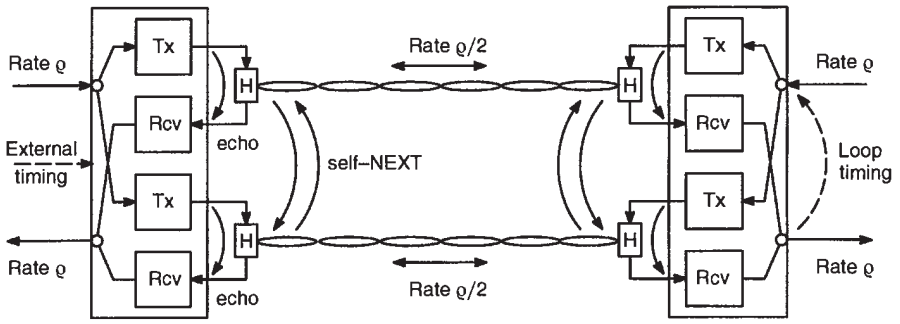


FIGURE 7.3 Model of a dual-duplex transmission system.

One of the transceivers in a full-duplex link will usually employ an externally provided reference clock for its transmit and receive operations. The other transceiver will extract timing from the received signal, and use this timing for its transmitter operations. This is known as *loop timing,* also illustrated in Fig. 7.3. If signals were transmitted in opposite directions with independent clocks, signals received from the remote transmitter would generally shift in phase relative to the also received echo signals. To cope with this effect, some form of interpolation would be required that can significantly increase the transceiver complexity [2].

In general, we consider baseband signalling techniques such that the signal at the output of the overall channel has nonnegligible excess bandwidth, i.e., nonnegligible spectral components at frequencies larger than half of the modulation rate, $|f| \geq 1/2T$. Therefore, to avoid aliasing, the signal $x(t)$ is sampled at twice the modulation rate or at a higher sampling rate. Assuming a sampling rate equal to $m/T, m > 1$, the ith sample during the nth modulation interval is given by

$$\begin{aligned} x\left[(nm+i)\frac{T}{m}\right] &= x_{nm+i} = r_{nm+i} + u_{nm+i} + w_{nm+i}, \qquad i = 0, \ldots, m-1 \\ &= \sum_{k=-\infty}^{\infty} h_{km+i} a^R_{n-k} + \sum_{k=-\infty}^{\infty} h_{E,km+i} a_{n-k} + w_{nm+i} \ , \end{aligned} \tag{7.2}$$

where $\{h_{nm+i},\ i = 0, \ldots, m-1\}$ and $\{h_{E,nm+i},\ i = 0, \ldots, m-1\}$ are the discrete-time impulse responses of the overall channel and the echo channel, respectively, and $\{w_{nm+i}, i = 0, \ldots, m-1\}$ is a sequence of Gaussian noise samples with zero mean and variance σ_w^2. Equation (7.2) suggests that the sequence of samples $\{x_{nm+i},\ i = 0, \ldots, m-1\}$ be regarded as a set of m interleaved sequences, each with a sampling rate equal to the modulation rate. Similarly, the sequence of echo samples $\{u_{nm+i},\ i = 0, \ldots, m-1\}$ can be regarded as a set of m interleaved sequences that are output by m independent echo channels with discrete-time impulse responses $\{h_{E,nm+i}\},\ i = 0, \ldots, m-1$, and an identical sequence $\{a_n\}$ of input symbols [7]. Hence, echo cancellation can be performed by m interleaved echo cancellers, as shown in Fig. 7.4. Since the performance of each canceller is independent of the other $m-1$ units, in the remaining part of this section we will consider the operations of a single echo canceller.

The echo canceller generates an estimate $\hat{u}_n$ of the echo signal. If we consider a transversal filter realization, $\hat{u}_n$ is obtained as the inner product of the vector of filter coefficients at time $t = nT$, $\boldsymbol{c}_n = (c_{n,0}, \ldots, c_{n,N-1})'$ and the vector of signals stored in the echo canceller delay line at the same instant, $\boldsymbol{a}_n = (a_n, \ldots, a_{n-N+1})'$, expressed by

$$\hat{u}_n = \boldsymbol{c}_n' \boldsymbol{a}_n = \sum_{k=0}^{N-1} c_{n,k} a_{n-k} \tag{7.3}$$

where $\boldsymbol{c}_n'$ denotes the transpose of the vector $\boldsymbol{c}_n$. The estimate of the echo is subtracted from the received signal. The result is defined as the cancellation error signal

$$z_n = x_n - \hat{u}_n = x_n - \boldsymbol{c}_n' \boldsymbol{a}_n \ . \tag{7.4}$$

The echo attenuation that must be provided by the echo canceller to achieve proper system operation depends on the application. For example, for the Integrated Services Digital Network (ISDN) U-Interface transceiver, the echo attenuation must be larger than 55 dB [10]. It is then required that the echo signals outside of the time span of the echo canceller delay line be negligible, i.e., $h_{E,n} \approx 0$ for $n < 0$ and $n > N-1$. As a measure

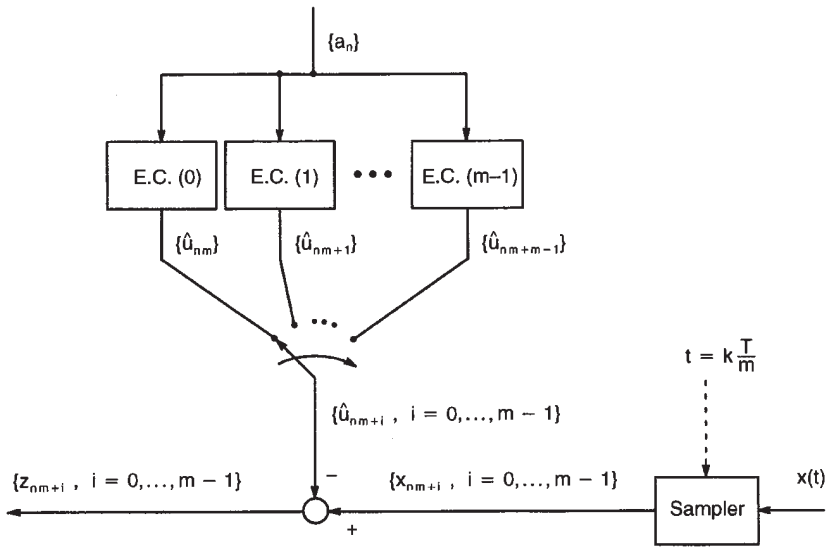


FIGURE 7.4 A set of m interleaved echo cancellers.

of system performance, we consider the mean square error ε_n^2 at the output of the echo canceller at time $t = nT$, defined by

$$\varepsilon_n^2 = E\left\{z_n^2\right\} , \tag{7.5}$$

where $\{z_n\}$ is the error sequence and $E\{\cdot\}$ denotes the expectation operator. For a particular coefficient vector $\boldsymbol{c}_n$, substitution of Eq. (7.4) into Eq. (7.5) yields

$$\varepsilon_n^2 = E\left\{x_n^2\right\} - 2\boldsymbol{c}_n'\boldsymbol{q} + \boldsymbol{c}_n'\boldsymbol{R}\,\boldsymbol{c}_n , \tag{7.6}$$

where $\boldsymbol{q} = E\{x_n\boldsymbol{a}_n\}$ and $\boldsymbol{R} = E\{\boldsymbol{a}_n\boldsymbol{a}_n'\}$. With the assumption of i.i.d. transmitted symbols, the correlation matrix $\boldsymbol{R}$ is diagonal. The elements on the diagonal are equal to the variance of the transmitted symbols, $\sigma_a^2 = (M^2 - 1)/3$. The minimum mean square error is given by

$$\varepsilon_{\min}^2 = E\left\{x_n^2\right\} - \boldsymbol{c}_{\text{opt}}'\boldsymbol{R}\,\boldsymbol{c}_{\text{opt}} , \tag{7.7}$$

where the optimum coefficient vector is $\boldsymbol{c}_{\text{opt}} = \boldsymbol{R}^{-1}\boldsymbol{q}$. We note that proper system operation is achieved only if the transmitted symbols are uncorrelated with the symbols from the remote transmitter. If this condition is satisfied, the optimum filter coefficients are given by the values of the discrete-time echo channel impulse response, i.e., $c_{\text{opt},k} = h_{E,k}, k = 0, \ldots, N-1$.

By the decision-directed stochastic gradient algorithm, also known as the least mean square (LMS) algorithm, the coefficients of the echo canceller converge in the mean to $\boldsymbol{c}_{\text{opt}}$. The LMS algorithm for an N-tap adaptive linear transversal filter is formulated as follows:

$$\boldsymbol{c}_{n+1} = \boldsymbol{c}_n - \frac{1}{2}\alpha\nabla_{\boldsymbol{c}}\left\{z_n^2\right\} = \boldsymbol{c}_n + \alpha z_n\boldsymbol{a}_n , \tag{7.8}$$

where α is the adaptation gain and

$$\nabla_{\boldsymbol{c}}\left\{z_n^2\right\} = \left(\frac{\partial z_n^2}{\partial c_{n,0}}, \ldots, \frac{\partial z_n^2}{\partial c_{n,N-1}}\right)' = -2z_n\boldsymbol{a}_n$$

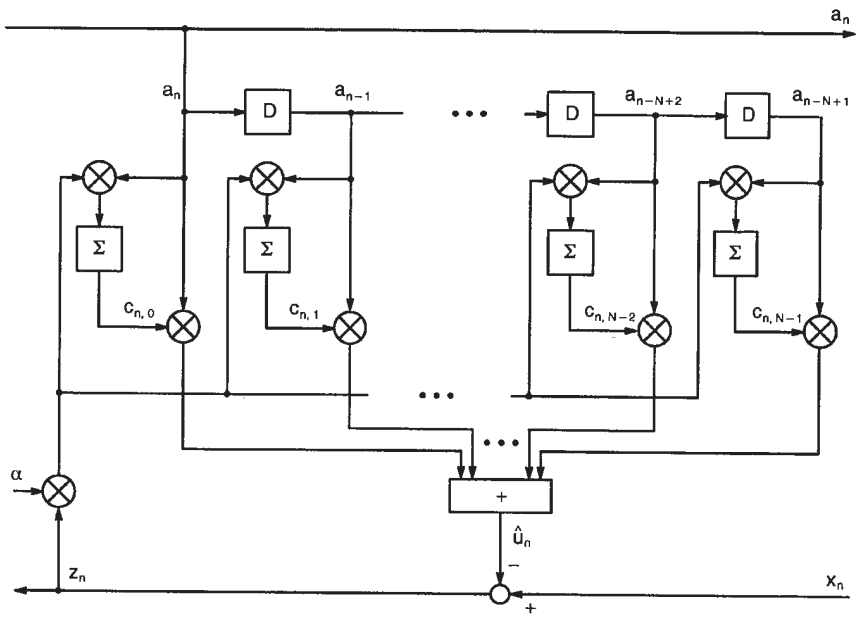


FIGURE 7.5 Block diagram of an adaptive transversal filter echo canceller.

is the gradient of the squared error with respect to the vector of coefficients. The block diagram of an adaptive transversal filter echo canceller is shown in Fig. 7.5.

If we define the vector $\boldsymbol{p}_n = \boldsymbol{c}_{\text{opt}} - \boldsymbol{c}_n$, the mean square error can be expressed as

$$\varepsilon_n^2 = \varepsilon_{\min}^2 + \boldsymbol{p}_n' \boldsymbol{R} \boldsymbol{p}_n \ , \tag{7.9}$$

where the term $\boldsymbol{p}_n' \boldsymbol{R} \boldsymbol{p}_n$ represents an 'excess mean square distortion' due to the misadjustment of the filter settings. The analysis of the convergence behavior of the excess mean square distortion was first proposed for adaptive equalizers [13] and later extended to adaptive echo cancellers [9]. Under the assumption that the vectors $\boldsymbol{p}_n$ and $\boldsymbol{a}_n$ are statistically independent, the dynamics of the mean square error are given by

$$E\left\{\varepsilon_n^2\right\} = \varepsilon_0^2 \left[1 - \alpha\sigma_a^2 \left(2 - \alpha N \sigma_a^2\right)\right]^n + \frac{2\varepsilon_{\min}^2}{2 - \alpha N \sigma_a^2} \ , \tag{7.10}$$

where ε_0^2 is determined by the initial conditions. The mean square error converges to a finite steady-state value ε_∞^2 if the stability condition $0 < \alpha < 2/(N\sigma_a^2)$ is satisfied. The optimum adaptation gain that yields fastest convergence at the beginning of the adaptation process is $\alpha_{\text{opt}} = 1/(N\sigma_a^2)$. The corresponding time constant and asymptotic mean square error are $\tau_{\text{opt}} = N$ and $\varepsilon_\infty^2 = 2\varepsilon_{\min}^2$, respectively.

We note that a fixed adaptation gain equal to α_{opt} could not be adopted in practice, since after echo cancellation the signal from the remote transmitter would be embedded in a residual echo having approximately the same power. If the time constant of the convergence mode is not a critical system parameter, an adaptation gain smaller than α_{opt} will be adopted to achieve an asymptotic mean square error close to $\varepsilon_{\min}^2$. On the other hand, if fast convergence is required, a variable gain will be chosen.

Several techniques have been proposed to increase the speed of convergence of the LMS algorithm. In particular, for echo cancellation in data transmission, the speed of adaptation is reduced by the presence of the signal from the remote transmitter in the cancellation error.

To mitigate this problem, the data signal can be adaptively removed from the cancellation error by a decision-directed algorithm [5].

Modified versions of the LMS algorithm have been also proposed to reduce system complexity. For example, the sign algorithm suggests that only the sign of the error signal be used to compute an approximation of the stochastic gradient [4]. An alternative means to reduce the implementation complexity of an adaptive echo canceller consists in the choice of a filter structure with a lower computational complexity than the transversal filter.

At high data rates, very large scale integration (VLSI) technology is needed for the implementation of transceivers for full-duplex data transmission. High-speed echo cancellers and near-end crosstalk cancellers that do not require multiplications represent an attractive solution because of their low complexity. As an example of an architecture suitable for VLSI implementation, we consider echo cancellation by a distributed-arithmetic filter, where multiplications are replaced by table lookup and shift-and-add operations [12]. By segmenting the echo canceller into filter sections of shorter lengths, various tradeoffs concerning the number of operations per modulation interval and the number of memory locations needed to store the lookup tables are possible. Adaptivity is achieved by updating the values stored in the lookup tables by the LMS algorithm.

To describe the principles of operations of a distributed-arithmetic echo canceller, we assume that the number of elements in the alphabet of input symbols is a power of two, $M = 2^W$. Therefore, each symbol is represented by the vector $(a_n^{(0)}, \ldots, a_n^{(W-1)})$, where $a_n^{(i)}, i = 0, \ldots, W-1$, are independent binary random variables, i.e.,

$$a_n = \sum_{w=0}^{W-1} \left(2a_n^{(w)} - 1\right) 2^w = \sum_{w=0}^{W-1} b_n^{(w)} 2^w \ , \tag{7.11}$$

where $b_n^{(w)} = (2a_n^{(w)} - 1) \in \{-1, +1\}$. By substituting Eq. (7.11) into Eq. (7.1) and segmenting the delay line of the echo canceller into L sections with $K = N/L$ delay elements each, we obtain

$$\hat{u}_n = \sum_{\ell=0}^{L-1} \sum_{w=0}^{W-1} 2^w \left[\sum_{k=0}^{K-1} b_{n-\ell K-k}^{(w)} c_{n,\ell K+k} \right] \ . \tag{7.12}$$

Equation (7.12) suggests that the filter output can be computed using a set of $L2^K$ values that are stored in L tables with 2^K memory locations each. The binary vectors $\boldsymbol{a}_{n,\ell}^{(w)} = (a_{n-(\ell+1)K+1}^{(w)}, \ldots, a_{n-\ell K}^{(w)})$, $w = 0, \ldots, W-1$, $\ell = 0, \ldots, L-1$, determine the addresses of the memory locations where the values that are needed to compute the filter output are stored. The filter output is obtained by WL table lookup and shift-and-add operations.

We observe that $\boldsymbol{a}_{n,\ell}^{(w)}$ and its binary complement $\bar{\boldsymbol{a}}_{n,\ell}^{(w)}$ select two values that differ only in their sign. This symmetry is exploited to halve the number of values to be stored. To determine the output of a distributed-arithmetic filter with reduced memory size, we reformulate Eq. (7.12) as

$$\hat{u}_n = \sum_{\ell=0}^{L-1} \sum_{w=0}^{W-1} 2^w b_{n-\ell K-k_0}^{(w)} \left[c_{n,\ell K+k_0} + b_{n-\ell K-k_0}^{(w)} \sum_{\substack{k=0 \\ k \neq k_0}}^{K-1} b_{n-\ell K-k}^{(w)} c_{n,\ell K+k} \right] \ , \tag{7.13}$$

where k_0 can be any element of the set $\{0, \ldots, K-1\}$. In the following, we take $k_0 = 0$. Then the binary symbols $b_{n-\ell K}^{(w)}$ determine whether the selected values are to be added or

subtracted. Each table has now 2^{K-1} memory locations, and the filter output is given by

$$\hat{u}_n = \sum_{\ell=0}^{L-1} \sum_{w=0}^{W-1} 2^w b_{n-\ell K}^{(w)} d_n \left(i_{n,\ell}^{(w)}, \ell \right) , \tag{7.14}$$

where $d_n(k,\ell)$, $k = 0, \ldots, 2^{K-1}-1$, $\ell = 0, \ldots, L-1$, are the look up values, and $i_{n,\ell}^{(w)}$, $w = 0, \ldots, W-1$, $\ell = 0, \ldots, L-1$, are the look up indices computed as follows:

$$i_{n,\ell}^{(w)} = \begin{cases} \displaystyle\sum_{k=1}^{K-1} a_{n-\ell K-k}^{(w)} 2^{k-1} & \text{if } a_{n-\ell K}^{(w)} = 1 \\ \displaystyle\sum_{k=1}^{K-1} \bar{a}_{n-\ell K-k}^{(w)} 2^{k-1} & \text{if } a_{n-\ell K}^{(w)} = 0 \end{cases} . \tag{7.15}$$

We note that, as long as Eqs. (7.12) and (7.13) hold for some coefficient vector $(c_{n,0}, \ldots, c_{n,N-1})$, the distributed-arithmetic filter emulates the operation of a linear transversal filter. For arbitrary values $d_n(k,\ell)$, however, a nonlinear filtering operation results.

The expression of the LMS algorithm to update the values of a distributed-arithmetic echo canceller takes the form

$$\boldsymbol{d}_{n+1} = \boldsymbol{d}_n - \frac{1}{2}\alpha \nabla_{\boldsymbol{d}} \left\{ z_n^2 \right\} = \boldsymbol{d}_n + \alpha z_n \boldsymbol{y}_n , \tag{7.16}$$

where $\boldsymbol{d}'_n = [\boldsymbol{d}'_n(0), \ldots, \boldsymbol{d}'_n(L-1)]$, with $\boldsymbol{d}'_n(\ell) = [d_n(0,\ell), \ldots, d_n(2^{K-1}-1,\ell)]$, and $\boldsymbol{y}'_n = [\boldsymbol{y}'_n(0), \ldots, \boldsymbol{y}'_n(L-1)]$, with

$$\boldsymbol{y}'_n(\ell) = \sum_{w=0}^{W-1} 2^w b_{n-\ell K}^{(w)} \left(\delta_{0,i_{n,\ell}^{(w)}}, \ldots, \delta_{2^{K-1}-1,i_{n,\ell}^{(w)}} \right) ,$$

are $L2^{K-1} \times 1$ vectors and where $\delta_{i,j}$ is the Kronecker delta. We note that at each iteration only those values that are selected to generate the filter output are updated. The block diagram of an adaptive distributed-arithmetic echo canceller with input symbols from a quaternary alphabet is shown in Fig. 7.6.

The analysis of the mean square error convergence behavior and steady-state performance has been extended to adaptive distributed-arithmetic echo cancellers [1]. The dynamics of the mean square error are given by

$$E\left\{\varepsilon_n^2\right\} = \varepsilon_0^2 \left[1 - \frac{\alpha\sigma_a^2}{2^{K-1}} \left(2 - \alpha L \sigma_a^2 \right) \right]^n + \frac{2\varepsilon_{\min}^2}{2 - \alpha L \sigma_a^2} . \tag{7.17}$$

The stability condition for the echo canceller is $0 < \alpha < 2/(L\sigma_a^2)$. For a given adaptation gain, echo canceller stability depends on the number of tables and on the variance of the transmitted symbols. Therefore, the time span of the echo canceller can be increased without affecting system stability, provided that the number L of tables is kept constant. In that case, however, mean square error convergence will be slower. From Eq. (7.17), we find that the optimum adaptation gain that permits the fastest mean square error convergence at the beginning of the adaptation process is $\alpha_{\text{opt}} = 1/(L\sigma_a^2)$. The time constant of the convergence mode is $\tau_{\text{opt}} = L2^{K-1}$. The smallest achievable time constant is proportional to the total number of values. The realization of a distributed-arithmetic echo canceller can be further simplified by updating at each iteration only the values that are addressed by the most significant bits of the symbols stored in the delay line. The complexity required for adaptation can thus be reduced at the price of a slower rate of convergence.

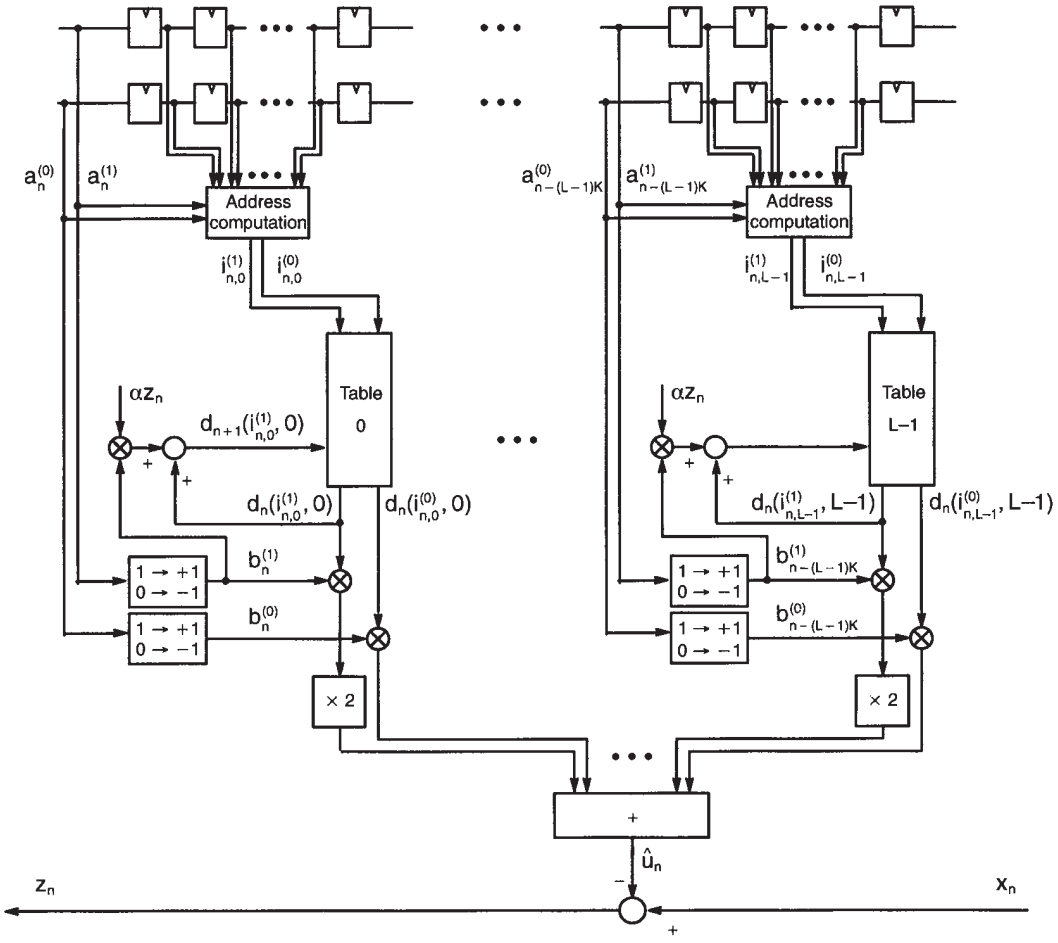


FIGURE 7.6 Block diagram of an adaptive distributed-arithmetic echo canceller.

7.3 Echo Cancellation for Quadrature Amplitude Modulation (QAM) Systems

Although most of the concepts presented in the preceding sections can be readily extended to echo cancellation for communications systems employing QAM, the case of full-duplex transmission over a voiceband data channel requires a specific discussion. We consider the system model shown in Fig. 7.7. The transmitter generates a sequence $\{a_n\}$ of i.i.d. complex-valued symbols from a two-dimensional constellation $\mathcal{A}$, which are modulated by the carrier $e^{j2\pi f_c nT}$, where T and f_c denote the modulation interval and the carrier frequency, respectively. The discrete-time signal at the output of the transmit Hilbert filter may be regarded as an analytic signal, which is generated at the rate of m/T samples/s, $m > 1$. The real part of the analytic signal is converted into an analog signal by a D/A converter and input to the channel. We note that by transmitting the real part of a complex-valued signal positive- and negative-frequency components become folded. The image band attenuation of the transmit Hilbert filter thus determines the achievable echo suppression. In fact, the receiver cannot extract aliasing image-band components from desired passband frequency components, and the echo canceller is able to suppress only echo arising from

transmitted passband components.

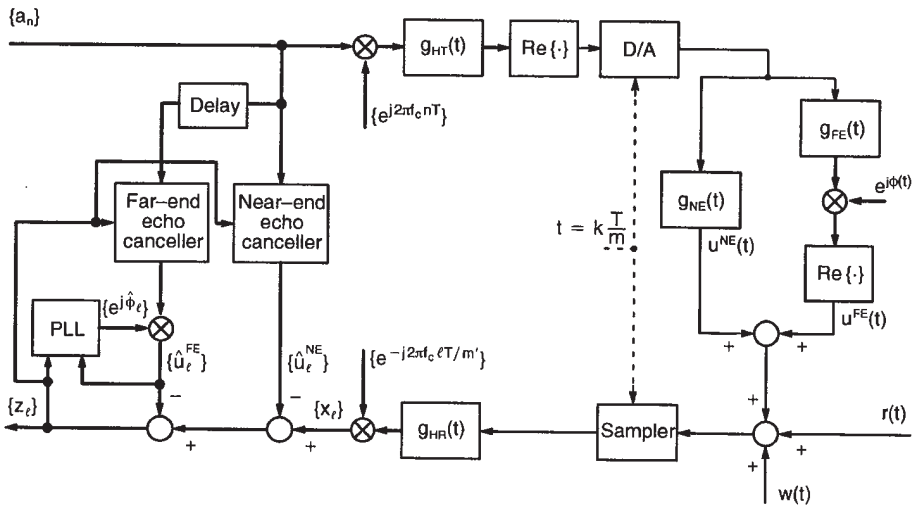


FIGURE 7.7 Configuration of an echo canceller for a QAM transmission system.

The output of the echo channel is represented as the sum of two contributions. The near-end echo $u^{\mathrm{NE}}(t)$ arises from the impedance mismatch between the hybrid and the transmission line, as in the case of baseband transmission. The far-end echo $u^{\mathrm{FE}}(t)$ represents the contribution due to echos that are generated at intermediate points in the telephone network. These echos are characterized by additional impairments, such as jitter and frequency shift, which are accounted for by introducing a carrier-phase rotation of an angle $\phi(t)$ in the model of the far-end echo.

At the receiver, samples of the signal at the channel output are obtained synchronously with the transmitter timing, at the sampling rate of m/T samples/s. The discrete-time received signal is converted to a complex-valued baseband signal $\{x_{nm'+i}, i = 0, \ldots, m'-1\}$, at the rate of m'/T samples/s, $1 < m' < m$, through filtering by the receive Hilbert filter, decimation, and demodulation. From delayed transmit symbols, estimates of the near- and far-end echo signals after demodulation, $\{\hat{u}^{\mathrm{NE}}_{nm'+i},\ i = 0, \ldots, m'-1\}$ and $\{\hat{u}^{\mathrm{FE}}_{nm'+i},\ i = 0, \ldots, m'-1\}$, respectively, are generated using m' interleaved near- and far-end echo cancellers. The cancellation error is given by

$$z_\ell = x_\ell - \hat{u}^{\mathrm{NE}}_\ell - \hat{u}^{\mathrm{FE}}_\ell \ . \tag{7.18}$$

A different model is obtained if echo cancellation is accomplished before demodulation. In this case, two equivalent configurations for the echo canceller may be considered. In one configuration, the modulated symbols are input to the transversal filter, which approximates the passband echo response. Alternatively, the modulator can be placed after the transversal filter, which is then called a baseband transversal filter [14].

In the considered realization, the estimates of the echo signals after demodulation are given by

$$\hat{u}^{\mathrm{NE}}_{nm'+i} = \sum_{k=0}^{N_{\mathrm{NE}}-1} c^{\mathrm{NE}}_{n,km'+i} a_{n-k}, \qquad i = 0, \ldots, m'-1 \ , \tag{7.19}$$

and

$$\hat{u}^{\mathrm{FE}}_{nm'+i} = \left[\sum_{k=0}^{N_{\mathrm{FE}}-1} c^{\mathrm{FE}}_{n,km'+i} a_{n-k-D_{\mathrm{FE}}} \right] e^{j\hat{\phi}_{nm'+i}}, \qquad i = 0, \ldots, m'-1 \ , \tag{7.20}$$

where $(c^{\mathrm{NE}}_{n,0}, \ldots, c^{\mathrm{NE}}_{n,m'N_{\mathrm{NE}}-1})$ and $(c^{\mathrm{FE}}_{n,0}, \ldots, c^{\mathrm{FE}}_{n,m'N_{\mathrm{FE}}-1})$ are the coefficients of the m' interleaved near- and far-end echo cancellers, respectively, $\{\hat{\phi}_{nm'+i}, i = 0, \ldots, m'-1\}$ is the sequence of far-end echo phase estimates, and D_{FE} denotes the bulk delay accounting for the round-trip delay from the transmitter to the point of echo generation. To prevent overlap of the time span of the near-end echo canceller with the time span of the far-end echo canceller, the condition $D_{\mathrm{FE}} > N_{\mathrm{NE}}$ must be satisfied. We also note that, because of the different nature of near- and far-end echo generation, the time span of the far-end echo canceller needs to be larger than the time span of the near-end echo canceller, i.e., $N_{\mathrm{FE}} > N_{\mathrm{NE}}$.

Adaptation of the filter coefficients in the near- and far-end echo cancellers by the LMS algorithm leads to

$$\begin{aligned} c^{\mathrm{NE}}_{n+1,km'+i} &= c^{\mathrm{NE}}_{n,km'+i} + \alpha z_{nm'+i}(a_{n-k})^* \\ k &= 0, \ldots, N_{\mathrm{NE}}-1, \qquad i = 0, \ldots, m'-1 \ , \end{aligned} \tag{7.21}$$

and

$$\begin{aligned} c^{\mathrm{FE}}_{n+1,km'+i} &= c^{\mathrm{FE}}_{n,km'+i} + \alpha z_{nm'+i}(a_{n-k-D_{\mathrm{FE}}})^* e^{-j\hat{\phi}_{nm'+i}} \\ k &= 0, \ldots, N_{\mathrm{FE}}-1, \qquad i = 0, \ldots, m'-1 \ , \end{aligned} \tag{7.22}$$

respectively, where the asterisk denotes complex conjugation.

The far-end echo phase estimate is computed by a second-order phase-lock loop algorithm, where the following stochastic gradient approach is adopted:

$$\begin{cases} \hat{\phi}_{\ell+1} = \hat{\phi}_\ell - \frac{1}{2}\gamma_{\mathrm{FE}} \nabla_{\hat{\phi}} |z_\ell|^2 + \Delta\phi_\ell \pmod{2\pi} \\ \Delta\phi_{\ell+1} = \Delta\phi_\ell - \frac{1}{2}\zeta_{\mathrm{FE}} \nabla_{\hat{\phi}} |z_\ell|^2 \end{cases} , \tag{7.23}$$

where $\ell = nm' + i$, $i = 0, \ldots, m'-1$, γ_{FE} and ζ_{FE} are step-size parameters, and

$$\nabla_{\hat{\phi}} |z_\ell|^2 = \frac{\partial |z_\ell|^2}{\partial \hat{\phi}_\ell} = -2\mathrm{Im}\left\{ z_\ell \left(\hat{u}^{\mathrm{FE}}_\ell\right)^* \right\} . \tag{7.24}$$

We note that algorithm (7.23) requires m' iterations per modulation interval, i.e., we cannot resort to interleaving to reduce the complexity of the computation of the far-end echo phase estimate.

7.4 Echo Cancellation for Orthogonal Frequency Division Multiplexing (OFDM) Systems

Orthogonal frequency division multiplexing (OFDM) is a modulation technique whereby blocks of M symbols are transmitted in parallel over M subchannels by employing M orthogonal subcarriers. We consider a real-valued discrete-time channel impulse response $\{h_i, i = 0, \ldots, L\}$ having length $L+1 \ll M$. To illustrate the basic principles of OFDM systems, let us consider a noiseless ideal channel with impulse response given by $\{h_i\} = \{\delta_i\}$, where $\{\delta_i\}$ is defined as the discrete-time delta function. Modulation of the complex-valued

input symbols at the n-th modulation interval, denoted by the vector $\boldsymbol{A}_n = \{A_n(i), i = 0, \ldots, M-1\}$, is performed by an inverse discrete Fourier transform (IDFT), as shown in Fig. 7.8. We assume that M is even, and that each block of symbols satisfies the Hermitian symmetry conditions, i.e., $A_n(0)$ and $A_n(M/2)$ are real valued, and $A_n(i) = A_n^*(M-i)$, $i = 1, \ldots, M/2-1$. Then the signals $\boldsymbol{a}_n = \{a_n(i), i = 0, \ldots, M-1\}$ obtained at the output of the IDFT are real valued. After parallel-to-serial conversion, the M signals are sent over the channel at the given transmission rate M/T, where T denotes the modulation interval. At the output of the channel, the noiseless signals are received without distortion. Serial-to-parallel conversion yields blocks of M elements, with boundaries placed such that each block obtained at the modulator output is also presented at the demodulator input. Then demodulation performed by a discrete Fourier transform (DFT) will reproduce the blocks of M input symbols. The overall input-output relationship is therefore equivalent to that of a bank of M parallel, independent subchannels.



FIGURE 7.8 Block diagram of an OFDM system.

In the general case of a noisy channel with impulse response having length greater than one, M independent subchannels are obtained by a variant of OFDM that is also known as discrete multitone modulation (DMT) [11]. In a DMT system, modulation by the IDFT is performed at the rate $1/T' = M/(M+L)T < 1/T$. After modulation, each block of M signals is cyclically extended by copying the last L signals in front of the block, and converted from parallel to serial. The resulting $L+M$ signals are sent over the channel. At the receiver, blocks of samples with length $L+M$ are taken. Block boundaries are placed such that the last M samples depend only on the elements of one cyclically extended block of signals. The first L samples are discarded, and the vector $\boldsymbol{x}_n$ of the last M samples of the block received at the n-th modulation interval can be expressed as

$$\boldsymbol{x}_n = \Gamma_n \boldsymbol{h} + \boldsymbol{w}_n \ , \tag{7.25}$$

where $\boldsymbol{h}$ is the vector of the impulse response extended with $M-L-1$ zeros, $\boldsymbol{w}_n$ is a vector of additive white Gaussian noise samples, and Γ_n is a $M \times M$ circulant matrix given by

$$\Gamma_n = \begin{bmatrix} a_n(0) & a_n(M-1) & \ldots & a_n(1) \\ a_n(1) & a_n(0) & \ldots & a_n(2) \\ \cdot & \cdot & & \cdot \\ \cdot & \cdot & & \cdot \\ \cdot & \cdot & & \cdot \\ a_n(M-1) & a_n(M-2) & \ldots & a_n(0) \end{bmatrix} . \tag{7.26}$$

Recalling that $\mathcal{F}_M \Gamma_n \mathcal{F}_M^{-1} = diag(\boldsymbol{A}_n)$, where $\mathcal{F}_M$ is the $M \times M$ DFT matrix defined as $\mathcal{F}_M = [(e^{-\frac{j2\pi}{M}})^{km}], k, m = 0, \ldots, M-1$, and $diag(\boldsymbol{A}_n)$ denotes the diagonal matrix with elements on the diagonal given by $\boldsymbol{A}_n$, we find that the output of the demodulator is given by

$$\boldsymbol{X}_n = diag(\boldsymbol{A}_n)\boldsymbol{H} + \boldsymbol{W}_n \ , \tag{7.27}$$

where $\boldsymbol{H}$ denotes the DFT of the vector $\boldsymbol{h}$, and $\boldsymbol{W}_n$ is a vector of independent Gaussian random variables. Equation (7.27) indicates that the sequence of transmitted symbol vectors

can be detected by assuming a bank of M independent subchannels, at the price of a decrease in the data rate by a factor $(M+L)/M$. Note that in practice the computationally more efficient inverse fast Fourier transform and fast Fourier transform are used instead of IDFT and DFT.

We discuss echo cancellation for OFDM with reference to a DMT system [6], as shown in Fig. 7.9. The real-valued discrete-time echo impulse response is $\{h_{E,i}, i = 0, \ldots, N-1\}$,

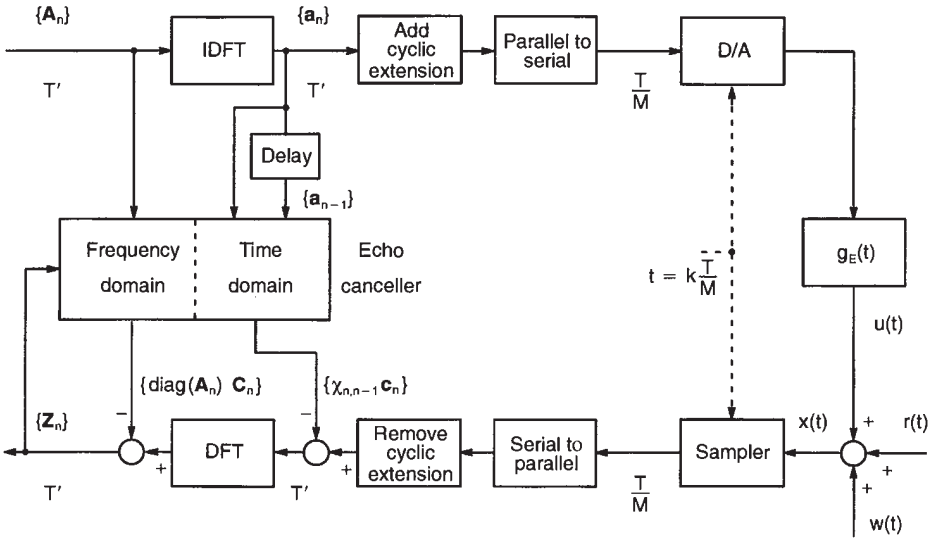


FIGURE 7.9 Configuration of an echo canceller for a DMT transmission system.

having length $N < M$. We initially assume $N \leq L+1$. Furthermore, we assume that the boundaries of the received blocks are placed such that the last M samples of the n-th received block are expressed by the vector

$$\boldsymbol{x}_n = \Gamma_n^R \boldsymbol{h} + \Gamma_n \boldsymbol{h}_E + \boldsymbol{w}_n \ , \tag{7.28}$$

where Γ_n^R is the circulant matrix with elements given by the signals from the remote transmitter, and $\boldsymbol{h}_E$ is the vector of the echo impulse response extended with $M-N$ zeros. In the frequency domain, the echo is expressed as $\boldsymbol{U}_n = diag(\boldsymbol{A}_n)\boldsymbol{H}_E$, where $\boldsymbol{H}_E$ denotes the DFT of the vector $\boldsymbol{h}_E$. In this case, the echo canceller provides an echo estimate that is given by $\hat{\boldsymbol{U}}_n = diag(\boldsymbol{A}_n)\boldsymbol{C}_n$, where $\boldsymbol{C}_n$ denotes the DFT of the vector $\boldsymbol{c}_n$ of the N coefficients of the echo canceller filter extended with $M-N$ zeros. In practice, however, we need to consider the case $N > L+1$. The expression of the cancellation error is then given by

$$\boldsymbol{z}_n = \boldsymbol{x}_n - \Psi_{n,n-1}\boldsymbol{c}_n \ , \tag{7.29}$$

where the vector of the last M elements of the n-th received block is now $\boldsymbol{x}_n = \Gamma_n^R \boldsymbol{h} + \Psi_{n,n-1}\boldsymbol{h}_E + \boldsymbol{w}_n$, and $\Psi_{n,n-1}$ is a $M \times M$ Toeplitz matrix given by

$$\Psi_{n,n-1} =$$

$$\begin{bmatrix} a_n(0) & a_n(M-1) & \cdots & a_n(M-L) & a_{n-1}(M-1) & \cdots & a_{n-1}(L+1) \\ a_n(1) & a_n(0) & \cdots & a_n(M-L+1) & a_n(M-L) & \cdots & a_{n-1}(L+2) \\ \vdots & & & \ddots & & & \vdots \\ a_n(M-1) & a_n(M-2) & \cdots & a_n(M-L-1) & a_n(M-L-2) & \cdots & a_n(0) \end{bmatrix} . \quad (7.30)$$

In the frequency domain, the cancellation error can be expressed as

$$\boldsymbol{Z}_n = \mathcal{F}_M \left(\boldsymbol{x}_n - \chi_{n,n-1} \boldsymbol{c}_n \right) - diag(\boldsymbol{A}_n) \boldsymbol{C}_n \ , \quad (7.31)$$

where $\chi_{n,n-1} = \Psi_{n,n-1} - \Gamma_n$ is a $M \times M$ upper triangular Toeplitz matrix. Equation (7.31) suggests a computationally efficient, two-part echo cancellation technique. First, in the time domain, a short convolution is performed and the result subtracted from the received signals to compensate for the insufficient length of the cyclic extension. Second, in the frequency domain, cancellation of the residual echo is performed over a set of M independent echo subchannels. Observing that Eq. (7.31) is equivalent to $\boldsymbol{Z}_n = \boldsymbol{X}_n - \tilde{\Psi}_{n,n-1} \boldsymbol{C}_n$, where $\tilde{\Psi}_{n,n-1} = \mathcal{F}_M \Psi_{n,n-1} \mathcal{F}_M^{-1}$, the echo canceller adaptation by the LMS algorithm in the frequency domain takes the form

$$\boldsymbol{C}_{n+1} = \boldsymbol{C}_n + \alpha \tilde{\Psi}^*_{n,n-1} \boldsymbol{Z}_n \ , \quad (7.32)$$

where α is the adaptation gain, and $\tilde{\Psi}^*_{n,n-1}$ denotes the transpose conjugate of $\tilde{\Psi}_{n,n-1}$. We note that, alternatively, echo canceller adaptation may also be performed by the algorithm $\boldsymbol{C}_{n+1} = \boldsymbol{C}_n + \alpha \, diag(\boldsymbol{A}^*_n) \boldsymbol{Z}_n$, which entails a substantially lower computational complexity than the LMS algorithm, at the price of a slower rate of convergence.

In DMT systems it is essential that the length of the channel impulse response be much less than the number of subchannels, so that the reduction in data rate due to the cyclic extension may be considered negligible. Therefore, equalization is adopted in practice to shorten the length of the channel impulse response. From Eq. (7.31), however, we observe that transceiver complexity depends on the relative lengths of the echo and of the channel impulse responses. To reduce the length of the cyclic extension as well as the computational complexity of the echo canceller, various methods have been proposed to shorten both the channel and the echo impulse responses jointly [8].

7.5 Summary and Conclusions

Digital signal processing techniques for echo cancellation provide large echo attenuation, and eliminate the need for additional line interfaces and digital-to-analog and analog-to-digital converters that are required by echo cancellation in the analog signal domain.

The realization of digital echo cancellers in transceivers for high-speed full-duplex data transmission today is possible at a low cost thanks to the advances in VLSI technology. Digital techniques for echo cancellation are also appropriate for near-end crosstalk cancellation in transceivers for transmission over voice-grade cables at rates of several megabits per second for local-area network applications.

In voiceband modems for data transmission over the telephone network, digital techniques for echo cancellation also allow a precise tracking of the carrier phase and frequency shift of far-end echos.

References

[1] Cherubini, G., Analysis of the convergence behavior of adaptive distributed-arithmetic echo cancellers. *IEEE Trans. Commun.*, 41(11), 1703–1714, 1993.

[2] Cherubini, G., Ölçer, S., and Ungerboeck, G., A quaternaty partial-response class-IV transceiver for 125 Mbit/s data transmission over unshielded twisted-pair cables: Principles of operation and VLSI realization. *IEEE J. Sel. Areas Commun.*, 13(9), 1656–1669, 1995.

[3] Cherubini, G., Creigh, J., Ölçer, S., Rao, S.K., and Ungerboeck, G., 100BASE-T2: A new standard for 100 Mb/s Ethernet transmission over voice-grade cables. *IEEE Commun. Mag.*, 35(11), 115–122, 1997.

[4] Duttweiler, D.L., Adaptive filter performance with nonlinearities in the correlation multiplier. *IEEE Trans. Acoust., Speech, Signal Processing*, 30(8), 578–586, 1982.

[5] Falconer, D.D., Adaptive reference echo-cancellation. *IEEE Trans. Commun.*, 30(9), 2083–2094, 1982.

[6] Ho, M., Cioffi, J.M. and Bingham, J.A.C., Discrete multitone echo cancellation. *IEEE Trans. Commun.*, 44(7), 817–825, 1996.

[7] Lee, E.A. and Messerschmitt, D.G., *Digital Communication*, 2nd ed., Kluwer Academic Publishers, Boston MA, 1994.

[8] Melsa, P.J.W., Younce, R.C., and Rohrs, C.E., Impulse response shortening for discrete multitone transceivers. *IEEE Trans. Commun.*, 44(12), 1662–1672, 1996.

[9] Messerschmitt, D.G., Echo cancellation in speech and data transmission. *IEEE J. Sel. Areas Commun.*, 2(2), 283–297, 1984.

[10] Messerschmitt, D.G., Design issues for the ISDN U-Interface transceiver. *IEEE J. Sel. Areas Commun.*, 4(8), 1281–1293, 1986.

[11] Ruiz, A., Cioffi, J.M., and Kasturia, S., Discrete multiple tone modulation with coset coding for the spectrally shaped channel. *IEEE Trans. Commun.*, 40(6), 1012–1029, 1992.

[12] Smith, M.J., Cowan, C.F.N., and Adams, P.F., Nonlinear echo cancellers based on transpose distributed arithmetic. *IEEE Trans. Circuits and Systems*, 35(1), 6–18, 1988.

[13] Ungerboeck, G., Theory on the speed of convergence in adaptive equalizers for digital communication. *IBM J. Res. Develop.*, 16(6), 546–555, 1972.

[14] Weinstein, S.B., A passband data-driven echo-canceller for full-duplex transmission on two-wire circuits. *IEEE Trans. Commun.*, 25(7), 654–666, 1977.

Further Information

For further information on adaptive transversal filters with application to echo cancellation, see *Adaptive Filters: Structures, Algorithms, and Applications*, M.L. Honig and D.G. Messerschmitt, Kluwer, 1984.

8

Pseudonoise Sequences

8.1 Introduction 8-1
8.2 m Sequences 8-2
8.3 The q-ary Sequences with Low Autocorrelation 8-4
8.4 Families of Sequences with Low Crosscorrelation 8-5
Gold and Kasami Sequences • Quaternary Sequences with Low Crosscorrelation • Binary Kerdock Sequences
8.5 Aperiodic Correlation 8-8
Barker Sequences • Sequences with High Merit Factor • Sequences with Low Aperiodic Crosscorrelation
8.6 Other Correlation Measures 8-10
Partial-Period Correlation • Mean Square Correlation • Optical Orthogonal Codes
Defining Terms 8-12
References 8-12
Further Information 8-13

Tor Helleseth
University of Bergen

P. Vijay Kumar
University of Southern California

8.1 Introduction

Pseudonoise sequences (PN sequences), also referred to as pseudorandom sequences, are sequences that are deterministically generated and yet possess some properties that one would expect to find in randomly generated sequences. Applications of PN sequences include signal synchronization, navigation, radar ranging, random number generation, spread-spectrum communications, multipath resolution, cryptography, and signal identification in multiple-access communication systems. The *correlation* between two sequences $\{x(t)\}$ and $\{y(t)\}$ is the complex inner product of the first sequence with a shifted version of the second sequence. The correlation is called 1) an autocorrelation if the two sequences are the same, 2) a crosscorrelation if they are distinct, 3) a periodic correlation if the shift is a cyclic shift, 4) an aperiodic correlation if the shift is not cyclic, and 5) a partial-period correlation if the inner product involves only a partial segment of the two sequences. More precise definitions are given subsequently.

Binary $\boldsymbol{m}$ **sequences**, defined in the next section, are perhaps the best-known family of PN sequences. The balance, run-distribution, and autocorrelation properties of these sequences mimic those of random sequences. It is perhaps the random-like correlation properties of PN sequences that makes them most attractive in a communications system, and it is common to refer to any collection of low-correlation sequences as a family of PN sequences.

0-8493-8597-0/99/$0.00+$.50

© 1999 by CRC Press LLC

Section 8.2 begins by discussing m sequences. Thereafter, the discussion continues with a description of sequences satisfying various correlation constraints along the lines of the accompanying self-explanatory figure, Fig. 8.1. Expanded tutorial discussions on pseudo-random sequences may be found in [14], in [15, Chapter 5] and in [6].

8.2 m Sequences

A binary $\{0,1\}$ **shift-register sequence** $\{s(t)\}$ is a sequence that satisfies a linear recurrence relation of the form

$$\sum_{i=0}^{r} f_i s(t+i) = 0\ , \qquad \text{for all } \ t \geq 0 \tag{8.1}$$

where $r \geq 1$ is the *degree* of the recursion; the coefficients f_i belong to the finite field $GF(2) = \{0,1\}$ where the leading coefficient $f_r = 1$. Thus, both sequences $\{a(t)\}$ and $\{b(t)\}$ appearing in Fig. 8.2 are shift-register sequences. A sequence satisfying a recursion of the form in Eq. (8.1) is said to have *characteristic polynomial* $f(x) = \sum_{i=0}^{r} f_i x^i$. Thus, $\{a(t)\}$ and $\{b(t)\}$ have characteristic polynomials given by $f(x) = x^3+x+1$ and $f(x) = x^3+x^2+1$, respectively.

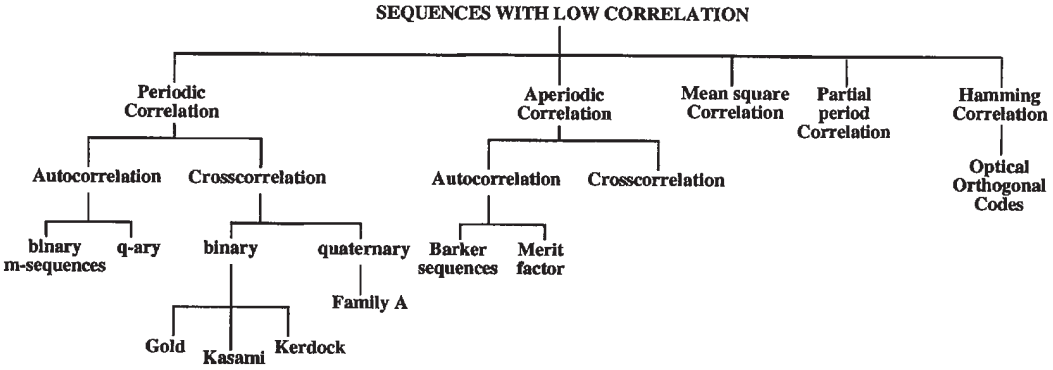


FIGURE 8.1 Overview of pseudonoise sequences.

Since an r-bit binary shift register can assume a maximum of 2^r different states, it follows that every shift-register sequence $\{s(t)\}$ is eventually periodic with period $n \leq 2^r$, i.e.,

$$s(t) = s(t+n), \qquad \text{for all } \ t \geq N$$

for some integer N. In fact, the maximum period of a shift-register sequence is $2^r - 1$, since a shift register that enters the all-zero state will remain forever in that state. The upper shift register in Fig. 8.2 when initialized with starting state 0 0 1 generates the periodic sequence $\{a(t)\}$ given by

$$0010111 \quad 0010111 \quad 0010111 \quad \cdots \tag{8.2}$$

of period $n = 7$. It follows then that this shift register generates sequences of maximal period starting from any nonzero initial state.

An m sequence is simply a binary shift-register sequence having maximal period. For every $r \geq 1$, m sequences are known to exist. The periodic **autocorrelation** function θ_s of

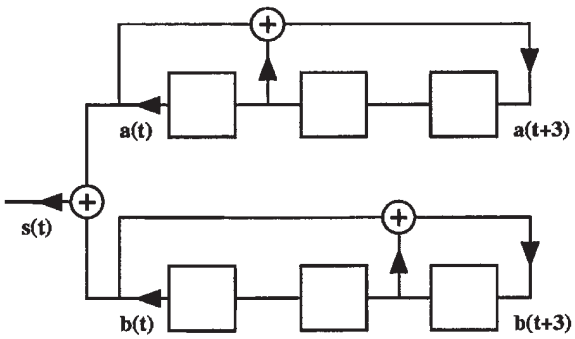


FIGURE 8.2 An example Gold sequence generator. Here $\{a(t)\}$ and $\{b(t)\}$ are m sequences of length 7.

a binary $\{0,1\}$ sequence $\{s(t)\}$ of period n is defined by

$$\theta_s(\tau) = \sum_{t=0}^{n-1} (-1)^{s(t+\tau)-s(t)} , \qquad 0 \le \tau \le n-1$$

An m sequence of length $2^r - 1$ has the following attributes. 1) *Balance property:* in each period of the m sequence there are 2^{r-1} ones and $2^{r-1} - 1$ zeros. 2) *Run property:* every nonzero binary s-tuple, $s \le r$ occurs 2^{r-s} times, the all-zero s-tuple occurs $2^{r-s} - 1$ times. 3) *Two-level autocorrelation function:*

$$\theta_s(\tau) = \begin{cases} n & \text{if } \tau = 0 \\ -1 & \text{if } \tau \neq 0 \end{cases} \tag{8.3}$$

The first two properties follow immediately from the observation that every nonzero r-tuple occurs precisely once in each period of the m sequence. For the third property, consider the difference sequence $\{s(t+\tau) - s(t)\}$ for $\tau \neq 0$. This sequence satisfies the same recursion as the m sequence $\{s(t)\}$ and is clearly not the all-zero sequence. It follows, therefore, that $\{s(t+\tau) - s(t)\} \equiv \{s(t+\tau')\}$ for some τ', $0 \le \tau' \le n-1$, i.e., is a different cyclic shift of the m sequence $\{s(t)\}$. The balance property of the sequence $\{s(t+\tau')\}$ then gives us attribute 3. The m sequence $\{a(t)\}$ in Eq. (8.2) can be seen to have the three listed properties.

If $\{s(t)\}$ is any sequence of period n and d is an integer, $1 \le d \le n$, then the mapping $\{s(t)\} \to \{s(dt)\}$ is referred to as a *decimation* of $\{s(t)\}$ by the integer d. If $\{s(t)\}$ is an m sequence of period $n = 2^r - 1$ and d is an integer relatively prime to $2^r - 1$, then the decimated sequence $\{s(dt)\}$ clearly also has period n. Interestingly, it turns out that the sequence $\{s(dt)\}$ is always also an m sequence of the same period. For example, when $\{a(t)\}$ is the sequence in Eq. (8.2), then

$$a(3t) = 0011101 \quad 0011101 \quad 0011101 \quad \cdots \tag{8.4}$$

and

$$a(2t) = 0111001 \quad 0111001 \quad 0111001 \quad \cdots \tag{8.5}$$

The sequence $\{a(3t)\}$ is also an m sequence of period 7, since it satisfies the recursion

$$s(t+3) + s(t+2) + s(t) = 0 \qquad \text{for all } t$$

of degree $r = 3$. In fact $\{a(3t)\}$ is precisely the sequence labeled $\{b(t)\}$ in Fig. 8.2. The sequence $\{a(2t)\}$ is simply a cyclically shifted version of $\{a(t)\}$ itself; this property holds in general. If $\{s(t)\}$ is any m sequence of period $2^r - 1$, then $\{s(2t)\}$ will always be a shifted

version of the same m sequence. Clearly, the same is true for decimations by any power of 2.

Starting from an m sequence of period $2^r - 1$, it turns out that one can generate all m sequences of the same period through decimations by integers d relatively prime to $2^r - 1$. The set of integers d, $1 \leq d \leq 2^r - 1$ satisfying $(d, 2^r - 1) = 1$ forms a group under multiplication modulo $2^r - 1$, with the powers $\{2^i | \, 0 \leq i \leq r - 1\}$ of 2 forming a subgroup of order r. Since decimation by a power of 2 yields a shifted version of the same m sequence, it follows that the number of distinct m sequences of period $2^r - 1$ is $[\phi(2^r - 1)/r]$ where $\phi(n)$ denotes the number of integers d, $1 \leq d \leq n$, relatively prime to n. For example, when $r = 3$, there are just two cyclically distinct m sequences of period 7, and these are precisely the sequences $\{a(t)\}$ and $\{b(t)\}$ discussed in the preceding paragraph. Tables provided in [12] can be used to determine the characteristic polynomial of the various m sequences obtainable through the decimation of a single given m sequence. The classical reference on m sequences is [4].

If one obtains a sequence of some large length n by repeatedly tossing an unbiased coin, then such a sequence will very likely satisfy the balance, run, and autocorrelation properties of an m sequence of comparable length. For this reason, it is customary to regard the extent to which a given sequence possesses these properties as a measure of randomness of the sequence. Quite apart from this, in many applications such as signal synchronization and radar ranging, it is desirable to have sequences $\{s(t)\}$ with low autocorrelation sidelobes i.e., $|\theta_s(\tau)|$ is small for $\tau \neq 0$. Whereas m sequences are a prime example, there exist other methods of constructing binary sequences with low out-of-phase autocorrelation.

Sequences $\{s(t)\}$ of period n having an autocorrelation function identical to that of an m sequence, i.e., having θ_s satisfying Eq. (8.3) correspond to well-studied combinatorial objects known as *cyclic Hadamard difference sets.* Known infinite families fall into three classes 1) Singer and Gordon, Mills and Welch, 2) quadratic residue, and 3) twin-prime difference sets. These correspond, respectively, to sequences of period n of the form $n = 2^r - 1, r \geq 1$; n prime; and $n = p(p+2)$ with both p and $p+2$ being prime in the last case. For a detailed treatment of cyclic difference sets, see [2]. A recent observation by Maschietti in [9] provides additional families of cyclic Hadamard difference sets that also correspond to sequences of period $n = 2^r - 1$.

8.3 The q-ary Sequences with Low Autocorrelation

As defined earlier, the autocorrelation of a binary $\{0, 1\}$ sequence $\{s(t)\}$ leads to the computation of the inner product of an $\{-1, +1\}$ sequence $\{(-1)^{s(t)}\}$ with a cyclically shifted version $\{(-1)^{s(t+\tau)}\}$ of itself. The $\{-1, +1\}$ sequence is transmitted as a phase shift by either 0° and 180° of a radio-frequency carrier, i.e., using binary phase-shift keying (PSK) modulation. If the modulation is q-ary PSK, then one is led to consider sequences $\{s(t)\}$ with symbols in the set Z_q, i.e., the set of integers modulo q. The relevant autocorrelation function $\theta_s(\tau)$ is now defined by

$$\theta_s(\tau) = \sum_{t=0}^{n-1} \omega^{s(t+\tau) - s(t)}$$

where n is the period of $\{s(t)\}$ and ω is a complex primitive qth root of unity. It is possible to construct sequences $\{s(t)\}$ over Z_q whose autocorrelation function satisfies

$$\theta_s(\tau) = \begin{cases} n & \text{if } \tau = 0 \\ 0 & \text{if } \tau \neq 0 \end{cases}$$

For obvious reasons, such sequences are said to have an *ideal autocorrelation function.*

We provide without proof two sample constructions. The sequences in the first construction are given by

$$s(t) = \begin{cases} t^2/2 \pmod{n} & \text{when } n \text{ is even} \\ t(t+1)/2 \pmod{n} & \text{when } n \text{ is odd} \end{cases}$$

Thus, this construction provides sequences with ideal autocorrelation for any period n. Note that the size q of the sequence symbol alphabet equals n when n is odd and $2n$ when n is even.

The second construction also provides sequences over Z_q of period n but requires that n be a perfect square. Let $n = r^2$ and let π be an arbitrary permutation of the elements in the subset $\{0, 1, 2, \ldots, (r-1)\}$ of Z_n: Let g be an arbitrary function defined on the subset $\{0, 1, 2, \ldots, r-1\}$ of Z_n. Then any sequence of the form

$$s(t) = rt_1\pi(t_2) + g(t_2) \pmod{n}$$

where $t = rt_1 + t_2$ with $0 \leq t_1, t_2 \leq r-1$ is the base-r decomposition of t, has an ideal autocorrelation function. When the alphabet size q equals or divides the period n of the sequence, ideal-autocorrelation sequences also go by the name *generalized bent functions.* For details, see [6].

8.4 Families of Sequences with Low Crosscorrelation

Given two sequences $\{s_1(t)\}$ and $\{s_2(t)\}$ over Z_q of period n, their **crosscorrelation** function $\theta_{1,2}(\tau)$ is defined by

$$\theta_{1,2}(\tau) = \sum_{t=0}^{n-1} \omega^{s_1(t+\tau)-s_2(t)}$$

where ω is a primitive qth root of unity. The crosscorrelation function is important in code-division multiple-access (CDMA) communication systems. Here, each user is assigned a distinct signature sequence and to minimize interference due to the other users, it is desirable that the signature sequences have pairwise, low values of crosscorrelation function. To provide the system in addition with a self-synchronizing capability, it is desirable that the signature sequences have low values of the autocorrelation function as well.

Let $\mathcal{F} = \{\{s_i(t)\} \mid 1 \leq i \leq M\}$ be a family of M sequences $\{s_i(t)\}$ over Z_q each of period n. Let $\theta_{i,j}(\tau)$ denote the crosscorrelation between the ith and jth sequence at shift τ, i.e.,

$$\theta_{i,j}(\tau) = \sum_{t=0}^{n-1} \omega^{s_i(t+\tau)-s_j(t)}, \qquad 0 \leq \tau \leq n-1$$

The classical goal in sequence design for CDMA systems has been minimization of the parameter

$$\theta_{\max} = \max\{|\theta_{i,j}(\tau)| \mid \text{ either } i \neq j \text{ or } \tau \neq 0\}$$

for fixed n and M. It should be noted though that, in practice, because of data modulation the correlations that one runs into are typically of an aperiodic rather than a periodic nature (see Section 8.5). The problem of designing for low aperiodic correlation, however, is a more difficult one. A typical approach, therefore, has been to design based on periodic correlation, and then to analyze the resulting design for its aperiodic correlation properties.

Again, in many practical systems, the mean square correlation properties are of greater interest than the worst-case correlation represented by a parameter such as $\theta_{\max}$. The mean square correlation is discussed in Section 8.6.

Bounds on the minimum possible value of $\theta_{\max}$ for given period n, family size M, and alphabet size q are available that can be used to judge the merits of a particular sequence design. The most efficient bounds are those due to Welch, Sidelnikov, and Levenshtein, see [6]. In CDMA systems, there is greatest interest in designs in which the parameter $\theta_{\max}$ is in the range $\sqrt{n} \leq \theta_{\max} \leq 2\sqrt{n}$. Accordingly, Table 8.1 uses the Welch, Sidelnikov, and Levenshtein bounds to provide an order-of-magnitude upper bound on the family size M for certain $\theta_{\max}$ in the cited range.

Practical considerations dictate that q be small. The bit-oriented nature of electronic hardware makes it preferable to have q a power of 2. With this in mind, a description of some efficient sequence families having low auto- and crosscorrelation values and alphabet sizes $q = 2$ and $q = 4$ are described next.

TABLE 8.1 Bounds on Family Size M for Given $n, \theta_{\max}$

$\theta_{\max}$	Upper bound on M $q = 2$	Upper Bound on M $q > 2$
$\sqrt{n}$	$n/2$	n
$\sqrt{2n}$	n	$n^2/2$
$2\sqrt{n}$	$3n^2/10$	$n^3/2$

8.4.1 Gold and Kasami Sequences

Given the low autocorrelation sidelobes of an m sequence, it is natural to attempt to construct families of low correlation sequences starting from m sequences. Two of the better known constructions of this type are the families of Gold and Kasami sequences.

Let r be odd and $d = 2^k + 1$ where $k, 1 \leq k \leq r-1$, is an integer satisfying $(k, r) = 1$. Let $\{s(t)\}$ be a cyclic shift of an m sequence of period $n = 2^r - 1$ that satisfies $S(dt) \not\equiv 0$ and let $\mathcal{G}$ be the *Gold* family of $2^r + 1$ sequences given by

$$\mathcal{G} = \{s(t)\} \cup \{s(dt)\} \cup \{\{s(t) + s(d[t+\tau])\} \mid 0 \leq \tau \leq n-1\}$$

Then each sequence in $\mathcal{G}$ has period $2^r - 1$ and the maximum-correlation parameter $\theta_{\max}$ of $\mathcal{G}$ satisfies

$$\theta_{\max} \leq \sqrt{2^{r+1}} + 1$$

An application of the Sidelnikov bound coupled with the information that $\theta_{\max}$ must be an odd integer yields that for the family $\mathcal{G}$, $\theta_{\max}$ is as small as it can possibly be. In this sense the family $\mathcal{G}$ is an optimal family. We remark that these comments remain true even when d is replaced by the integer $d = 2^{2k} - 2^k + 1$ with the conditions on k remaining unchanged.

The Gold family remains the best-known family of m sequences having low crosscorrelation. Applications include the Navstar Global Positioning System whose signals are based on Gold sequences.

The family of Kasami sequences has a similar description. Let $r = 2v$ and $d = 2^v + 1$. Let $\{s(t)\}$ be a cyclic shift of an m sequence of period $n = 2^r - 1$ that satisfies $s(dt) \not\equiv 0$, and consider the family of Kasami sequences given by

$$\mathcal{K} = \{s(t)\} \cup \{\{s(t) + s(d[t+\tau])\} \mid 0 \leq \tau \leq 2^v - 2\}$$

Then the Kasami family $\mathcal{K}$ contains 2^v sequences of period $2^r - 1$. It can be shown that in this case

$$\theta_{\max} = 1 + 2^v$$

This time an application of the Welch bound and the fact that $\theta_{\max}$ is an integer shows that the Kasami family is optimal in terms of having the smallest possible value of $\theta_{\max}$ for given n and M.

8.4.2 Quaternary Sequences with Low Crosscorrelation

The entries in Table 8.1 suggest that nonbinary (i.e., $q > 2$) designs may be used for improved performance. A family of quaternary sequences that outperform the Gold and Kasami sequences is now discussed below.

Let $f(x)$ be the characteristic polynomial of a binary m sequence of length $2^r - 1$ for some integer r. The coefficients of $f(x)$ are either 0 or 1. Now, regard $f(x)$ as a polynomial over Z_4 and form the product $(-1)^r f(x)f(-x)$. This can be seen to be a polynomial in x^2. Define the polynomial $g(x)$ of degree r by setting $g(x^2) = (-1)^r f(x)f(-x)$. Let $g(x) = \sum_{i=0}^{r} g_i x^i$ and consider the set of all quaternary sequences $\{a(t)\}$ satisfying the recursion $\sum_{i=0}^{r} g_i a(t+i) = 0$ for all t.

It turns out that with the exception of the all-zero sequence, all of the sequences generated in this way have period $2^r - 1$. Thus, the recursion generates a family $\mathcal{A}$ of $2^r + 1$ cyclically distinct quaternary sequences. Closer study reveals that the maximum correlation parameter $\theta_{\max}$ of this family satisfies $\theta_{\max} \leq 1 + \sqrt{2^r}$. Thus, in comparison to the family of Gold sequences, the family $\mathcal{A}$ offers a lower value of $\theta_{\max}$ (by a factor of $\sqrt{2}$) for the same family size. In comparison to the set of Kasami sequences, it offers a much larger family size for the same bound on $\theta_{\max}$. Family $\mathcal{A}$ sequences may be found discussed in [16, 3].

We illustrate with an example. Let $f(x) = x^3 + x + 1$ be the characteristic polynomial of the m sequence $\{a(t)\}$ in Eq. (8.1). Then over Z_4

$$g\left(x^2\right) = (-1)^3 f(x)f(-x) = x^6 + 2x^4 + x^2 + 3$$

so that $g(x) = x^3 + 2x^2 + x + 3$. Thus, the sequences in family $\mathcal{A}$ are generated by the recursion $s(t+3) + 2s(t+2) + s(t+1) + 3s(t) = 0 \bmod 4$. The corresponding shift register is shown in Fig. 8.3. By varying initial conditions, this shift register can be made to generate nine cyclically distinct sequences, each of length 7. In this case $\theta_{\max} \leq 1 + \sqrt{8}$.

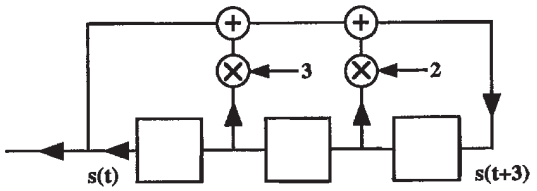


FIGURE 8.3 Shift register that generates family A quaternary sequences $\{s(t)\}$ of period 7.

8.4.3 Binary Kerdock Sequences

The Gold and Kasami families of sequences are closely related to binary linear cyclic codes. It is well known in coding theory that there exists nonlinear binary codes whose performance

exceeds that of the best possible linear code. Surprisingly, some of these examples come from binary codes, which are images of *linear quaternary* ($q = 4$) *codes* under the Gray map: $0 \to 00$, $1 \to 01$, $2 \to 11$, $3 \to 10$. A prime example of this is the Kerdock code, which recently has been shown to be the Gray image of a quaternary linear code. Thus, it is not surprising that the Kerdock code yields binary sequences that significantly outperform the family of Kasami sequences.

The Kerdock sequences may be constructed as follows: let $f(x)$ be the characteristic polynomial of an m sequence of period $2^r - 1, r$ odd. As before, regarding $f(x)$ as a polynomial over Z_4 (which happens to have $\{0,1\}$ coefficients), let the polynomial $g(x)$ over Z_4 be defined via $g(x^2) = -f(x)f(-x)$. [Thus, $g(x)$ is the characteristic polynomial of a family $\mathcal{A}$ sequence set of period $2^r - 1$.] Set $h(x) = -g(-x) = \sum_{i=0}^{r} h_i x^i$, and let S be the set of all Z_4 sequences satisfying the recursion $\sum_{i=0}^{r} h_i s(t+i) = 0$. Then S contain 4^r-distinct sequences corresponding to all possible distinct initializations of the shift register.

Let T denote the subset S of size 2^r-consisting of those sequences corresponding to initializations of the shift register only using the symbols 0 and 2 in Z_4. Then the set $S - T$ of size $4^r - 2^r$ contains a set $\mathcal{U}$ of 2^{r-1} cyclically distinct sequences each of period $2(2^r - 1)$. Given $x = a + 2b \in Z_4$ with $a, b \in \{0,1\}$, let μ denote the most significant bit (MSB) map $\mu(x) = b$. Let $\mathcal{K}_E$ denote the family of 2^{r-1} binary sequences obtained by applying the map μ to each sequence in $\mathcal{U}$. It turns out that each sequence in $\mathcal{U}$ also has period $2(2^r - 1)$ and that, furthermore, for the family $\mathcal{K}_E$, $\theta_{\max} \leq 2 + \sqrt{2^{r+1}}$. Thus, $\mathcal{K}_E$ is a much larger family than the Kasami family, while having almost exactly the same value of $\theta_{\max}$.

For example, taking $r = 3$ and $f(x) = x^3 + x + 1$, we have from the previous family $\mathcal{A}$ example that $g(x) = x^3 + 2x^2 + x + 3$, so that $h(x) = -g(-x) = x^3 + 2x^2 + x + 1$. Applying the MSB map to the head of the shift register, and discarding initializations of the shift register involving only 0's and 2's yields a family of four cyclically distinct binary sequences of period 14. Kerdock sequences are discussed in [6, 11, 1, 17].

8.5 Aperiodic Correlation

Let $\{x(t)\}$ and $\{y(t)\}$ be complex-valued sequences of length (or period) n, not necessarily distinct. Their *aperiodic correlation* values $\{\rho_{x,y}(\tau) | -(n-1) \leq \tau \leq n-1\}$ are given by

$$\rho_{x,y}(\tau) = \sum_{t=\max\{0,-\tau\}}^{\min\{n-1,n-1-\tau\}} x(t+\tau)y^*(t)$$

where $y^*(t)$ denotes the complex conjugate of $y(t)$. When $x \equiv y$, we will abbreviate and write ρ_x in place of $\rho_{x,y}$. The sequences described next are perhaps the most famous example of sequences with low-aperiodic autocorrelation values.

8.5.1 Barker Sequences

A binary $\{-1, +1\}$ sequence $\{s(t)\}$ of length n is said to be a *Barker sequence* if the aperiodic autocorrelation values $\rho_s(\tau)$ satisfy $|\rho_s(\tau)| \leq 1$ for all $\tau, -(n-1) \leq \tau \leq n-1$. The Barker property is preserved under the following transformations:

$$s(t) \to -s(t), \qquad s(t) \to (-1)^t s(t) \quad \text{and} \quad s(t) \to s(n-1-t)$$

as well as under compositions of the preceding transformations. Only the following Barker sequences are known:

$$\begin{aligned} n = 2 &\quad ++ \\ n = 3 &\quad ++- \\ n = 4 &\quad +++- \\ n = 5 &\quad +++-+ \\ n = 7 &\quad +++--+- \\ n = 11 &\quad +++---+--+- \\ n = 13 &\quad +++++--++-+-+ \end{aligned}$$

where $+$ denotes $+1$ and $-$ denotes -1 and sequences are generated from these via the transformations already discussed. It is known that if any other Barker sequence exists, it must have length $n > 1{,}898{,}884$, that is a multiple of 4.

For an upper bound to the maximum out-of-phase aperiodic autocorrelation of an m sequence, see [13].

8.5.2 Sequences with High Merit Factor

The *merit factor* F of a $\{-1, +1\}$ sequence $\{s(t)\}$ is defined by

$$F = \frac{n^2}{2\sum_{\tau=1}^{n-1} \rho_s^2(\tau)}$$

Since $\rho_s(\tau) = \rho_s(-\tau)$ for $1 \leq |\tau| \leq n-1$ and $\rho_s(0) = n$, factor F may be regarded as the ratio of the square of the in-phase autocorrelation, to the sum of the squares of the out-of-phase aperiodic autocorrelation values. Thus, the merit factor is one measure of the aperiodic autocorrelation properties of a binary $\{-1, +1\}$ sequence. It is also closely connected with the signal to self-generated noise ratio of a communication system in which coded pulses are transmitted and received.

Let F_n denote the largest merit factor of any binary $\{-1, +1\}$ sequence of length n. For example, at length $n = 13$, the Barker sequence of length 13 has a merit factor $F = F_{13} = 14.08$. Assuming a certain ergodicity postulate it was established by Golay that $\lim_{n\to\infty} F_n = 12.32$. Exhaustive computer searches carried out for $n \leq 40$ have revealed the following.

1. For $1 \leq n \leq 40$, $n \neq 11, 13$,

$$3.3 \leq F_n \leq 9.85 \ ,$$

2. $F_{11} = 12.1$, $F_{13} = 14.08$.

The value F_{11} is also achieved by a Barker sequence. From partial searches, for lengths up to 117, the highest known merit factor is between 8 and 9.56; for lengths from 118 to 200, the best-known factor is close to 6. For lengths > 200, statistical search methods have failed to yield a sequence having merit factor exceeding 5.

An *offset sequence* is one in which a fraction θ of the elements of a sequence of length n are chopped off at one end and appended to the other end, i.e., an offset sequence is a cyclic shift of the original sequence by $n\theta$ symbols. It turns out that the asymptotic merit factor of m sequences is equal to 3 and is independent of the particular offset of the m sequence. There exist offsets of sequences associated with quadratic-residue and twin-prime difference sets that achieve a larger merit factor of 6. Details may be found in [7].

8.5.3 Sequences with Low Aperiodic Crosscorrelation

If $\{u(t)\}$ and $\{v(t)\}$ are sequences of length $2n-1$ defined by

$$u(t) = \begin{cases} x(t) & \text{if } 0 \le t \le n-1 \\ 0 & \text{if } n \le t \le 2n-2 \end{cases}$$

and

$$v(t) = \begin{cases} y(t) & \text{if } 0 \le t \le n-1 \\ 0 & \text{if } n \le t \le 2n-2 \end{cases}$$

then

$$\{\rho_{x,y}(\tau) \mid -(n-1) \le \tau \le n-1\} = \{\theta_{u,v}(\tau) \mid 0 \le \tau \le 2n-2\} \tag{8.6}$$

Given a collection

$$U = \{\{x_i(t)\} \mid 1 \le i \le M\}$$

of sequences of length n over Z_q, let us define

$$\rho_{\max} = \max\{|\rho_{a,b}(\tau)| \mid a, b \in U \ , \ \text{either } a \ne b \text{ or } \tau \ne 0\}$$

It is clear from Eq. (8.6) how bounds on the *periodic* correlation parameter $\theta_{\max}$ can be adapted to give bounds on $\rho_{\max}$. Translation of the Welch bound gives that for every integer $k \ge 1$,

$$\rho_{\max}^{2k} \ge \left(\frac{n^{2k}}{M(2n-1)-1}\right)\left\{\frac{M(2n-1)}{\binom{2n+k-2}{k}} - 1\right\}$$

Setting $k = 1$ in the preceding bound gives

$$\rho_{\max} \ge n\sqrt{\frac{M-1}{M(2n-1)-1}}$$

Thus, for fixed M and large n, Welch's bound gives

$$\rho_{\max} \ge \mathcal{O}\left(n^{1/2}\right)$$

There exist sequence families which asymptotically achieve $\rho_{\max} \approx \mathcal{O}(n^{1/2})$, [10].

8.6 Other Correlation Measures

8.6.1 Partial-Period Correlation

The *partial-period (p-p) correlation* between the sequences $\{u(t)\}$ and $\{v(t)\}$ is the collection $\{\Delta_{u,v}(l,\tau,t_0) \mid 1 \le l \le n, 0 \le \tau \le n-1, 0 \le t_0 \le n-1\}$ of inner products

$$\Delta_{u,v}(l,\tau,t_0) = \sum_{t=t_0}^{t=t_0+l-1} u(t+\tau)v^*(t)$$

where l is the length of the partial period and the sum $t+\tau$ is again computed modulo n.

In direct-sequence CDMA systems, the pseudorandom signature sequences used by the various users are often very long for reasons of data security. In such situations, to minimize receiver hardware complexity, correlation over a partial period of the signature sequence is

often used to demodulate data, as well as to achieve synchronization. For this reason, the p-p correlation properties of a sequence are of interest.

Researchers have attempted to determine the moments of the p-p correlation. Here the main tool is the application of the Pless power-moment identities of coding theory [8]. The identities often allow the first and second p-p correlation moments to be completely determined. For example, this is true in the case of m sequences (the remaining moments turn out to depend upon the specific characteristic polynomial of the m sequence). Further details may be found in [15].

8.6.2 Mean Square Correlation

Frequently in practice, there is a greater interest in the mean-square correlation distribution of a sequence family than in the parameter $\theta_{\max}$. Quite often in sequence design, the sequence family is derived from a linear, binary cyclic code of length n by picking a set of cyclically distinct sequences of period n. The families of Gold and Kasami sequences are so constructed. In this case, as pointed out by Massey, the mean square correlation of the family can be shown to be either optimum or close to optimum, under certain easily satisfied conditions, imposed on the minimum distance of the dual code. A similar situation holds even when the sequence family does not come from a linear cyclic code. In this sense, mean square correlation is not a very discriminating measure of the correlation properties of a family of sequences. An expanded discussion of this issue may be found in [5].

8.6.3 Optical Orthogonal Codes

Given a pair of $\{0,1\}$ sequences $\{s_1(t)\}$ and $\{s_2(t)\}$ each having period n, we define the *Hamming correlation* function $\theta_{12}(\tau)$, $0 \leq \tau \leq n-1$, by

$$\theta_{12}(\tau) = \sum_{t=0}^{n-1} s_1(t+\tau)s_2(t)$$

Such correlations are of interest, for instance, in optical communication systems where the 1's and 0's in a sequence correspond to the presence or absence of pulses of transmitted light.

An (n, w, λ) optical orthogonal code (OOC) is a family $\mathcal{F} = \{\{s_i(t)\} \mid i = 1, 2, \ldots, M\}$, of M $\{0,1\}$ sequences of period n, constant Hamming weight w, where w is an integer lying between 1 and $n-1$ satisfying $\theta_{ij}(\tau) \leq \lambda$ whenever either $i \neq j$ or $\tau \neq 0$.

Note that the Hamming distance $d_{a,b}$ between a period of the corresponding codewords $\{a(t)\}$, $\{b(t)\}$, $0 \leq t \leq n-1$ in an (n, w, λ) OOC having Hamming correlation $\rho, 0 \leq \rho \leq \lambda$, is given by $d_{a,b} = 2(w - \rho)$, and, thus, OOCs are closely related to constant-weight error correcting codes. Given an (n, w, λ) OOC, by enlarging the OOC to include every cyclic shift of each sequence in the code, one obtains a constant-weight, minimum distance $d_{\min} \geq 2(w - \lambda)$ code. Conversely, given a constant-weight cyclic code of length n, weight w and minimum distance $d_{\min}$, one can derive an (n, w, λ) OOC code with $\lambda \leq w - d_{\min}/2$ by partitioning the code into cyclic equivalence classes and then picking precisely one representative from each equivalence class of size n.

By making use of this connection, one can derive bounds on the size of an OOC from known bounds on the size of constant-weight codes. The bound given next follows directly from the Johnson bound for constant weight codes [8]. The number $M(n, w, \lambda)$ of codewords

in a (n, w, λ) OOC satisfies

$$M(n,w,\lambda) \leq \frac{1}{w}\left\lfloor \frac{n-1}{w-1} \cdots \left\lfloor \frac{n-\lambda+1}{w-\lambda+1}\left\lfloor \frac{n-\lambda}{w-\lambda}\right\rfloor\right\rfloor \cdots \right\rfloor$$

An OOC code that achieves the Johnson bound is said to be optimal. A family $\{\mathcal{F}_n\}$ of OOCs indexed by the parameter n and arising from a common construction is said to be asymptotically optimum if

$$\lim_{n\to\infty} \frac{|\mathcal{F}_n|}{M(n,w,\lambda)} = 1$$

Constructions for optical orthogonal codes are available for the cases when $\lambda = 1$ and $\lambda = 2$. For larger values of λ, there exist constructions which are asymptotically optimum. Further details may be found in [6].

Defining Terms

Autocorrelation of a sequence: The complex inner product of the sequence with a shifted version itself.

Crosscorrelation of two sequences: The complex inner product of the first sequence with a shifted version of the second sequence.

***m* Sequence:** A periodic binary $\{0, 1\}$ sequence that is generated by a shift register with linear feedback and which has maximal possible period given the number of stages in the shift register.

Pseudonoise sequences: Also referred to as pseudorandom sequences (PN), these are sequences that are deterministically generated and yet possess some properties that one would expect to find in randomly generated sequences.

Shift-register sequence: A sequence with symbols drawn from a field, which satisfies a linear-recurrence relation and which can be implemented using a shift register.

References

[1] Barg, A. On small families of sequences with low periodic correlation, *Lecture Notes in Computer Science,* 781, 154–158, Berlin, Springer-Verlag, 1994.

[2] Baumert, L.D. *Cyclic Difference Sets,* Lecture Notes in Mathematics 182, Springer–Verlag, New York, 1971.

[3] Boztaş, S., Hammons, R., and Kumar, P.V. 4-phase sequences with near-optimum correlation properties, *IEEE Trans. Inform. Theory,* IT-38, 1101–1113, 1992.

[4] Golomb, S.W. *Shift Register Sequences,* Aegean Park Press, San Francisco, CA, 1982.

[5] Hammons, A.R., Jr. and Kumar, P.V. On a recent 4-phase sequence design for CDMA. *IEICE Trans. Commun.,* E76-B(8), 1993.

[6] Helleseth, T. and Kumar, P.V. (planned). Sequences with low correlation. In *Handbook of Coding Theory,* ed., V.S. Pless and W.C. Huffman, Elsevier Science Publishers, Amsterdam, 1998.

[7] Jensen, J.M., Jensen, H.E., and Høholdt, T. The merit factor of binary sequences related to difference sets. *IEEE Trans. Inform. Theory,* IT-37(May), 617–626, 1991.

[8] MacWilliams, F.J. and Sloane, N.J.A. *The Theory of Error-Correcting Codes,* North-Holland, Amsterdam, 1977.

[9] Maschietti, A. Difference sets and hyperovals, *Designs, Codes and Cryptography,* 14, 89–98, 1998.

[10] Mow, W.H. On McEliece's open problem on minimax aperiodic correlation. In *Proc. IEEE Intern. Symp. Inform. Theory,* 75, 1994.
[11] Nechaev, A. The Kerdock code in a cyclic form, *Discrete Math. Appl.,* 1, 365–384, 1991.
[12] Peterson, W.W. and Weldon, E.J., Jr. *Error-Correcting Codes,* 2nd ed. MIT Press, Cambridge, MA, 1972.
[13] Sarwate, D.V. An upper bound on the aperiodic autocorrelation function for a maximal-length sequence. *IEEE Trans. Inform. Theory,* IT-30(July), 685–687, 1984.
[14] Sarwate, D.V. and Pursley, M.B. Crosscorrelation properties of pseudorandom and related sequences. *Proc. IEEE,* 68(May), 593–619, 1980.
[15] Simon, M.K., Omura, J.K., Scholtz, R.A., and Levitt, B.K. *Spread Spectrum Communications Handbook,* revised ed., McGraw Hill, New York, 1994.
[16] Solé, P. A quaternary cyclic code and a family of quadriphase sequences with low correlation properties, *Coding Theory and Applications, Lecture Notes in Computer Science,* 388, 193–201, Berlin, Springer-Verlag, 1989.
[17] Udaya, P. and Siddiqi, M. Optimal biphase sequences with large linear complexity derived from sequences over Z_4, *IEEE Trans. Inform. Theory,* IT-42 (Jan), 206–216, 1996.

Further Information

A more in-depth treatment of pseudonoise sequences, may be found in the following.

[1] Golomb, S.W. *Shift Register Sequences,* Aegean Park Press, San Francisco, 1982.
[2] Helleseth, T. and Kumar, P.V. Sequences with Low Correlation, in *Handbook of Coding Theory,* edited by V.S. Pless and W.C. Huffman, Elsevier Science Publishers, Amsterdam, 1998 (planned).
[3] Sarwate, D.V. and Pursley, M.B. Crosscorrelation Properties of Pseudorandom and Related Sequences, *Proc. IEEE,* 68, May, 593–619, 1980.
[4] Simon, M.K., Omura, J.K., Scholtz, R.A., and Levitt, B.K. *Spread Spectrum Communications Handbook,* revised ed., McGraw Hill, New York, 1994.

9

Optimum Receivers

9.1 Introduction 9-1
9.2 Preliminaries 9-2
9.3 Karhunen–Loève Expansion 9-2
9.4 Detection Theory 9-4
9.5 Performance 9-5
9.6 Signal Space 9-6
9.7 Standard Binary Signalling Schemes 9-7
9.8 M-ary Optimal Receivers 9-8
9.9 More Realistic Channels 9-9
Random Phase Channels • Rayleigh Channel
9.10 Dispersive Channels 9-13
Defining Terms 9-14
References 9-14
Further Information 9-15

Geoffrey C. Orsak
Southern Methodist University

9.1 Introduction

Every engineer strives for optimality in design. This is particularly true for communications engineers since in many cases implementing suboptimal receivers and sources can result in dramatic losses in performance. As such, this chapter focuses on design principles leading to the implementation of optimum receivers for the most common communication environments.

The main objective in digital communications is to transmit a sequence of bits to a remote location with the highest degree of accuracy. This is accomplished by first representing bits (or more generally short bit sequences) by distinct waveforms of finite time duration. These time-limited waveforms are then transmitted (broadcasted) to the remote sites in accordance with the data sequence.

Unfortunately, because of the nature of the **communication channel,** the remote location receives a corrupted version of the concatenated signal waveforms. The most widely accepted model for the communication channel is the so-called **additive white Gaussian noise**[1] **channel (AWGN channel).** Mathematical arguments based upon the central

[1] For those unfamiliar with AWGN, a random process (waveform) is formally said to be white Gaussian noise if all collections of instantaneous observations of the process are jointly Gaussian and mutually independent. An important consequence of this property is that the power spectral density of the process

0-8493-8597-0/99/$0.00+$.50

© 1999 by CRC Press LLC

limit theorem [7], together with supporting empirical evidence, demonstrate that many common communication channels are accurately modeled by this abstraction. Moreover, from the design perspective, this is quite fortuitous since design and analysis with respect to this channel model is relatively straightforward.

9.2 Preliminaries

To better describe the digital communications process, we shall first elaborate on so-called binary communications. In this case, when the source wishes to transmit a bit value of 0, the transmitter broadcasts a specified waveform $s_0(t)$ over the **bit interval** $t \in [0, T]$. Conversely, if the source seeks to transmit the bit value of 1, the transmitter alternatively broadcasts the signal $s_1(t)$ over the same bit interval. The received waveform $R(t)$ corresponding to the first bit is then appropriately described by the following hypotheses testing problem:

$$\begin{array}{ll} H_0 : R(t) = s_0(t) + \eta(t) & 0 \leq t \leq T \\ H_1 : R(t) = s_1(t) + \eta(t) & \end{array} \tag{9.1}$$

where, as stated previously, $\eta(t)$ corresponds to AWGN with spectral height nominally given by $N_0/2$. It is the objective of the receiver to determine the bit value, i.e., the most accurate hypothesis from the received waveform $R(t)$.

The optimality criterion of choice in digital communication applications is the **total probability of error** normally denoted as P_e. This scalar quantity is expressed as

$$\begin{aligned} P_e \;=\; & Pr(\text{ declaring } 1 \,|\, 0 \text{ transmitted}) Pr(0 \text{ transmitted}) \\ & + Pr(\text{ declaring } 0 \,|\, 1 \text{ transmitted}) Pr(1 \text{ transmitted}) \end{aligned} \tag{9.2}$$

The problem of determining the optimal binary receiver with respect to the probability of error is solved by applying stochastic representation theory [10] to detection theory [5, 9]. The specific waveform representation of relevance in this application is the **Karhunen–Loève (KL) expansion.**

9.3 Karhunen–Loève Expansion

The Karhunen–Loève expansion is a generalization of the Fourier series designed to represent a random process in terms of deterministic basis functions and uncorrelated random variables derived from the process. Whereas the Fourier series allows one to model or represent deterministic time-limited energy signals in terms of linear combinations of complex exponential waveforms, the Karhunen–Loève expansion allows us to represent a second-order random process in terms of a set of **orthonormal** basis functions scaled by a sequence of random variables. The objective in this representation is to choose the basis of time functions so that the coefficients in the expansion are mutually uncorrelated random variables.

To be more precise, if $R(t)$ is a zero mean second-order random process defined over $[0, T]$ with covariance function $K_R(t, s)$, then so long as the basis of deterministic functions satisfy

is a constant with respect to frequency variation (spectrally flat). For more on AWGN, see Papoulis [4].

certain integral constraints [9], one may write $R(t)$ as

$$R(t) = \sum_{i=1}^{\infty} R_i \phi_i(t) \qquad 0 \leq t \leq T \tag{9.3}$$

where

$$R_i = \int_0^T R(t)\phi_i(t)\ \mathrm{d}t$$

In this case the R_i will be mutually uncorrelated random variables with the ϕ_i being deterministic basis functions that are complete in the space of square integrable time functions over $[0, T]$. Importantly, in this case, equality is to be interpreted as **mean-square equivalence,** i.e.,

$$\lim_{N\to\infty} E\left[\left(R(t) - \sum_{i=1}^{N} R_i\phi_i(t)\right)^2\right] = 0$$

for all $0 \leq t \leq T$.

FACT 9.1 *If $R(t)$ is AWGN, then any basis of the vector space of square integrable signals over $[0, T]$ results in uncorrelated and therefore independent Gaussian random variables.*

The use of Fact 9.1 allows for a conversion of a continuous time detection problem into a finite-dimensional detection problem. Proceeding, to derive the optimal binary receiver, we first construct our set of basis functions as the set of functions defined over $t \in [0, T]$ beginning with the signals of interest $s_0(t)$ and $s_1(t)$. That is,

$$\{s_0(t), s_1(t),\ \text{plus a countable number of functions which complete the basis}\}$$

In order to insure that the basis is orthonormal, we must apply the Gramm–Schmidt procedure[2] [6] to the full set of functions beginning with $s_0(t)$ and $s_1(t)$ to arrive at our final choice of basis $\{\phi_i(t)\}$.

FACT 9.2 *Let $\{\phi_i(t)\}$ be the resultant set of basis functions.*
Then for all $i > 2$, the $\phi_i(t)$ are orthogonal to $s_0(t)$ and $s_1(t)$. That is,

$$\int_0^T \phi_i(t)s_j(t)\,\mathrm{d}t = 0$$

for all $i > 2$ and $j = 0, 1$.

Using this fact in conjunction with Eq. (9.3), one may recognize that only the coefficients R_1 and R_2 are functions of our signals of interest. Moreover, since the R_i are mutually independent, the optimal receiver will, therefore, only be a function of these two values.

[2]The Gramm-Schmidt procedure is a deterministic algorithm that simply converts an arbitrary set of basis functions (vectors) into an equivalent set of orthonormal basis functions (vectors).

Thus, through the application of the KL expansion, we arrive at an equivalent hypothesis testing problem to that given in Eq. (9.1),

$$\begin{aligned} H_0 : \boldsymbol{R} &= \begin{bmatrix} \int_0^T \phi_1(t)s_0(t)\ \mathrm{d}t \\ \int_0^T \phi_2(t)s_0(t)\ \mathrm{d}t \end{bmatrix} + \begin{bmatrix} \eta_1 \\ \eta_2 \end{bmatrix} \\ H_1 : \boldsymbol{R} &= \begin{bmatrix} \int_0^T \phi_1(t)s_1(t)\ \mathrm{d}t \\ \int_0^T \phi_2(t)s_1(t)\ \mathrm{d}t \end{bmatrix} + \begin{bmatrix} \eta_1 \\ \eta_2 \end{bmatrix} \end{aligned} \tag{9.4}$$

where it is easily shown that η_1 and η_2 are mutually independent, zero-mean, Gaussian random variables with variance given by $N_0/2$, and where ϕ_1 and ϕ_2 are the first two functions from our orthonormal set of basis functions. Thus, the design of the optimal binary receiver reduces to a simple two-dimensional detection problem that is readily solved through the application of detection theory.

9.4 Detection Theory

It is well known from detection theory [5] that under the minimum P_e criterion, the optimal detector is given by the *maximum a posteriori rule* (*MAP*),

$$\text{choose}_i \ \text{ largest } p_{H_i|\boldsymbol{R}}(H_i \mid \boldsymbol{R} = \boldsymbol{r}) \tag{9.5}$$

i.e., determine the hypothesis that is most likely, given that our observation vector is $\boldsymbol{r}$. By a simple application of Bayes theorem [4], we immediately arrive at the central result in detection theory: the optimal binary detector is given by the likelihood ratio test (LRT),

$$L(\boldsymbol{R}) = \frac{p_{\boldsymbol{R}|H_1}(\boldsymbol{R})}{p_{\boldsymbol{R}|H_0}(\boldsymbol{R})} \underset{H_0}{\overset{H_1}{\gtrless}} \frac{\pi_0}{\pi_1} \tag{9.6}$$

where the π_i are the a priori probabilities of the hypotheses H_i being true. Since in this case we have assumed that the noise is white and Gaussian, the LRT can be written as

$$L(\boldsymbol{R}) = \frac{\prod_1^2 \frac{1}{\sqrt{\pi N_0}} \exp\left(-\frac{1}{2} \frac{(R_i - s_{1,i})^2}{N_0/2} \right)}{\prod_1^2 \frac{1}{\sqrt{\pi N_0}} \exp\left(-\frac{1}{2} \frac{(R_i - s_{0,i})^2}{N_0/2} \right)} \underset{H_0}{\overset{H_1}{\gtrless}} \frac{\pi_0}{\pi_1} \tag{9.7}$$

where

$$s_{j,i} = \int_0^T \phi_i(t) s_j(t)\, \mathrm{d}t$$

By taking the logarithm and cancelling common terms, it is easily shown that the optimum binary receiver can be written as

$$\frac{2}{N_0} \sum_1^2 \boldsymbol{R}_i \left(s_{1,i} - s_{0,i} \right) - \frac{1}{N_0} \sum_1^2 \left(s_{1,i}^2 - s_{0,i}^2 \right) \underset{H_0}{\overset{H_1}{\gtrless}} \ln \frac{\pi_0}{\pi_1} \tag{9.8}$$

This finite-dimensional version of the optimal receiver can be converted back into a continuous time receiver by the direct application of Parseval's theorem [4] where it is easily shown that

$$\begin{aligned} \sum_{i=1}^{2} R_i s_{k,i} &= \int_0^T R(t) s_k(t)\, \mathrm{d}t \\ \sum_{i=1}^{2} s_{k,i}^2 &= \int_0^T s_k^2(t)\, \mathrm{d}t \end{aligned} \tag{9.9}$$

By applying Eq. (9.9) to Eq. (9.8) the final receiver structure is then given by

$$\int_0^T R(t)\left[s_1(t) - s_0(t)\right] \mathrm{d}t - \frac{1}{2}\left(E_1 - E_0\right) \underset{H_0}{\overset{H_1}{\gtrless}} \frac{N_0}{2} \ln \frac{\pi_0}{\pi_1} \tag{9.10}$$

where E_1 and E_0 are the energies of signals $s_1(t)$ and $s_0(t)$, respectively. (See Fig. 9.1 for a block diagram.) Importantly, if the signals are equally likely ($\pi_0 = \pi_1$), the optimal receiver is independent of the typically unknown spectral height of the background noise.

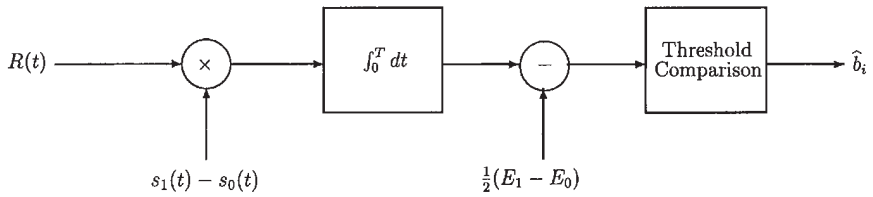


FIGURE 9.1 Optimal correlation receiver structure for binary communications.

One can readily observe that the optimal binary communication receiver correlates the received waveform with the difference signal $s_1(t) - s_0(t)$ and then compares the statistic to a threshold. This operation can be interpreted as identifying the signal waveform $s_i(t)$ that best correlates with the received signal $R(t)$. Based on this interpretation, the receiver is often referred to as the **correlation receiver.**

As an alternate means of implementing the correlation receiver, we may reformulate the computation of the left-hand side of Eq. (9.10) in terms of standard concepts in filtering. Let $h(t)$ be the impulse response of a linear, time-invariant (LTI) system. By letting $h(t) = s_1(T-t) - s_0(T-t)$, then it is easily verified that the output of $R(t)$ to a LTI system with impulse response given by $h(t)$ and then sampled at time $t = T$ gives the desired result. (See Fig. 9.2 for a block diagram.) Since the impulse response is matched to the signal waveforms, this implementation is often referred to as the **matched filter receiver.**

9.5 Performance

Because of the nature of the statistics of the channel and the relative simplicity of the receiver, performance analysis of the optimal binary receiver in AWGN is a straightforward task. Since the conditional statistics of the log likelihood ratio are Gaussian random vari-

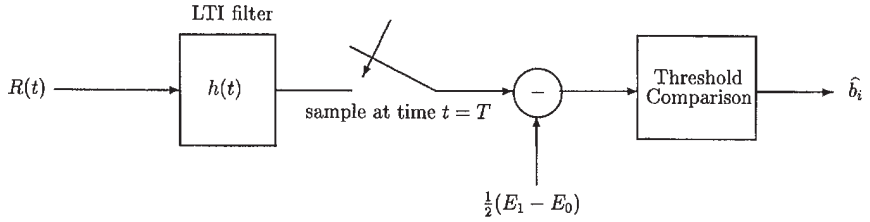


FIGURE 9.2 Optimal matched filter receiver structure for binary communications. In this case $h(t) = s_1(T - t) - s_0(t - t)$.

ables, the probability of error can be computed directly in terms of Marcum Q functions[3] as

$$P_e = Q\left(\frac{\|\boldsymbol{s}_0 - \boldsymbol{s}_1\|}{\sqrt{2N_0}}\right)$$

where the $\boldsymbol{s}_i$ are the two-dimensional signal vectors obtained from Eq. (9.4), and where $\|\boldsymbol{x}\|$ denotes the Euclidean length of the vector $\boldsymbol{x}$. Thus, $\|\boldsymbol{s}_0 - \boldsymbol{s}_1\|$ is best interpreted as the distance between the respective signal representations. Since the Q function is monotonically decreasing with an increasing argument, one may recognize that the probability of error for the optimal receiver decreases with an increasing separation between the signal representations, i.e., the more dissimilar the signals, the lower the P_e.

9.6 Signal Space

The concept of a **signal space** allows one to view the signal classification problem (receiver design) within a geometrical framework. This offers two primary benefits: first it supplies an often more intuitive perspective on the receiver characteristics (e.g., performance) and second it allows for a straightforward generalization to standard M-ary signalling schemes.

To demonstrate this, in Fig. 9.3, we have plotted an arbitrary signal space for the binary signal classification problem. The axes are given in terms of the basis functions $\phi_1(t)$ and $\phi_2(t)$. Thus, every point in the signal space is a time function constructed as a linear combination of the two basis functions. By Fact 9.2, we recall that both signals $s_0(t)$ and $s_1(t)$ can be constructed as a linear combination of $\phi_1(t)$ and $\phi_2(t)$ and as such we may identify these two signals in this figure as two points.

Since the decision statistic given in Eq. (9.8) is a linear function of the observed vector $\boldsymbol{R}$ which is also located in the signal space, it is easily shown that the set of vectors under which the receiver declares hypothesis H_i is bounded by a line in the signal space. This so-called **decision boundary** is obtained by solving the equation $\ln[L(\boldsymbol{R})] = 0$. (Here again we have assumed equally likely hypotheses.) In the case under current discussion, this decision boundary is simply the hyperplane separating the two signals in signal space. Because of the generality of this formulation, many problems in communication system design are best cast in terms of the signal space, that is, signal locations and decision boundaries.

[3]The Q function is the probability that a standard normal random variable exceeds a specified constant, i.e., $Q(x) = \int_x^\infty 1/\sqrt{2\pi}\exp(-z^2/2)\,dz$.

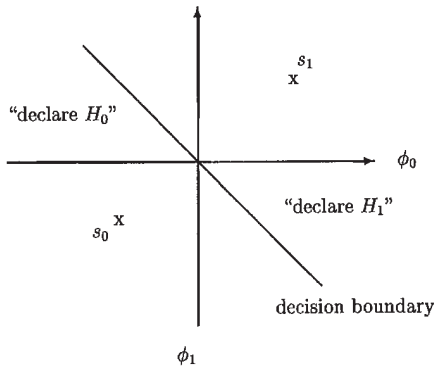


FIGURE 9.3 Signal space and decision boundary for optimal binary receiver.

9.7 Standard Binary Signalling Schemes

The framework just described allows us to readily analyze the most popular signalling schemes in binary communications: amplitude-shift keying (ASK), frequency-shift keying (FSK), and phase-shift keying (PSK). Each of these examples simply constitute a different selection for signals $s_0(t)$ and $s_1(t)$.

In the case of ASK, $s_0(t) = 0$, while $s_1(t) = \sqrt{2E/T}\sin(2\pi f_c t)$, where E denotes the energy of the waveform and f_c denotes the frequency of the carrier wave with $f_c T$ being an integer. Because $s_0(t)$ is the null signal, the signal space is a one-dimensional vector space with $\phi_1(t) = \sqrt{2/T}\sin(2\pi f_c t)$. This, in turn, implies that $\|s_0 - s_1\| = \sqrt{E}$. Thus, the corresponding probability of error for ASK is

$$P_e(\text{ ASK}) = Q\left(\sqrt{\frac{E}{2N_0}}\right)$$

For FSK, the signals are given by equal amplitude sinusoids with distinct center frequencies, that is, $s_i(t) = \sqrt{2E/T}\sin(2\pi f_i t)$ with $f_i T$ being two distinct integers. In this case, it is easily verified that the signal space is a two-dimensional vector space with $\phi_i(t) = \sqrt{2/T}\sin(2\pi f_i t)$ resulting in $\|\boldsymbol{s}_0 - \boldsymbol{s}_1\| = \sqrt{2\boldsymbol{E}}$. The corresponding error rate is given to be

$$P_e(\text{FSK}) = Q\left(\sqrt{\frac{E}{N_0}}\right)$$

Finally, with regard to PSK signalling, the most frequently utilized binary PSK signal set is an example of an antipodal signal set. Specifically, the antipodal signal set results in the greatest separation between the signals in the signal space subject to an energy constraint on both signals. This, in turn, translates into the energy constrained signal set with the minimum P_e. In this case, the $s_i(t)$ are typically given by $\sqrt{2E/T}\sin[2\pi f_c t + \theta(i)]$, where $\theta(0) = 0$ and $\theta(1) = \pi$. As in the ASK case, this results in a one-dimensional signal space, however, in this case $\|\boldsymbol{s}_0 - \boldsymbol{s}_1\| = 2\sqrt{\boldsymbol{E}}$ resulting in probability of error given by

$$P_e(\text{PSK}) = Q\left(\sqrt{\frac{2E}{N_0}}\right)$$

In all three of the described cases, one can readily observe that the resulting performance is a function of only the signal-to-noise ratio E/N_0. In the more general case, the performance

will be a function of the intersignal energy to noise ratio. To gauge the relative difference in performance of the three signalling schemes, in Fig. 9.4, we have plotted the P_e as a function of the SNR. Please note the large variation in performance between the three schemes for even moderate values of SNR.

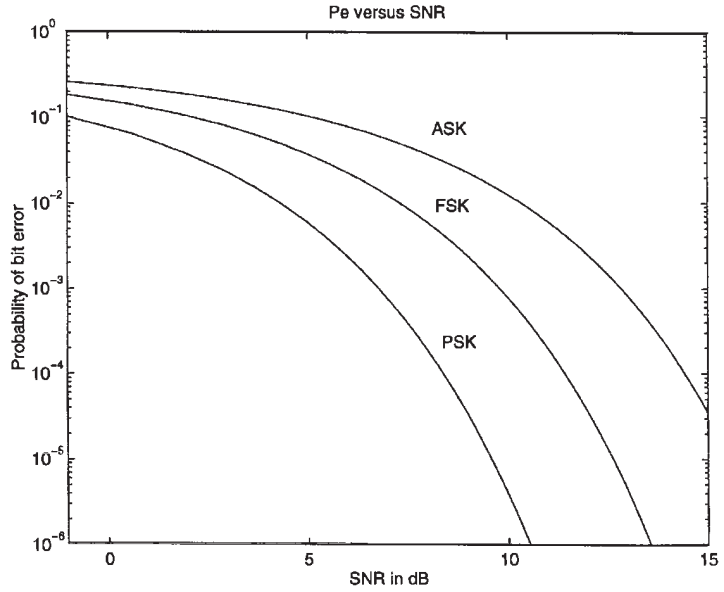


FIGURE 9.4 P_e vs. the signal to noise ratio in decibels [dB $= 10\log(E/N_0)$] for amplitude-shift keying, frequency-shift keying, and phase-shift keying; note that there is a 3-dB difference in performance from ASK to FSK to PSK.

9.8 *M*-ary Optimal Receivers

In binary signalling schemes, one seeks to transmit a single bit over the bit interval $[0, T]$. This is to be contrasted with M-ary signalling schemes where one transmits multiple bits simultaneously over the so-called symbol interval $[0, T]$. For example, using a signal set with 16 separate waveforms will allow one to transmit a length four-bit sequence per symbol (waveform). Examples of M-ary waveforms are quadrature phase-shift keying (QPSK) and quadrature amplitude modulation (QAM).

The derivation of the optimum receiver structure for M-ary signalling requires the straightforward application of fundamental results in detection theory. As with binary signalling, the Karhunen–Loève expansion is the mechanism utilized to convert a hypotheses testing problem based on continuous waveforms into a vector classification problem. Depending on the complexity of the M waveforms, the signal space can be as large as an M-dimensional vector space.

By extending results from the binary signalling case, it is easily shown that the optimum M-ary receiver computes

$$\xi_i[R(t)] = \int_0^T s_i(t)R(t)\ \mathrm{d}t - \frac{E_i}{2} + \frac{N_0}{2}\ln \pi_i \qquad i = 1, \ldots, M$$

where, as before, the $s_i(t)$ constitute the signal set with the π_i being the corresponding a priori probabilities. After computing M separate values of ξ_i, the minimum probability of error receiver simply chooses the largest amongst this set. Thus, the M-ary receiver is implemented with a bank of correlation or matched filters followed by choose-largest decision logic.

In many cases of practical importance, the signal sets are selected so that the resulting signal space is a two-dimensional vector space irrespective of the number of signals. This simplifies the receiver structure in that the sufficient statistics are obtained by implementing only two matched filters. Both QPSK and QAM signal sets fit into this category. As an example, in Fig. 9.5, we have depicted the signal locations for standard 16-QAM signalling with the associated decision boundaries. In this case we have assumed an equally likely signal set. As can be seen, the optimal decision rule selects the signal representation that is closest to the received signal representation in this two-dimensional signal space.

9.9 More Realistic Channels

As is unfortunately often the case, many channels of practical interest are not accurately modeled as simply an AWGN channel. It is often that these channels impose nonlinear effects on the transmitted signals. The best example of this are channels that impose a random phase and random amplitude onto the signal. This typically occurs in applications such as in mobile communications, where one often experiences rapidly changing path lengths from source to receiver.

Fortunately, by the judicious choice of signal waveforms, it can be shown that the selection of the ϕ_i in the Karhunen–Loève transformation is often independent of these unwanted parameters. In these situations, the random amplitude serves only to scale the signals in signal space, whereas the random phase simply imposes a rotation on the signals in signal space.

Since the Karhunen–Loève basis functions typically do not depend on the unknown parameters, we may again convert the continuous time classification problem to a vector channel problem where the received vector $\boldsymbol{R}$ is computed as in Eq. (9.3). Since this vector is a function of both the unknown parameters (i.e., in this case amplitude A and phase ν), to obtain a likelihood ratio test independent of A and ν, we simply apply Bayes theorem to obtain the following form for the LRT:

$$L(\boldsymbol{R}) = \frac{E\left[p_{\boldsymbol{R}\,|H_1,A,\nu}\left(\boldsymbol{R}\mid H_1,A,\nu\right)\right]}{E\left[p_{\boldsymbol{R}\,|H_0,A,\nu}\left(\boldsymbol{R}\mid H_0,A,\nu\right)\right]} \begin{array}{c} H_1 \\ > \\ < \\ H_0 \end{array} \frac{\pi_0}{\pi_1}$$

where the expectations are taken with respect to A and ν, and where $p_{\boldsymbol{R}|H_i,A,\nu}$ are the conditional probability density functions of the signal representations. Assuming that the background noise is AWGN, it can be shown that the LRT simplifies to choosing the largest amongst

$$\xi_i[R(t)] = \pi_i \int_{A,\nu} \exp\left\{\frac{2}{N_0}\int_0^T R(t)s_i(t\,|\,A,\nu)\;\mathrm{d}t - \frac{E_i(A,\nu)}{N_0}\right\} p_{A,\nu}(A,\nu)\;\mathrm{d}A\,\mathrm{d}\nu$$

$$i = 1,\ldots,M \qquad (9.11)$$

It should be noted that in the Eq. (9.11) we have explicitly shown the dependence of the transmitted signals s_i on the parameters A and ν. The final receiver structures, together

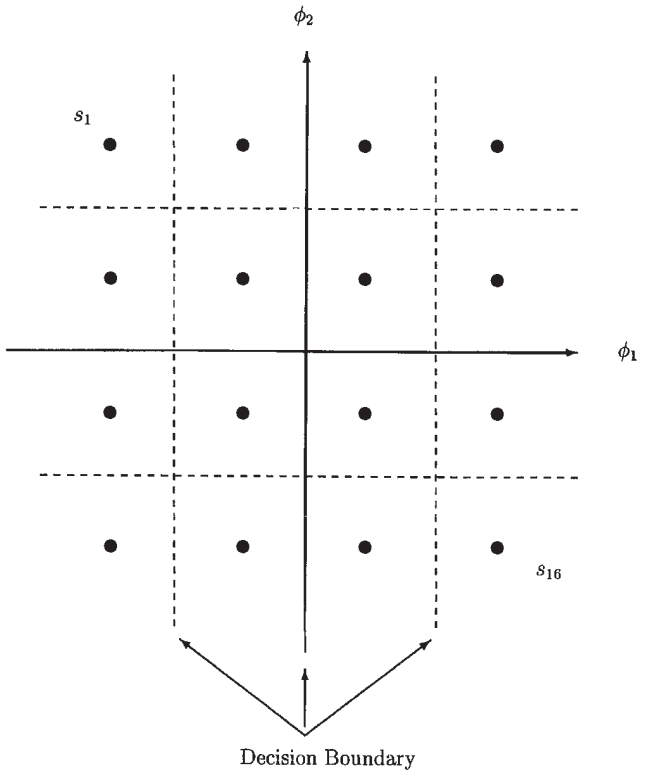


FIGURE 9.5 Signal space representation of 16-QAM signal set. Optimal decision regions for equally likely signals are also noted.

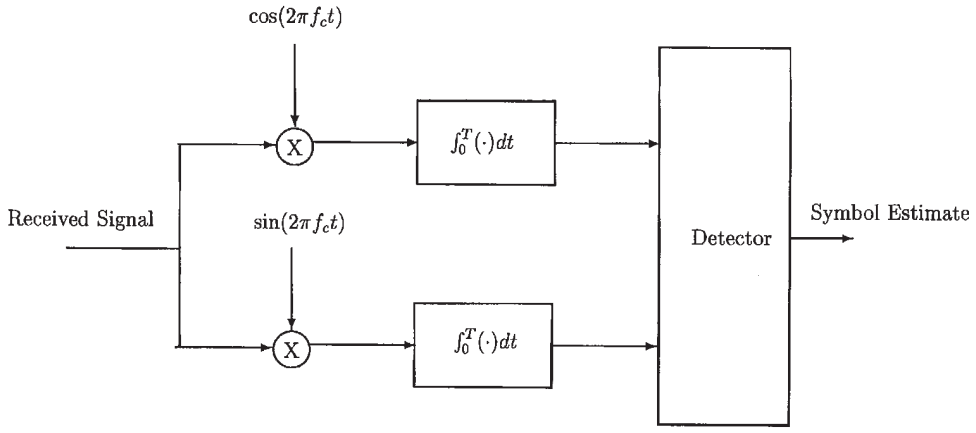


FIGURE 9.6 Optimum receiver structure for noncoherent (random or unknown phase) ASK demodulation.

with their corresponding performance are, thus, a function of both the choice of signal sets and the probability density functions of the random amplitude and random phase.

9.9.1 Random Phase Channels

If we consider first the special case where the channel simply imposes a uniform random phase on the signal, then it can be easily shown that the so-called in-phase and quadrature statistics obtained from the received signal $R(t)$ (denoted by R_I and R_Q, respectively), are sufficient statistics for the signal classification problem. These quantities are computed as

$$R_I(i) = \int_0^T R(t) \cos\left[2\pi f_c(i)t\right] \; \mathrm{d}t$$

and

$$R_Q(i) = \int_0^T R(t) \sin\left[2\pi f_c(i)t\right] \; \mathrm{d}t$$

where in this case the index i corresponds to the center frequencies of hypotheses H_i, (e.g., FSK signalling). The optimum binary receiver selects the largest from amongst

$$\xi_i[R(t)] = \pi_i \exp\left(-\frac{E_i}{N_0}\right) I_0\left[\frac{2}{N_0}\sqrt{R_I^2(i) + R_Q^2(i)}\right] \qquad i = 1, \ldots, M$$

where I_0 is a zeroth-order, modified Bessel function of the first kind. If the signals have equal energy and are equally likely (e.g., FSK signalling), then the optimum receiver is given by

$$R_I^2(1) + R_Q^2(1) \underset{H_0}{\overset{H_1}{\gtrless}} R_I^2(0) + R_Q^2(0)$$

One may readily observe that the optimum receiver bases its decision on the values of the two envelopes of the received signal $\sqrt{R_I^2(i) + R_Q^2(i)}$ and, as a consequence, is often referred to as an envelope or square-law detector. Moreover, it should be observed that the computation of the envelope is independent of the underlying phase of the signal and is as such known as a noncoherent receiver.

The computation of the error rate for this detector is a relatively straightforward exercise resulting in

$$P_e(\text{ noncoherent}) = \frac{1}{2} \exp\left(-\frac{E}{2N_0}\right)$$

As before, note that the error rate for the noncoherent receiver is simply a function of the SNR.

9.9.2 Rayleigh Channel

As an important generalization of the described random phase channel, many communication systems are designed under the assumption that the channel introduces both a random amplitude and a random phase on the signal. Specifically, if the original signal sets are of the form $s_i(t) = m_i(t)\cos(2\pi f_c t)$ where $m_i(t)$ is the baseband version of the message (i.e., what distinguishes one signal from another), then the so-called **Rayleigh channel** introduces random distortion in the received signal of the following form:

$$s_i(t) = A m_i(t) \cos\left(2\pi f_c t + \nu\right)$$

where the amplitude A is a Rayleigh random variable[4] and where the random phase ν is a uniformly distributed between zero and 2π.

To determine the optimal receiver under this distortion, we must first construct an alternate statistical model for $s_i(t)$. To begin, it can be shown from the theory of random variables [4] that if X_I and X_Q are statistically independent, zero mean, Gaussian random variables with variance given by σ^2, then

$$Am_i(t)\cos(2\pi f_c t + \nu) = m_i(t)X_I \cos(2\pi f_c t) + m_i(t)X_Q \sin(2\pi f_c t)$$

Equality here is to be interpreted as implying that both A and ν will be the appropriate random variables. From this, we deduce that the combined uncertainty in the amplitude and phase of the signal is incorporated into the Gaussian random variables X_I and X_Q. The in-phase and quadrature components of the signal $s_i(t)$ are given by $s_{Ii}(t) = m_i(t)\cos(2\pi f_c t)$ and $s_{Q_i}(t) = m_i(t)\sin(2\pi f_c t)$, respectively. By appealing to Eq. (9.11), it can be shown that the optimum receiver selects the largest from

$$\xi_i[R(t)] = \frac{\pi_i}{1 + \dfrac{2E_i}{N_0}\sigma^2} \exp\left[\frac{\sigma^2}{\dfrac{1}{2} + \dfrac{E_i}{N_0}\sigma^2}\left(\langle R(t), s_{Ii}(t)\rangle^2 + \langle R(t), s_{Q_i}(t)\rangle^2\right)\right]$$

where the inner product

$$\langle R(t), S_i(t)\rangle = \int_0^T R(t)s_i(t)\ \mathrm{d}t$$

Further, if we impose the conditions that the signals be equally likely with equal energy over the symbol interval, then optimum receiver selects the largest amongst

$$\xi_i[R(t)] = \sqrt{\langle R(t), s_{Ii}(t)\rangle^2 + \langle R(t), s_{Q_i}(t)\rangle^2}$$

Thus, much like for the random phase channel, the optimum receiver for the Rayleigh channel computes the projection of the received waveform onto the in-phase and quadrature components of the hypothetical signals. From a signal space perspective, this is akin to computing the length of the received vector in the subspace spanned by the hypothetical signal. The optimum receiver then chooses the largest amongst these lengths.

As with the random phase channel, computing the performance is a straightforward task resulting in (for the equally likely, equal energy case)

$$P_e(\text{ Rayleigh}) = \frac{\dfrac{1}{2}}{\left(1 + \dfrac{E\sigma^2}{N_0}\right)}$$

Interestingly, in this case the performance depends not only on the SNR, but also on the variance (spread) of the Rayleigh amplitude A. Thus, if the amplitude spread is large, we expect to often experience what is known as deep fades in the amplitude of the received waveform and as such expect a commensurate loss in performance.

[4]The density of a Rayleigh random variable is given by $p_A(a) = a/\sigma^2 \exp(-a^2/2\sigma^2)$ for $a \geq 0$.

9.10 Dispersive Channels

The **dispersive channel** model assumes that the channel not only introduces AWGN but also distorts the signal through a filtering process. This model incorporates physical realities such as multipath effects and frequency selective fading. In particular, the standard model adopted is depicted in the block diagram given in Fig. 9.7. As can be seen, the receiver observes a filtered version of the signal plus AWGN. If the impulse response of the channel is known, then we arrive at the optimum receiver design by applying the previously presented theory. Unfortunately, the duration of the filtered signal can be a complicating factor. More often than not, the channel will increase the duration of the transmitted signals, hence, leading to the description, dispersive channel.

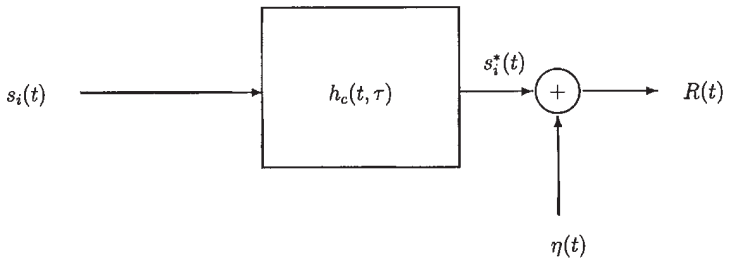


FIGURE 9.7 Standard model for dispersive channel. The time varying impulse response of the channel is denoted by $h_c(t,\tau)$.

However, if the designers take this into account by shortening the duration of $s_i(t)$ so that the duration of $s_i^*(t)$ is less than T, then the optimum receiver chooses the largest amongst

$$\xi_i(R(t)) = \frac{N_0}{2}\ln\pi_i + \langle R(t), s_i^*(t)\rangle - \frac{1}{2}E_i^*$$

If we limit our consideration to equally likely binary signal sets, then the minimum P_e matches the received waveform to the filtered versions of the signal waveforms. The resulting error rate is given by

$$P_e(\text{ dispersive}) = Q\left(\frac{\|s_0^* - s_0^*\|}{\sqrt{2N_0}}\right)$$

Thus, in this case the minimum P_e is a function of the separation of the filtered version of the signals in the signal space.

The problem becomes substantially more complex if we cannot insure that the filtered signal durations are less than the symbol lengths. In this case we experience what is known as **intersymbol interference (ISI)**. That is, observations over one symbol interval contain not only the symbol information of interest but also information from previous symbols. In this case we must appeal to optimum sequence estimation [5] to take full advantage of the information in the waveform. The basis for this procedure is the maximization of the joint likelihood function conditioned on the sequence of symbols. This procedure not only defines the structure of the optimum receiver under ISI but also is critical in the decoding of convolutional codes and coded modulation. Alternate adaptive techniques to solve this problem involve the use of channel equalization.

Defining Terms

Additive white Gaussian noise (AWGN) channel: The channel whose model is that of corrupting a transmitted waveform by the addition of white (i.e., spectrally flat) Gaussian noise.

Bit (symbol) interval: The period of time over which a single symbol is transmitted.

Communication channel: The medium over which communication signals are transmitted. Examples are fiber optic cables, free space, or telephone lines.

Correlation or matched filter receiver: The optimal receiver structure for digital communications in AWGN.

Decision boundary: The boundary in signal space between the various regions where the receiver declares H_i. Typically a hyperplane when dealing with AWGN channels.

Dispersive channel: A channel that elongates and distorts the transmitted signal. Normally modeled as a time-varying linear system.

Intersymbol interference: The ill-effect of one symbol smearing into adjacent symbols thus interfering with the detection process. This is a consequence of the channel filtering the transmitted signals and therefore elongating their duration, see dispersive channel.

Karhunen–Loève expansion: A representation for second-order random processes. Allows one to express a random process in terms of a superposition of deterministic waveforms. The scale values are uncorrelated random variables obtained from the waveform.

Mean-square equivalence: Two random vectors or time-limited waveforms are mean-square equivalent if and only if the expected value of their mean-square error is zero.

Orthonormal: The property of two or more vectors or time-limited waveforms being mutually orthogonal and individually having unit length. Orthogonality and length are typically measured by the standard Euclidean inner product.

Rayleigh channel: A channel that randomly scales the transmitted waveform by a Rayleigh random variable while adding an independent uniform phase to the carrier.

Signal space: An abstraction for representing a time limited waveform in a low-dimensional vector space. Usually arrived at through the application of the Karhunen–Loève transformation.

Total probability of error: The probability of classifying the received waveform into any of the symbols that were not transmitted over a particular bit interval.

References

[1] Gibson, J.D., *Principles of Digital and Analog Communications,* 2nd ed., MacMillan, New York, 1993.

[2] Haykin, S., *Communication Systems,* 3rd ed., John Wiley & Sons, New York, 1994.

[3] Lee, E.A. and Messerschmitt, D.G., *Digital Communication,* Kluwer Academic Publishers, Norwell, MA, 1988.

[4] Papoulis, A., *Probability, Random Variables, and Stochastic Processes,* 3rd ed., McGraw-Hill, New York, 1991.
[5] Poor, H.V., *An Introduction to Signal Detection and Estimation,* Springer-Verlag, New York, 1988.
[6] Proakis, J.G., *Digital Communications,* 2nd ed., McGraw-Hill, New York, 1989.
[7] Shiryayev, A.N., *Probability,* Springer-Verlag, New York, 1984.
[8] Sklar, B., *Digital Communications, Fundamentals and Applications,* Prentice Hall, Englewood Cliffs, NJ, 1988.
[9] Van Trees, H.L., *Detection, Estimation, and Modulation Theory, Part I,* John Wiley & Sons, New York, 1968.
[10] Wong, E. and Hajek, B., *Stochastic Processes in Engineering Systems,* Springer-Verlag, New York, 1985.
[11] Wozencraft, J.M. and Jacobs, I., *Principles of Communication Engineering,* reissue, Waveland Press, Prospect Heights, Illinois, 1990.
[12] Ziemer, R.E. and Peterson, R.L., *Introduction to Digital Communication,* Macmillan, New York, 1992.

Further Information

The fundamentals of receiver design were put in place by Wozencraft and Jacobs in their seminal book. Since that time, there have been many outstanding textbooks in this area. For a sampling see [1, 2, 3, 8, 12]. For a complete treatment on the use and application of detection theory in communications see [5, 9]. For deeper insights into the Karhunen–Loève expansion and its use in communications and signal processing see [10].

10

Forward Error Correction Coding

10.1 Introduction 10-1
10.2 Fundamentals of Block Coding 10-3
10.3 Structure and Decoding of Block Codes 10-3
10.4 Important Classes of Block Codes 10-5
10.5 Principles of Convolutional Coding 10-6
10.6 Decoding of Convolutional Codes 10-10
10.7 Trellis-Coded Modulation 10-10
10.8 Additional Measures 10-13
10.9 Turbo Codes 10-13
10.10 Applications 10-14
Defining Terms 10-15
References 10-17
Further Information 10-17

V.K. Bhargava
University of Victoria

I.J. Fair
University of Alberta

10.1 Introduction

In 1948, Claude Shannon issued a challenge to communications engineers by proving that communication systems could be made arbitrarily reliable as long as a fixed percentage of the transmitted signal was redundant [9]. He showed that limits exist only on the rate of communication and not its accuracy, and went on to prove that errorless transmission could be achieved in an additive white Gaussian noise (AWGN) environment with infinite bandwidth if the ratio of energy per data bit to noise power spectral density exceeds the **Shannon Limit**. He did not, however, indicate how this could be achieved. Subsequent research has led to a number of techniques that introduce redundancy to allow for correction of errors without retransmission. These techniques, collectively known as forward error correction (FEC) coding techniques, are used in systems where a reverse channel is not available for requesting retransmission, the delay with retransmission would be excessive, the expected number of errors would require a large number of retransmissions, or retransmission would be awkward to implement [10].

A simplified model of a digital communication system which incorporates FEC coding is shown in Fig. 10.1. The FEC code acts on a **discrete data channel** comprising all system elements between the encoder output and decoder input. The encoder maps the source data to q-ary code symbols which are modulated and transmitted. During transmission, this signal can be corrupted, causing errors to arise in the demodulated symbol sequence. The FEC decoder attempts to correct these errors and restore the original source data.

0-8493-8597-0/99/$0.00+$.50

© 1999 by CRC Press LLC

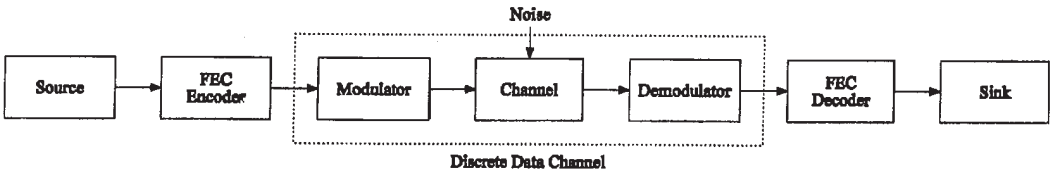


FIGURE 10.1 Block diagram of a digital communication system with forward error correction.

A demodulator which outputs only a value for the q-ary symbol received during each symbol interval is said to make **hard decisions.** In the **binary symmetric channel** (BSC), hard decisions are made on binary symbols and the probability of error is independent of the value of the symbol. One example of a BSC is the coherently demodulated binary phase-shift-keyed (BPSK) signal corrupted by AWGN. The conditional probability density functions which result with this system are depicted in Fig. 10.2. The probability of error is given by the area under the density functions that lies across the decision threshold, and is a function of the symbol energy E_s and the one-sided noise power spectral density N_0.

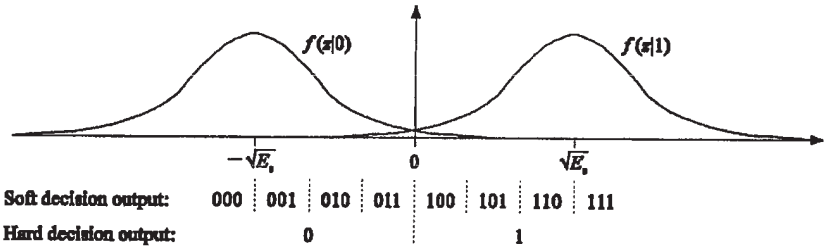


FIGURE 10.2 Hard and soft decision demodulation of a coherently demodulated BPSK signal corrupted by AWGN. $f(z \mid 1)$ and $f(z \mid 0)$ are the Gaussianly distributed conditional probability density functions at the threshold device.

Alternatively, the demodulator can make **soft decisions** or output an estimate of the symbol value along with an indication of its confidence in this estimate. For example, if the BPSK demodulator uses three-bit quantization, the two least significant bits can be taken as a confidence measure. Possible soft-decision thresholds for the BPSK signal are depicted in Fig. 10.2. In practice, there is little to be gained by using many soft-decision quantization levels.

Block and convolutional codes introduce redundancy by adding parity symbols to the message data. They map k source symbols to n code symbols and are said to have **code rate** $R = k/n$. With fixed information rates, this redundancy results in increased bandwidth and lower energy per transmitted symbol. At low signal-to-noise ratios, these codes cannot compensate for these impairments, and performance is degraded. At higher ratios of information symbol energy E_b to noise spectral density N_0, however, there is **coding gain** since the performance improvement offered by coding more than compensates for these impairments. Coding gain is usually defined as the reduction in required E_b/N_0 to achieve a specific error rate in an error-control coded system over one without coding. In contrast to block and convolutional codes, trellis-coded modulation introduces redundancy by expanding the size of the signal set rather than increasing the number of symbols transmitted, and so offers the advantages of coding to band-limited systems.

Each of these coding techniques is considered in turn. Following a discussion of **inter-**

leaving and concatenated coding, this chapter gives an overview of a recent and significant advance in coding, the development of Turbo codes, and concludes with a brief overview of FEC applications.

10.2 Fundamentals of Block Coding

In block codes there is a one-to-one mapping between k-symbol source words and n-symbol codewords. With q-ary signalling, q^k out of the q^n possible n-tuples are valid code vectors. The set of all n-tuples forms a **vector space** in which the q^k code vectors are distributed. The **Hamming distance** between any two code vectors is the number of symbols in which they differ; the **minimum distance** $d_{\min}$ of the code is the smallest Hamming distance between any two codewords.

There are two contradictory objectives of block codes. The first is to distribute the code vectors in the vector space such that the distance between them is maximized. Then, if the decoder receives a corrupted vector, by evaluating the nearest valid code vector it will decode the correct word with high probability. The second is to pack the vector space with as many code vectors as possible to reduce the redundancy in transmission.

When code vectors differ in at least $d_{\min}$ positions, a decoder which evaluates the nearest code vector to each received word is guaranteed to correct up to t random symbol errors per word if

$$d_{\min} \geq 2t + 1 \tag{10.1}$$

Alternatively, all $q^n - q^k$ illegal words can be detected, including all error patterns with $d_{\min} - 1$ or fewer errors. In general, a block code can correct all patterns of t or fewer errors and detect all patterns of u or fewer errors provided that $u \geq t$ and

$$d_{\min} \geq t + u + 1 \tag{10.2}$$

If $q = 2$, knowledge of the positions of the errors is sufficient for their correction; if $q > 2$, the decoder must determine both the positions and values of the errors. If the demodulator indicates positions in which the symbol values are unreliable, the decoder can assume their value unknown and has only to solve for the value of these symbols. These positions are called **erasures.** A block code can correct up to t errors and v erasures in each word if

$$d_{\min} \geq 2t + v + 1 \tag{10.3}$$

10.3 Structure and Decoding of Block Codes

Shannon showed that the performance limit of codes with fixed code rate improves as the block length increases. As n and k increase, however, practical implementation requires that the mapping from message to code vector not be arbitrary but that an underlying structure to the code exist. The structures developed to date limit the error correcting capability of these codes to below what Shannon proved possible, on average, for a code with random codeword assignments. Although Turbo codes have made significant strides towards approaching the Shannon Limit, the search for good constructive codes continues.

A property which simplifies implementation of the coding operations is that of code linearity. A code is **linear** if the addition of any two code vectors forms another code vector, which implies that the code vectors form a subspace of the vector space of n-tuples. This subspace, which contains the all-zero vector, is spanned by any set of k linearly independent

code vectors. Encoding can be described as the multiplication of the information k-tuple by a **generator matrix** $\boldsymbol{G}$, of dimension $k \times n$, which contains these basis vectors as rows. That is, a message vector $\boldsymbol{m}_i$ is mapped to a code vector $\boldsymbol{c}_i$ according to

$$\boldsymbol{c}_i = \boldsymbol{m}_i \boldsymbol{G}, \qquad i = 0, 1, \ldots, q^k - 1 \tag{10.4}$$

where elementwise arithmetic is defined in the **finite field** GF(q). In general, this encoding procedure results in code vectors with nonsystematic form in that the values of the message symbols cannot be determined by inspection of the code vector. However, if $\boldsymbol{G}$ has the form $[\boldsymbol{I}_k, \boldsymbol{P}]$ where $\boldsymbol{I}_k$ is the $k \times k$ identity matrix and $\boldsymbol{P}$ is a $k \times (n-k)$ matrix of parity checks, then the k most significant symbols of each code vector are identical to the message vector and the code has **systematic** form. This notation assumes that vectors are written with their most significant or first symbols in time on the left, a convention used throughout this chapter.

For each generator matrix there is an $(n-k) \times k$ **parity check matrix** $\boldsymbol{H}$ whose rows are orthogonal to the rows in $\boldsymbol{G}$, i.e., $\boldsymbol{G}\boldsymbol{H}^T = \boldsymbol{0}$. If the code is systematic, $\boldsymbol{H} = [-\boldsymbol{P}^T, \boldsymbol{I}_{n-k}]$. Since all codewords are linear sums of the rows in $\boldsymbol{G}$, it follows that $\boldsymbol{c}_i \boldsymbol{H}^T = \boldsymbol{0}$ for all $i, i = 0, 1, \ldots, q^k - 1$, and that the validity of the demodulated vectors can be checked by performing this multiplication. If a codeword $\boldsymbol{c}$ is corrupted during transmission so that the hard-decision demodulator outputs the vector $\hat{\boldsymbol{c}} = \boldsymbol{c} + \boldsymbol{e}$, where $\boldsymbol{e}$ is a nonzero error pattern, the result of this multiplication is an $(n-k)$-tuple that is indicative of the validity of the sequence. This result, called the **syndrome** $\boldsymbol{s}$, is dependent only on the error pattern since

$$\boldsymbol{s} = \hat{\boldsymbol{c}}\boldsymbol{H}^T = (\boldsymbol{c} + \boldsymbol{e})\boldsymbol{H}^T = \boldsymbol{c}\boldsymbol{H}^T + \boldsymbol{e}\boldsymbol{H}^T = \boldsymbol{e}\boldsymbol{H}^T \tag{10.5}$$

If the error pattern is a code vector, the errors go undetected. For all other error patterns, however, the syndrome is nonzero. Since there are $q^{n-k} - 1$ nonzero syndromes, $q^{n-k} - 1$ error patterns can be corrected. When these patterns include all those with t or fewer errors and no others, the code is said to be a **perfect code.** Few codes are perfect; most codes are capable of correcting some patterns with more than t errors. **Standard array decoders** use lookup tables to associate each syndrome with an error pattern but become impractical as the block length and number of parity symbols increases. Algebraic decoding algorithms have been developed for codes with stronger structure. These algorithms are simplified with imperfect codes if the patterns corrected are limited to those with t or fewer errors, a simplification called **bounded distance decoding.**

Cyclic codes are a subclass of linear block codes with an algebraic structure that enables encoding to be implemented with a linear feedback shift register and decoding to be implemented without a lookup table. As a result, most block codes in use today are cyclic or are closely related to cyclic codes. These codes are best described if vectors are interpreted as polynomials and the arithmetic follows the rules for polynomials where the elementwise operations are defined in GF(q). In a cyclic code, all codeword polynomials are multiples of a **generator polynomial** $g(x)$ of degree $n-k$. This polynomial is chosen to be a divisor of $x^n - 1$ so that a cyclic shift of a code vector yields another code vector, giving this class of codes its name. A message polynomial $m_i(x)$ can be mapped to a codeword polynomial $c_i(x)$ in nonsystematic form as

$$c_i(x) = m_i(x)g(x), \qquad i = 0, 1, \ldots, q^k - 1 \tag{10.6}$$

In systematic form, codeword polynomials have the form

$$c_i(x) = m_i(x)x^{n-k} - r_i(x), \qquad i = 0, 1, \ldots, q^k - 1 \tag{10.7}$$

where $r_i(x)$ is the remainder of $m_i(x)x^{n-k}$ divided by $g(x)$. Polynomial multiplication and division can be easily implemented with shift registers [5].

The first step in decoding the demodulated word is to determine if the word is a multiple of $g(x)$. This is done by dividing it by $g(x)$ and examining the remainder. Since polynomial division is a linear operation, the resulting syndrome $s(x)$ depends only on the error pattern. If $s(x)$ is the all-zero polynomial, transmission is errorless or an undetectable error pattern has occurred. If $s(x)$ is nonzero, at least one error has occurred. This is the principle of the **cyclic redundancy check** (CRC). It remains to determine the most likely error pattern that could have generated this syndrome.

Single error correcting binary codes can use the syndrome to immediately locate the bit in error. More powerful codes use this information to determine the locations and values of multiple errors. The most prominent approach of doing so is with the iterative technique developed by Berlekamp. This technique, which involves computing an error-locator polynomial and solving for its roots, was subsequently interpreted by Massey in terms of the design of a minimum-length shift register. Once the location and values of the errors are known, Chien's search algorithm efficiently corrects them. The implementation complexity of these decoders increases only as the square of the number of errors to be corrected [4] but does not generalize easily to accommodate soft-decision information. Other decoding techniques, including Chase's algorithm and threshold decoding, are easier to implement with soft-decision input [6]. Berlekamp's algorithm can be used in conjunction with transform-domain decoding, which involves transforming the received block with a finite field Fourier-like transform and solving for errors in the transform domain. Since the implementation complexity of these decoders depends on the block length rather than the number of symbols corrected, this approach results in simpler circuitry for codes with high redundancy [13].

Other block codes have also been constructed, including codes that are based on transform-domain spectral properties, codes that are designed specifically for correction of burst errors, and codes that are decodable with straightforward threshold or majority logic decoders [5, 6, 7].

10.4 Important Classes of Block Codes

When errors occur independently, Bose–Chaudhuri–Hocquenghem (BCH) codes provide one of the best performances of known codes for a given block length and code rate. They are cyclic codes with $n = q^m - 1$, where m is any integer greater than 2. They are designed to correct up to t errors per word and so have **designed distance** $d = 2t + 1$; the minimum distance may be greater. Generator polynomials for these codes are listed in many texts, including [6]. These polynomials are of degree less than or equal to mt, and so $k \geq n - mt$. BCH codes can be shortened to accommodate system requirements by deleting positions for information symbols.

Some subclasses of these codes are of special interest. Hamming codes are perfect single error correcting binary BCH codes. Full length codes have $n = 2^m - 1$ and $k = n - m$ for any m greater than 2. The duals of these codes are maximal-length codes, with $n = 2^m - 1$, $k = m$, and $d_{\min} = 2^{m-1}$. All $2^m - 1$ nonzero code vectors in these codes are cyclic shifts of a single nonzero code vector. Reed–Solomon (RS) codes are nonbinary BCH codes defined over GF(q), where q is often taken as a power of two so that symbols can be represented by a sequence of bits. In these cases, correction of even a single symbol allows for correction of a burst of bit errors. The block length is $n = q - 1$, and the minimum distance $d_{\min} = 2t + 1$ is achieved using only $2t$ parity symbols. Since RS codes meet the Singleton bound of

$d_{\min} \leq n-k+1$, they have the largest possible minimum distance for these values of n and k and are called **maximum distance separable** codes.

The Golay codes are the only nontrivial perfect codes that can correct more than one error. The (11, 6) ternary Golay code has minimum distance 5. The (23, 12) binary code is a triple error correcting BCH code with $d_{\min} = 7$. To simplify implementation, it is often extended to a (24, 12) code through the addition of an extra parity bit. The extended code has $d_{\min} = 8$.

The (23, 12) Golay code is also a binary quadratic residue code. These cyclic codes have prime length of the form $n = 8m \pm 1$, with $k = (n+1)/2$ and $d_{\min} \geq \sqrt{n}$. Some of these codes are as good as the best codes known with these values of n and k, but it is unknown if there are good quadratic residue codes with large n [5].

Reed-Muller codes are equivalent to binary cyclic codes with an additional overall parity bit. For any m, the rth-order Reed-Muller code has $n = 2^m$, $k = \Sigma_{i=0}^{r} \binom{m}{i}$, and $d_{\min} = 2^{m-r}$. The rth-order and $(m-r-1)$th-order codes are duals, and the first-order codes are similar to maximal-length codes. These codes, and the closely related Euclidean geometry and projective geometry codes, can be decoded with threshold decoding.

The performance of several of these block codes is shown in Fig. 10.3 in terms of decoded bit error probability vs. E_b/N_0 for systems using coherent, hard-decision demodulated BPSK signalling. Many other block codes have also been developed, including Goppa codes, quasicyclic codes, burst error correcting Fire codes, and other lesser known codes.

10.5 Principles of Convolutional Coding

Convolutional codes map successive information k-tuples to a series of n-tuples such that the sequence of n-tuples has distance properties that allow for detection and correction of errors. Although these codes can be defined over any alphabet, their implementation has largely been restricted to binary signals, and only binary convolutional codes are considered here.

In addition to the code rate $R = k/n$, the **constraint length** K is an important parameter for these codes. Definitions vary; we will use the definition that K equals the number of k-tuples that affect formation of each n-tuple during encoding. That is, the value of an n-tuple depends on the k-tuple that arrives at the encoder during that encoding interval as well as the $K-1$ previous information k-tuples.

Binary convolutional encoders can be implemented with kK-stage shift registers and n modulo-2 adders, an example of which is given in Fig. 10.4(a) for a rate 1/2, constraint length 3 code. The encoder shifts in a new k-tuple during each encoding interval and samples the outputs of the adders sequentially to form the coded output.

Although connection diagrams similar to that of Fig. 10.4(a) completely describe the code, a more concise description can be given by stating the values of n, k, and K and giving the adder connections in the form of vectors or polynomials. For instance, the rate 1/2 code has the generator vectors $\boldsymbol{g}_1 = 111$ and $\boldsymbol{g}_2 = 101$, or equivalently, the generator polynomials $g_1(x) = x^2 + x + 1$ and $g_2(x) = x^2 + 1$. Alternatively, a convolutional code can be characterized by its impulse response, the coded sequence generated due to input of a single logic-1. It is straightforward to verify that the circuit in Fig. 10.4(a) has the impulse response 111011. Since modulo-2 addition is a linear operation, convolutional codes are linear, and the coded output can be viewed as the convolution of the input sequence with the impulse response, hence the name of this coding technique. Shifted versions of the impulse response or generator vectors can be combined to form an infinite-order generator matrix which also describes the code.

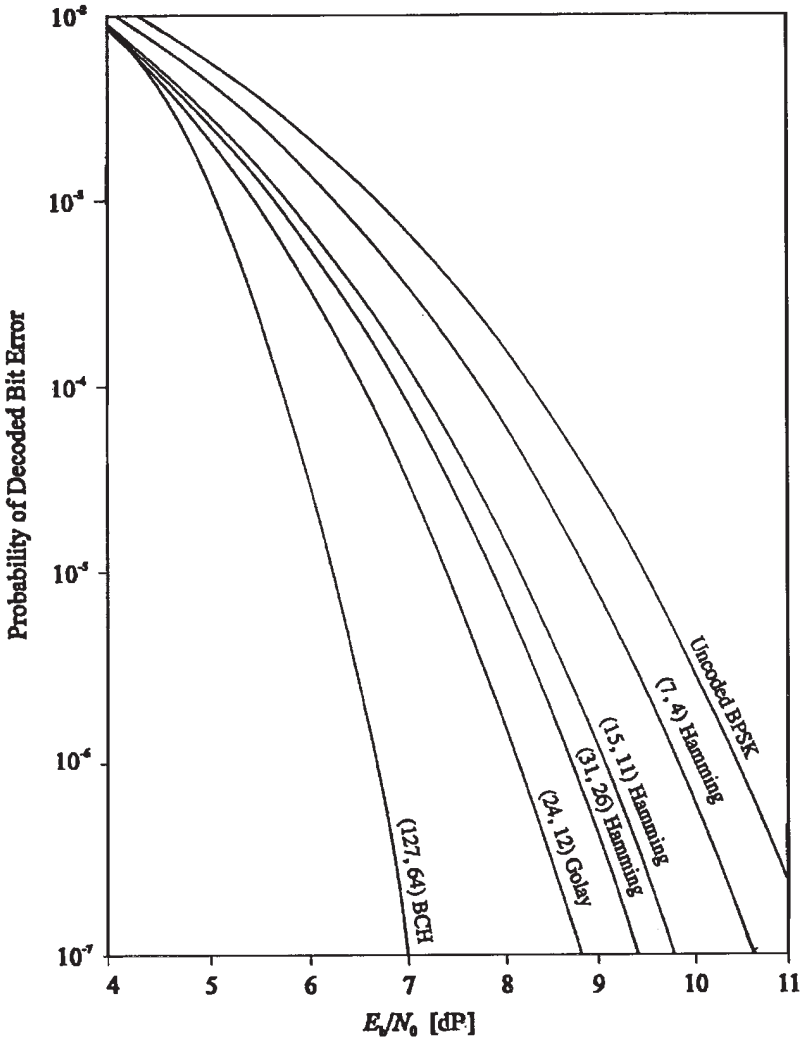
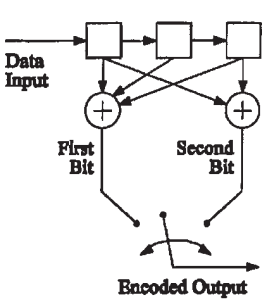


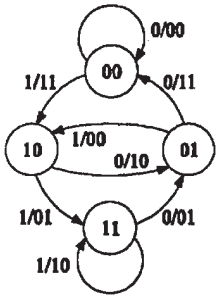
FIGURE 10.3 Block code performance. *Source:* Sklar, B., 1988, *Digital Communications: Fundamentals and Applications,* © 1988, p. 300. Reprinted by permission of Prentice-Hall, Inc., Englewood Cliffs, NJ.

Shift register circuits can be modeled as finite state machines. A Mealy machine description of a convolutional encoder requires $2^{k(K-1)}$ states, each describing a different value of the $K-1$ k-tuples which have most recently entered the shift register. Each state has 2^k exit paths which correspond to the value of the incoming k-tuple. A state machine description for the rate 1/2 encoder depicted in Fig. 10.4(a) is given in Fig. 10.4(b). States are labeled with the contents of the two leftmost register stages; edges are labeled with information bit values and their corresponding coded output.

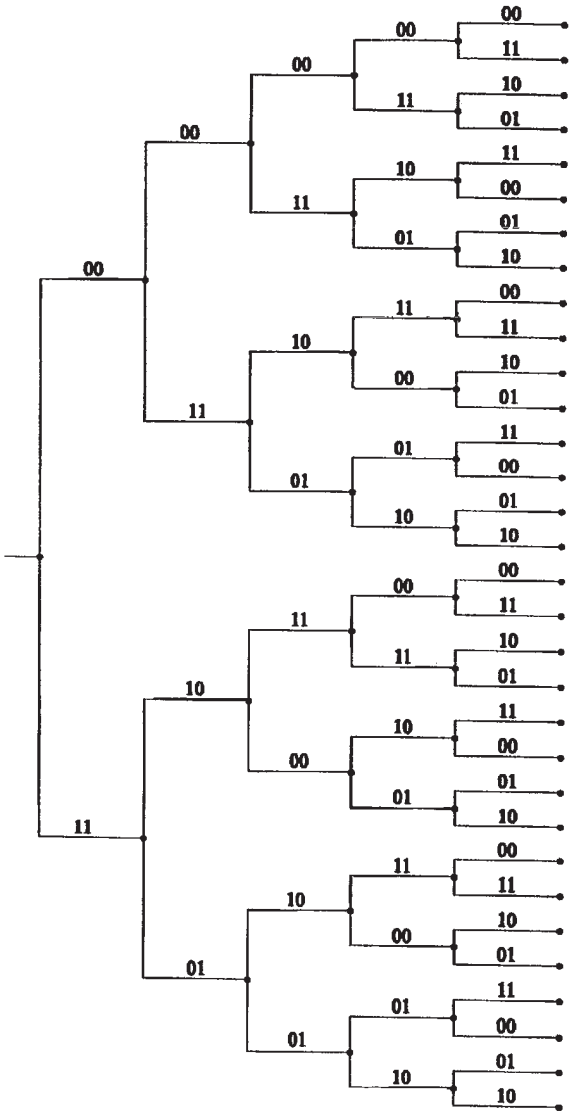
The dimension of time is added to the description of the encoder with tree and trellis diagrams. The tree diagram for the rate 1/2 convolutional code is given in Fig. 10.4(c), assuming the shift register is initially clear. Each node represents an encoding interval, from which the upper branch is taken if the input bit is a 0 and the lower branch is taken if the input bit is a 1. Each branch is labeled with the corresponding output bit sequence. A drawback of the tree representation is that it grows without bound as the length of the



(a) Connection diagram



(b) State machine model



(c) Tree diagram

FIGURE 10.4 A rate 1/2, constraint length 3 convolutional code.

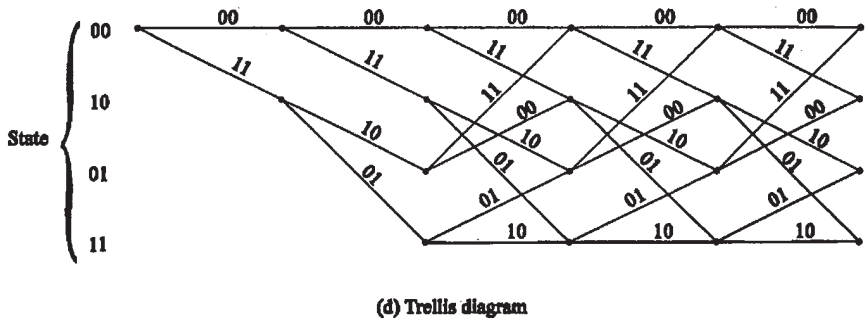


FIGURE 10.4 (*Continued*).

input sequence increases. This is overcome with the trellis diagram depicted in Fig. 10.4(d), Again, encoding results in left-to-right movement, where the upper of the two branches is taken whenever the input is a 0, the lower branch is taken when the input is a 1, and the output is the bit sequence which weights the branch taken. Each level of nodes corresponds to a state of the encoder as shown on the left-hand side of the diagram.

If the received sequence contains errors, it may no longer depict a valid path through the tree or trellis. It is the job of the decoder to determine the original path. In doing so, the decoder does not so much correct errors as find the closest valid path to the received sequence. As a result, the error correcting capability of a convolutional code is more difficult to quantify than that of a block code; it depends on how valid paths differ. One measure of this difference is the **column distance** $d_c(i)$, the minimum Hamming distance between all coded sequences generated over i encoding intervals which differ in the first interval. The nondecreasing sequence of column distance values is the **distance profile** of the code. The column distance after K intervals is the minimum distance of the code and is important for evaluating the performance of a code that uses threshold decoding. As i increases, $d_c(i)$ approaches the **free distance** of the code, d_{free}, which is the minimum Hamming distance in the set of arbitrarily long paths that diverge and then remerge in the trellis.

With maximum likelihood decoding, convolutional codes can generally correct up to t errors within three to five constraint lengths, depending on how the errors are distributed, where

$$d_{\text{free}} \geq 2t + 1 \tag{10.8}$$

The free distance can be calculated by exhaustively searching for the minimum-weight path that returns to the all-zero state, or evaluating the term of lowest degree in the generating function of the code.

The objective of a convolutional code is to maximize these distance properties. They generally improve as the constraint length of the code increases, and nonsystematic codes generally have better properties than systematic ones. Good codes have been found by computer search and are tabulated in many texts, including [6]. Convolutional codes with high code rate can be constructed by **puncturing** or periodically deleting coded symbols from a low rate code. A list of low rate codes and perforation matrices that result in good high rate codes can be found in many sources, including [13]. The performance of good punctured codes approaches that of the best convolutional codes known with similar rate, and decoder implementation is significantly less complex.

Convolutional codes can be **catastrophic,** having the potential to generate an unlimited number of decoded bit errors in response to a finite number of errors in the demodulated bit sequence. Catastrophic error propagation is avoided if the code has generator polynomials with a greatest common divisor of the form x^a for any a or, equivalently, if there are no

closed-loop paths in the state diagram with all-zero output other than the one taken with all-zero input. **Systematic codes** are not catastrophic.

10.6 Decoding of Convolutional Codes

In 1967, Viterbi developed a maximum likelihood decoding algorithm that takes advantage of the trellis structure to reduce the complexity of the evaluation. This algorithm has become known as the **Viterbi algorithm.** With each received n-tuple, the decoder computes a **metric** or measure of likelihood for all paths that could have been taken during that interval and discards all but the most likely to terminate on each node. An arbitrary decision is made if path metrics are equal. The metrics can be formed using either hard or soft decision information with little difference in implementation complexity.

If the message has finite length and the encoder is subsequently flushed with zeros, a single decoded path remains. With a BSC, this path corresponds to the valid code sequence with minimum Hamming distance from the demodulated sequence. Full-length decoding becomes impractical as the length of the message sequence increases. The most likely paths tend to have a common stem, however, and selecting the trace value four or five times the constraint length prior to the present decoding depth results in near-optimum performance. Since the number of paths examined during each interval increases exponentially with the constraint length, the Viterbi algorithm also becomes impractical for codes with large constraint length. To date, Viterbi decoding has been implemented for codes with constraint lengths up to ten. Other decoding techniques, such as sequential and threshold decoding, can be used with larger constraint lengths.

Sequential decoding was proposed by Wozencraft, and the most widely used algorithm was developed by Fano. Rather than tracking multiple paths through the trellis, the sequential decoder operates on a single path while searching the code tree for a path with high probability. It makes tentative decisions regarding the transmitted sequence, computes a metric between its proposed path and the demodulated sequence, and moves forward through the tree as long as the metric indicates that the path is likely. If the likelihood of the path becomes low, the decoder moves backward, searching other paths until it finds one with high probability. The number of computations involved in this procedure is almost independent of the constraint length and is typically quite small, but it can be highly variable, depending on the channel. Buffers must be provided to store incoming sequences as the decoder searches the tree. Their overflow is a significant limiting factor in the performance of these decoders.

Figure 10.5 compares the performance of the Viterbi and sequential decoding algorithms for several convolutional codes operating on coherently demodulated BPSK signals corrupted by AWGN. Other decoding algorithms have also been developed, including syndrome decoding methods such as table look-up feedback decoding and threshold decoding [6]. These algorithms are easily implemented but offer suboptimal performance. Techniques such as the one discussed by [1] have been developed to support both soft input and soft output, but these decoding techniques typically increase decoder complexity.

10.7 Trellis-Coded Modulation

Trellis-coded modulation (TCM) has received considerable attention since its development by Ungerboeck in the late 1970s [11]. Unlike block and convolutional codes, TCM schemes achieve coding gain by increasing the size of the signal alphabet and using multilevel/phase signalling. Like convolutional codes, sequences of coded symbols are restricted to certain

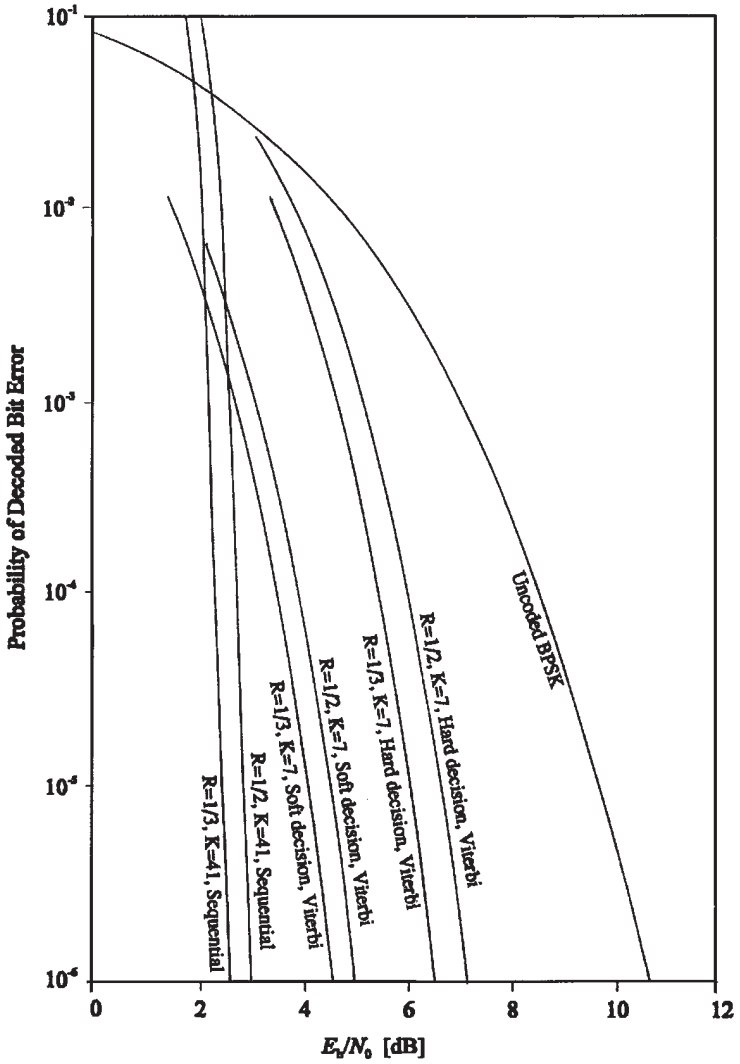


FIGURE 10.5 Convolutional code performance. *Source:* Omura, J.K. and Levitt, B.K., © 1982 IEEE, "Coded Error Probability Evaluation for Antijam Communication Systems," *IEEE Trans. Commun.*, vol. COM-30, no. 5, pp. 896–903. Reprinted by permission of IEEE.

valid patterns. In TCM, these patterns are chosen to have large Euclidean distance from one another so that a large number of corrupted sequences can be corrected. The Viterbi algorithm is often used to decode these sequences. Since the symbol transmission rate does not increase, coded and uncoded signals require the same transmission bandwidth. If transmission power is held constant, the signal constellation of the coded signal is denser. The loss in symbol separation, however, is more than overcome by the error correction capability of the code.

Ungerboeck investigated the increase in channel capacity that can be obtained by increasing the size of the signal set and restricting the pattern of transmitted symbols, and concluded that almost all of the additional capacity can be gained by doubling the number of points in the signal constellation. This is accomplished by encoding the binary data

with a rate $R = k/(k+1)$ code and mapping sequences of $k+1$ coded bits to points in a constellation of 2^{k+1} symbols. For example, the rate 2/3 encoder of Fig. 10.6(a) encodes pairs of source bits to three coded bits. Figure 10.6(b) depicts one stage in the trellis of the coded output where, as with the convolutional code, the state of the encoder is defined by the values of the two most recent bits to enter the shift register. Note that unlike the trellis for the convolutional code, this trellis contains parallel paths between nodes.

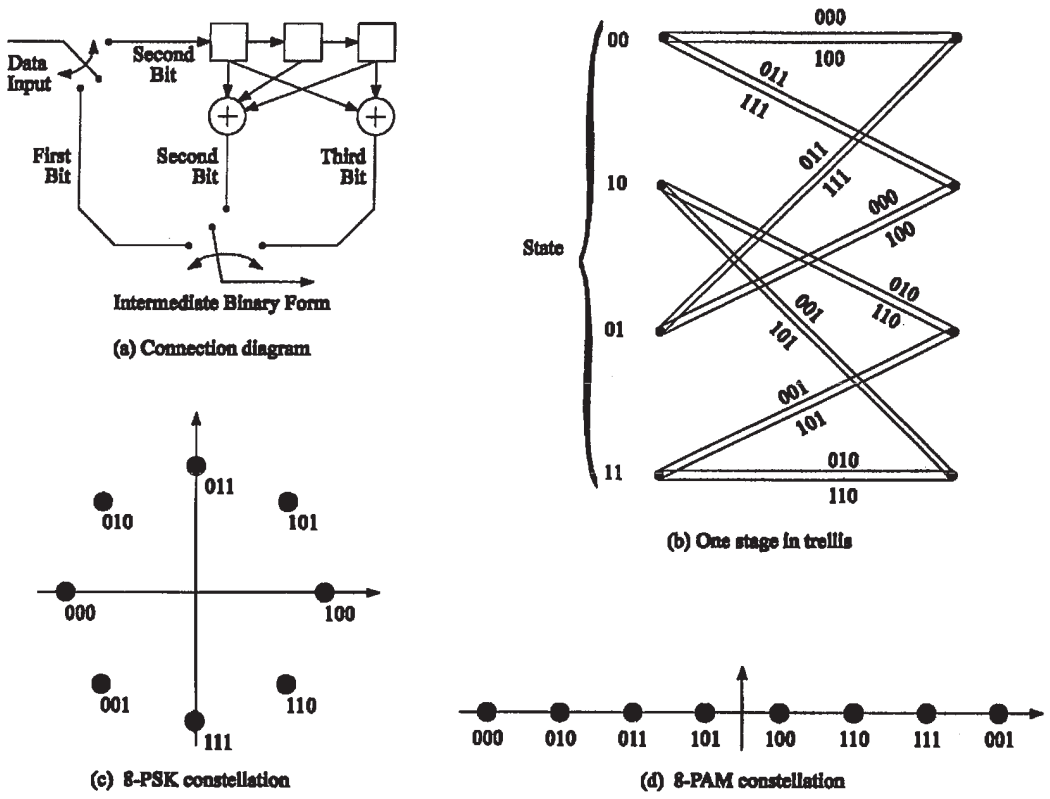


FIGURE 10.6 Rate 2/3 trellis-coded modulation.

The key to improving performance with TCM is to map the coded bits to points in the signal space such that the Euclidean distance between transmitted sequences is maximized. A method that ensures improved Euclidean distance is the method of **set partitioning.** This involves separating all parallel paths on the trellis with maximum distance and assigning the next greatest distance to paths that diverge from or merge onto the same node. Figures 10.6(c) and 10.6(d) give examples of mappings for the rate 2/3 code with 8-PSK and 8-PAM signal constellations, respectively.

As with convolutional codes, the free distance of a TCM code is defined as the minimum distance between paths through the trellis, where the distance of concern is now Euclidean distance rather than Hamming distance. The free distance of an uncoded signal is defined as the distance between the closest signal points. When coded and uncoded signals have the same average power, the coding gain of the TCM system is defined as

$$\text{coding gain} = 20\log_{10}\left(\frac{d_{\text{free, coded}}}{d_{\text{free, uncoded}}}\right) \tag{10.9}$$

It can be shown that the simple, rate 2/3 8 phase-shift keying (PSK) and 8 pulse-amplitude modulation (PAM) TCM systems provide gains of 3 dB and 3.3 dB, respectively, [6]. More complex TCM systems yield gains up to 6 dB. Tables of good codes are given in [11].

10.8 Additional Measures

When the demodulated sequence contains bursts of errors, the performance of codes designed to correct independent errors improves if coded sequences are **interleaved** prior to transmission and deinterleaved prior to decoding. Deinterleaving separates the burst errors, making them appear more random and increasing the likelihood of accurate decoding. It is generally sufficient to interleave several block lengths of a block coded signal or several constraint lengths of a convolutionally encoded signal. Block interleaving is the most straightforward approach, but delay and memory requirements are halved with convolutional and helical interleaving techniques. Periodicity in the way sequences are combined is avoided with pseudorandom interleaving.

Serially **concatenated codes,** first investigated by Forney, use two levels of coding to achieve a level of performance with less complexity than a single coding stage would require. The inner code interfaces with the modulator and demodulator and corrects the majority of the errors; the outer code corrects errors that appear at the output of the inner-code decoder. A convolutional code with Viterbi decoding is usually chosen as the inner code, and an RS code is often chosen as the outer code due to its ability to correct the bursts of bit errors which can result with incorrect decoding of trellis-coded sequences. Interleaving and deinterleaving outer-code symbols between coding stages offers further protection against the burst error output of the inner code.

Product codes effectively place the data in a two dimensional array and use FEC techniques over both the rows and columns of this array. Not only do these codes result in error protection in two dimensions, but the manner in which the array is constructed can offer advantages similar to those achieved through interleaving.

10.9 Turbo Codes

The most recent significant achievement in FEC coding is the development of **Turbo codes** [3]. The principle of this coding technique is to encode the data with two or more **constituent codes** concatenated in parallel form. The received sequence is decoded in an iterative, serial approach using soft-input, soft-output decoders. This iterative decoding approach involves feedback of information in a manner similar to processes within the turbo engine, giving this coding technique its name.

Turbo codes effectively result in the construction of relatively long codewords with few codewords being close in terms of Hamming distance, while at the same time constraining the implementation complexity of the decoder to practical limits. The first Turbo codes developed used recursive systematic convolutional codes as the constituent codes, and punctured them to improve the code rate. The use of other constituent codes has since been considered. Two or more of these codes are concatenated in parallel,where code concatenation is combined with interleaving in order to increase the independence of the data sequences encoded by the constituent encoders. This apparent increase in randomness, implemented with simple interleavers, is an important contributing factor to the excellent performance of the decoders.

As in other multi-stage coding techniques, the complexity of the decoder is limited through use of separate decoding stages for each constituent code. The input to the first

stage is the soft output of the demodulator for a finite-length received symbol sequence. Subsequent stages use both the demodulator output and an output of the previous decoding stage which is indicative of the reliability of the symbols. This information, gleaned from soft-output decoders, is called **extrinsic information**.

Decoding proceeds by iterating through constituent decoders, each forwarding updated extrinsic information to the next decoder, until a predefined number of iterations has been completed or the extrinsic information indicates that high reliability has been achieved. This approach results in very good performance at low values of E_b/N_0. Simulations have demonstrated error rates of 10^{-5} at signal-to-noise ratios appreciably less than 1 dB. At higher values of E_b/N_0, however, the performance curves can exhibit flattening if constituent codes are chosen in a manner that results in an overall small Hamming distance for the code.

Although this coding technique has shown great promise, there remains considerable work with regard to optimizing code parameters. Great strides have been made over the last few years in understanding the structure of these codes and relating them to serially concatenated and product codes, but many researchers are still examining these codes in order to advance their development. With this research will come optimization of the Turbo code process and application of these codes in various communication systems.

10.10 Applications

FEC coding remained of theoretical interest until advances in digital technology and improvements in decoding algorithms made their implementation possible. It has since become an attractive alternative to improving other system components or boosting transmission power. FEC codes are commonly used in digital storage systems, deep-space and satellite communication systems, terrestrial radio and band limited wireline systems, and have also been proposed for fiber optic transmission. Accordingly, the theory and practice of error correcting codes now occupies a prominent position in the field of communications engineering.

Deep-space systems began using forward error correction in the early 1970s to reduce transmission power requirements, and used multiple error correcting RS codes for the first time in 1977 to protect against corruption of compressed image data in the Voyager missions [12]. The Consultative Committee for Space Data Systems (CCSDS) has since recommended use of a concatenated coding system which uses a rate 1/2, constraint length 7 convolutional inner code and a (255, 223) RS outer code.

Coding is now commonly used in satellite systems to reduce power requirements and overall hardware costs and to allow closer orbital spacing of geosynchronous satellites [2]. FEC codes play integral roles in the VSAT, MSAT, INTELSAT, and INMARSAT systems [13]. Further, a (31, 15) RS code is used in the joint tactical information distribution system (JTIDS), a (7, 2) RS code is used in the air force satellite communication system (AFSATCOM), and a (204, 192) RS code has been designed specifically for satellite time division multiple access (TDMA) systems. Another code designed for military applications involves concatenation of a Golay and RS code with interleaving to ensure an imbalance of 1's and 0's in the transmitted symbol sequence and enhance signal recovery under severe noise and interference [2].

TCM has become commonplace in transmission of data over voiceband telephone channels. Modems developed since 1984 use trellis coded QAM modulation to provide robust communication at rates above 9.6 kb/s. Various coding techniques are used in the new digital cellular and personal communication standards, with an emphasis on convolutional and cyclic redundancy check codes [8].

FEC codes have also been widely used in digital recording systems, most prominently in the compact disc digital audio system. This system uses two levels of coding and interleaving in the cross-interleaved RS coding (CIRC) system to correct errors that result from disc imperfections and dirt and scratches which accumulate during use. Steps are also taken to mute uncorrectable sequences [12].

Defining Terms

Binary symmetric channel: A memoryless discrete data channel with binary signalling, hard-decision demodulation, and channel impairments that do not depend on the value of the symbol transmitted.

Bounded distance decoding: Limiting the error patterns which are corrected in an imperfect code to those with t or fewer errors.

Catastrophic code: A convolutional code in which a finite number of code symbol errors can cause an unlimited number of decoded bit errors.

Code rate: The ratio of source word length to codeword length, indicative of the amount of information transmitted per encoded symbol.

Coding gain: The reduction in signal-to-noise ratio required for specified error performance in a block or convolutional coded system over an uncoded system with the same information rate, channel impairments, and modulation and demodulation techniques. In TCM, the ratio of the squared free distance in the coded system to that of the uncoded system.

Column distance: The minimum Hamming distance between convolutionally encoded sequences of a specified length with different leading n-tuples.

Constituent codes: Two or more FEC codes that are combined in concatenated coding techniques.

Cyclic code: A block code in which cyclic shifts of code vectors are also code vectors.

Cyclic redundancy check: When the syndrome of a cyclic block code is used to detect errors.

Designed distance: The guaranteed minimum distance of a BCH code designed to correct up to t errors.

Discrete data channel: The concatenation of all system elements between FEC encoder output and decoder input.

Distance profile: The minimum Hamming distance after each encoding interval of convolutionally encoded sequences which differ in the first interval.

Erasure: A position in the demodulated sequence where the symbol value is unknown.

Extrinsic information: The output of a constituent soft decision decoder that is forwarded as input to the next decoding stage in iterative decoding of Turbo codes.

Finite field: A finite set of elements and operations of addition and multiplication that satisfy specific properties. Often called Galois fields and denoted GF(q), where q is the number of elements in the field. Finite fields exist for all q which are prime or the power of a prime.

Free distance: The minimum Hamming weight of convolutionally encoded sequences that diverge and remerge in the trellis. Equals the maximum column distance and the limiting value of the distance profile.

Generator matrix: A matrix used to describe a linear code. Code vectors equal the information vectors multiplied by this matrix.

Generator polynomial: The polynomial that is a divisor of all codeword polynomials in a cyclic block code; a polynomial that describes circuit connections in a convolutional encoder.

Hamming distance: The number of symbols in which codewords differ.

Hard decision: Demodulation that outputs only a value for each received symbol.

Interleaving: Shuffling the coded bit sequence prior to modulation and reversing this operation following demodulation. Used to separate and redistribute burst errors over several codewords (block codes) or constraint lengths (trellis codes) for higher probability of correct decoding by codes designed to correct random errors.

Linear code: A code whose code vectors form a vector space. Equivalently, a code where the addition of any two code vectors forms another code vector.

Maximum distance separable: A code with the largest possible minimum distance given the block length and code rate. These codes meet the Singleton bound of $d_{\min} \leq n - k + 1$.

Metric: A measure of goodness against which items are judged. In the Viterbi algorithm, an indication of the probability of a path being taken given the demodulated symbol sequence.

Minimum distance: In a block code, the smallest Hamming distance between any two codewords. In a convolutional code, the column distance after K intervals.

Parity check matrix: A matrix whose rows are orthogonal to the rows in the generator matrix of a linear code. Errors can be detected by multiplying the received vector by this matrix.

Perfect code: A t error correcting (n, k) block code in which $q^{n-k} - 1 = \Sigma_{i=1}^{t} \binom{n}{i}$.

Puncturing: Periodic deletion of code symbols from the sequence generated by a convolutional encoder for purposes of constructing a higher rate code. Also, deletion of parity bits in a block code.

Set partitioning: Rules for mapping coded sequences to points in the signal constellation that always result in a larger Euclidean distance for a TCM system than an uncoded system, given appropriate construction of the trellis.

Shannon Limit: The ratio of energy per data bit E_b to one-sided noise power spectral density N_0 in an AWGN channel above which errorless transmission is possible when bandwidth limitations are not placed on the signal and transmission is at channel capacity. This limit has the value $\ln 2 = 0.693 = -1.6$ dB.

Soft decision: Demodulation that outputs an estimate of the received symbol value along with an indication of the reliability of this value. Usually implemented by quantizing the received signal to more levels than there are symbol values.

Standard array decoding: Association of an error pattern with each syndrome by way of a lookup table.

Syndrome: An indication of whether or not errors are present in the demodulated symbol sequence.

Systematic code: A code in which the values of the message symbols can be identified by inspection of the code vector.

Vector space: An algebraic structure comprised of a set of elements in which operations of vector addition and scalar multiplication are defined. For our purposes, a

set of n-tuples consisting of symbols from GF(q) with addition and multiplication defined in terms of elementwise operations from this finite field.

Viterbi algorithm: A maximum-likelihood decoding algorithm for trellis codes that discards low-probability paths at each stage of the trellis, thereby reducing the total number of paths that must be considered.

References

[1] Bahl, L.R., Cocke, J., Jelinek, F., and Raviv, J., Optimal Decoding of Linear Codes for Minimizing Symbol Error Rate. *IEEE Transactions on Information Theory,* 20, 248–287, 1974.

[2] Berlekamp, E.R., Peile, R.E., and Pope, S.P., The application of error control to communications. *IEEE Commun. Mag.,* 25(4), 44–57, 1987.

[3] Berrou, C., Glavieux, A., and Thitimajshima, P., Near Shannon Limit Error-Correcting Coding and Decoding: Turbo Codes. *Proceedings of ICC'93,* Geneva, Switzerland, 1064–1070, 1993. Later expanded and published as: Berrou, C., Glavieux, A., 1996. Near Optimum Error Correcting Coding and Decoding. *IEEE Transactions on Communications,* 44(10), 1261–1271, 1996.

[4] Bhargava, V.K., Forward error correction schemes for digital communications. *IEEE Commun. Mag.,* 21(1), 11–19, 1983.

[5] Blahut, R.E., *Theory and Practice of Error Control Codes,* Addison-Wesley, Reading, MA, 1983.

[6] Clark, G.C. Jr. and Cain, J.B., *Error Correction Coding for Digital Communications,* Plenum Press, New York, 1981.

[7] Lin, S. and Costello, D.J. Jr., *Error Control Coding: Fundamentals and Applications,* Prentice-Hall, Englewood Cliffs, NJ, 1983.

[8] Rappaport, T.S., *Wireless Communications, Principles and Practice,* Prentice-Hall and IEEE Press, NJ, 1996.

[9] Shannon, C.E., A mathematical theory of communication. *Bell Syst. Tech. J.,* 27(3), 379–423 and 623–656, 1948.

[10] Sklar, B., *Digital Communications: Fundamentals and Applications,* Prentice-Hall, Englewood Cliffs, NJ, 1988.

[11] Ungerboeck, G., Trellis-coded modulation with redundant signal sets. *IEEE Commun. Mag.,* 25(2), 5–11 and 12–21, 1987.

[12] Wicker, S.B. and Bhargava, V.K., *Reed-Solomon Codes and Their Applications,* IEEE Press, NJ, 1994.

[13] Wu, W.W., Haccoun, D., Peile, R., and Hirata, Y., Coding for satellite communication. *IEEE J. Selected Areas in Commun.,* SAC-5(4), 724–748, 1987.

Further Information

There is now a large amount of literature on the subject of FEC coding. An introduction to the philosophy and limitations of these codes can be found in the second chapter of Lucky's book *Silicon Dreams: Information, Man, and Machine,* St. Martin's Press, New York, 1989. More practical introductions can be found in overview chapters of many communications texts. The number of texts devoted entirely to this subject also continues to grow. Although these texts summarize the algebra underlying block codes, more in-depth treatments can be found in mathematical texts. Survey papers appear occasionally in the literature, but the interested reader is directed to the seminal papers by Shannon, Ham-

ming, Reed and Solomon, Bose and Chaudhuri, Hocquenghem, Wozencraft, Fano, Forney, Berlekamp, Massey, Viterbi, Ungerboeck, Berrou and Glavieux, among others. The most recent advances in the theory and implementation of error control codes are published in *IEEE Transactions on Information Theory, IEEE Transactions on Communications,* and special issues of *IEEE Journal on Selected Areas in Communications.*

11

Spread Spectrum Communications

Laurence B. Milstein
University of California

Marvin K. Simon
Jet Propulsion Laboratory

11.1 A Brief History 11-1
11.2 Why Spread Spectrum? 11-1
11.3 Basic Concepts and Terminology 11-2
11.4 Spread Spectrum Techniques 11-2
Direct Sequence Modulation • Frequency Hopping Modulation • Time Hopping Modulation • Hybrid Modulations
11.5 Applications of Spread Spectrum 11-8
Military • Commercial
Defining Terms 11-13
References 11-14

11.1 A Brief History

Spread spectrum (SS) has its origin in the military arena where the friendly communicator is 1) susceptible to detection/interception by the enemy and 2) vulnerable to intentionally introduced unfriendly interference (jamming). Communication systems that employ spread spectrum to reduce the communicator's detectability and combat the enemy-introduced interference are respectively referred to as **low probability of intercept (LPI)** and **antijam** (AJ) **communication systems**. With the change in the current world political situation wherein the U.S. Department of Defense (DOD) has reduced its emphasis on the development and acquisition of new communication systems for the original purposes, a host of new commercial applications for SS has evolved, particularly in the area of cellular mobile communications. This shift from military to commercial applications of SS has demonstrated that the basic concepts that make SS techniques so useful in the military can also be put to practical peacetime use. In the next section, we give a simple description of these basic concepts using the original military application as the basis of explanation. The extension of these concepts to the mentioned commercial applications will be treated later on in the chapter.

11.2 Why Spread Spectrum?

Spread spectrum is a communication technique wherein the transmitted modulation is *spread* (increased) in bandwidth prior to transmission over the channel and then *despread* (decreased) in bandwidth by the same amount at the receiver. If it were not for the fact that the communication channel introduces some form of narrowband (relative to the spread bandwidth) interference, the receiver performance would be transparent to the spreading

0-8493-8597-0/99/$0.00+$.50
© 1999 by CRC Press LLC

and despreading operations (assuming that they are identical inverses of each other). That is, after **despreading** the received signal would be identical to the transmitted signal prior to **spreading**. In the presence of narrowband interference, however, there is a significant advantage to employing the spreading/despreading procedure described. The reason for this is as follows. Since the interference is introduced after the transmitted signal is spread, then, whereas the despreading operation at the receiver shrinks the desired signal back to its original bandwidth, at the same time it spreads the undesired signal (interference) in bandwidth by the same amount, thus reducing its power spectral density. This, in turn, serves to diminish the effect of the interference on the receiver performance, which depends on the amount of interference power in the despread bandwidth. It is indeed this very simple explanation, which is at the heart of all spread spectrum techniques.

11.3 Basic Concepts and Terminology

To describe this process analytically and at the same time introduce some terminology that is common in spread spectrum parlance, we proceed as follows. Consider a communicator that desires to send a message using a transmitted power S Watts (W) at an information rate R_b bits/s (bps). By introducing a SS modulation, the bandwidth of the transmitted signal is increased from R_b Hz to W_{SS} Hz where $W_{\text{SS}} \gg R_b$ denotes the **spread spectrum bandwidth**. Assume that the channel introduces, in addition to the usual thermal noise (assumed to have a single-sided power spectral density (PSD) equal to N_0 W/Hz), an additive interference (jamming) having power J distributed over some bandwidth W_J. After despreading, the desired signal bandwidth is once again now equal to R_b Hz and the interference PSD is now $N_J = J/W_{\text{SS}}$. Note that since the thermal noise is assumed to be white, i.e., it is uniformly distributed over all frequencies, its PSD is unchanged by the despreading operation and, thus, remains equal to N_0. Regardless of the signal and interferer waveforms, the equivalent bit energy-to-total noise spectral density ratio is, in terms of the given parameters,

$$\frac{E_b}{N_t} = \frac{E_b}{N_0 + N_J} = \frac{S/R_b}{N_0 + J/W_{\text{SS}}} \tag{11.1}$$

For most practical scenarios, the jammer limits performance and, thus, the effects of receiver noise in the channel can be ignored. Thus, assuming $N_J \gg N_0$, we can rewrite Eq. (11.1) as

$$\frac{E_b}{N_t} \cong \frac{E_b}{N_J} = \frac{S/R_b}{J/W_{\text{SS}}} = \frac{S}{J}\frac{W_{\text{SS}}}{R_b} \tag{11.2}$$

where the ratio J/S is the *jammer-to-signal power ratio* and the ratio W_{SS}/R_b is the **spreading ratio** and is defined as the **processing gain** of the system. Since the ultimate error probability performance of the communication receiver depends on the ratio E_b/N_J, we see that from the communicator's viewpoint his goal should be to minimize J/S (by choice of S) and maximize the processing gain (by choice of W_{SS} for a given desired information rate). The possible strategies for the jammer will be discussed in the section on military applications dealing with AJ communications.

11.4 Spread Spectrum Techniques

By far the two most popular spreading techniques are **direct sequence (DS) modulation** and **frequency hopping (FH) modulation**. In the following subsections, we present a brief description of each.

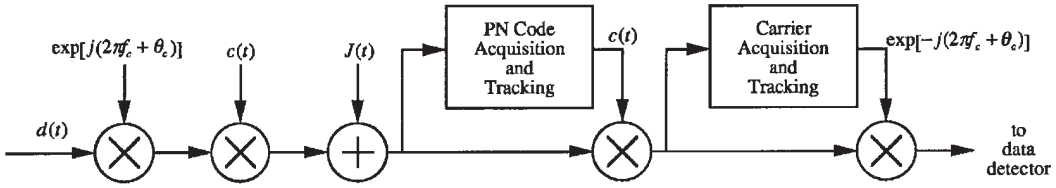


FIGURE 11.1 A DS-BPSK system (complex form).

11.4.1 Direct Sequence Modulation

A direct sequence modulation $c(t)$ is formed by linearly modulating the output sequence $\{c_n\}$ of a pseudorandom number generator onto a train of pulses, each having a duration T_c called the **chip time**. In mathematical form,

$$c(t) = \sum_{n=-\infty}^{\infty} c_n p(t - nT_c) \tag{11.3}$$

where $p(t)$ is the basic pulse shape and is assumed to be of rectangular form. This type of modulation is usually used with binary phase-shift-keyed (BPSK) information signals, which have the complex form $d(t)\exp\{j(2\pi f_c t + \theta_c)\}$, where $d(t)$ is a binary-valued data waveform of rate $1/T_b$ bits/s and f_c and θ_c are the frequency and phase of the data-modulated carrier, respectively. As such, a DS/BPSK signal is formed by multiplying the BPSK signal by $c(t)$ (see Fig. 11.1), resulting in the real transmitted signal

$$x(t) = \mathrm{Re}\{c(t)d(t)\exp[j(2\pi f_c t + \theta_c)]\} \tag{11.4}$$

Since T_c is chosen so that $T_b \gg T_c$, then relative to the bandwidth of the BPSK information signal, the bandwidth of the DS/BPSK signal[1] is effectively increased by the ratio $T_b/T_c = W_{SS}/2R_b$, which is one-half the spreading factor or processing gain of the system. At the receiver, the sum of the transmitted DS/BPSK signal and the channel interference $I(t)$ (as discussed before, we ignore the presence of the additive thermal noise) are ideally multiplied by the identical DS modulation (this operation is known as despreading), which returns the DS/BPSK signal to its original BPSK form whereas the real interference signal is now the real wideband signal $\mathrm{Re}\{I(t)c(t)\}$. In the previous sentence, we used the word ideally, which implies that the PN waveform used for despreading at the receiver is identical to that used for spreading at the transmitter. This simple implication covers up a multitude of tasks that a practical DS receiver must perform. In particular, the receiver must first acquire the PN waveform. That is, the local PN random generator that generates the PN waveform at the receiver used for despreading must be aligned (synchronized) to within one chip of the PN waveform of the received DS/BPSK signal. This is accomplished by employing some sort of **search algorithm** which typically steps the local PN waveform sequentially in time by a fraction of a chip (e.g., half a chip) and at each position searches for a high degree of correlation between the received and local PN reference waveforms. The search terminates when the correlation exceeds a given threshold, which is an indication that the alignment has been achieved. After bringing the two PN waveforms into **coarse alignment**, a **tracking algorithm** is employed to maintain **fine alignment**. The most

[1] For the usual case of a rectangular spreading pulse $p(t)$, the PSD of the DS/BPSK modulation will have $(\sin x/x)^2$ form with first zero crossing at $1/T_c$, which is nominally taken as one-half the spread spectrum bandwidth W_{SS}.

popular forms of tracking loops are the continuous time **delay-locked loop** and its time-multiplexed version the **tau–dither loop**. It is the difficulty in synchronizing the receiver PN generator to subnanosecond accuracy that limits PN chip rates to values on the order of hundreds of Mchips/s, which implies the same limitation on the DS spread spectrum bandwidth W_{SS}.

11.4.2 Frequency Hopping Modulation

A **frequency hopping (FH) modulation** $c(t)$ is formed by nonlinearly modulating a train of pulses with a sequence of pseudorandomly generated frequency shifts $\{f_n\}$. In mathematical terms, $c(t)$ has the complex form

$$c(t) = \sum_{n=-\infty}^{\infty} \exp\{j(2\pi f_n + \phi_n)\} p(t - nT_h) \tag{11.5}$$

where $p(t)$ is again the basic pulse shape having a duration T_h, called the **hop time** and $\{\phi_n\}$ is a sequence of random phases associated with the generation of the hops. FH modulation is traditionally used with multiple-frequency-shift-keyed (MFSK) information signals, which have the complex form $\exp\{j[2\pi(f_c + d(t))t]\}$, where $d(t)$ is an M-level digital waveform (M denotes the symbol alphabet size) representing the information frequency modulation at a rate $1/T_s$ symbols/s (sps). As such, an FH/MFSK signal is formed by complex multiplying the MFSK signal by $c(t)$ resulting in the real transmitted signal

$$x(t) = \mathrm{Re}\{c(t)\exp\{j[2\pi(f_c + d(t))t]\}\} \tag{11.6}$$

In reality, $c(t)$ is never generated in the transmitter. Rather, $x(t)$ is obtained by applying the sequence of pseudorandom frequency shifts $\{f_n\}$ directly to the frequency synthesizer that generates the carrier frequency f_c (see Fig. 11.2). In terms of the actual implementation,

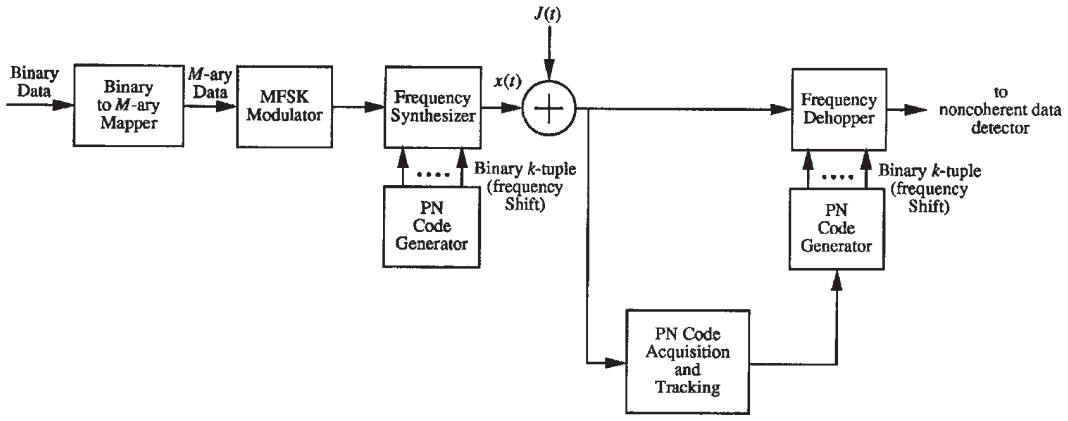


FIGURE 11.2 An FH-MFSK system.

successive (not necessarily disjoint) k-chip segments of a PN sequence drive a frequency synthesizer, which hops the carrier over 2^k frequencies. In view of the large bandwidths over which the frequency synthesizer must operate, it is difficult to maintain phase coherence from hop to hop, which explains the inclusion of the sequence $\{\phi_n\}$ in the Eq. (11.5) model for $c(t)$. On a short term basis, e.g., within a given hop, the signal bandwidth is identical

to that of the MFSK information modulation, which is typically much smaller than W_{SS}. On the other hand, when averaged over many hops, the signal bandwidth is equal to W_{SS}, which can be on the order of several GHz, i.e., an order of magnitude larger than that of implementable DS bandwidths. The exact relation between W_{SS}, T_h, T_s and the number of frequency shifts in the set $\{f_n\}$ will be discussed shortly.

At the receiver, the sum of the transmitted FH/MFSK signal and the channel interference $I(t)$ is ideally complex multiplied by the identical FH modulation (this operation is known as **dehopping**), which returns the FH/MFSK signal to its original MFSK form, whereas the real interference signal is now the wideband (in the average sense) signal $\mathrm{Re}\{I(t)c(t)\}$. Analogous to the DS case, the receiver must acquire and track the FH signal so that the dehopping waveform is as close to the hopping waveform $c(t)$ as possible.

FH systems are traditionally classified in accordance with the relationship between T_h and T_s. **Fast frequency-hopped (FFH)** systems are ones in which there exists one or more hops per data symbol, that is, $T_s = NT_h$ (N an integer) whereas **slow frequency-hopped (SFH)** systems are ones in which there exists more than one symbol per hop, that is, $T_h = NT_s$. It is customary in SS parlance to refer to the FH/MFSK tone of shortest duration as a "chip", despite the same usage for the PN chips associated with the code generator that drives the frequency synthesizer. Keeping this distinction in mind, in an FFH system where, as already stated, there are multiple hops per data symbol, a chip is equal to a hop. For SFH, where there are multiple data symbols per hop, a chip is equal to an MFSK symbol. Combining these two statements, the chip rate R_c in an FH system is given by the larger of $R_h = 1/T_h$ and $R_s = 1/T_s$ and, as such, is the highest system clock rate.

The frequency spacing between the FH/MFSK tones is governed by the chip rate R_c and is, thus, dependent on whether the FH modulation is FFH or SFH. In particular, for SFH where $R_c = R_s$, the spacing between FH/MFSK tones is equal to the spacing between the MFSK tones themselves. For noncoherent detection (the most commonly encountered in FH/MFSK systems), the separation of the MFSK symbols necessary to provide orthogonality[2] is an integer multiple of R_s. Assuming the minimum spacing, i.e., R_s, the entire spread spectrum band is then partitioned into a total of $N_t = W_{SS}/R_s = W_{SS}/R_c$ equally spaced FH tones. One arrangement, which is by far the most common, is to group these N_t tones into $N_b = N_t/M$ contiguous, nonoverlapping bands, each with bandwidth $MR_s = MR_c$; see Fig. 11.3a. Assuming symmetric MFSK modulation around the carrier frequency, then the center frequencies of the $N_b = 2^k$ bands represent the set of hop carriers, each of which is assigned to a given k-tuple of the PN code generator. In this fixed arrangement, each of the N_t FH/MFSK tones corresponds to the combination of a unique hop carrier (PN code k-tuple) and a unique MFSK symbol. Another arrangement, which provides more protection against the sophisticated interferer (jammer), is to overlap adjacent M-ary bands by an amount equal to R_c; see Fig. 11.3b. Assuming again that the center frequency of each band corresponds to a possible hop carrier, then since all but $M-1$ of the N_t tones are available as center frequencies, the number of hop carriers has been increased from N_t/M to $N_t-(M-1)$, which for $N_t \gg M$ is approximately an increase in randomness by a factor of M.

[2]An optimum noncoherent MFSK detector consists of a bank of energy detectors each matched to one of the M frequencies in the MFSK set. In terms of this structure, the notion of *orthogonality* implies that for a given transmitted frequency there will be no crosstalk (energy spillover) in any of the other $M-1$ energy detectors.

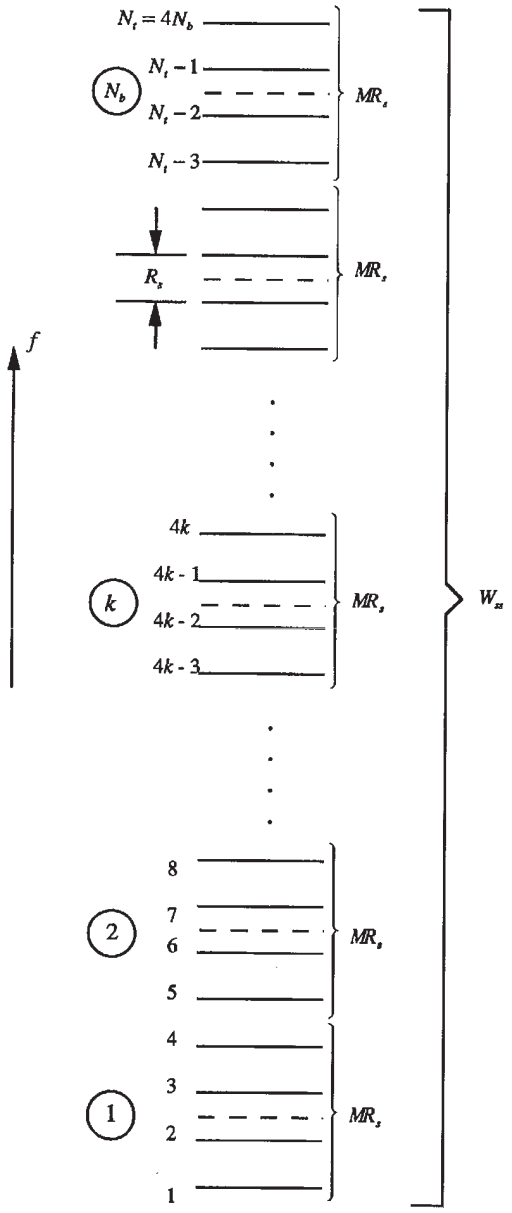


Figure 11.3a Frequency distribution for FH-4FSK—nonoverlapping bands. Dashed lines indicate location of hop frequencies.

For FFH, where $R_c = R_h$, the spacing between FH/MFSK tones is equal to the hop rate. Thus, the entire spread spectrum band is partitioned into a total of $N_t = W_{SS}/R_h = W_{SS}/R_c$ equally spaced FH tones, each of which is assigned to a unique k-tuple of the PN code generator that drives the frequency synthesizer. Since for FFH there are R_h/R_s hops per symbol, then the metric used to make a noncoherent decision on a particular symbol is obtained by summing up R_h/R_s detected chip (hop) energies, resulting in a so-called *noncoherent combining loss.*

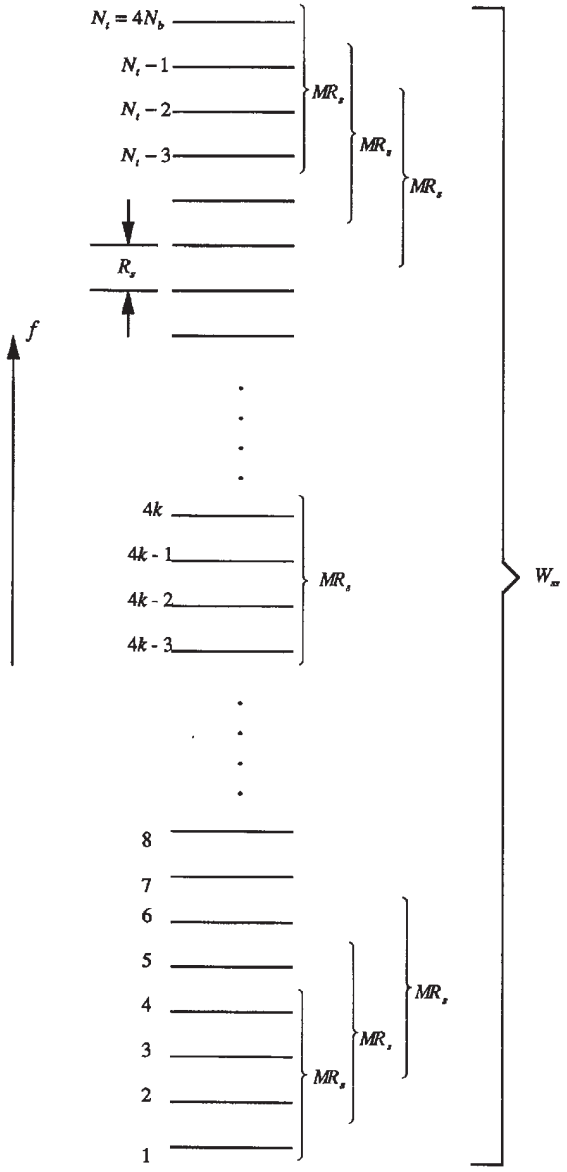


Figure 11.3b Frequency distribution for FH-4FSK—over-lapping bands.

11.4.3 Time Hopping Modulation

Time hopping (TH) is to spread spectrum modulation what pulse position modulation (PPM) is to information modulation. In particular, consider segmenting time into intervals of T_f seconds and further segment each T_f interval into M_T increments of width T_f/M_T. Assuming a pulse of maximum duration equal to T_f/M_T, then a **time hopping spread spectrum** modulation would take the form

$$c(t) = \sum_{n=-\infty}^{\infty} p\left[t - \left(n + \frac{a_n}{M_T}\right) T_f\right] \tag{11.7}$$

where a_n denotes the pseudorandom position (one of M_T uniformly spaced locations) of the pulse within the T_f-second interval.

For DS and FH, we saw that *multiplicative* modulation, that is the transmitted signal is the product of the SS and information signals, was the natural choice. For TH, *delay* modulation is the natural choice. In particular, a TH-SS modulation takes the form

$$x(t) = \mathrm{Re}\left\{c(t - d(t)) \exp\left[j\left(2\pi f_c + \phi_T\right)\right]\right\} \tag{11.8}$$

where $d(t)$ is a digital information modulation at a rate $1/T_s$ sps. Finally, the dehopping procedure at the receiver consists of removing the sequence of delays introduced by $c(t)$, which restores the information signal back to its original form and spreads the interferer.

11.4.4 Hybrid Modulations

By blending together several of the previous types of SS modulation, one can form **hybrid** modulations that, depending on the system design objectives, can achieve a better performance against the interferer than can any of the SS modulations acting alone. One possibility is to multiply several of the $c(t)$ wideband waveforms [now denoted by $c^{(i)}(t)$ to distinguish them from one another] resulting in a SS modulation of the form

$$c(t) = \prod_i c^{(i)}(t) \tag{11.9}$$

Such a modulation may embrace the advantages of the various $c^{(i)}(t)$, while at the same time mitigating their individual disadvantages.

11.5 Applications of Spread Spectrum

11.5.1 Military

Antijam (AJ) Communications

As already noted, one of the key applications of spread spectrum is for antijam communications in a hostile environment. The basic mechanism by which a **direct sequence spread spectrum** receiver attenuates a noise jammer was illustrated in Section 11.3. Therefore, in this section, we will concentrate on tone jamming.

Assume the received signal, denoted $r(t)$, is given by

$$r(t) = Ax(t) + I(t) + n_w(t) \tag{11.10}$$

where $x(t)$ is given in Eq. (11.4), A is a constant amplitude,

$$I(t) = \alpha \cos\left(2\pi f_c t + \theta\right) \tag{11.11}$$

and $n_w(t)$ is additive white Gaussian noise (AWGN) having two-sided spectral density $N_0/2$. In Eq. (11.11), α is the amplitude of the tone jammer and θ is a random phase uniformly distributed in $[0, 2\pi]$.

If we employ the standard correlation receiver of Fig. 11.4, it is straightforward to show that the final test statistic out of the receiver is given by

$$g(T_b) = AT_b + \alpha \cos\theta \int_0^{T_b} c(t)\,\mathrm{d}t + N\left(T_b\right) \tag{11.12}$$

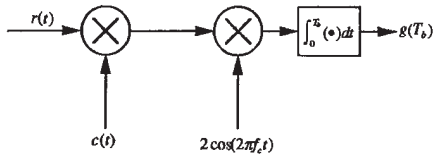


FIGURE 11.4 Standard correlation receiver.

where $N(T_b)$ is the contribution to the test statistic due to the AWGN. Noting that, for rectangular chips, we can express

$$\int_0^{T_b} c(t)\,\mathrm{d}t = T_c \sum_{i=1}^{M} c_i \tag{11.13}$$

where

$$M \triangleq \frac{T_b}{T_c} \tag{11.14}$$

is one-half of the processing gain, it is straightforward to show that, for a given value of θ, the signal-to-noise-plus-interference ratio, denoted by S/N_{total}, is given by

$$\frac{S}{N_{\text{total}}} = \frac{1}{\frac{N_0}{2E_b} + \left(\frac{J}{MS}\right)\cos^2\theta} \tag{11.15}$$

In Eq. (11.15), the jammer power is

$$J \triangleq \frac{\alpha^2}{2} \tag{11.16}$$

and the signal power is

$$S \triangleq \frac{A^2}{2} \tag{11.17}$$

If we look at the second term in the denominator of Eq. (11.15), we see that the ratio J/S is divided by M. Realizing that J/S is the ratio of the jammer power to the signal power before despreading, and J/MS is the ratio of the same quantity after despreading, we see that, as was the case for noise jamming, the benefit of employing direct sequence spread spectrum signalling in the presence of tone jamming is to reduce the effect of the jammer by an amount on the order of the processing gain.

Finally, one can show that an estimate of the average probability of error of a system of this type is given by

$$P_e = \frac{1}{2\pi}\int_0^{2\pi} \phi\left(-\sqrt{\frac{S}{N_{\text{total}}}}\right)\mathrm{d}\theta \tag{11.18}$$

where

$$\phi(x) \triangleq \frac{1}{\sqrt{2\pi}}\int_{-\infty}^{x} e^{-y^2/2}\,\mathrm{d}y \tag{11.19}$$

If Eq. (11.18) is evaluated numerically and plotted, the results are as shown in Fig. 11.5. It is clear from this figure that a large initial power advantage of the jammer can be overcome by a sufficiently large value of the processing gain.

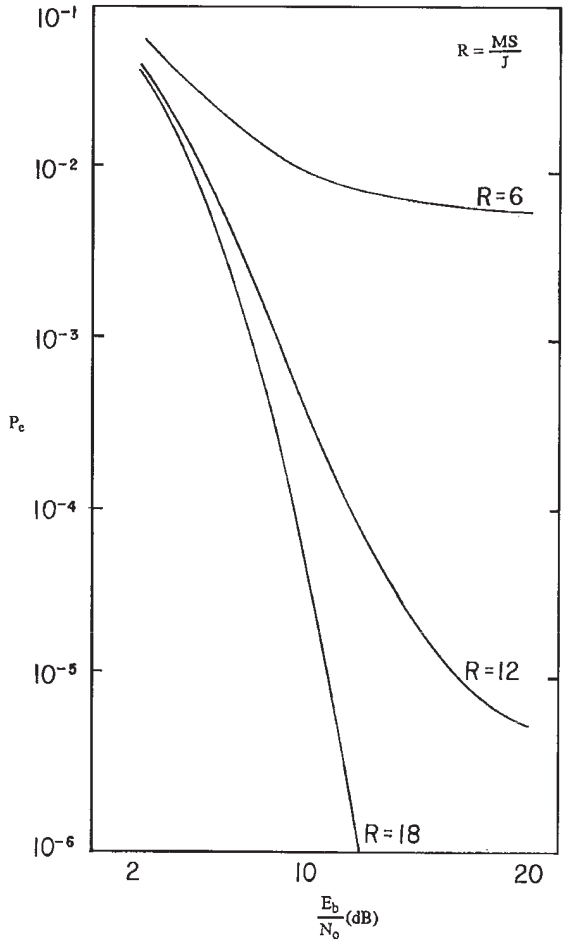


FIGURE 11.5 Plotted results of Eq. (11.18).

Low-Probability of Intercept (LPI)

The opposite side of the AJ problem is that of LPI, that is, the desire to hide your signal from detection by an intelligent adversary so that your transmissions will remain unnoticed and, thus, neither jammed nor exploited in any manner. This idea of designing an LPI system is achieved in a variety of ways, including transmitting at the smallest possible power level, and limiting the transmission time to as short an interval in time as is possible. The choice of signal design is also important, however, and it is here that spread spectrum techniques become relevant.

The basic mechanism is reasonably straightforward; if we start with a conventional narrowband signal, say a BPSK waveform having a spectrum as shown in Fig. 11.6a, and then spread it so that its new spectrum is as shown in Fig. 11.6b, the peak amplitude of the spectrum after spreading has been reduced by an amount on the order of the processing gain relative to what it was before spreading. Indeed, a sufficiently large processing gain will result in the spectrum of the signal after spreading falling below the ambient thermal noise level. Thus, there is no easy way for an unintended listener to determine that a transmission is taking place.

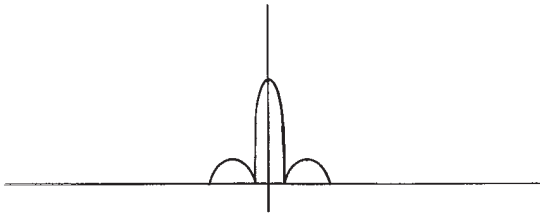


Figure 11.6a



Figure 11.6b

That is not to say the spread signal cannot be detected, however, merely that it is more difficult for an adversary to learn of the transmission. Indeed, there are many forms of so-called intercept receivers that are specifically designed to accomplish this very task. By way of example, probably the best known and simplest to implement is a **radiometer**, which is just a device that measures the total power present in the received signal. In the case of our intercept problem, even though we have lowered the power spectral density of the transmitted signal so that it falls below the noise floor, we have not lowered its power (i.e., we have merely spread its power over a wider frequency range). Thus, if the radiometer integrates over a sufficiently long period of time, it will eventually determine the presence of the transmitted signal buried in the noise. The key point, of course, is that the use of the spreading makes the interceptor's task much more difficult, since he has no knowledge of the spreading code and, thus, cannot despread the signal.

11.5.2 Commercial

Multiple Access Communications

From the perspective of commercial applications, probably the most important use of spread spectrum communications is as a multiple accessing technique. When used in this manner, it becomes an alternative to either frequency division multiple access (FDMA) or time division multiple access (TDMA) and is typically referred to as either code division multiple access (CDMA) or spread spectrum multiple access (SSMA). When using CDMA, each signal in the set is given its own spreading sequence. As opposed to either FDMA, wherein all users occupy disjoint frequency bands but are transmitted simultaneously in time, or TDMA, whereby all users occupy the same bandwidth but transmit in disjoint intervals of time, in CDMA, all signals occupy the same bandwidth and are transmitted simultaneously in time; the different waveforms in CDMA are distinguished from one another at the receiver by the specific spreading codes they employ.

Since most CDMA detectors are correlation receivers, it is important when deploying such a system to have a set of spreading sequences that have relatively low-pairwise cross-correlation between any two sequences in the set. Further, there are two fundamental types of operation in CDMA, synchronous and asynchronous. In the former case, the symbol transition times of all of the users are aligned; this allows for orthogonal sequences to be used as the spreading sequences and, thus, eliminates interference from one user to another.

Alternately, if no effort is made to align the sequences, the system operates asychronously; in this latter mode, multiple access interference limits the ultimate channel capacity, but the system design exhibits much more flexibility.

CDMA has been of particular interest recently for applications in wireless communications. These applications include cellular communications, personal communications services (PCS), and wireless local area networks. The reason for this popularity is primarily due to the performance that spread spectrum waveforms display when transmitted over a multipath fading channel.

To illustrate this idea, consider DS signalling. As long as the duration of a single chip of the spreading sequence is less than the multipath delay spread, the use of DS waveforms provides the system designer with one of two options. First, the multipath can be treated as a form of interference, which means the receiver should attempt to attenuate it as much as possible. Indeed, under this condition, all of the multipath returns that arrive at the receiver with a time delay greater than a chip duration from the multipath return to which the receiver is synchronized (usually the first return) will be attenuated because of the processing gain of the system.

Alternately, the multipath returns that are separated by more than a chip duration from the main path represent independent "looks" at the received signal and can be used constructively to enhance the overall performance of the receiver. That is, because all of the multipath returns contain information regarding the data that is being sent, that information can be extracted by an appropriately designed receiver. Such a receiver, typically referred to as a RAKE receiver, attempts to resolve as many individual multipath returns as possible and then to sum them coherently. This results in an *implicit* diversity gain, comparable to the use of *explicit* diversity, such as receiving the signal with multiple antennas.

The condition under which the two options are available can be stated in an alternate manner. If one envisions what is taking place in the frequency domain, it is straightforward to show that the condition of the chip duration being smaller than the multipath delay spread is equivalent to requiring that the spread bandwidth of the transmitted waveform exceed what is called the coherence bandwidth of the channel. This latter quantity is simply the inverse of the multipath delay spread and is a measure of the range of frequencies that fade in a highly correlated manner. Indeed, anytime the coherence bandwidth of the channel is less than the spread bandwidth of the signal, the channel is said to be *frequency selective* with respect to the signal. Thus, we see that to take advantage of DS signalling when used over a multipath fading channel, that signal should be designed such that it makes the channel appear frequency selective.

In addition to the desirable properties that spread spectrum signals display over multipath channels, there are two other reasons why such signals are of interest in cellular-type applications. The first has to do with a concept known as the reuse factor. In conventional cellular systems, either analog or digital, in order to avoid excessive interference from one cell to its neighbor cells, the frequencies used by a given cell are not used by its immediate neighbors (i.e., the system is designed so that there is a certain spatial separation between cells that use the same carrier frequencies). For CDMA, however, such spatial isolation is typically not needed, so that so-called *universal reuse* is possible.

Further, because CDMA systems tend to be interference limited, for those applications involving voice transmission, an additional gain in the capacity of the system can be achieved by the use of *voice activity detection.* That is, in any given two-way telephone conversation, each user is typically talking only about 50% of the time. During the time when a user is quiet, he is not contributing to the instantaneous interference. Thus, if a sufficiently large number of users can be supported by the system, statistically only about one-half of them will be active simultaneously, and the effective capacity can be doubled.

Interference Rejection

In addition to providing multiple accessing capability, spread spectrum techniques are of interest in the commercial sector for basically the same reasons they are in the military community, namely their AJ and LPI characteristics. However, the motivations for such interest differ. For example, whereas the military is interested in ensuring that systems they deploy are robust to interference generated by an intelligent adversary (i.e., exhibit jamming resistance), the interference of concern in commercial applications is unintentional. It is sometimes referred to as cochannel interference (CCI) and arises naturally as the result of many services using the same frequency band at the same time. And while such scenarios almost always allow for some type of spatial isolation between the interfering waveforms, such as the use of narrow-beam antenna patterns, at times the use of the inherent interference suppression property of a spread spectrum signal is also desired. Similarly, whereas the military is very much interested in the LPI property of a spread spectrum waveform, as indicated in Section 11.3, there are applications in the commercial segment where the same characteristic can be used to advantage.

To illustrate these two ideas, consider a scenario whereby a given band of frequencies is somewhat sparsely occupied by a set of conventional (i.e., nonspread) signals. To increase the overall spectral efficiency of the band, a set of spread spectrum waveforms can be overlaid on the same frequency band, thus forcing the two sets of users to share common spectrum. Clearly, this scheme is feasible only if the mutual interference that one set of users imposes on the other is within tolerable limits. Because of the interference suppression properties of spread spectrum waveforms, the despreading process at each spread spectrum receiver will attenuate the components of the final test statistic due to the overlaid narrowband signals. Similarly, because of the LPI characteristics of spread spectrum waveforms, the increase in the overall noise level as seen by any of the conventional signals, due to the overlay, can be kept relatively small.

Defining Terms

Antijam communication system: A communication system designed to resist intentional jamming by the enemy.

Chip time (interval): The duration of a single pulse in a direct sequence modulation; typically much smaller than the information symbol interval.

Coarse alignment: The process whereby the received signal and the despreading signal are aligned to within a single chip interval.

Dehopping: Despreading using a frequency-hopping modulation.

Delay-locked loop: A particular implementation of a closed-loop technique for maintaining fine alignment.

Despreading: The notion of decreasing the bandwidth of the received (spread) signal back to its information bandwidth.

Direct sequence modulation: A signal formed by linearly modulating the output sequence of a pseudorandom number generator onto a train of pulses.

Direct sequence spread spectrum: A spreading technique achieved by multiplying the information signal by a direct sequence modulation.

Fast frequency-hopping: A spread spectrum technique wherein the hop time is less than or equal to the information symbol interval, i.e., there exist one or more hops per data symbol.

Fine alignment: The state of the system wherein the received signal and the despreading signal are aligned to within a small fraction of a single chip interval.

Frequency-hopping modulation: A signal formed by nonlinearly modulating a train of pulses with a sequence of pseudorandomly generated frequency shifts.

Hop time (interval): The duration of a single pulse in a frequency-hopping modulation.

Hybrid spread spectrum: A spreading technique formed by blending together several spread spectrum techniques, e.g., direct sequence, frequency-hopping, etc.

Low-probability-of-intercept communication system: A communication system designed to operate in a hostile environment wherein the enemy tries to detect the presence and perhaps characteristics of the friendly communicator's transmission.

Processing gain (spreading ratio): The ratio of the spread spectrum bandwidth to the information data rate.

Radiometer: A device used to measure the total energy in the received signal.

Search algorithm: A means for coarse aligning (synchronizing) the despreading signal with the received spread spectrum signal.

Slow frequency-hopping: A spread spectrum technique wherein the hop time is greater than the information symbol interval, i.e., there exists more than one data symbol per hop.

Spread spectrum bandwidth: The bandwidth of the transmitted signal after spreading.

Spreading: The notion of increasing the bandwidth of the transmitted signal by a factor far in excess of its information bandwidth.

Tau–dither loop: A particular implementation of a closed-loop technique for maintaining fine alignment.

Time-hopping spread spectrum: A spreading technique that is analogous to pulse position modulation.

Tracking algorithm: An algorithm (typically closed loop) for maintaining fine alignment.

References

[1] Cook, C.F., Ellersick, F.W., Milstein, L.B., and Schilling, D.L., *Spread Spectrum Communications*, IEEE Press, 1983.

[2] Dixon, R.C., *Spread Spectrum Systems*, 3rd ed., John Wiley and Sons, Inc. 1994.

[3] Holmes, J.K., *Coherent Spread Spectrum Systems*, John Wiley and Sons, Inc. 1982.

[4] Simon, M.K., Omura, J.K., Scholtz, R.A., and Levitt, B.K., *Spread Spectrum Communications Handbook*, McGraw Hill, 1994 (previously published as *Spread Spectrum Communications*, Computer Science Press, 1985).

[5] Ziemer, R.E. and Peterson, R.L., *Digital Communications and Spread Spectrum Techniques*, Macmillan, 1985.

12

Diversity

12.1 Introduction 12-1
12.2 Diversity Schemes 12-3
Space Diversity • Polarization Diversity • Angle Diversity • Frequency Diversity • Path Diversity • Time Diversity • Transformed Diversity
12.3 Diversity Combining Techniques 12-6
Selection Combining • Maximal Ratio Combining • Equal Gain Combining • Loss of Diversity Gain Due to Branch Correlation and Unequal Branch Powers
12.4 Effect of Diversity Combining on Bit Error Rate 12-10
12.5 Concluding Remarks 12-11
Defining Terms 12-11
References 12-11

Arogyaswami J. Paulraj
Stanford University

12.1 Introduction

Diversity is a commonly used technique in mobile radio systems to combat signal **fading.** The basic principle of diversity is as follows. If several replicas of the same information-carrying signal are received over multiple channels with comparable strengths, which exhibit independent fading, then there is a good likelihood that at least one or more of these received signals will not be in a fade at any given instant in time, thus making it possible to deliver adequate signal level to the receiver. Without diversity techniques, in noise limited conditions, the transmitter would have to deliver a much higher power level to protect the link during the short intervals when the channel is severely faded. In mobile radio, the power available on the reverse link is severely limited by the battery capacity of hand-held subscriber units. Diversity methods play a crucial role in reducing transmit power needs. Also, cellular communication networks are mostly interference limited and, once again, mitigation of channel fading through use of diversity can translate into reduced variability of carrier-to-interference ratio (C/I), which in turn means lower C/I margin and hence better reuse factors and higher system capacity.

The basic principles of diversity have been known since 1927 when the first experiments in space diversity were reported. There are many techniques for obtaining independently fading branches, and these can be subdivided into two main classes. The first are explicit techniques where explicit redundant signal transmission is used to exploit diversity channels. Use of dual polarized signal transmission and reception in many point-to-point radios is an example of explicit diversity. Clearly such redundant signal transmission involves a penalty in frequency spectrum or additional power. In the second class are implicit diversity tech-

0-8493-8597-0/99/$0.00+$.50

© 1999 by CRC Press LLC

niques: the signal is transmitted only once, but the decorrelating effects in the propagation medium such as multipaths are exploited to receive signals over multiple diversity channels. A good example of implicit diversity is the **RAKE receiver** in code division multiple access (CDMA) systems, which uses independent fading of resolvable multipaths to achieve diversity gain. Figure 12.1 illustrates the principle of diversity where two independently fading signals are shown along with the selection diversity output signal which selects the stronger signal. The fades in the resulting signal have been substantially smoothed out while also yielding higher average power.

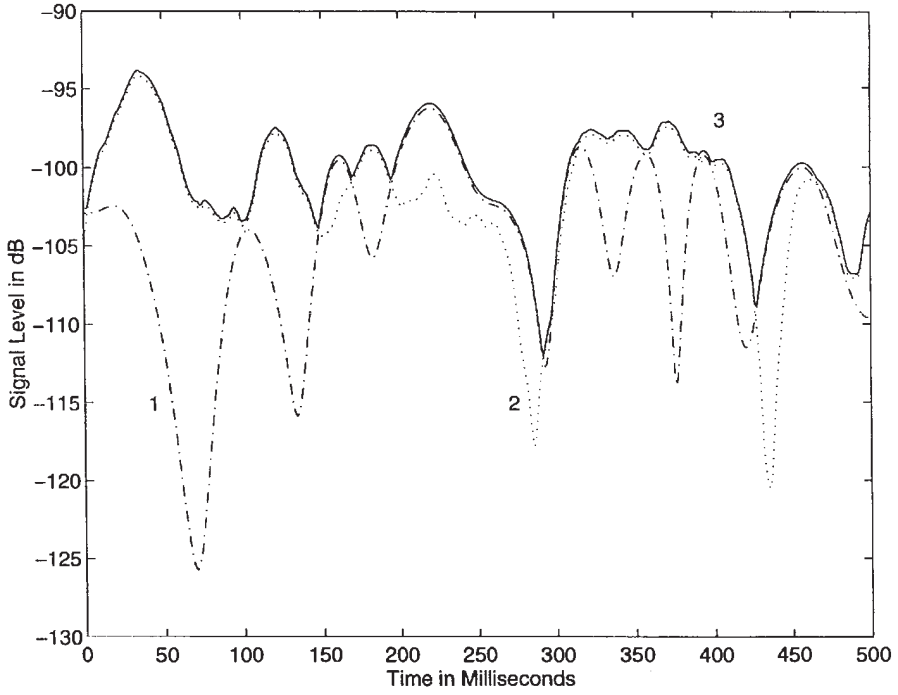


FIGURE 12.1 Example of diversity combining. Two independently fading signals 1 and 2. The signal 3 is the result of selecting the strongest signal.

If antennas are used in transmit, they can be exploited for diversity. If the transmit channel is known, the antennas can be driven with complex conjugate channel weighting to co-phase the signals at the receive antenna. If the forward channel is not known, we have several methods to convert space selective fading at the transmit antennas to other forms of diversity exploitable in the receiver.

Exploiting diversity needs careful design of the communication link. In explicit diversity, multiple copies of the same signal are transmitted in channels using either a frequency, time, or polarization dimension. At the receiver end we need arrangements to receive the different diversity branches (this is true for both explicit and implicit diversity). The different diversity branches are then combined to reduce signal **outage probability** or bit error rate.

In practice, the signals in the diversity branches may not show completely independent fading. The envelope cross correlation ρ between these signals is a measure of their inde-

pendence.

$$\rho = \frac{E\left[\left[r_1 - \bar{r}_1\right]\left[r_2 - \bar{r}_2\right]\right]}{\sqrt{E\left|r_1 - \bar{r}_1\right|^2 E\left|r_2 - \bar{r}_2\right|^2}}$$

where r_1 and r_2 represent the instantaneous envelope levels of the normalized signals at the two receivers and $\bar{r_1}$ and $\bar{r_2}$ are their respective means. It has been shown that a cross correlation of 0.7 [3] between signal envelopes is sufficient to provide a reasonable degree of diversity gain. Depending on the type of diversity employed, these diversity channels must be sufficiently *separated* along the appropriate diversity dimension. For spatial diversity, the antennas should be separated by more than the *coherence distance* to ensure a cross correlation of less than 0.7. Likewise in frequency diversity, the frequency separation must be larger than the *coherence bandwidth,* and in time diversity the separation between channel reuse in time should be longer than the *coherence time.* These coherence factors in turn depend on the channel characteristics. The coherence distance, coherence bandwidth and coherence time vary inversely as the angle spread, delay spread, and Doppler spread, respectively.

If the receiver has a number of diversity branches, it has to combine these branches to maximize the signal level. Several techniques have been studied for diversity combining. We will describe three main techniques: selection combining, equal gain combining, and maximal ratio combining.

Finally, we should note that diversity is primarily used to combat fading and if the signal does not show significant fading in the first place, for example when there is a direct path component, diversity combining may not provide significant diversity gain. In the case of antenna diversity, array gain proportional to the number of antennas will still be available.

12.2 Diversity Schemes

There are several techniques for obtaining diversity branches, sometimes also known as diversity dimensions. The most important of these are discussed in the following sections.

12.2.1 Space Diversity

This has historically been the most common form of diversity in mobile radio base stations. It is easy to implement and does not require additional frequency spectrum resources. Space diversity is exploited on the reverse link at the base station receiver by spacing antennas apart so as to obtain sufficient decorrelation. The key for obtaining minimum uncorrelated fading of antenna outputs is adequate spacing of the antennas. The required spacing depends on the degree of multipath angle spread. For example if the multipath signals arrive from all directions in the azimuth, as is usually the case at the mobile, antenna spacing (coherence distance) of the order of 0.5λ to 0.8λ is quite adequate [5]. On the other hand if the multipath angle spread is small, as in the case of base stations, the coherence distance is much larger. Also empirical measurements show a strong coupling between antenna height and spatial correlation. Larger antenna heights imply larger coherence distances. Typically 10λ to 20λ separation is adequate to achieve $\rho = 0.7$ at base stations in suburban settings when the signals arrive from the broadside direction. The coherence distance can be 3 to 4 times larger for endfire arrivals. The endfire problem is averted in base stations with trisectored antennas as each sector needs to handle only signals arriving $\pm 60°$ off the broadside. The coherence distance depends strongly on the terrain. Large multipath angle spread means smaller coherence distance. Base stations normally use space

diversity in the horizontal plane only. Separation in the vertical plane can also be used, and the necessary spacing depends upon vertical multipath angle spread. This can be small for distant mobiles making vertical plane diversity less attractive in most applications.

Space diversity is also exploitable at the transmitter. If the forward channel is known, it works much like receive space diversity. If it is not known, then space diversity can be transformed to another form of diversity exploitable at the receiver. (See Section 12.2.7 below).

If antennas are used at transmit and receive, the M transmit and N receive antennas both contribute to diversity. It can be shown that if simple weighting is used without additional bandwidth or time/memory processing, then maximum diversity gain is obtained if the transmitter and receiver use the left and right singular vectors of the $M \times N$ channel matrix, respectively. However, to approach the maximum $M \times N$ order diversity order will require the use of additional bandwidth or time/memory-based methods.

12.2.2 Polarization Diversity

In mobile radio environments, signals transmitted on orthogonal polarizations exhibit low fade correlation, and therefore, offer potential for diversity combining. Polarization diversity can be obtained either by explicit or implicit techniques. Note that with polarization only two diversity branches are available as against space diversity where several branches can be obtained using multiple antennas. In explicit polarization diversity, the signal is transmitted and received in two orthogonal polarizations. For a fixed total transmit power, the power in each branch will be 3 dB lower than if single polarization is used. In the implicit polarization technique, the signal is launched in a single polarization, but is received with cross-polarized antennas. The propagation medium couples some energy into the cross-polarization plane. The observed cross-polarization coupling factor lies between 8 to 12 dB in mobile radio [8, 1]. The cross-polarization envelope decorrelation has been found to be adequate. However, the large branch imbalance reduces the available diversity gain.

With hand-held phones, the handset can be held at random orientations during a call. This results in energy being launched with varying polarization angles ranging from vertical to horizontal. This further increases the advantage of cross-polarized antennas at the base station since the two antennas can be combined to match the received signal polarization. This makes polarization diversity even more attractive. Recent work [4] has shown that with variable launch polarization, a cross-polarized antenna can give comparable overall (matching plus diversity) performance to a vertically polarized space diversity antenna.

Finally, we should note that cross-polarized antennas can be deployed in a compact antenna assembly and do not need large physical separation needed in space diversity antennas. This is an important advantage in the **PCS** base stations where low profile antennas are needed.

12.2.3 Angle Diversity

In situations where the angle spread is very high, such as indoors or at the mobile unit in urban locations, signals collected from multiple nonoverlapping beams offer low fade correlation with balanced power in the diversity branches. Clearly, since directional beams imply use of antenna aperture, angle diversity is closely related to space diversity. Angle diversity has been utilized in indoor wireless LANs, where its use allows substantial increase in LAN throughputs [2].

12.2.4 Frequency Diversity

Another technique to obtain decorrelated diversity branches is to transmit the same signal over different frequencies. The frequency separation between carriers should be larger than the coherence bandwidth. The coherence bandwidth, of course, depends on the multipath delay spread of the channel. The larger the delay spread, the smaller the coherence bandwidth and the more closely we can space the frequency diversity channels. Clearly, frequency diversity is an explicit diversity technique and needs additional frequency spectrum.

A common form of frequency diversity is multicarrier (also known as multitone) modulation. This technique involves sending redundant data over a number of closely spaced carriers to benefit from frequency diversity, which is then exploited by applying **interleaving** and **channel coding/forward error correction** across the carriers. Another technique is to use **frequency hopping** wherein the interleaved and channel coded data stream is transmitted with widely separated frequencies from burst to burst. The wide frequency separation is chosen to guarantee independent fading from burst to burst.

12.2.5 Path Diversity

This implicit diversity is available if the signal bandwidth is much larger than the channel coherence bandwidth. The basis for this method is that when the multipath arrivals can be resolved in the receiver and since the paths fade independently, diversity gain can be obtained. In CDMA systems, the multipath arrivals must be separated by more than one *chip* period and the RAKE receiver provides the diversity [9]. In TDMA systems, the multipath arrivals must be separated by more than one *symbol* period and the MLSE receiver provides the diversity.

12.2.6 Time Diversity

In mobile communications channels, the mobile motion together with scattering in the vicinity of the mobile causes time selective fading of the signal with Rayleigh fading statistics for the signal envelope. Signal fade levels separated by the *coherence time* show low correlation and can be used as diversity branches if the same signal can be transmitted at multiple instants separated by the coherence time. The coherence time depends on the Doppler spread of the signal, which in turn is a function of the mobile speed and the carrier frequency.

Time diversity is usually exploited via interleaving, forward-error correction (FEC) coding, and **automatic request for repeat** (ARQ). These are sophisticated techniques to exploit channel coding and time diversity. One fundamental drawback with time diversity approaches is the delay needed to collect the repeated or interleaved transmissions. If the coherence time is large, as for example when the vehicle is slow moving, the required delay becomes too large to be acceptable for interactive voice conversation.

The statistical properties of fading signals depend on the field component used by the antenna, the vehicular speed, and the carrier frequency. For an idealized case of a mobile surrounded by scatterers in all directions, the autocorrelation function of the received signal $x(t)$ (note this is not the envelope $r(t)$) can be shown to be

$$E\left[x(t)x(t+\tau)\right] = J_0\left(2\pi\tau v/\lambda\right)$$

where J_0 is a Bessel function of the 0th order and v is the mobile velocity.

12.2.7 Transformed Diversity

In transformed diversity, the space diversity branches at the transmitter are transformed into other forms of diversity branches exploitable at the receiver. This is used when the forward channel is not known and shifts the responsibility of diversity combining to the receiver which has the necessary channel knowledge.

Space to Frequency

- *Antenna-delay.* Here the signal is transmitted from two or more antennas with delays of the order of a chip or symbol period in CDMA or TDMA, respectively. The different transmissions simulate resolved path arrivals that can be used as diversity branches by the RAKE or MLSE equalizer.
- *Multicarrier modulation.* The data stream after interleaving and coding is modulated as a multicarrier output using an inverse DFT. The carriers are then mapped to the different antennas. The space selective fading at the antennas is now transformed to frequency selective fading and diversity is obtained during decoding.

Space to Time

- *Antenna hopping/phase rolling.* In this method the data stream after coding and interleaving is switched randomly from antenna to antenna. The space selective fading at the transmitter is converted into a time selective fading at the receiver. This is a form of "active" fading.
- *Space-time coding.* The approach in space-time coding is to split the encoded data into multiple data streams each of which is modulated and simultaneously transmitted from different antennas. The received signal is a superposition of the multiple transmitted signals. Channel decoding can be used to recover the data sequence. Since the encoded data arrive over uncorrelated fade branches, diversity gain can be realized.

12.3 Diversity Combining Techniques

Several diversity combining methods are known. We describe three main techniques: selection, maximal ratio, and equal gain. They can be used with each of the diversity schemes discussed above.

12.3.1 Selection Combining

This is the simplest and perhaps the most frequently used form of diversity combining. In this technique, one of the two diversity branches with the highest carrier-to-noise ratio (C/N) is connected to the output. See Fig. 12.2(a).

The performance improvement due to selection diversity can be seen as follows. Let the signal in each branch exhibit Rayleigh fading with mean power σ^2. The density function of the envelope is given by

$$p(r_i) = \frac{r_i}{\sigma^2} e^{\frac{-r_i^2}{2\sigma^2}} \tag{12.1}$$

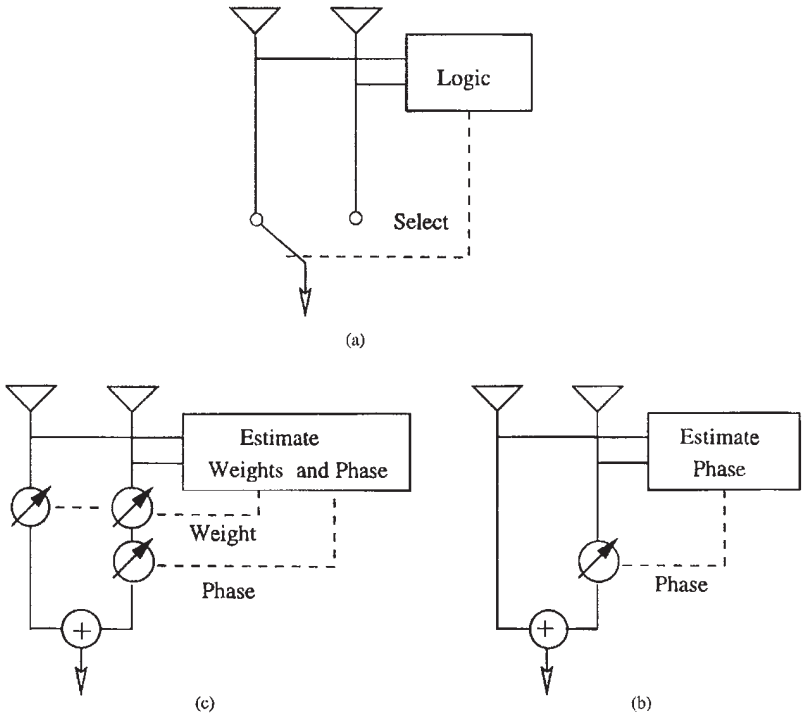


FIGURE 12.2 Diversity combining methods for two diversity branches.

where r_i is the signal envelope in each branch. If we define two new variables

$$\gamma_i = \frac{\text{Instantaneous signal power in each branch}}{\text{Mean noise power}}$$

$$\Gamma = \frac{\text{Mean signal power in each branch}}{\text{Mean noise power}}$$

then the probability that the C/N is less than or equal to some specified value γ_s is

$$\text{Prob}\left[\gamma_i \leq \gamma_s\right] = 1 - e^{-\gamma_s/\Gamma} \tag{12.2}$$

The probability that γ_i in all branches with independent fading will be simultaneously less than or equal to γ_s is then

$$\text{Prob}\left[\gamma_1, \gamma_2, \ldots \gamma_M \leq \gamma_s\right] = \left(1 - e^{-\gamma_s/\Gamma}\right)^M \tag{12.3}$$

This is the distribution of the best signal envelope from the two diversity branches. Figure 12.3 shows the distribution of the combiner output C/N for M = 1,2,3, and 4 branches. The improvement in signal quality is significant. For example at 99% reliability level, the improvement in C/N is 10 dB for two branches and 16 dB for four branches.

Selection combining also increases the mean C/N of the combiner output and can be shown to be [3]

$$\text{Mean}\left(\gamma_s\right) = \Gamma \sum_{k=1}^{M} \frac{1}{k} \tag{12.4}$$

This indicates that with 4 branches, for example, the mean C/N of the selected branch is 2.08 better than the mean C/N in any one branch.

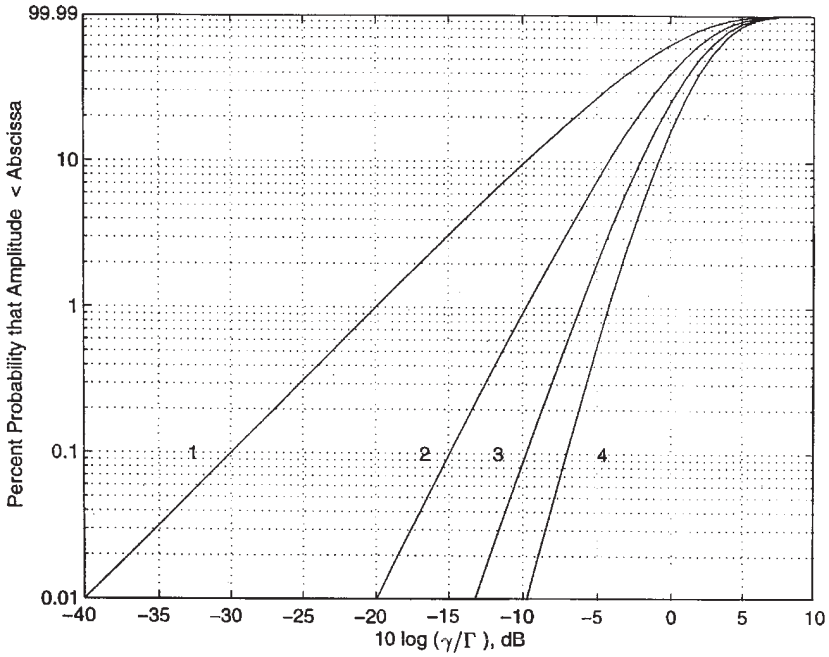


FIGURE 12.3 Probability distribution of signal envelope for selection combining.

12.3.2 Maximal Ratio Combining

In this technique the M diversity branches are first co-phased and then weighted proportionally to their signal level before summing. See Fig. 12.2(b). The distribution of the maximal ratio combiner has been shown to be [5]

$$\text{Prob}\left[\gamma \leq \gamma_m\right] = 1 - e^{(-\gamma_m/\Gamma)} \sum_{k=1}^{M} \frac{(\gamma_m/\Gamma)^{k-1}}{(k-1)!} \tag{12.5}$$

The distribution of output of a maximal ratio combiner is shown in Fig. 12.4. Maximal ratio combining is known to be optimal in the sense that it yields the best statistical reduction of fading of any linear diversity combiner. In comparison to the selection combiner, at 99% reliability level, the maximal ratio combiner provides a 11.5 dB gain for two branches and a 19 dB gain for four branches, an improvement of 1.5 and 3 dB, respectively, over the selection diversity combiner.

The mean C/N of the combined signal may be easily shown to be

$$\text{Mean}\left(\gamma_m\right) = M\Gamma \tag{12.6}$$

Therefore, combiner output mean varies linearly with M. This confirms the intuitive result that the output C/N averaged over fades should provide gain proportional to the number of diversity branches. This is a situation similar to conventional beamforming.

12.3.3 Equal Gain Combining

In some applications, it may be difficult to estimate the amplitude accurately, the combining gains may all be set to unity, and the diversity branches merely summed after co-phasing. [See Fig. 12.2(c)].

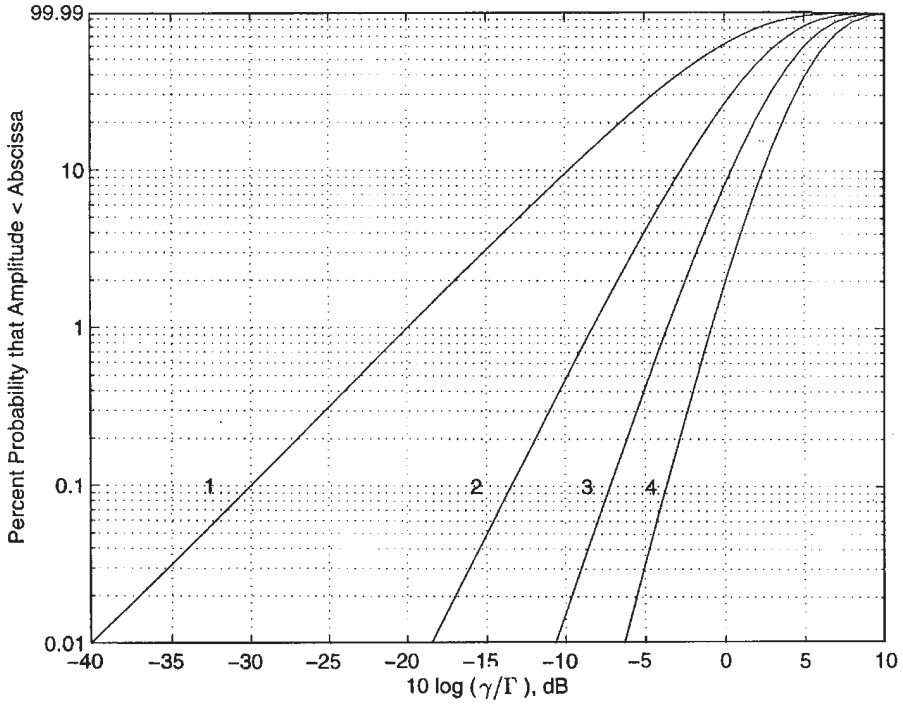


FIGURE 12.4 Probability distribution for signal envelope for maximal ratio combining.

The distribution of equal gain combiner does not have a neat expression and has been computed by numerical evaluation. Its performance has been shown to be very close to within a decibel to maximal ratio combining. The mean C/N can be shown to be [3]

$$\text{Mean}\,(\gamma_e) = \Gamma\left[1 + \frac{\pi}{4}(M-1)\right] \tag{12.7}$$

Like maximal ratio combining, the mean C/N for equal gain combining grows almost linearly with M and is approximately only one decibel poorer than maximal ratio combiner even with an infinite number of branches.

12.3.4 Loss of Diversity Gain Due to Branch Correlation and Unequal Branch Powers

The above analysis assumed that the fading signals in the diversity branches were all uncorrelated and of equal power. In practice, this may be difficult to achieve and as we saw earlier, the branch cross-correlation coefficient $\rho = 0.7$ is considered to be acceptable. Also, equal mean powers in diversity branches are rarely available. In such cases we can expect a certain loss of diversity gain. However, since most of the damage in fading is due to deep fades, and also since the chance of coincidental deep fades is small even for moderate branch correlation, one can expect a reasonable tolerance to branch correlation.

The distribution of the output signal envelope of maximal ratio combiner has been shown to be [6]:

$$\text{Prob}\,[\gamma_m] = \sum_{n=1}^{M} \frac{A_n}{2\lambda_n} e^{-\gamma_m/2\lambda_n} \tag{12.8}$$

where λ_n are the eigenvalues of the M $\times$ M branch envelope covariance matrix whose elements are defined by

$$\mathbf{R}_{ij} = E\left[r_i r_j^*\right] \tag{12.9}$$

and A_n is defined by

$$A_n = \prod_{\substack{k=1 \\ k \neq n}}^{M} \frac{1}{1 - \lambda_k/\lambda_n} \tag{12.10}$$

12.4 Effect of Diversity Combining on Bit Error Rate

So far we have studied the distribution of the instantaneous envelope or C/N after diversity combining. We will now briefly survey how diversity combining affects BER performance in digital radio links; we assume maximal ratio combining.

To begin let us first examine the effect of Rayleigh fading on the BER performance of digital transmission links. This has been studied by several authors and is summarized in [7]. Table 12.1 gives the BER expressions in the large E_b/N_0 case for coherent binary PSK and coherent binary orthogonal FSK for unfaded and Rayleigh faded AWGN (additive white Gaussian noise channels) channels. $\bar{E}_b/N_0$ represents the average E_b/N_0 for the fading channel.

TABLE 12.1 Comparison of BER Performance for Unfaded and Rayleigh Faded Signals

Modulaton	Unfaded BER	Faded BER
Coh BPSK	$\frac{1}{2}\text{erfc}\left(\sqrt{E_b/N_0}\right)$	$\frac{1}{4\left(\bar{E}_b/N_0\right)}$
Coh FSK	$\frac{1}{2}\text{erfc}\left(\sqrt{\frac{1}{2}E_b/N_0}\right)$	$\frac{1}{2\left(\bar{E}_b/N_0\right)}$

Observe that error rates decrease only inversely with SNR as against exponential decreases for the unfaded channel. Also note that for fading channels, coherent binary PSK is 3 dB better than coherent binary FSK, exactly the same advantage as in unfaded case. Even for modest target BER of 10^{-2} that is usually needed in mobile communications, the loss due to fading can be very high—17.2 dB.

To obtain the BER with maximal ratio diversity combining we have to average the BER expression for the unfaded BER with the distribution obtained for the maximal ratio combiner given in (12.5). Analytical expressions have been derived for these in [7]. For a branch SNR greater than 10 dB, the BER after maximal ratio diversity combining is given in Table 12.2.

We observe that the probability of error varies as $1/\bar{E}_b/N_0$ raised to the Lth power. Thus, diversity reduces the error rate exponentially as the number of independent branches increases.

TABLE 12.2 BER Performance for Coherent BPSK and FSK with Diversity

Modulaton	Post Diversity BER
Coherent BPSK	$\left(\frac{1}{4\ \bar{E}_b/N_0}\right)^L \left(\begin{array}{c} 2L-1 \\ L \end{array}\right)$
Coherent FSK	$\left(\frac{1}{2\bar{E}_b/N_0}\right)^L \left(\begin{array}{c} 2L-1 \\ L \end{array}\right)$

12.5 Concluding Remarks

Diversity provides a powerful technique for combating fading in mobile communication systems. Diversity techniques seek to generate and exploit multiple branches over which the signal shows low fade correlation. To obtain the best diversity performance, the multiple access, modulation, coding and antenna design of the wireless link must all be carefully chosen so as to provide a rich and reliable level of well-balanced, low-correlation diversity branches in the target propagation environment. Successful diversity exploitation can impact a mobile network in several ways. Reduced power requirements can result in increased coverage or improved battery life. Low signal outage improves voice quality and handoff performance. Finally, reduced fade margins directly translate to better reuse factors and, hence, increased system capacity.

Defining Terms

Automatic request for repeat: An error control mechanism in which received packets that cannot be corrected are retransmitted.

Channel coding/Forward error correction: A technique that inserts redundant bits during transmission to help detect and correct bit errors during reception.

Fading: Fluctuation in the signal level due to shadowing and multipath effects.

Frequency hopping: A technique where the signal bursts are transmitted at different frequencies separated by random spacing that are multiples of signal bandwidth.

Interleaving: A form of data scrambling that spreads burst of bit errors evenly over the received data allowing efficient forward error correction.

Outage probability: The probability that the signal level falls below a specified minimum level.

PCS: Personal Communications Services.

RAKE receiver: A receiver used in direct sequence spread spectrum signals. The receiver extracts energy in each path and then adds them together with appropriate weighting and delay.

References

[1] Adachi, F., Feeney, M.T., Williason, A.G., and Parsons, J.D., Crosscorrelation between the envelopes of 900 MHz signals received at a mobile radio base station site. *Proc. IEE,* 133(6), 506–512, 1986.

[2] Freeburg, T.A., Enabling technologies for in-building network communications—four technical challenges and four solutions. *IEEE Trans. Veh. Tech.,* 29(4), 58–64, 1991.

[3] Jakes, W.C., *Microwave Mobile Communications,* John Wiley & Sons, New York, 1974.

[4] Jefford, P.A., Turkmani, A.M.D., Arowojulu, A.A., and Kellet, C.J., An experimental evaluation of the performance of the two branch space and polarization schemes at 1800 MHz. *IEEE Trans. Veh. Tech.*, VT-44(2), 318–326, 1995.

[5] Lee, W.C.Y., *Mobile Communications Engineering*, McGraw-Hill, New York, 1982.

[6] Pahlavan, K. and Levesque, A.H., *Wireless Information Networks*, John Wiley & Sons, New York, 1995.

[7] Proakis, J.G., *Digital Communications*, McGraw-Hill, New York, 1989.

[8] Vaughan, R.G., Polarization diversity system in mobile communications. *IEEE Trans. Veh. Tech.*, VT-39(3), 177–186, 1990.

[9] Viterbi, A.J., *CDMA: Principle of Spread Spectrum Communications*, Addison-Wesley, Reading, MA, 1995.

13

Digital Communication System Performance[1]

13.1 Introduction 13-1
The Channel • The Link
13.2 Bandwidth and Power Considerations 13-3
The Bandwidth Efficiency Plane • M-ary Signalling • Bandwidth-Limited Systems • Power-Limited Systems • Minimum Bandwidth Requirements for MPSK and MFSK Signalling
13.3 Example 1: Bandwidth-Limited Uncoded System 13-7
Solution to Example 1
13.4 Example 2: Power-Limited Uncoded System 13-9
Solution to Example 2
13.5 Example 3: Bandwidth-Limited Power-Limited Coded System 13-10
Solution to Example 3 • Calculating Coding Gain
13.6 Example 4: Direct-Sequence Spread-Spectrum Coded System 13-15
Processing Gain • Channel Parameters for Example 13.4 • Solution to Example 13.4
13.7 Conclusion 13-19
Appendix: Received E_b/N_0 Is Independent of the Code Parameters 13-19
References 13-20
Further Information 13-20

Bernard Sklar
Communications Engineering Services

13.1 Introduction

In this section we examine some fundamental tradeoffs among bandwidth, power, and error performance of digital communication systems. The criteria for choosing modulation and coding schemes, based on whether a system is bandwidth limited or power limited, are reviewed for several system examples. Emphasis is placed on the subtle but straightforward relationships we encounter when transforming from data-bits to channel-bits to symbols to chips.

[1] A version of this chapter has appeared as a paper in the *IEEE Communications Magazine*, November 1993, under the title "Defining, Designing, and Evaluating Digital Communication Systems."

0-8493-8597-0/99/$0.00+$.50

© 1999 by CRC Press LLC

The design or definition of any digital communication system begins with a description of the communication link. The *link* is the name given to the communication transmission path from the modulator and transmitter, through the channel, and up to and including the receiver and demodulator. The *channel* is the name given to the propagating medium between the transmitter and receiver. A link description quantifies the average signal power that is received, the available bandwidth, the noise statistics, and other impairments, such as fading. Also needed to define the system are basic requirements, such as the data rate to be supported and the error performance.

13.1.1 The Channel

For radio communications, the concept of *free space* assumes a channel region free of all objects that might affect radio frequency (RF) propagation by absorption, reflection, or refraction. It further assumes that the atmosphere in the channel is perfectly uniform and nonabsorbing, and that the earth is infinitely far away or its reflection coefficient is negligible. The RF energy arriving at the receiver is assumed to be a function of distance from the transmitter (simply following the inverse-square law of optics). In practice, of course, propagation in the atmosphere and near the ground results in refraction, reflection, and absorption, which modify the free space transmission.

13.1.2 The Link

A radio transmitter is characterized by its average output signal power P_t and the gain of its transmitting antenna G_t. The name given to the product $P_t G_t$, with reference to an isotropic antenna is *effective radiated power* (*EIRP*) in watts (or dBW). The predetection average signal power S arriving at the output of the receiver antenna can be described as a function of the *EIRP*, the gain of the receiving antenna G_r, the path loss (or space loss) L_s, and other losses, L_o, as follows [14, 15]:

$$S = \frac{EIRP\, G_r}{L_s L_o} \tag{13.1}$$

The path loss L_s can be written as follows [15]:

$$L_s = \left(\frac{4\pi d}{\lambda}\right)^2 \tag{13.2}$$

where d is the distance between the transmitter and receiver and λ is the wavelength.

We restrict our discussion to those links distorted by the mechanism of additive white Gaussian noise (AWGN) only. Such a noise assumption is a very useful model for a large class of communication systems. A valid approximation for average received noise power N that this model introduces is written as follows [5, 9]:

$$N \cong kT^{\circ}W \tag{13.3}$$

where k is Boltzmann's constant (1.38×10^{-23} joule/K), T° is effective temperature in kelvin, and W is bandwidth in hertz. Dividing Eq. (13.3) by bandwidth, enables us to write the received noise-power spectral density N_0 as follows:

$$N_0 = \frac{N}{W} = kT^{\circ} \tag{13.4}$$

Dividing Eq. (13.1) by N_0 yields the received average signal-power to noise-power spectral density S/N_0 as

$$\frac{S}{N_0} = \frac{EIRP\, G_r/T^\circ}{kL_sL_o} \tag{13.5}$$

where G_r/T° is often referred to as the receiver figure of merit. A link budget analysis is a compilation of the power gains and losses throughout the link; it is generally computed in decibels, and thus takes on the bookkeeping appearance of a business enterprise, highlighting the assets and liabilities of the link. Once the value of S/N_0 is specified or calculated from the link parameters, we then shift our attention to optimizing the choice of signalling types for meeting system bandwidth and error performance requirements.

Given the received S/N_0, we can write the received bit-energy to noise-power spectral density E_b/N_0, for any desired data rate R, as follows:

$$\frac{E_b}{N_0} = \frac{ST_b}{N_0} = \frac{S}{N_0}\left(\frac{1}{R}\right) \tag{13.6}$$

Equation (13.6) follows from the basic definitions that received bit energy is equal to received average signal power times the bit duration and that bit rate is the reciprocal of bit duration. Received E_b/N_0 is a key parameter in defining a digital communication system. Its value indicates the apportionment of the received waveform energy among the bits that the waveform represents. At first glance, one might think that a system specification should entail the symbol-energy to noise-power spectral density E_s/N_0 associated with the arriving waveforms. We will show, however, that for a given S/N_0 the value of E_s/N_0 is a function of the modulation and coding. The reason for defining systems in terms of E_b/N_0 stems from the fact that E_b/N_0 depends only on S/N_0 and R and is unaffected by any system design choices, such as modulation and coding.

13.2 Bandwidth and Power Considerations

Two primary communications resources are the received power and the available transmission bandwidth. In many communication systems, one of these resources may be more precious than the other and, hence, most systems can be classified as either bandwidth limited or power limited. In bandwidth-limited systems, spectrally efficient modulation techniques can be used to save bandwidth at the expense of power; in power-limited systems, power efficient modulation techniques can be used to save power at the expense of bandwidth. In both bandwidth- and power-limited systems, error-correction coding (often called channel coding) can be used to save power or to improve error performance at the expense of bandwidth. Recently, trellis-coded modulation (TCM) schemes have been used to improve the error performance of bandwidth-limited channels without any increase in bandwidth [17], but these methods are beyond the scope of this chapter.

13.2.1 The Bandwidth Efficiency Plane

Figure 13.1 shows the abscissa as the ratio of bit-energy to noise-power spectral density E_b/N_0 (in decibels) and the ordinate as the ratio of throughput, R (in bits per second), that can be transmitted per hertz in a given bandwidth W. The ratio R/W is called bandwidth efficiency, since it reflects how efficiently the bandwidth resource is utilized. The plot stems from the Shannon–Hartley capacity theorem [12, 13, 15], which can be stated as

$$C = W \log_2\left(1 + \frac{S}{N}\right) \tag{13.7}$$

where S/N is the ratio of received average signal power to noise power. When the logarithm is taken to the base 2, the capacity C, is given in bits per second. The capacity of a channel defines the maximum number of bits that can be reliably sent per second over the channel. For the case where the data (information) rate R is equal to C, the curve separates a region of practical communication systems from a region where such communication systems cannot operate reliably [12, 15].

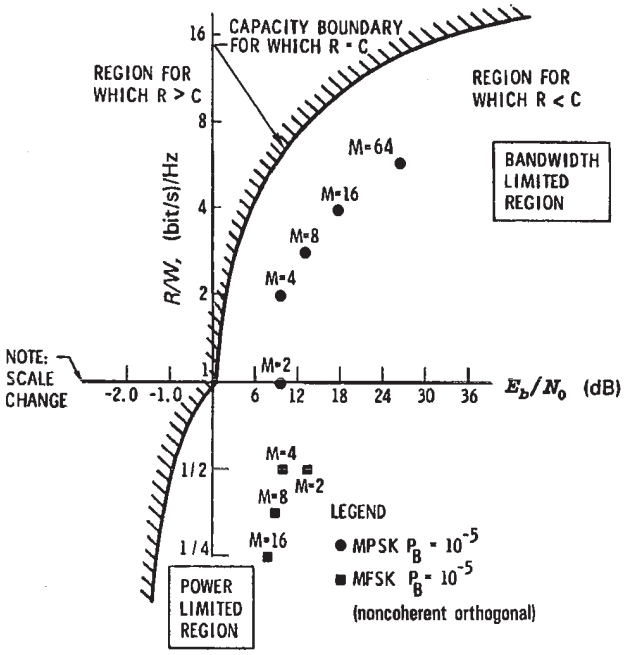


FIGURE 13.1 Bandwidth-efficiency plane.

13.2.2 *M*-ary Signalling

Each symbol in an M-ary alphabet can be related to a unique sequence of m bits, expressed as

$$M = 2^m \qquad \text{or} \qquad m = \log_2 M \tag{13.8}$$

where M is the size of the alphabet. In the case of digital transmission, the term symbol refers to the member of the M-ary alphabet that is transmitted during each symbol duration T_s. To transmit the symbol, it must be mapped onto an electrical voltage or current waveform. Because the waveform represents the symbol, the terms symbol and waveform are sometimes used interchangeably. Since one of M symbols or waveforms is transmitted during each symbol duration T_s, the data rate R in bits per second can be expressed as

$$R = \frac{m}{T_s} = \frac{\log_2 M}{T_s} \tag{13.9}$$

Data-bit-time duration is the reciprocal of data rate. Similarly, symbol-time duration is the reciprocal of symbol rate. Therefore, from Eq. (13.9), we write that the effective time

duration T_b of each bit in terms of the symbol duration T_s or the symbol rate R_s is

$$T_b = \frac{1}{R} = \frac{T_s}{m} = \frac{1}{mR_s} \tag{13.10}$$

Then, using Eqs. (13.8) and (13.10) we can express the symbol rate R_s in terms of the bit rate R as follows:

$$R_s = \frac{R}{\log_2 M} \tag{13.11}$$

From Eqs. (13.9) and (13.10), any digital scheme that transmits $m = \log_2 M$ bits in T_s seconds, using a bandwidth of W hertz, operates at a bandwidth efficiency of

$$\frac{R}{W} = \frac{\log_2 M}{WT_s} = \frac{1}{WT_b} \qquad \text{(b/s)/Hz} \tag{13.12}$$

where T_b is the effective time duration of each data bit.

13.2.3 Bandwidth-Limited Systems

From Eq. (13.12), the smaller the WT_b product, the more bandwidth efficient will be any digital communication system. Thus, signals with small WT_b products are often used with bandwidth-limited systems. For example, the European digital mobile telephone system known as Global System for Mobile Communications (GSM) uses Gaussian minimum shift keying (GMSK) modulation having a WT_b product equal to 0.3 Hz/(b/s), where W is the 3-dB bandwidth of a Gaussian filter [4].

For uncoded bandwidth-limited systems, the objective is to maximize the transmitted information rate within the allowable bandwidth, at the expense of E_b/N_0 (while maintaining a specified value of bit-error probability P_B). The operating points for coherent M-ary phase-shift keying (MPSK) at $P_B = 10^{-5}$ are plotted on the bandwidth-efficiency plane of Fig. 13.1. We assume Nyquist (ideal rectangular) filtering at baseband [10]. Thus, for MPSK, the required double-sideband (DSB) bandwidth at an intermediate frequency (IF) is related to the symbol rate as follows:

$$W = \frac{1}{T_s} = R_s \tag{13.13}$$

where T_s is the symbol duration and R_s is the symbol rate. The use of Nyquist filtering results in the minimum required transmission bandwidth that yields zero intersymbol interference; such ideal filtering gives rise to the name Nyquist minimum bandwidth.

From Eqs. (13.12) and (13.13), the bandwidth efficiency of MPSK modulated signals using Nyquist filtering can be expressed as

$$R/W = \log_2 M \qquad \text{(b/s)/Hz} \tag{13.14}$$

The MPSK points in Fig. 13.1 confirm the relationship shown in Eq. (13.14). Note that MPSK modulation is a bandwidth-efficient scheme. As M increases in value, R/W also increases. MPSK modulation can be used for realizing an improvement in bandwidth efficiency at the cost of increased E_b/N_0. Although beyond the scope of this chapter, many highly bandwidth-efficient modulation schemes are under investigation [1].

13.2.4 Power-Limited Systems

Operating points for noncoherent orthogonal M-ary FSK (MFSK) modulation at $P_B = 10^{-5}$ are also plotted on Fig. 13.1. For MFSK, the IF minimum bandwidth is as follows [15]

$$W = \frac{M}{T_s} = MR_s \tag{13.15}$$

where T_s is the symbol duration and R_s is the symbol rate. With MFSK, the required transmission bandwidth is expanded M-fold over binary FSK since there are M different orthogonal waveforms, each requiring a bandwidth of $1/T_s$. Thus, from Eqs. (13.12) and (13.15), the bandwidth efficiency of noncoherent orthogonal MFSK signals can be expressed as

$$\frac{R}{W} = \frac{\log_2 M}{M} \qquad \text{(b/s)/Hz} \tag{13.16}$$

The MFSK points plotted in Fig. 13.1 confirm the relationship shown in Eq. (13.16). Note that MFSK modulation is a bandwidth-expansive scheme. As M increases, R/W decreases. MFSK modulation can be used for realizing a reduction in required E_b/N_0 at the cost of increased bandwidth.

In Eqs. (13.13) and (13.14) for MPSK, and Eqs. (13.15) and (13.16) for MFSK, and for all the points plotted in Fig. 13.1, ideal filtering has been assumed. Such filters are not realizable! For realistic channels and waveforms, the required transmission bandwidth must be increased in order to account for realizable filters.

In the examples that follow, we will consider radio channels that are disturbed only by additive white Gaussian noise (AWGN) and have no other impairments, and for simplicity, we will limit the modulation choice to constant-envelope types, i.e., either MPSK or noncoherent orthogonal MFSK. For an uncoded system, MPSK is selected if the channel is bandwidth limited, and MFSK is selected if the channel is power limited. When error-correction coding is considered, modulation selection is not as simple, because coding techniques can provide power-bandwidth tradeoffs more effectively than would be possible through the use of any M-ary modulation scheme considered in this chapter [3].

In the most general sense, M-ary signalling can be regarded as a waveform-coding procedure, i.e., when we select an M-ary modulation technique instead of a binary one, we in effect have replaced the binary waveforms with better waveforms—either better for bandwidth performance (MPSK) or better for power performance (MFSK). Even though orthogonal MFSK signalling can be thought of as being a coded system, i.e., a first-order Reed-Muller code [8], we restrict our use of the term coded system to those traditional error-correction codes using redundancies, e.g., block codes or convolutional codes.

13.2.5 Minimum Bandwidth Requirements for MPSK and MFSK Signalling

The basic relationship between the symbol (or waveform) transmission rate R_s and the data rate R was shown in Eq. (13.11). Using this relationship together with Eqs. (13.13–13.16) and $R = 9600$ b/s, a summary of symbol rate, minimum bandwidth, and bandwidth efficiency for MPSK and noncoherent orthogonal MFSK was compiled for $M = 2, 4, 8, 16,$ and 32 (Table 13.1). Values of E_b/N_0 required to achieve a bit-error probability of 10^{-5} for MPSK and MFSK are also given for each value of M. These entries (which were computed using relationships that are presented later in this chapter) corroborate the tradeoffs shown in Fig. 13.1. As M increases, MPSK signalling provides more bandwidth efficiency at the

cost of increased E_b/N_0, whereas MFSK signalling allows for a reduction in E_b/N_0 at the cost of increased bandwidth.

TABLE 13.1 Symbol Rate, Minimum Bandwidth, Bandwidth Efficiency, and Required E_b/N_0 for MPSK and Noncoherent Orthogonal MFSK Signalling at 9600 bit/s

M	m	R (b/s)	R_s (symb/s)	MPSK Minimum Bandwidth (Hz)	MPSK R/W	MPSK E_b/N_0 (dB) $P_B = 10^{-5}$	Noncoherent Orthog MFSK Min Bandwidth (Hz)	MFSK R/W	MFSK E_b/N_0 (dB) $P_B = 10^{-5}$
2	1	9600	9600	9600	1	9.6	19,200	1/2	13.4
4	2	9600	4800	4800	2	9.6	19,200	1/2	10.6
8	3	9600	3200	3200	3	13.0	25,600	3/8	9.1
16	4	9600	2400	2400	4	17.5	38,400	1/4	8.1
32	5	9600	1920	1920	5	22.4	61,440	5/32	7.4

13.3 Example 1: Bandwidth-Limited Uncoded System

Suppose we are given a bandwidth-limited AWGN radio channel with an available bandwidth of $W = 4000$ Hz. Also, suppose that the link constraints (transmitter power, antenna gains, path loss, etc.) result in the ratio of received average signal-power to noise-power spectral density S/N_0 being equal to 53 dB-Hz. Let the required data rate R be equal to 9600 b/s, and let the required bit-error performance P_B be at most 10^{-5}. The goal is to choose a modulation scheme that meets the required performance. In general, an error-correction coding scheme may be needed if none of the allowable modulation schemes can meet the requirements. In this example, however, we shall find that the use of error-correction coding is not necessary.

13.3.1 Solution to Example 1

For any digital communication system, the relationship between received S/N_0 and received bit-energy to noise-power spectral density, E_b/N_0 was given in Eq. (13.6) and is briefly rewritten as

$$\frac{S}{N_0} = \frac{E_b}{N_0} R \tag{13.17}$$

Solving for E_b/N_0 in decibels, we obtain

$$\begin{aligned} \frac{E_b}{N_0}\ (\text{dB}) &= \frac{S}{N_0}\ (\text{dB-Hz}) - R\ (\text{dB-b/s}) \\ &= 53\ \text{dB-Hz} - (10 \times \log_{10} 9600)\ \text{dB-b/s} \\ &= 13.2\ \text{dB (or 20.89)} \end{aligned} \tag{13.18}$$

Since the required data rate of 9600 b/s is much larger than the available bandwidth of 4000 Hz, the channel is bandwidth limited. We therefore select MPSK as our modulation scheme. We have confined the possible modulation choices to be constant-envelope types; without such a restriction, we would be able to select a modulation type with greater bandwidth efficiency. To conserve power, we compute the *smallest possible* value of M such that the MPSK minimum bandwidth does not exceed the available bandwidth of 4000 Hz.

Table 13.1 shows that the smallest value of M meeting this requirement is $M = 8$. Next we determine whether the required bit-error performance of $P_B \leq 10^{-5}$ can be met by using 8-PSK modulation alone or whether it is necessary to use an error-correction coding scheme. Table 13.1 shows that 8-PSK alone will meet the requirements, since the required E_b/N_0 listed for 8-PSK is less than the received E_b/N_0 derived in Eq. (13.18). Let us imagine that we do not have Table 13.1, however, and evaluate whether or not error-correction coding is necessary.

Figure 13.2 shows the basic modulator/demodulator (MODEM) block diagram summarizing the functional details of this design. At the modulator, the transformation from data bits to symbols yields an output symbol rate R_s, that is, a factor $\log_2 M$ smaller than the input data-bit rate R, as is seen in Eq. (13.11). Similarly, at the input to the demodulator, the symbol-energy to noise-power spectral density E_S/N_0 is a factor $\log_2 M$ larger than E_b/N_0, since each symbol is made up of $\log_2 M$ bits. Because E_S/N_0 is larger than E_b/N_0 by the same factor that R_s is smaller than R, we can expand Eq. (13.17), as follows:

$$\frac{S}{N_0} = \frac{E_b}{N_0} R = \frac{E_s}{N_0} R_s \tag{13.19}$$

The demodulator receives a waveform (in this example, one of $M = 8$ possible phase shifts) during each time interval T_s. The probability that the demodulator makes a symbol error $P_E(M)$ is well approximated by the following equation for $M > 2$ [6]:

$$P_E(M) \cong 2Q\left[\sqrt{\frac{2E_s}{N_0}} \sin\left(\frac{\pi}{M}\right)\right] \tag{13.20}$$

where $Q(x)$, sometimes called the complementary error function, represents the probability under the tail of a zero-mean unit-variance Gaussian density function. It is defined as follows [18]:

$$Q(x) = \frac{1}{\sqrt{2\pi}} \int_x^\infty \exp\left(-\frac{u^2}{2}\right) \mathrm{d}u \tag{13.21}$$

A good approximation for $Q(x)$, valid for $x > 3$, is given by the following equation [2]

$$Q(x) \cong \frac{1}{x\sqrt{2\pi}} \exp\left(-\frac{x^2}{2}\right) \tag{13.22}$$

In Fig. 13.2 and all of the figures that follow, rather than show explicit probability relationships, the generalized notation $f(x)$ has been used to indicate some functional dependence on x.

A traditional way of characterizing communication efficiency in digital systems is in terms of the received E_b/N_0 in decibels. This E_b/N_0 description has become standard practice, but recall that there are no bits at the input to the demodulator; there are only waveforms that have been assigned bit meanings. The received E_b/N_0 represents a bit-apportionment of the arriving waveform energy.

To solve for $P_E(M)$ in Eq. (13.20), we first need to compute the ratio of received symbol-energy to noise-power spectral density E_s/N_0. Since from Eq. (13.18)

$$\frac{E_b}{N_0} = 13.2 \text{ dB (or } 20.89)$$

and because each symbol is made up of $\log_2 M$ bits, we compute the following using $M = 8$.

$$\frac{E_s}{N_0} = (\log_2 M) \frac{E_b}{N_0} = 3 \times 20.89 = 62.67 \tag{13.23}$$

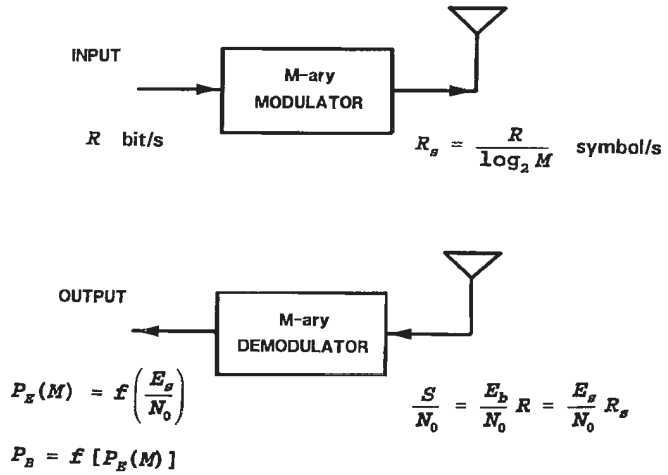


FIGURE 13.2 Basic modulator/demodulator (MODEM) without channel coding.

Using the results of Eq. (13.23) in Eq. (13.20), yields the symbol-error probability $P_E = 2.2 \times 10^{-5}$. To transform this to bit-error probability, we use the relationship between bit-error probability P_B and symbol-error probability P_E, for multiple-phase signalling [8] for $P_E \ll 1$ as follows:

$$P_B \cong \frac{P_E}{\log_2 M} = \frac{P_E}{m} \tag{13.24}$$

which is a good approximation when Gray coding is used for the bit-to-symbol assignment [6]. This last computation yields $P_B = 7.3 \times 10^{-6}$, which meets the required bit-error performance. No error-correction coding is necessary, and 8-PSK modulation represents the design choice to meet the requirements of the bandwidth-limited channel, which we had predicted by examining the required E_b/N_0 values in Table 13.1.

13.4 Example 2: Power-Limited Uncoded System

Now, suppose that we have exactly the same data rate and bit-error probability requirements as in Example 1, but let the available bandwidth W be equal to 45 kHz, and the available S/N_0 be equal to 48 dB-Hz. The goal is to choose a modulation or modulation/coding scheme that yields the required performance. We shall again find that error-correction coding is not required.

13.4.1 Solution to Example 2

The channel is clearly not bandwidth limited since the available bandwidth of 45 kHz is more than adequate for supporting the required data rate of 9600 bit/s. We find the received E_b/N_0 from Eq. (13.18), as follows:

$$\frac{E_b}{N_0}\ (\text{dB}) = 48\ \text{dB-Hz} - (10 \times \log_{10} 9600)\ \text{dB-b/s} = 8.2\ \text{dB (or 6.61)} \tag{13.25}$$

Since there is abundant bandwidth but a relatively small E_b/N_0 for the required bit-error probability, we consider that this channel is power limited and choose MFSK as the modulation scheme. To conserve power, we search for the *largest possible* M such that the MFSK minimum bandwidth is not expanded beyond our available bandwidth of 45 kHz. A search results in the choice of $M = 16$ (Table 13.1). Next, we determine whether the required error performance of $P_B \leq 10^{-5}$ can be met by using 16-FSK alone, i.e., without error-correction coding. Table 13.1 shows that 16-FSK alone meets the requirements, since the required E_b/N_0 listed for 16-FSK is less than the received E_b/N_0 derived in Eq. (13.25). Let us imagine again that we do not have Table 13.1, and evaluate whether or not error-correction coding is necessary.

The block diagram in Fig. 13.2 summarizes the relationships between symbol rate R_s, and bit rate R, and between E_s/N_0 and E_b/N_0, which is identical to each of the respective relationships in Example 1. The 16-FSK demodulator receives a waveform (one of 16 possible frequencies) during each symbol time interval T_s. For noncoherent orthogonal MFSK, the probability that the demodulator makes a symbol error $P_E(M)$ is approximated by the following upper bound [20]:

$$P_E(M) \leq \frac{M-1}{2} \exp\left(-\frac{E_s}{2N_0}\right) \tag{13.26}$$

To solve for $P_E(M)$ in Eq. (13.26), we compute E_S/N_0, as in Example 1. Using the results of Eq. (13.25) in Eq. (13.23), with $M = 16$, we get

$$\frac{E_s}{N_0} = (\log_2 M)\frac{E_b}{N_0} = 4 \times 6.61 = 26.44 \tag{13.27}$$

Next, using the results of Eq. (13.27) in Eq. (13.26), yields the symbol-error probability $P_E = 1.4 \times 10^{-5}$. To transform this to bit-error probability, P_B, we use the relationship between P_B and P_E for orthogonal signalling [20], given by

$$P_B = \frac{2^{m-1}}{(2^m - 1)} P_E \tag{13.28}$$

This last computation yields $P_B = 7.3 \times 10^{-6}$, which meets the required bit-error performance. Thus, we can meet the given specifications for this power-limited channel by using 16-FSK modulation, without any need for error-correction coding, as we had predicted by examining the required E_b/N_0 values in Table 13.1.

13.5 Example 3: Bandwidth-Limited and Power-Limited Coded System

We start with the same channel parameters as in Example 1 ($W = 4000$ Hz, $S/N_0 = 53$ dB-Hz, and $R = 9600$ b/s), with one exception.

In this example, we specify that P_B must be at most 10^{-9}. Table 13.1 shows that the system is both bandwidth limited and power limited, based on the available bandwidth of 4000 Hz and the available E_b/N_0 of 20.2 dB, from Eq. (13.18); 8-PSK is the only possible choice to meet the bandwidth constraint; however, the available E_b/N_0 of 20.2 dB is certainly insufficient to meet the required P_B of 10^{-9}. For this small value of P_B, we need to consider the performance improvement that error-correction coding can provide within the available bandwidth. In general, one can use convolutional codes or block codes.

The Bose–Chaudhuri–Hocquenghem (BCH) codes form a large class of powerful error-correcting cyclic (block) codes [7]. To simplify the explanation, we shall choose a block code from the BCH family. Table 13.2 presents a partial catalog of the available BCH codes in terms of n, k, and t, where k represents the number of information (or data) bits that the code transforms into a longer block of n coded bits (or channel bits), and t represents the largest number of incorrect channel bits that the code can correct within each n-sized block. The rate of a code is defined as the ratio k/n; its inverse represents a measure of the code's redundancy [7].

TABLE 13.2
BCH Codes (Partial Catalog)

n	k	t
7	4	1
15	11	1
	7	2
	5	3
31	26	1
	21	2
	16	3
	11	5
63	57	1
	51	2
	45	3
	39	4
	36	5
	30	6
127	120	1
	113	2
	106	3
	99	4
	92	5
	85	6
	78	7
	71	9
	64	10

13.5.1 Solution to Example 3

Since this example has the same bandwidth-limited parameters given in Example 1, we start with the same 8-PSK modulation used to meet the stated bandwidth constraint. We now employ error-correction coding, however, so that the bit-error probability can be lowered to $P_B \leq 10^{-9}$.

To make the optimum code selection from Table 13.2, we are guided by the following goals.

1. The output bit-error probability of the combined modulation/coding system must meet the system error requirement.
2. The rate of the code must not expand the required transmission bandwidth beyond the available channel bandwidth.
3. The code should be as simple as possible. Generally, the shorter the code, the simpler will be its implementation.

The uncoded 8-PSK minimum bandwidth requirement is 3200 Hz (Table 13.1) and the allowable channel bandwidth is 4000 Hz, and so the uncoded signal bandwidth can be increased by no more than a factor of 1.25 (i.e., an expansion of 25%). The very first step in this (simplified) code selection example is to eliminate the candidates in Table 13.2 that would expand the bandwidth by more than 25%. The remaining entries form a much reduced set of bandwidth-compatible codes (Table 13.3).

In Table 13.3, a column designated Coding Gain G (for MPSK at $P_B = 10^{-9}$) has been added. Coding gain in decibels is defined as follows:

$$G = \left(\frac{E_b}{N_0}\right)_{\text{uncoded}} - \left(\frac{E_b}{N_0}s\right)_{\text{coded}} \tag{13.29}$$

G can be described as the reduction in the required E_b/N_0 (in decibels) that is needed due to the error-performance properties of the channel coding. G is a function of the

TABLE 13.3 Bandwidth-Compatible BCH Codes

n	k	t	Coding Gain, G (dB) MPSK, $P_B = 10^{-9}$
31	26	1	2.0
63	57	1	2.2
	51	2	3.1
127	120	1	2.2
	113	2	3.3
	106	3	3.9

modulation type and bit-error probability, and it has been computed for MPSK at $P_B = 10^{-9}$ (Table 13.3). For MPSK modulation, G is relatively independent of the value of M. Thus, for a particular bit-error probability, a given code will provide about the same coding gain when used with any of the MPSK modulation schemes. Coding gains were calculated using a procedure outlined in the subsequent Calculating Coding Gain section.

A block diagram summarizes this system, which contains both modulation and coding (Fig. 13.3). The introduction of encoder/decoder blocks brings about additional transformations. The relationships that exist when transforming from R b/s to R_c channel-b/s to R_s symbol/s are shown at the encoder/modulator. Regarding the channel-bit rate R_c, some authors prefer to use the units of channel-symbol/s (or code-symbol/s). The benefit is that error-correction coding is often described more efficiently with nonbinary digits. We reserve the term symbol for that group of bits mapped onto an electrical waveform for transmission, and we designate the units of R_c to be channel-b/s (or coded-b/s).

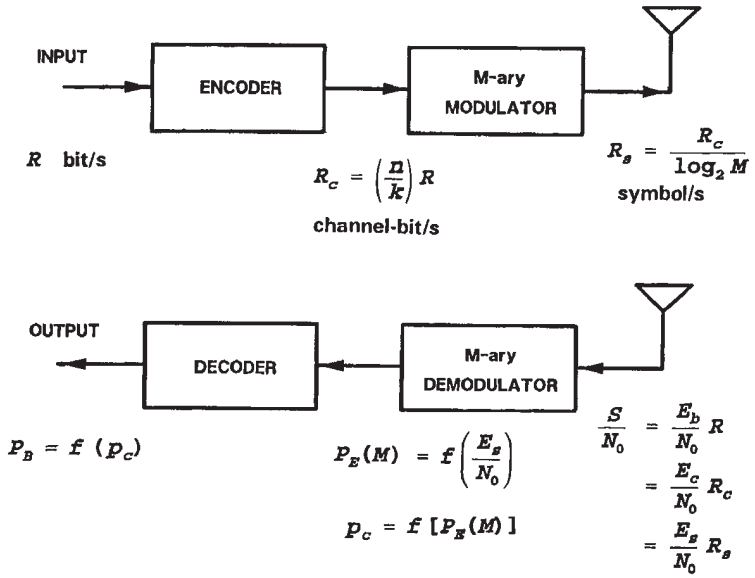


FIGURE 13.3 MODEM with channel coding.

We assume that our communication system cannot tolerate any message delay, so that the channel-bit rate R_c must exceed the data-bit rate R by the factor n/k. Further, each symbol is made up of $\log_2 M$ channel bits, and so the symbol rate R_s is less than R_c by the factor $\log_2 M$. For a system containing both modulation and coding, we summarize the

rate transformations as follows:

$$R_c = \left(\frac{n}{k}\right) R \tag{13.30}$$

$$R_s = \frac{R_c}{\log_2 M} \tag{13.31}$$

At the demodulator/decoder in Fig.13.3, the transformations among data-bit energy, channel- bit energy, and symbol energy are related (in a reciprocal fashion) by the same factors as shown among the rate transformations in Eqs. (13.30) and (13.31). Since the encoding transformation has replaced k data bits with n channel bits, then the ratio of channel-bit energy to noise-power spectral density E_c/N_0 is computed by decrementing the value of E_b/N_0 by the factor k/n. Also, since each transmission symbol is made up of $\log_2 M$ channel bits, then E_S/N_0, which is needed in Eq. (13.20) to solve for P_E, is computed by incrementing E_c/N_0 by the factor $\log_2 M$. For a system containing both modulation and coding, we summarize the energy to noise-power spectral density transformations as follows:

$$\frac{E_c}{N_0} = \left(\frac{k}{n}\right) \frac{E_b}{N_0} \tag{13.32}$$

$$\frac{E_s}{N_0} = (\log_2 M) \frac{E_c}{N_0} \tag{13.33}$$

Using Eqs. (13.30) and (13.31), we can now expand the expression for S/N_0 in Eq. (13.19), as follows (Appendix).

$$\frac{S}{N_0} = \frac{E_b}{N_0} R = \frac{E_c}{N_0} R_c = \frac{E_s}{N_0} R_s \tag{13.34}$$

As before, a standard way of describing the link is in terms of the received E_b/N_0 in decibels. However, there are no data bits at the input to the demodulator, and there are no channel bits; there are only waveforms that have bit meanings and, thus, the waveforms can be described in terms of bit-energy apportionments.

Since S/N_0 and R were given as 53 dB-Hz and 9600 b/s, respectively, we find as before, from Eq. (13.18), that the received $E_b/N_0 = 13.2$ dB. The received E_b/N_0 is fixed and independent of n, k, and t (Appendix). As we search, in Table 13.3 for the ideal code to meet the specifications, we can iteratively repeat the computations suggested in Fig. 13.3. It might be useful to program on a personal computer (or calculator) the following four steps as a function of n, k, and t. Step 1 starts by combining Eqs. (13.32) and (13.33), as follows.

Step 1:

$$\frac{E_s}{N_0} = (\log_2 M) \frac{E_c}{N_0} = (\log_2 M) \left(\frac{k}{n}\right) \frac{E_b}{N_0} \tag{13.35}$$

Step 2:

$$P_E(M) \cong 2Q \left[\sqrt{\frac{2E_s}{N_0}} \sin\left(\frac{\pi}{M}\right)\right] \tag{13.36}$$

which is the approximation for symbol-error probability P_E rewritten from Eq. (13.20). At each symbol-time interval, the demodulator makes a symbol decision, but it delivers a channel-bit sequence representing that symbol to the decoder. When the channel-bit output of the demodulator is quantized to two levels, 1 and 0, the demodulator is said to make hard decisions. When the output is quantized to more than two levels, the demodulator

is said to make soft decisions [15]. Throughout this paper, we shall assume hard-decision demodulation.

Now that we have a decoder block in the system, we designate the channel-bit-error probability out of the demodulator and into the decoder as p_c, and we reserve the notation P_B for the bit-error probability out of the decoder. We rewrite Eq. (13.24) in terms of p_c for $P_E \ll 1$ as follows.

Step 3:

$$p_c \cong \frac{P_E}{\log_2 M} = \frac{P_E}{m} \tag{13.37}$$

relating the channel-bit-error probability to the symbol-error probability out of the demodulator, assuming Gray coding, as referenced in Eq. (13.24).

For traditional channel-coding schemes and a given value of received S/N_0, the value of E_s/N_0 with coding will always be less than the value of E_s/N_0 without coding. Since the demodulator with coding receives less E_s/N_0, it makes more errors! When coding is used, however, the system error-performance does not only depend on the performance of the demodulator, it also depends on the performance of the decoder. For error-performance improvement due to coding, the decoder must provide enough error correction to more than compensate for the poor performance of the demodulator.

The final output decoded bit-error probability P_B depends on the particular code, the decoder, and the channel-bit-error probability p_c. It can be expressed by the following approximation [11].

Step 4:

$$P_B \cong \frac{1}{n} \sum_{j=t+1}^{n} j \binom{n}{j} p_c^j (1-p_c)^{n-j} \tag{13.38}$$

where t is the largest number of channel bits that the code can correct within each block of n bits. Using Eqs. (13.35–13.38) in the four steps, we can compute the decoded bit-error probability P_B as a function of n, k, and t for each of the codes listed in Table 13.3. The entry that meets the stated error requirement with the largest possible code rate and the smallest value of n is the double-error correcting (63, 51) code. The computations are as follows.

Step 1:

$$\frac{E_s}{N_0} = 3\left(\frac{51}{63}\right) 20.89 = 50.73$$

where $M = 8$, and the received $E_b/N_0 = 13.2$ dB (or 20.89).

Step 2:

$$P_E \cong 2Q\left[\sqrt{101.5} \times \sin\left(\frac{\pi}{8}\right)\right] = 2Q(3.86) = 1.2 \times 10^{-4}$$

Step 3:

$$p_c \cong \frac{1.2 \times 10^{-4}}{3} = 4 \times 10^{-5}$$

Step 4:

$$\begin{aligned} P_B &\cong \frac{3}{63}\binom{63}{3}\left(4 \times 10^{-5}\right)^3 \left(1 - 4 \times 10^{-5}\right)^{60} \\ &\quad + \frac{4}{63}\binom{63}{4}\left(4 \times 10^{-5}\right)^4 \left(1 - 4 \times 10^{-5}\right)^{59} + \cdots \\ &= 1.2 \times 10^{-10} \end{aligned}$$

where the bit-error-correcting capability of the code is $t = 2$. For the computation of P_B in step 4, we need only consider the first two terms in the summation of Eq. (13.38) since the other terms have a vanishingly small effect on the result. Now that we have selected the (63, 51) code, we can compute the values of channel-bit rate R_c and symbol rate R_s using Eqs. (13.30) and (13.31), with $M = 8$,

$$\begin{aligned} R_c &= \left(\frac{n}{k}\right) R = \left(\frac{63}{51}\right) 9600 \approx 11{,}859 \text{ channel-b/s} \\ R_s &= \frac{R_c}{\log_2 M} = \frac{11859}{3} = 3953 \text{ symbol/s} \end{aligned}$$

13.5.2 Calculating Coding Gain

Perhaps a more direct way of finding the simplest code that meets the specified error performance is to first compute how much coding gain G is required in order to yield $P_B = 10^{-9}$ when using 8-PSK modulation alone; then, from Table 13.3, we can simply choose the code that provides this performance improvement. First, we find the uncoded E_s/N_0 that yields an error probability of $P_B = 10^{-9}$, by writing from Eqs. (13.24) and (13.36), the following:

$$P_B \cong \frac{P_E}{\log_2 M} \cong \frac{2Q\left[\sqrt{\frac{2E_s}{N_0}}\sin\left(\frac{\pi}{M}\right)\right]}{\log_2 M} = 10^{-9} \tag{13.39}$$

At this low value of bit-error probability, it is valid to use Eq. (13.22) to approximate $Q(x)$ in Eq. (13.39) By trial and error (on a programmable calculator), we find that the uncoded $E_s/N_0 = 120.67 = 20.8$ dB, and since each symbol is made up of $\log_2 8 = 3$ bits, the required $(E_b/N_0)_{\text{uncoded}} = 120.67/3 = 40.22 = 16$ dB. From the given parameters and Eq. (13.18), we know that the received $(E_b/N_0)_{\text{coded}} = 13.2$ dB. Using Eq. (13.29), the required coding gain to meet the bit-error performance of $P_B = 10^{-9}$ in decibels is

$$G = \left(\frac{E_b}{N_0}\right)_{\text{uncoded}} - \left(\frac{E_b}{N_0}\right)_{\text{coded}} = 16 - 13.2 = 2.8$$

To be precise, each of the E_b/N_0 values in the preceding computation must correspond to exactly the same value of bit-error probability (which they do not). They correspond to $P_B = 10^{-9}$ and $P_B = 1.2 \times 10^{-10}$, respectively. At these low probability values, however, even with such a discrepancy, this computation still provides a good approximation of the required coding gain. In searching Table 13.3 for the simplest code that will yield a coding gain of at least 2.8 dB, we see that the choice is the (63, 51) code, which corresponds to the same code choice that we made earlier.

13.6 Example 4: Direct-Sequence (DS) Spread-Spectrum Coded System

Spread-spectrum systems are not usually classified as being bandwidth- or power-limited. They are generally perceived to be power-limited systems, however, because the bandwidth occupancy of the information is much larger than the bandwidth that is intrinsically needed for the information transmission. In a direct-sequence spread-spectrum (DS/SS) system, spreading the signal bandwidth by some factor permits lowering the signal-power spectral density by the same factor (the total average signal power is the same as before spreading).

The bandwidth spreading is typically accomplished by multiplying a relatively narrowband data signal by a wideband spreading signal. The spreading signal or spreading code is often referred to as a pseudorandom code or PN code.

13.6.1 Processing Gain

A typical DS/SS radio system is often described as a two-step BPSK modulation process. In the first step, the carrier wave is modulated by a bipolar data waveform having a value $+1$ or -1 during each data-bit duration; in the second step, the output of the first step is multiplied (modulated) by a bipolar PN-code waveform having a value $+1$ or -1 during each PN-code-bit duration. In reality, DS/SS systems are usually implemented by first multiplying the data waveform by the PN-code waveform and then making a single pass through a BPSK modulator. For this example, however, it is useful to characterize the modulation process in two separate steps—the outer modulator/demodulator for the data, and the inner modulator/demodulator for the PN code (Fig. 13.4).

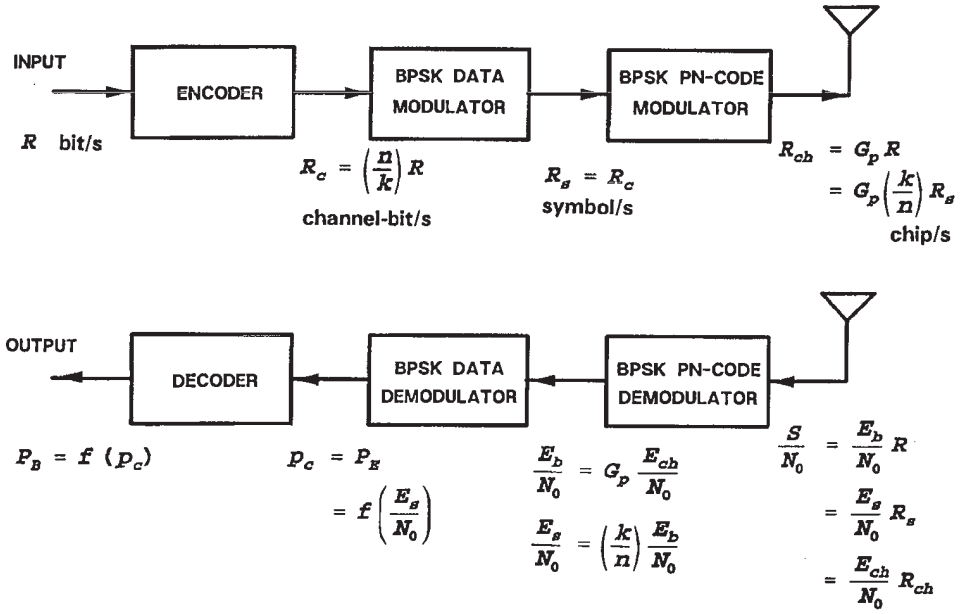


FIGURE 13.4 Direct-sequence spread-spectrum MODEM with channel coding.

A spread-spectrum system is characterized by a processing gain G_p, that is defined in terms of the spread-spectrum bandwidth W_{ss} and the data rate R as follows [20]:

$$G_p = \frac{W_{\text{ss}}}{R} \tag{13.40}$$

For a DS/SS system, the PN-code bit has been given the name chip, and the spread-spectrum signal bandwidth can be shown to be about equal to the chip rate R_{ch} as follows:

$$G_p = \frac{R_{\text{ch}}}{R} \tag{13.41}$$

Some authors define processing gain to be the ratio of the spread-spectrum bandwidth to

the symbol rate. This definition separates the system performance that is due to bandwidth spreading from the performance that is due to error-correction coding. Since we ultimately want to relate all of the coding mechanisms relative to the information source, we shall conform to the most usually accepted definition for processing gain, as expressed in Eqs. (13.40) and (13.41).

A spread-spectrum system can be used for interference rejection and for multiple access (allowing multiple users to access a communications resource simultaneously). The benefits of DS/SS signals are best achieved when the processing gain is very large; in other words, the chip rate of the spreading (or PN) code is much larger than the data rate. In such systems, the large value of G_p allows the signalling chips to be transmitted at a power level well below that of the thermal noise. We will use a value of $G_p = 1000$. At the receiver, the despreading operation correlates the incoming signal with a synchronized copy of the PN code and, thus, accumulates the energy from multiple (G_p) chips to yield the energy per data bit. The value of G_p has a major influence on the performance of the spread-spectrum system application. We shall see, however, that the value of G_p has no effect on the received E_b/N_0. In other words, spread spectrum techniques offer no error-performance advantage over thermal noise. For DS/SS systems, there is no disadvantage either! Sometimes such spread-spectrum radio systems are employed only to enable the transmission of very small power-spectral densities and thus avoid the need for FCC licensing [16].

13.6.2 Channel Parameters for Example 13.4

Consider a DS/SS radio system that uses the same (63, 51) code as in the previous example. Instead of using MPSK for the data modulation, we shall use BPSK. Also, we shall use BPSK for modulating the PN-code chips. Let the received $S/N_0 = 48$ dB-Hz, the data rate $R = 9600$ b/s, and the required $P_B \leq 10^{-6}$. For simplicity, assume that there are no bandwidth constraints. Our task is simply to determine whether or not the required error performance can be achieved using the given system architecture and design parameters. In evaluating the system, we will use the same type of transformations used in the previous examples.

13.6.3 Solution to Example 13.4

A typical DS/SS system can be implemented more simply than the one shown in Fig. 13.4. The data and the PN code would be combined at baseband, followed by a single pass through a BPSK modulator. We will, however, assume the existence of the individual blocks in Fig. 13.4 because they enhance our understanding of the transformation process. The relationships in transforming from data bits, to channel bits, to symbols, and to chips Fig. 13.4 have the same pattern of subtle but straightforward transformations in rates and energies as previous relationships (Figs. 13.2 and 13.3). The values of R_c, R_s, and R_{ch} can now be calculated immediately since the (63, 51) BCH code has already been selected. From Eq. (13.30) we write

$$R_c = \left(\frac{n}{k}\right) R = \left(\frac{63}{51}\right) 9600 \approx 11{,}859 \text{ channel-b/s}$$

Since the data modulation considered here is BPSK, then from Eq. (13.31) we write

$$R_s = R_c \approx 11{,}859 \text{ symbol/s}$$

and from Eq. (13.41), with an assumed value of $G_p = 1000$

$$R_{\text{ch}} = G_p R = 1000 \times 9600 = 9.6 \times 10^6 \text{ chip/s}$$

Since we have been given the same S/N_0 and the same data rate as in Example 2, we find the value of received E_b/N_0 from Eq. (13.25) to be 8.2 dB (or 6.61). At the demodulator, we can now expand the expression for S/N_0 in Eq. (13.34) and the Appendix as follows:

$$\frac{S}{N_0} = \frac{E_b}{N_0} R = \frac{E_c}{N_0} R_c = \frac{E_s}{N_0} R_s = \frac{E_{\text{ch}}}{N_0} R_{\text{ch}} \tag{13.42}$$

Corresponding to each transformed entity (data bit, channel bit, symbol, or chip) there is a change in rate and, similarly, a reciprocal change in energy-to-noise spectral density for that received entity. Equation (13.42) is valid for any such transformation when the rate and energy are modified in a reciprocal way. There is a kind of *conservation of power* (or energy) phenomenon that exists in the transformations. The total received average power (or total received energy per symbol duration) is fixed regardless of how it is computed, on the basis of data bits, channel bits, symbols, or chips.

The ratio E_{ch}/N_0 is much lower in value than E_b/N_0. This can be seen from Eqs. (13.42) and (13.41), as follows:

$$\frac{E_{\text{ch}}}{N_0} = \frac{S}{N_0}\left(\frac{1}{R_{\text{ch}}}\right) = \frac{S}{N_0}\left(\frac{1}{G_p R}\right) = \left(\frac{1}{G_p}\right)\frac{E_b}{N_0} \tag{13.43}$$

But, even so, the despreading function (when properly synchronized) accumulates the energy contained in a quantity G_p of the chips, yielding the same value $E_b/N_0 = 8.2$ dB, as was computed earlier from Eq. (13.25). Thus, the DS spreading transformation has no effect on the error performance of an AWGN channel [15], and the value of G_p has no bearing on the value of P_B in this example.

From Eq. (13.43), we can compute, in decibels,

$$\begin{aligned} \frac{E_{\text{ch}}}{N_0} &= E_b/N_0 - G_p \\ &= 8.2 - (10 \times \log_{10} 1000) \\ &= -21.8 \end{aligned} \tag{13.44}$$

The chosen value of processing gain ($G_p = 1000$) enables the DS/SS system to operate at a value of chip energy well below the thermal noise, with the same error performance as without spreading.

Since BPSK is the data modulation selected in this example, each message symbol therefore corresponds to a single channel bit, and we can write

$$\frac{E_s}{N_0} = \frac{E_c}{N_0} = \left(\frac{k}{n}\right)\frac{E_b}{N_0} = \left(\frac{51}{63}\right) \times 6.61 = 5.35 \tag{13.45}$$

where the received $E_b/N_0 = 8.2$ dB (or 6.61). Out of the BPSK data demodulator, the symbol-error probability P_E (and the channel-bit error probability p_c) is computed as follows [15]:

$$p_c = P_E = Q\left(\sqrt{\frac{2E_c}{N_0}}\right) \tag{13.46}$$

Using the results of Eq. (13.45) in Eq. (13.46) yields

$$p_c = Q(3.27) = 5.8 \times 10^{-4}$$

Finally, using this value of p_c in Eq. (13.38) for the (63,51) double-error correcting code yields the output bit-error probability of $P_B = 3.6 \times 10^{-7}$. We can, therefore, verify that for the given architecture and design parameters of this example the system does, in fact, achieve the required error performance.

13.7 Conclusion

The goal of this section has been to review fundamental relationships used in evaluating the performance of digital communication systems. First, we described the concept of a link and a channel and examined a radio system from its transmitting segment up through the output of the receiving antenna. We then examined the concept of bandwidth-limited and power-limited systems and how such conditions influence the system design when the choices are confined to MPSK and MFSK modulation. Most important, we focused on the definitions and computations involved in transforming from data bits to channel bits to symbols to chips. In general, most digital communication systems share these concepts; thus, understanding them should enable one to evaluate other such systems in a similar way.

Appendix: Received E_b/N_0 Is Independent of the Code Parameters

Starting with the basic concept that the received average signal power S is equal to the received symbol or waveform energy, E_s, divided by the symbol-time duration, T_s (or multiplied by the symbol rate, R_s), we write

$$\frac{S}{N_0} = \frac{E_s/T_s}{N_0} = \frac{E_s}{N_0} R_s \tag{A13.1}$$

where N_0 is noise-power spectral density.

Using Eqs. (13.27) and (13.25), rewritten as

$$\frac{E_s}{N_0} = (\log_2 M)\frac{E_c}{N_0} \qquad \text{and} \qquad R_s = \frac{R_c}{\log_2 M}$$

let us make substitutions into Eq. (A13.1), which yields

$$\frac{S}{N_0} = \frac{E_c}{N_0} R_c \tag{A13.2}$$

Next, using Eqs. (13.26) and (13.24), rewritten as

$$\frac{E_c}{N_0} = \left(\frac{k}{n}\right)\frac{E_b}{N_0} \qquad \text{and} \qquad R_c = \left(\frac{n}{k}\right) R$$

let us now make substitutions into Eq. (A13.2), which yields the relationship expressed in Eq. (13.11)

$$\frac{S}{N_0} = \frac{E_b}{N_0} R \tag{A13.3}$$

Hence, the received E_b/N_0 is only a function of the received S/N_0 and the data rate R. It is independent of the code parameters, n, k, and t. These results are summarized in Fig. 13.3.

References

[1] Anderson, J.B. and Sundberg, C.-E.W., Advances in constant envelope coded modulation, *IEEE Commun., Mag.*, 29(12), 36–45, 1991.

[2] Borjesson, P.O. and Sundberg, C.E., Simple approximations of the error function $Q(x)$ for communications applications, *IEEE Trans. Comm.*, COM-27, 639–642, Mar. 1979.

[3] Clark Jr., G.C. and Cain, J.B., *Error-Correction Coding for Digital Communications,* Plenum Press, New York, 1981.

[4] Hodges, M.R.L., The GSM radio interface, *British Telecom Technol. J.*, 8(1), 31–43, 1990.

[5] Johnson, J.B., Thermal agitation of electricity in conductors, *Phys. Rev.*, 32, 97–109, Jul. 1928.

[6] Korn, I., *Digital Communications,* Van Nostrand Reinhold Co., New York, 1985.

[7] Lin, S. and Costello Jr., D.J., *Error Control Coding: Fundamentals and Applications,* Prentice-Hall, Englewood Cliffs, NJ, 1983.

[8] Lindsey, W.C. and Simon, M.K., *Telecommunication Systems Engineering,* Prentice-Hall, Englewood Cliffs, NJ, 1973.

[9] Nyquist, H., Thermal agitation of electric charge in conductors, *Phys. Rev.*, 32, 110–113, Jul. 1928.

[10] Nyquist, H., Certain topics on telegraph transmission theory, *Trans. AIEE,* 47, 617–644, Apr. 1928.

[11] Odenwalder, J.P., *Error Control Coding Handbook.* Linkabit Corp., San Diego, CA, Jul. 15, 1976.

[12] Shannon, C.E., A mathematical theory of communication, *BSTJ.* 27, 379–423, 623–657, 1948.

[13] Shannon, C.E., Communication in the presence of noise, *Proc. IRE.* 37(1), 10–21, 1949.

[14] Sklar, B., What the system link budget tells the system engineer or how I learned to count in decibels, *Proc. of the Intl. Telemetering Conf.*, San Diego, CA, Nov. 1979.

[15] Sklar, B., *Digital Communications: Fundamentals and Applications,* Prentice-Hall, Englewood Cliffs, NJ, 1988.

[16] Title 47, *Code of Federal Regulations,* Part 15 Radio Frequency Devices.

[17] Ungerboeck, G., Trellis-coded modulation with redundant signal sets, Pt. I and II, *IEEE Comm. Mag.*, 25, 5–21. Feb. 1987.

[18] Van Trees, H.L., *Detection, Estimation, and Modulation Theory,* Pt. I, John Wiley & Sons, New York, 1968.

[19] Viterbi, A.J., *Principles of Coherent Communication,* McGraw-Hill, New York, 1966.

[20] Viterbi, A.J., Spread spectrum communications—myths and realities, *IEEE Comm. Mag.*, 11–18, May, 1979.

Further Information

A useful compilation of selected papers can be found in: *Cellular Radio & Personal Communications–A Book of Selected Readings,* edited by Theodore S. Rappaport, Institute of Electrical and Electronics Engineers, Inc., Piscataway, New Jersey, 1995. Fundamental design issues, such as propagation, modulation, channel coding, speech coding, multiple-accessing and networking, are well represented in this volume.

Another useful sourcebook that covers the fundamentals of mobile communications in great detail is: *Mobile Radio Communications,* edited by Raymond Steele, Pentech Press, London 1992. This volume is also available through the Institute of Electrical and Electronics Engineers, Inc., Piscataway, New Jersey.

For spread spectrum systems, an excellent reference is: *Spread Spectrum Communications Handbook,* by Marvin K. Simon, Jim K. Omura, Robert A. Scholtz, and Barry K. Levitt, McGraw-Hill Inc., New York, 1994.

14

Telecommunications Standardization

14.1 Introduction 14-1
14.2 Global Standardization 14-2
ITU-T • ITU-R • BDT • ISO/IEC JTC 1
14.3 Regional Standardization 14-6
CITEL
14.4 National Standardization 14-9
ANSI T1 • TIA • TTC
14.5 Intellectual Property 14-12
14.6 Standards Coordination 14-13
14.7 Scientific 14-14
14.8 Standards Development Cycle 14-14
Defining Terms 14-15
Further Information 14-16

Spiros Dimolitsas
Lawrence Livermore National Laboratory

Michael Onufry
COMSAT Laboratories

14.1 Introduction

National economies are increasingly becoming information based, where networking and information transport provide a foundation for productivity and economic growth. Concurrently, many countries are rapidly adopting deregulation policies that are resulting in a telecommunications industry that is increasingly multicarrier and multivendor based, and where interconnectivity and compatibility between different networks is emerging as key to the success of this technological and regulatory transition. The communications industry has, consequently, become more interested in standardization; **standards** give manufacturers, service providers, and users freedom of choice at reasonable cost.

In this chapter, a review is provided of the primary telecommunications standards setting bodies. As will be seen, these bodies are often driven by slightly different underlying philosophies, but the output of their activities, i.e., the standards, possess essentially the same characteristics. An all-encompassing review of standardization bodies is not attempted here; this would clearly take many volumes to describe. Furthermore, as country after country increasingly deregulates its telecommunication industry, new standards setting bodies emerge to fill in the void of the de-facto (but no longer existing) standards setting bodies: the national telecommunications administration.

The principal communications standards bodies that will be covered are the following: the International Telecommunications Union (**ITU**); the United States **ANSI** Committee

0-8493-8597-0/99/$0.00+$.50

© 1999 by CRC Press LLC

T1 on Telecommunications; the Telecommunications Industry Association (**TIA**); the European Telecommunications Standards Institute (**ETSI**); the Inter-American Telecommunications Commission (**CITEL**); the Japanese Telecommunications Technology Committee (**TTC**); and the Institute of Electrical and Electronics Engineers (**IEEE**). Not addressed explicitly are other standards setting bodies that are either national or regional in character, even though it is recognized that sometimes there is overlap in scope with the bodies explicitly covered here.

Most notably, standards setting bodies that are not covered, but that are worth noting, include: the United States ANSI Committee X3; the International Standards Organization (**ISO**), the International Electrotechnical Commission (**IEC**) [except ISO/IEC joint technical committee (JTC) 1], the Telecommunications Standards Advisory Council of Canada (TSACC), the Australian Telecommunications Standardization Committee (ATSC), the Telecommunication Technology Association (TTA) in Korea, and several forums (whose scope is, in principle, somewhat different) such as the asynchronous transfer mode (ATM) forum, the frame relay forum, the integrated digital services network (ISDN) users' forum, and telocator. As will be described later, many of these bodies operate in a coherent fashion through a mechanism developed by the Interregional Telecommunications Standards Conference (ITSC) and its successor, the Global Standards Collaboration (**GSC**).

14.2 Global Standardization

When it comes to setting global communications standards, the ITU comes to the forefront. The ITU is an intergovernmental organization, whereby each sovereign state that is a member of the United Nations may become a member of the ITU. Member governments (in most cases represented by their telecommunications administrations) are constitutional members with a right to vote. Other organizations, such as network and service providers, manufacturers, and scientific and industrial organizations also participate in ITU activities but with a lower legal status.

ITU traces its history back to 1865 in the era of telegraphy. The supreme organ of the ITU is the plenipotentiary conference, which is held not less than every five years and plays a major role in the management of ITU. In 1993 the ITU as a U.N.-specialized agency was reorganized into three sectors (see Fig. 14.1): The *telecommunications standardization* sector (**ITU-T**), the *radiocommunications* sector (**ITU-R**), and the *development* sector (BDT). These sectors' activities are, respectively, standardization of telecommunications, including radio communications; regulation of telecommunications (mainly for radio communications); and development of telecommunications.

It should be noted that, in general, the ITU-T is the successor of the international telephone and telegraph consultative committee (**CCITT**) of the ITU with additional responsibilities for standardization of network-related radio communications. Similarly, the ITU-R is the successor of the international radio consultative committee (**CCIR**) and the international frequency registration bureau (IFRB) of the ITU (after transferring some of its standardization activities to the ITU-T). The BDT is a new sector, which became operational in 1989.

14.2.1 ITU-T

Within the ITU structure, standardization work is undertaken by a number of study groups (SG) dealing with specific areas of communications. There are currently 14 study groups, as shown in Table 14.1.

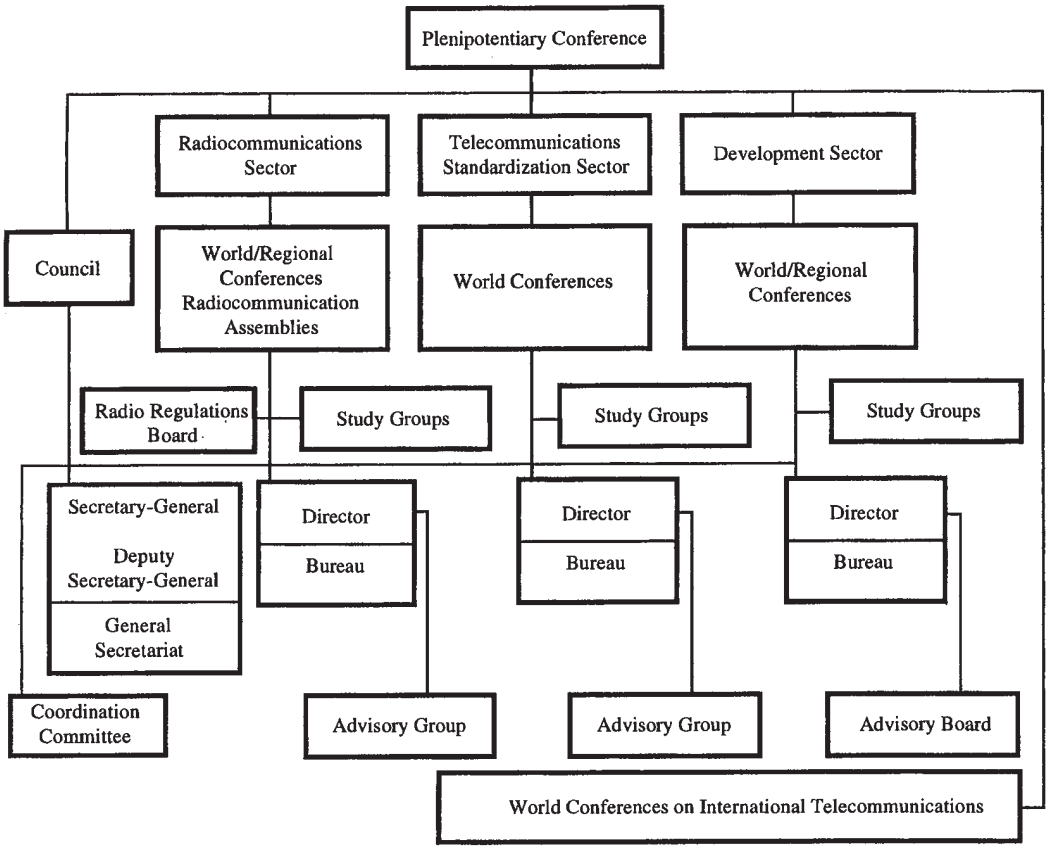


FIGURE 14.1 The ITU structure.

Study groups develop standards for their respective work areas, which then have to be agreed upon by consensus—a process that for the time being is reserved to administrations only. The standards so developed are called **recommendations** to indicate their legal nonbinding nature. Technically, however, there is no distinction between recommendations developed by the ITU and standards developed by other standards setting bodies.

The study groups' work is undertaken by delegation members, sent or sponsored by their national administrations, and delegates from recognized private operating organizations (RPOA), scientific and industrial organizations (SIO) or international organizations. Because an ITU-T study group can typically have from 100 to more than 500 participating members and deal with 20–50 project standards, the work of each study group is often divided among working parties (WP). Such working parties are usually split further into experts' groups led by a chair or "rapporteur" with responsibility for leading the work defined in an approved active question or subelement of a question.

To coordinate standardization work that spans several study groups, two joint coordination groups (**JCG**) have also been established (not shown in Fig. 14.1): International Mobile Communications (IMT-2000) and Satellite Matters.

Such groups do not have executive powers but are merely there to coordinate work of pervasive interest within the ITU-T sector.

Also part of the ITU-T structure is the telecommunications standardization bureau (TSB) or, as it was formerly called, the CCITT secretariat. The TSB is responsible for the organization of numerous meetings held by the sector each year as well as all other support

TABLE 14.1 ITU-T Study Group Structure

SG 2	Network and service operation Lead SG on Service definition, Numbering, Routing and Global Mobility
SG 3	Tariff and accounting principles
SG 4	TMN and network maintenance Lead SG on Telecommunication management network (TMN) studies
SG 5	Protection against electromagnetic environmental effects
SG 6	Outside plant
SG 7	Data networks and open systems communications Lead SG on Open Distributed Processing (ODP), Frame Relay and for Communications System Security
SG 8	Characteristics of telematic services Lead SG on Facsimile
SG 9	Television and sound transmission
SG 10	Languages and general software aspects for telecommunications systems
SG 11	Signalling requirements and protocols Lead SG on Intelligent Network and IMT-2000
SG 12	End-to-end transmission performance of networks and terminals
SG 13	General network aspects Lead SG on General network aspects Global Information Infrastructures and Broadband ISDN
SG 15	Transport networks, systems and equipment Lead SG on Access Network Transport
SG 16	Transmission systems and equipment Lead SG on Multimedia services and systems

services required to ensure the smooth and efficient operation of the sector (including, but not limited to, document production and distribution). The TSB is headed by a director, who holds the executive power and, in collaboration with the study groups, bears full responsibility for the ITU-T activities. In this structure, unlike other U.N. organizations, the secretary general is the legal representative of the ITU, with the executive powers being vested in the director.

Finally, the ITU-T is supported by an advisory group, i.e., the telecommunications standardization advisory group (TSAG), which together with interested ITU members, the ITU-T Director, and ITU-T SG chairman, guides standardization activities.

14.2.2 ITU-R

The radiocommunications sector emphasizes the regulatory and pure radio-interface aspects. The functional structure of the ITU-R currently includes eight study groups, (shown in Table 14.2) a radiocommunications bureau, and an advisory board. The role of the latter two elements is very similar to the ITU-T and, thus, need not be repeated here.

As within the ITU-T, there are areas of pervasive interest, and so areas of common interest can be found between the ITU-T and ITU-R where activities need to be coordinated. To achieve this objective, two intersector coordination groups (**ICG**) have been established (not shown in Fig. 14.1) dealing with international mobile telecommunications (IMT-2000), and satellite matters.

Three major special activities have been organized within ITU-R:

- IMT-2000 (formerly known as Future Public Land Mobile Telecommunications Systems FPLMTS). The objective of the International Mobile Telecommunications (IMT)-2000 activity is to provide seamless satellite and terrestrial operation

TABLE 14.2 ITU-R Study Group Structure

SG 1	Spectrum management
SG 3	Radio wave propagation
SG 4	Fixed satellite service
SG 7	Science services
SG 8	Mobile, radio determination, amateur and related satellite services
SG 9	Fixed service
SG 10	Broadcasting services: sound
SG 11	Broadcasting services: television

of mobile terminals throughout the world—anywhere, anytime—where communication coverage requires interoperation of satellite and terrestrial networks. This is to be accomplished using technology available around the year 2000.

- Mobile-satellite and radionavigation-satellite service (MSS-RNSS). The rapid growth of service in these areas has created a need to focus attention on interference and spectrum allocation.
- Wireless Access Systems (WAS). This is an application of radio technology and personal communications systems directed toward lowering the installation and maintenance cost of the local access network. The traditional high cost has prevented penetration of basic telephone service in evolving and developing countries of the world. Overcoming this barrier is an objective of the BDT, described next.

14.2.3 BDT

Unlike the ITU-T (and to some extent ITU-R), which deals with standardization, the BDT deals with aspects that promote the integration and deployment of communications in developing countries. Typical outputs from this sector include implementation guides that expand the utility of ITU recommendations and ensure their expeditious implementation. Communications has been recognized as a necessary element for economic growth. The BDT also seeks to arrange special financing involving communication suppliers and governments or authorized carriers within developing countries to enable provision of basic communications service where otherwise it would not be possible.

14.2.4 ISO/IEC JTC 1

Two global organizations are active in the information processing systems area, the International Standards Organization (ISO) and the International Electrotechnical Commission (IEC), particularly through the Joint Technical Committee 1 (JTC 1).

The ISO comprises national standards bodies, which have the responsibility for promoting and distributing ISO standards within their own countries. ISO technical work is carried out by some 200 technical committees (TC). Technical committees are established by the ISO council and their work program is approved by the technical board on behalf of the council.

The IEC comprises national committees (one from each country) and deals with almost all spheres of electrotechnology, including power, electronics, telecommunications, and nuclear energy. IEC technical work is performed by some 200 TCs set up by its council and some 700 working groups. Part of this organization, a President's Advisory Committee on future technology (PACT) advises the IEC president on new technologies which require preliminary

or immediate standardization work. PACT is designed to form a direct link with private and public research and development activities, keeping the IEC abreast of accelerating technological changes and the accompanying demand for new standards. Small industrial project teams examine new work initiatives which can be introduced into the regular IEC working structure.

In 1987 a joint technical committee was established incorporating ISO TC97, IEC TC83, and subcommittee 47B to deal with generic information technology. The international standards developed by JTC1 are published under the ISO and IEC logos. The activities of ISO/IEC/JTC 1 are listed in Table 14.3 expressed in terms of its subcommittees (SC).

TABLE 14.3 ISO/IEC/JTC1 Subcommittees

SC 1	Vocabulary
SC 2	Coded character sets
SC 6	Telecommunications information exchange between systems
SC 7	Software engineering
SC 11	Flexible magnetic media for digital data interchange
SC 17	Identification cards and related devices
SC 22	Programming languages, their environments and systems software interfaces
SC 23	Optical disk cartridges for information interchange
SC 24	Computer graphics and image processing
SC 25	Interconnection information technology management
SC 26	Microprocessor systems
SC 27	IT security techniques
SC 28	Office equipment
SC 29	Coding of audio, picture, multimedia and hypermedia information
SC 31	Automatic data capture
SC 32	Data management services
SC 33	Distributed application services

The ISO and IEC jointly issue directions for the work of the technical committees. The scope (or area of activity) of each technical committee (TC)/subcommittee (SC) is defined by the TC/SC itself, and then submitted to the Committee of Action (CA)/parent TC for approval. The TCs/SCs prepare technical documents on specific subjects within their respective scopes, which area then submitted to the National Committees for voting with a view to their approval as international standards.

14.3 Regional Standardization

Today the ETSI comes closest to being a true regional standards setting body, together with CITEL, the regional (Latin-American) standardization body.

ETSI is the result of the Single Act of the European community and the EC commission green paper in 1987 that analyzed the consequences of the Single Act and recommended that a European telecommunications standards body be created to develop common standards for telecommunications equipment and networks. Out of this recommendation, the Committee for Harmonization (CCH) and the European Conference for Post and Telecommunications (**CEPT**) evolved into ETSI, which formally came into being in March 1988. It should be noted, however, that even though ETSI attributes at least part of its existence to the European Community, its membership is wider than just the European Union Nations.

Because of the way ETSI came into being, ETSI is characterized by a unique aspect, namely, it is often called upon by the European Commission to develop standards that are necessary to implement legislation. Such standards, which are referred to as technical basis reports (TBR) and whose application is usually mandatory, are often needed in public procurements, as well as in provisioning for open network interconnection as national telecommunications administrations are being deregulated. Like ITU, however, ETSI also develops voluntary standards in accordance with common international understanding against which industry is not obliged to produce conforming products. These standards fall into either the European technical standard (**ETS**) class when fully approved, or into the interim-ETS class, when not fully stable or proven.

ETSI standards are typically sought when either the subject matter is not studied at the global level (such as when it may be required to support some piece of legislation), or the development of the standard is justified by market needs that exist in Europe and not in other parts of the world. In some cases, it may be necessary to adapt ITU standards for the European continent, although a simple endorsement of an ITU standard as a European standard is also possible. A more delicate case arises when both the ITU and ETSI are pursuing parallel standards activities, in which case close coordination with the ITU is sought either through member countries that may input ETSI standards to the ITU for consideration or through the global standards collaboration process.

The highest authority of ETSI is the general assembly, which determines ETSI's policy, appoints its director and deputy, adopts the budget, and approves the audited accounts. The more technical issues are addressed by the technical assembly, which approves technical standards, advises on the work to be undertaken, and sets priorities. The ETSI technical committees are listed in Table 14.4.

TABLE 14.4 ETSI Technical Committees

TCEE	Environmental engineering
TCHF	Human factors
TCMTS	Methods for testing and specification
TCSEC	Security
TCSPS	Signalling protocols and switching
TCTM	Transmission and multiplexing
TCERM	EMC and radio spectrum matters
TCICC	Integrated circuit cards
TCNA	Network aspects
TCSES	Satellite earth stations and systems
TCSTQ	Speech processing, transmission and quality
TCTMN	Telecommunications management networks
ECMA TC32	Communication, networks and systems interconnection
EBU/CENELEC/ETSI JTC	Joint technical committee

It can be seen that ETSI currently comprises 14 technical committees reporting to the technical assembly. These committees are responsible for the development of technical standards. In addition, these committees are responsible for prestandardization activities, that is, activities lead to ETSI technical reports (ETR) that eventually become the basis for future standards.

In addition to the technical assembly, a strategic review committee (SRC) is responsible for prospective examination of a single technical domain, whereas an intellectual property rights committee defines ETSI's policy in the area of intellectual property. Although by no means unique to ETSI, the rapid pace of technological progress has resulted in more standards being adopted that embrace technologies that are still under patent protection. This creates a fundamental conflict between the private, exclusive nature of industrial property rights, and the open, public nature of standards. Harmonizing those conflicting claims has emerged as a thorny issue in all standards organizations; ETSI has established a formal function for this purpose. Finally, the ETS/EBU technical committee coordinates activities with the European broadcasting union (EBU), whereas the ISDN committee is in charge of managing and coordinating the standardization process for narrowband ISDN.

14.3.1 CITEL

On June 11, 1993, the Organization of American States (OAS) General Assembly revised the existing Inter-American Telecommunication Commission (CITEL) strengthening and reorganizing the activities of CITEL, creating a position for the executive secretariat of CITEL and opening the doors, as associate members, to enterprises, organisms, and private telecommunication organizations, to act as observers of the permanent consultative committees of CITEL and its working groups.

CITEL's objectives include facilitating and promoting the continuous development of telecommunications in the hemisphere. It serves as the organization's principal advisory body on matters related to telecommunications. The commission represents all the members states. It has a permanent executive committee consisting of 11 members, and three permanent consultative committees. The permanent consultative committees, whose members are all member states of the organization, also have associate members that represent various private telecommunications agencies or companies.

The general assembly of CITEL, through resolution CITEL Res.8(I-94) established the following specific mandates for the three permanent consultative committees and the steering committee.

Permanent Consultative Committee I: Public Telecommunication Services. To promote and watch over the integration and strengthening of networks and public telecommunication services operating in the countries of the Americas, taking into account the need for modernization of networks and promotion of universal telephone basic services, as well as for increasing the public availability of specialized services and the promotion of the use of international ITU standards and radio regulations.

Permanent Consultative Committee II: Broadcasting. To stimulate and encourage the regional presence of broadcasting services, promoting the use of modern technologies and improving the public availability of such communication media, including audio and video systems, and the promotion of the use of international ITU standards and radio regulations.

Permanent Consultative Committee III: Radiocommunications. To promote the harmonization of radiocommunication services bearing especially in mind the need for a reduction to the minimum of those factors that may cause harmful interferences in the performance and operation of networks and services. To promote the use of modern technologies and the application of the ITU radio regulations and standards.

Steering Committee. The Steering Committee shall be formed by the chairman and vice-chairman of COM/CITEL and the chairman of the PCCs. The committee will be responsible for the revision and proposal to COM/CITEL of the continuous updating of

the regulations, mandates and work programs of CITEL bodies; the executive secretary of CITEL will act as the secretary of said committee.

14.4 National Standardization

As standardization moves from global to regional and then to national levels, the number of actual participating entities rapidly grows. Here, the function of two national standards bodies are reviewed, primarily because these have been in existence the longest and secondarily because they also represent major markets for commercial communications.

14.4.1 ANSI T1

Unlike the ETSI, which came into being partly as a consequence of legislative recommendations, the ANSI Committee T1 on telecommunications came into being as a result of the realization that with the breakup of the Bell System, de-facto standards could no longer be expected. In fact, T1 came into being the very same year (1984) that the breakup of the Bell System came into effect.

The T1 membership comprises four types of interest groups: users and general interest groups, manufacturers, interexchange carriers, and exchange carriers. This rather broad membership is reflected, to some extent, by the scope to which T1 standards are being applied; this means that nontraditional telecommunications service providers are utilizing the technologies standardized by committee T1. This situation is the result of the rapid evolution and convergence of the telecommunications, computer, and cable television industries in the United States, and advances in wireless technology.

Committee T1 currently addresses approximately 150 approved projects, which led to the establishment of six, primarily functionally oriented, technical subcommittees (TSC), as shown in Table 14.5 and Fig. 14.2 [although not evident from Table 14.3, subcommittee T1P1 has primary responsibility for management of activities on personal communications systems (PCS)]. In-turn, each of these six subcommittees is divided into a number of subtending working groups, and subworking groups.

TABLE 14.5 T1 Subcommittee Structure

TSC: T1A1	Performance and signal processing
TSC: T1E1	Network interfaces and environmental considerations
TSC: T1M1	Interwork operations, administration, maintenance, and provisioning
TSC: T1P1	Systems engineering, standards planning, and program management
TSC: T1S1	Services, architecture, and signalling
TSC: T1X1	Digital hierarchy and synchronization

Committee T1 also has an advisory group (**T1AG**) made up of elected representatives from each of the four interest groups to carry out committee T1 directives and to develop proposals for consideration by the T1 membership.

In parallel to serving as the forum that establishes ANSI telecommunications network standards, committee T1 technical subcommittees draft candidate U.S. technical contributions to the ITU. These contributions are submitted to the U.S. Department of State National Committee for the ITU, which administers U.S. participation and contributions to the ITU (see Fig. 14.3). In this manner, activities within T1 are coordinated with